DYNAMICS OF OCEAN WAVES IN A CONTINUOUS SEA ICE COVER

by

Vernon A. Squire

A dissertation submitted for the degree of
Doctor of Philosophy
in the University of Cambridge

Short title:
Waves in ice

Trinity College,
Cambridge.
October 1978.

PREFACE

This dissertation is an account of my work carried out while a research student at the Scott Polar Research Institute in the period October 1975 to October 1978 under the direction of my supervisor Dr Peter Wadhams.

The dissertation does not exceed 80 000 words. Unless otherwise stated, it is the original work of the author and not the outcome of work done in collaboration. It has not been and is not being submitted for a degree at any other university.

Vernon Squire.

Vernon A. Squire
October 1978

To Mum and Dad,

and Sam

ABSTRACT

Waves and swell incident on a continuous cover of sea ice can become coupled to the ice and propagate as flexural-gravity waves. These ice-coupled waves are determined by a dispersion equation and attenuation coefficient which depend critically on the material properties of the sea ice.

Two models of sea ice are proposed:- a linearly viscoelastic thin plate with uniform properties throughout; and a thermorheologically simple, viscoelastic thin plate whose properties vary through the ice sheet due to the temperature gradient across its thickness. Using the former model, an approximate solution consisting of the superposition of three ice-coupled waves is found for deep water waves impinging on ice at normal incidence. The characteristic properties of these waves are discussed in detail. The latter, more complicated model is developed and solved assuming that the viscoelastic Poisson's ratio is constant and the viscoelastic Young's modulus at a particular reference temperature satisfies some sea ice model proposed in the literature. Flexural-gravity wave solutions are discussed with emphasis laid on their temperature dependence and the effects of rotatory inertia and transverse shear.

Obliquely incident waves are also considered. It is shown that the presence of significant attenuation within the ice cover leads to inhomogeneous flexural-gravity waves near the ice edge but the degree of inhomogeneity and angular spread decreases with distance. The existence of a critical angle of incidence enhances this effect considerably.

Experiments carried out using strain measuring instruments on fast ice in Newfoundland are discussed and the data obtained are compared with theoretical predictions. It is shown that the direction and magnitude of wave components at some locations may be found using a rosette of three instruments but that large errors may occur in the subsequent data processing. A method avoiding

these errors is proposed and implemented. Additional observations of ice-coupled waves recorded at Strathcona Sound are reported and possible mechanisms for their generation are suggested.

ACKNOWLEDGEMENTS

I would like to thank my supervisor, Dr Peter Wadhams, who has given me constant help and encouragement during the last three years. His enthusiasm and sustained interest in my project have developed into a friendship which will outlive our academic interests.

My work has been strongly influenced by Dr G. de Q. Robin, Director of the Scott Polar Research Institute, who first introduced me to the waves-in-ice problem. My thanks go to him and other members of the Institute for providing such comfortable working conditions; to Dr Dougal Goodman whose knowledge on the physics of ice frequently guided my mathematics; and to Kolumban Hutter whose mathematics often guided my physics.

The *in situ* experimental program was the result of a collaboration between S.P.R.I. and C-CORE, Memorial University of Newfoundland, and in this connection I would like to acknowledge Harold Snyder for his continued support. Alastair Allan organized and led the field work and with the help of Jamie Rossiter, Terry Ridings and Gene Lau, contributed much to a successful series of experiments. I thank these and other members of C-CORE for teaching me much about sea ice.

Many others have helped both before and after, as well as during experiments. I would especially like to thank Ken Butt for electronic wizardry; Brian Gamberg for invaluable assistance on a small computer; and Ray Horne for invaluable assistance on a large computer.

Special thanks are due to Alida Short and family for their generosity and cheerfulness over the years I have been in Cambridge.

Lastly, I would like to thank Mrs Pat Little for her rapid and accurate typing; Stuart Moore for his photographic guidance; and Pat Langhorne who patiently tolerated the ups and downs of a research student writing his thesis.

During my three years as a research student at S.P.R.I. I was supported by a grant from the Natural Environmental Research Council.

CONTENTS

CHAPTER 1

INTRODUCTION AND SURVEY

INTRODUCTION AND SURVEY

For most of the year approximately 7% of the earth's surface is covered with sea ice. This constitutes an area of about 38×10^6 km^2, yet owing to the considerable variability of sea ice and the difficulties associated with field work in a harsh and dynamic environment, we are far from understanding many of its subtle properties. In this introduction we shall discuss briefly only those physical and engineering properties which are considered relevant to wave studies. A survey of both theoretical and experimental work in waves-on-ice will also be given.

1.1 Sea Ice Formation and Structure

Two important factors determine the initial growth of sea ice in the oceans:- a decrease in the freezing point of sea water with increasing salinity; and the absence of a temperature of maximum density in sea water with salinity above 24.7 ‰. As the surface temperature decreases convection currents will be set up which will carry the colder surface waters downwards to a depth prescribed by mixing and the vertical density gradient of the sea. Water of greater salinity from beneath will then gradually replace the surface waters until at some point the temperature is such that the freezing point for water of that salinity is reached and freezing commences. The first crystals to form are minute spheres of pure ice. These rapidly form into thin discoids which spread laterally across the surface of the water and freeze together to give the sea surface a greasy appearance. This type of ice is called frazil. In calm waters the orientation of the c-axes would be completely vertical and the frazil would then thicken to form nilas, a thin, clear layer of ice with sufficient elasticity to bend to a wave. However, since water conditions are rarely, if ever, calm, some discoids are caught with their c-axes inclined to the vertical and the surface skim shows crystals at almost every orientation. Under wind and wave action the ice layer may then be fractured and knocked together to form pancake ice or piled-up to form the thick polycrystalline composite often seen off the coast

INTRODUCTION AND SURVEY

For most of the year approximately 7% of the earth's surface is covered with sea ice. This constitutes an area of about 38×10^6 km^2, yet owing to the considerable variability of sea ice and the difficulties associated with field work in a harsh and dynamic environment, we are far from understanding many of its subtle properties. In this introduction we shall discuss briefly only those physical and engineering properties which are considered relevant to wave studies. A survey of both theoretical and experimental work in waves-on-ice will also be given.

1.1 Sea Ice Formation and Structure

Two important factors determine the initial growth of sea ice in the oceans:- a decrease in the freezing point of sea water with increasing salinity; and the absence of a temperature of maximum density in sea water with salinity above 24.7 ‰. As the surface temperature decreases convection currents will be set up which will carry the colder surface waters downwards to a depth prescribed by mixing and the vertical density gradient of the sea. Water of greater salinity from beneath will then gradually replace the surface waters until at some point the temperature is such that the freezing point for water of that salinity is reached and freezing commences. The first crystals to form are minute spheres of pure ice. These rapidly form into thin discoids which spread laterally across the surface of the water and freeze together to give the sea surface a greasy appearance. This type of ice is called frazil. In calm waters the orientation of the c-axes would be completely vertical and the frazil would then thicken to form nilas, a thin, clear layer of ice with sufficient elasticity to bend to a wave. However, since water conditions are rarely, if ever, calm, some discoids are caught with their c-axes inclined to the vertical and the surface skim shows crystals at almost every orientation. Under wind and wave action the ice layer may then be fractured and knocked together to form pancake ice or piled-up to form the thick polycrystalline composite often seen off the coast

of Newfoundland.

Once an initial skim has formed the ice begins to thicken. The crystals have now lost a degree of growth freedom so that any tendency towards anisotropy in the initial skim will produce geometric selection. Since the directions of easiest growth for a single ice crystal lie in the basal plane (perpendicular to the c-axis), crystals with their c-axes at large angles to the vertical will grow in preference to those with their c-axes nearly vertical. This results in a gradual transition from the surface ice, where most of the c-axes are near vertical, to the columnar zone, where most of the c-axes are near horizontal. Beneath the columnar zone we have a zone in direct contact with the underlying sea water. This zone is called the skeletal layer.

Examination of the skeletal layer throws some light on the mechanisms involved in a growing sea ice sheet. The layer shows the crystals to be made up of parallel rows of individual platelets with layers of brine between them. As the ice thickens, these platelets may trap the brine to form isolated pockets known as brine cells. Further, the relative position of the brine cells will change with respect to the ice/water interface with the result that they are cooled. Their volume will therefore decrease with a corresponding increase in the salinity of the entrapped brine.

Once the ice has formed, desalination changes its properties further. Four possible mechanisms have been proposed: brine cell migration, brine expulsion, gravity drainage and flushing. These mechanisms are felt to be out of place in this account. The interested reader is referred to Cox and Weeks (1975).

Further discussions on the physical properties of sea ice may be found in reviews by Pounder (1965), Weeks (1966) and Lewis (1971).

1.2 Engineering Properties

The engineer or off-shore technologist who wishes to use sea ice

as a material may require to know something of its mechanical, frictional, thermal or electromagnetic properties. Fortunately, the problem of waves propagating in ice-covered waters does not require such a broad outlook and we shall limit ourselves to aspects of the mechanical and thermal behaviour of sea ice which are relevant to the present case. These include the elastic, viscoelastic and thermomechanical properties.

Ice is an unusual material in that it does not have a distinct yield point below which almost all the strain is elastic and above which it is plastic. Instead creep occurs under any stress. In many problems in ice engineering, however, the stresses are applied sufficiently transiently that an elastic analysis is adequate to determine solutions. An engineer may then require to know any of the following properties: Young's modulus, Poisson's ratio, compressive strength, tensile strength, flexural strength or shear strength. In problems of flexure the Young's modulus E and Poisson's ratio ν would be required together with various measures of the tensile strength. Bearing in mind what we have said in section 1.1 regarding the complex structure of sea ice, we might expect these three parameters to be functions of the fractional volume of brine (and air) trapped in the material and its crystal structure.

Of all the material properties of ice, the determination of Young's modulus has attracted the most attention. Two basic experimental methods have evolved:- the static method whereby Young's modulus is found directly from the stress-strain curve; and the dynamic method where for in situ measurements, seismic techniques are used, or for laboratory measurements either natural resonance or acoustical measurements are used. Static experiments tend to predict lower values than dynamic methods since the ice can flow during the finite period over which the stress is applied. Detailed studies of the relation between Young's modulus and brine volume show a general decrease in E as brine volume increases (Schwarz and Weeks, 1977). In comparison with Young's modulus, Poisson's ratio shows very little variation with brine volume

(Weeks and Assur, 1967; Hutter, 1975c, 1976). Dykins (1970) has shown the tensile strength in uniaxial tests to be strongly dependent on the direction of load and to vary linearly with the square root of the brine volume. He found that there was no appreciable dependence on crystal size.

Empirical studies on the viscoelastic properties of sea ice have been carried out by Tabata (1955a, 1958a, 1958b) using *in situ* cantilever beams and beams fixed to the ice sheet at both ends. Viscoelastic experiments are necessarily *in situ* to avoid the brine drainage problems that would be encountered when small samples are stressed for long periods. However, care must be taken to ensure that the open water cuts alongside the beams do not modify the vertical temperature distribution within the beam. Tabata found that the viscoelastic behaviour of sea ice may be represented by a rheological model composed of a Maxwell unit and a Voigt unit connected in series. Unfortunately, there are insufficient data to obtain any correlation between the measured viscoelastic properties and the state of the sea ice. Tabata's model can only be an approximation to the real behaviour of sea ice which is governed by dislocation generation and movement characteristics of the ice crystal lattice (Goodman, 1977). The approximation is useful, however, as a mathematical tool for solving problems in the dynamical behaviour of ice sheets. The present author knows of no further *in situ* experimental work of this type on sea ice. Theoretical calculations based on viscoelastic models of sea ice (linear and non-linear) are becoming popular at the present time, however, so that hopefully more valuable experimental work in this field will be carried out in the near future. A review of recent experimental work is included in Nevel (1976).

To the author's knowledge no experimental work has been carried out on sea ice to measure its thermomechanical properties when the material is allowed to flow as well as behave elastically. This behaviour, called thermoviscoelasticity, is relatively new to sea ice research and empirical studies have not yet had time to catch up with theoretical work. The original equations due to Hutter

(1975b) and Williams (1976) have been developed in the present work so that engineering problems may not only be posed but also solved. Communication between the present author and Kolumban Hutter has resulted in a further report (Hutter, 1978) based on a series of two lectures given at the Memorial University of Newfoundland in Spring, 1977.

1.3 Waves-in-Ice. A Survey

Towards the end of the nineteenth century, Greenhill (1887) showed theoretically that ice floating on the surface of water can support flexural wave-type solutions. To the present author's knowledge, Greenhill's solution represents the earliest theoretical analysis on this particular aspect of floating ice though flexural waves had no doubt been observed on many occasions prior to that date. Such waves are a common sight in sea ice near open water and early whalers and sealers in the Greenland Sea could not fail to notice the slight but perceptible motion associated with their presence. Greenhill chose to represent the ice as a thin elastic plate with negligible Poisson's ratio floating on water of uniform depth. This model, in a slightly more general form, has been used consistently by engineers to solve both dynamical and static problems in ice research.

Nearly fifty years later, Ewing *et al* (1934) and Ewing and Crary (1934) used seismographs to detect the existence of longitudinal, transverse and flexural waves in a sheet of fresh water ice. The waves were generated by the explosion of blasting caps placed in holes in the ice. Using essentially the equations derived by Greenhill (1887) with modification to include Poisson's ratio and a compressible water column, Ewing and Crary plotted the group velocity for the flexural vibrations as a function of frequency. The data showed the waves to be highly dispersive over the range of frequencies present. Similar experiments were carried out several years later by Press *et al* (1951) and Press and Ewing (1951). The former authors produced elastic waves in lake ice by detonating small explosive charges at various depths in the water,

within the ice, and in the air. It was found that the position of the explosion was critical in determining the type of waves produced. Explosions within the ice or water produced the same dispersive flexural waves found by Ewing and Crary, whereas explosions in the air produced a new type of wave referred to as air-coupled flexural waves. The latter paper (Press and Ewing, 1951) considered theoretical wave solutions for the propagation of elastic waves in a floating ice sheet.

It was not until 1954 that experiments equivalent to the above were reported for Arctic sea ice (Oliver et al, 1954). In these tests, air-coupled as well as dispersive flexural waves were generated by shots fired above and below the ice surface with the purpose of deducing ice thickness. It was found that although the air-coupled waves gave a reasonable estimate, the predicted thickness consistently fell below the measured value. In a later paper Anderson (1963) developed the ideas of Oliver et al and suggested that in addition to measuring ice thickness, elastic waves could permit a detailed description to be made of the mechanical properties of sea ice. He noted, however, that the anisotropy of sea ice is critical in determining those properties and cannot be neglected when using elastic waves. The suggestions of Anderson have prompted considerable experimental work on the determination of mechanical properties by seismic methods (Weeks and Assur, 1967).

Early in the 1950's another line of research concerned with flexural waves in an ice cover led to several papers which neglected the flexural rigidity of the ice and assumed it to be a floating mat of small, non-interacting particles. Peters (1950) considered the deep water solution for a wave impinging from an open water region on to a region covered with such a mat. In a later paper Weitz and Keller (1953) generalized Peters' solution to water of arbitrary depth and waves impinging at any angle of incidence. In the same year Shapiro and Simpson (1953) quantified the effect of an ice field on impinging open water waves by deriving practical formulae for forecasting swells in ice-covered seas. Unfortunately, their paper caontains an error in the calculation of the transmission coefficient

which forced them to postulate a fictitious "pressure energy" term. Wadhams (1976b, app.C) discusses the correct solution. Two further papers by Keller and Goldstein (1953) and Keller and Weitz (1953) looked more deeply into reflection and transmission coefficients at an ice edge.

Early observations of naturally-occurring ice vibrations were reported by Crary et al (1952) and Crary and Goldstein (1957). Their gravity meter data showed the existence of a ubiquitous vertical ice oscillation of very small amplitude in the period range 5-40 s. The measurements, however, formed part of a much larger geophysical survey to carry out ocean sounding and to measure ice movement and gravity anomalies, so that no processing of the wave data was attempted. A more detailed study of waves in an ice-covered ocean was carried out by Hunkins (1962) from four floating ice stations. The data showed waves to be present over a range of period from about 15 to 60 s, though the calculated amplitude spectra are believed to be in error due to the failure to remove a trend from the data. Similar errors are present in LeSchack and Haubrich (1964) and LeSchack (1965) for wave data obtained at stations on pack ice, ice islands and shelf ice. Wadhams (1973b) discusses these errors in detail. The significance of these papers is therefore not in their quantative results but in their observations. Hunkins concluded that the measured wave motions were due to a combination of both waves entering from open water and to wind generation (or enhancement) of waves within the sea ice cover. This latter mechanism is discussed more fully by Sytinskiy and Tripol'nikov (1964) who used a tripartite array of seismographs to observe the progressive waves produced by a wind gust as well as the usual background oscillations.

During a voyage from Stanley to Halley Bay in the Antarctic by R.R.S. "John Biscoe", Robin (1963a) had the opportunity to make systematic wave recordings in ice-covered waters. Ten-minute recordings were made at six-hour intervals using a shipborne wave recorder designed at the Institute of Oceanographic Sciences. The resulting power spectral densities showed a gradual elimination

of the energy of shorter period waves as the ship moved further into the ice cover. The long period component of the spectrum, however, showed little change until very large floes were encountered. Similar experiments were carried out by Dean (1965) in the small-floe zone near a compacted ice edge. Dean found that the energy decay with distance was not simply exponential. Wadhams (1973b) analysed Dean's data more thoroughly and showed that the apparent decay was due to a change in floe size distribution some way in from the ice edge. It must be noted that the observations reported by both Robin and Dean were concerned with pack ice and so do not relate directly to measurements of the decay of flexural waves. An individual ice floe will possess unique flexural, hydrodynamical and scattering properties, all of which contribute to the observed energy decay. A comprehensive discussion of the mechanisms involved in this more general situation can be found in review papers by Robin (1963b, 1966).

The observations of Robin (1963a) stimulated a renewed interest in theoretical treatments of the waves-in-ice problem. Hendrickson and Webb (1963) considered the problem originally posed by Peters (1950) but did not neglect the flexural rigidity term. The derived solution however was an approximation since the velocity potentials within the open water region and ice region could only be matched at the surface. The finite submergence of the ice was also neglected. Nevertheless Hendrickson and Webb's treatment represented a significant improvement on existing theories. Two further papers by the Staff of the National Engineering Science Company (1965) and Hendrickson (1966) generalized the earlier paper further by considering an ice sheet of finite length on deep water and water of arbitrary depth respectively. Both these theoretical works were accompanied by thorough laboratory simulations using polythene sheet to model the floating sea ice. Similar experiments by Ofuya and Reynolds (1967) with polythene sheet demonstrated selective damping of incident waves. Long waves passed through the sheet with little energy loss whereas shorter waves experienced high attenuation. They concluded that this energy loss was due to three factors:- hysteresis in the

bending sheet; dissipation in the boundary layer beneath the sheet; and overtopping of water during wave motion. Further ice floe simulation experiments were reported by Henry (1968).

More recent work on waves in sea ice has been carried out by Wadhams (1973a, 1973b, 1978). Wadhams has investigated a variety of decay mechanisms including scattering of waves by individual floes, hysteresis losses due to bending, and hydrodynamical effects. His theoretical and experimental work using laser profilometry and inverted echo sounding in the Arctic show excellent agreement. In the Antarctic, Wadhams has found good agreement between theory and the observations of Robin (1963a) and Dean (1965). Further work in the Antarctic using Wadhams (1973a) has been carried out by Keliher (1976).

The first direct measurement of the strain at the surface of an ice cover due to flexural waves were made by Goodman et al (1975) and Allan (1975). The instruments used were developed at the Scott Polar Research Institute from strainmeters originally designed to measure earth tides. Subsequent work in this field has been reported in Squire (1978), Allan and Squire (1978), and Squire and Allan (1979).

CHAPTER 2

THE TEMPERATURE INDEPENDENT FLEXURAL-GRAVITY WAVE

THE TEMPERATURE INDEPENDENT FLEXURAL-GRAVITY WAVE

2.1 Introduction

Considerable research into the engineering properties of sea ice has been carried out over the last decade prompted by the growing interest in ice infested waters by oil companies. A recent review of the literature by Schwarz and Weeks (1977) clearly demonstrates that although we are able to provide an engineer with relevant information, based on empirical observations, we are still a long way from understanding the physics of sea ice. Indeed, it is only recently that a book on current sea ice research has become available (Doronin and Kheisin, 1977). Unfortunately many of the references cited are Russian and difficult to obtain.

The specific problem of 'waves-in-ice' has attracted a little attention over the years, as discussed in Chapter 1, but although the hydrodynamics are reasonably well understood, the material properties of the floating sea ice are not. The presence of ice on the surface of water could provide an extremely complex surface boundary condition depending on those properties and it is clear that some degree of approximation is inevitable if progress is to be made. However, how does one approximate when the original behaviour is unknown? Work by Glen (1955) has yielded a flow law for the long-term creep of non-saline, polycrystalline ice but no corresponding experiments have been carried out for sea ice. Perhaps sea ice is so variable a material that no simple, ubiquitous flow law exists.

Because of the current trend amongst theoretical physicists working on sea ice to adopt linear viscoelastic theory as a starting point (Nevel, 1966, 1976; Kheisin, 1967; Katona, 1974; Vaudrey and Katona, 1975), the present author has chosen this approach. The sea ice is therefore represented as a floating viscoelastic sheet. Although by no means necessary (see Chapter 6) we shall assume that the ice-coupled flexural waves are generated by normally incident sea waves so that the problem may essentially be regarded as one-dimensional. The ice will be assumed thin (valid for the

wavelengths considered) so that thin plate theory and its associated extensive literature may be used. In this chapter we shall also suppose that the ice is isotropic though the validity of this assumption is questionable. With all these assumptions, the problem is soluble but perhaps one should ask if the sea ice has been replaced by another material with much simpler properties.

2.2 The Viscoelastic Model

Using a variational approach, Biot (1955) has derived a general equation for the flexural bending of an isotropic, linearly viscoelastic, thin plate of thickness h. In terms of two material operators Q and R which are rational function of $\partial/\partial t$, he assumes a stress-strain relation

$$\sigma_{ij} = 2Q\varepsilon_{ij} + R\delta_{ij}\varepsilon_{kk} , \qquad (2.1)$$

where σ_{ij}, ε_{ij} are the stress and strain respectively and δ_{ij} is the Kronecker delta. Following Biot, we may write down an equation for the vertical displacement $w(x;t)$ as follows

$$B_1 \frac{\partial^4 w}{\partial x^4} + \rho h \frac{\partial^2 w}{\partial t^2} = q(x;t) , \qquad (2.2)$$

where ρ is the mass density of the plate and q is the load per unit area on the plate. The parameter B_1 is a function of the operators Q and R and corresponds to the flexural rigidity for a linearly elastic thin plate. Explicitly,

$$B_1 = \frac{Q(Q+R)h^3}{3(2Q+R)} . \qquad (2.3)$$

In an earlier paper, Biot (1954) shows that if the plate is assumed to be elastic under hydrostatic stresses, the material operators Q and R are simply related:-

$$R = K - \frac{2}{3}Q , \qquad (2.4)$$

where K is the bulk elastic modulus. Substitution into (2.3) yields an alternative expression for B_1,

$$B_1 = \frac{Q(Q+3K)h^3}{3(4Q+3K)} . \qquad (2.5)$$

This expression for B_1 in terms of Q, an integro-differential material operator corresponding to the shear modulus (Read, 1950), and K, the constant bulk elastic modulus, may be further simplified if the material is assumed to be incompressible (Squire and Allan, 1979). Such an assumption is intuitive rather than empirical since there appears to be no data discussing the bulk modulus of sea ice. However, one would not expect a sphere of ice under hydrostatic loading to show much volume change with time. For snow, on the other hand, there would be compaction with time. For an incompressible material, $K \to \infty$, so that (2.5) becomes

$$B_1 = \frac{h^3 Q}{3} . \qquad (2.6)$$

Unfortunately, the assumption that $K \to \infty$ imposes an unrealistic restriction on ν, namely $\nu = \frac{1}{2}$. For this reason we shall consider the sea ice to behave elastically under hydrostatic loading but not necessarily to be incompressible. Given that K is constant, its value may be estimated from known elastic properties. With a Young's modulus of 6.0×10^9 N m^{-2} and a Poisson's ratio of 0.3, the bulk modulus $K = 5.0 \times 10^9$ N m^{-2} (Jaeger, 1956, sect.13). Rather than choose this value of K outright however, we shall assign various reasonable values of K in order to find out whether the final solution is strongly dependent on the compressibility. Hence, the displacement equation (2.2) may be written explicitly as

$$\frac{Q(Q+3K)h^3}{3(4Q+3K)} \frac{\partial^4 w}{\partial x^4} + \rho h \frac{\partial^2 w}{\partial t^2} = q . \qquad (2.7)$$

So far, the form of the integro-differential operator Q has not been discussed and in order to proceed some Q must be found which adequately models the behaviour of sea ice. If, for example, Q were assumed to be constant, then B_1 reduces to the familiar elastic

flexural rigidity and equation (2.7) becomes the equation for elastic bending of an isotropic thin plate (Hetényi, 1946). Such a formulation has been used many times to study the 'waves-in-ice' problem (see for example, Hendrickson et al, 1962; Hendrickson and Webb, 1963; Hendrickson, 1966; Evans and Davies, 1968). A propagating wave with no attenuation is predicted, however, which does not agree with the frequency dependent attenuation observed in nature. Wadhams (1973b) has investigated the possibility of dissipation of energy by hydrodynamical effects and has concluded that the observed attenuation is too large to be credited to hydrodynamical effects alone. We therefore suspect that a suitable expression for Q for waves propagating under a sea ice cover must allow for some energy loss due to creep.

Tabata (1955 , 1958a) has carried out in situ cantilever beam tests on sea ice and has found that the operator E, corresponding to Young's modulus, fits a Maxwell-Voigt model (Flügge, 1975) over the range of stress considered. Similar results were obtained in the laboratory by Jellinek and Brill (1956) for non-saline ice under uniaxial tension. A schematic diagram representing this model is shown in figure 2.1. The model may essentially be divided into two parts; a spring in series with a dashpot and a spring in parallel with a dashpot. All elements are assumed to be linear though more general mechanical analogies have been proposed (Sala and Olkkonen, 1973).

From Flügge (1975), a differential equation for the linear, one-dimensional Maxwell-Voigt model may be written down:

$$\left(\frac{\partial^2}{\partial t^2} + a_1 \frac{\partial}{\partial t} + a_2 \right) \sigma = \left(b_0 \frac{\partial^2}{\partial t^2} + b_1 \frac{\partial}{\partial t} \right) \varepsilon, \qquad (2.8)$$

where a_i and b_i are material constants which may be related to the elastic and viscous properties of the model. We suppose that this equation represents the behaviour of a sample of sea ice in a uniaxial test, so that

$$E \equiv \left(b_0 \frac{\partial^2}{\partial t^2} + b_1 \frac{\partial}{\partial t} \right) \Big/ \left(\frac{\partial^2}{\partial t^2} + a_1 \frac{\partial}{\partial t} + a_2 \right). \qquad (2.9)$$

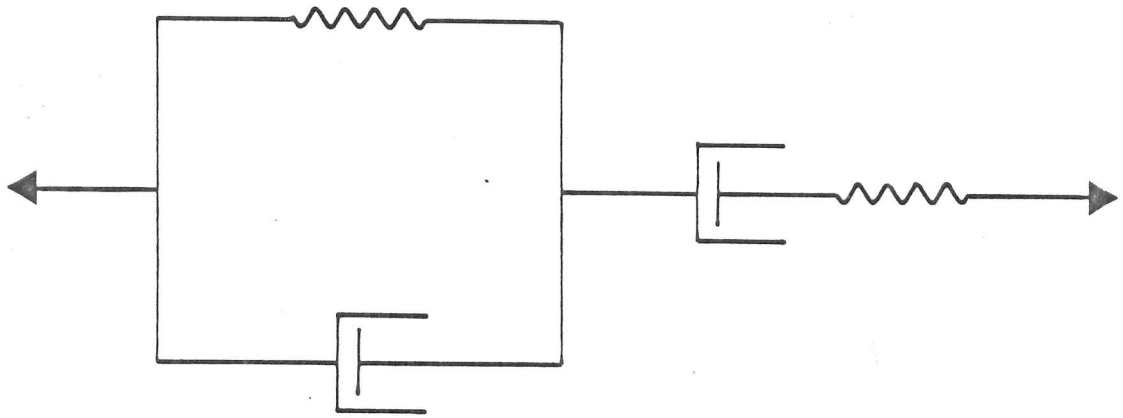

Fig. 2.1 The Maxwell-Voigt spring-dashpot sea ice model.

At this stage we shall restrict ourselves to problems which are periodic with a circular frequency ω, then writing

$$\sigma = \mathring{\sigma} e^{-i\omega t}, \quad \varepsilon = \mathring{\varepsilon} e^{-i\omega t}, \tag{2.10}$$

it may be shown that

$$\mathring{\sigma} = E^*(i\omega)\mathring{\varepsilon}, \tag{2.11}$$

where

$$E^*(i\omega) = \frac{b_0\omega^2 + ib_1\omega}{(\omega^2 - a_2) + ia_1\omega}. \tag{2.12}$$

The quantity $E^*(i\omega)$ is called the complex Young's modulus. In order to relate $E^*(i\omega)$ to the complex shear modulus $Q^*(i\omega)$, say, we use the expression

$$E^*(i\omega) = \frac{9Q^*(i\omega)K}{Q^*(i\omega) + 3K}, \tag{2.13}$$

(Christensen, 1971, sect.1.8). Hence, the complex flexural rigidity is given by

$$B_1^*(i\omega) = \frac{3K^2E^*(i\omega)h^3}{[9K - E^*(i\omega)][E^*(i\omega) + 3K]}. \tag{2.14}$$

Whence, the displacement equation (2.7) becomes

$$\frac{3K^2E^*(i\omega)h^3}{[9K - E^*(i\omega)][E^*(i\omega) + 3K]} \frac{\partial^4 w}{\partial x^4} - \rho h\omega^2 w = q, \tag{2.15}$$

Equation (2.15) is assumed to model the behaviour of a thin sheet of floating sea ice under flexure. We suppose that the region $-\infty < x < 0$ represents open water whereas the region $0 \leqslant x < \infty$ represents the floating sea ice (fig.2.2). We seek a solution to the problem of an infinitestimal monochromatic wave propagating in the positive x-direction towards a linear, semi-infinite viscoelastic sea ice sheet.

2.3 Hydrodynamics

If the hydrodynamics are assumed to be linear and irrotational then we may define a velocity potential Φ such that at every point

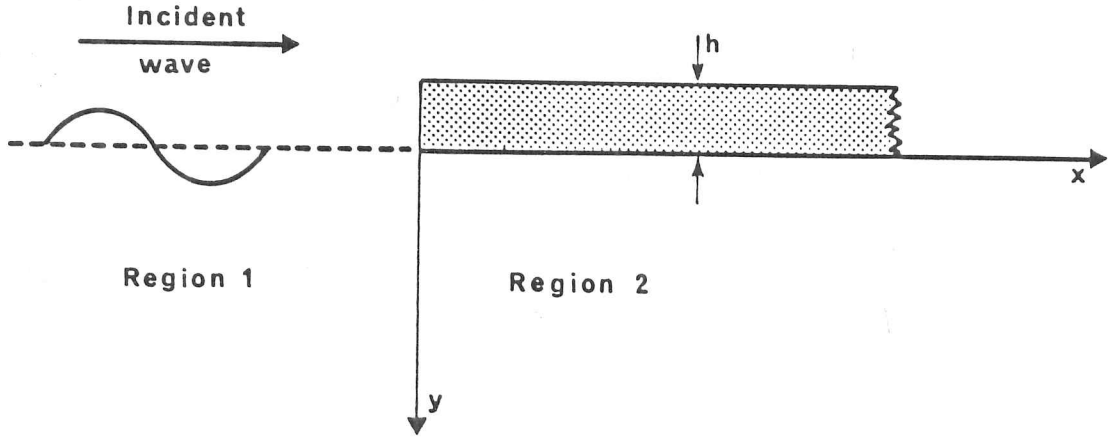

Fig. 2.2 Schematic representation of wave/ice interaction.

Laplace's equation

$$\nabla^2\Phi = 0, \tag{2.16}$$

is satisfied (Stoker, 1957). The operator ∇^2 represents $\frac{\partial^2}{\partial x^2} + \frac{\partial^2}{\partial y^2}$ (fig.2.2). The water is assumed to be deep, so that

$$\left.\frac{\partial\Phi}{\partial z}\right|_{z\to\infty} = 0. \tag{2.17}$$

The domain within which a deep water condition is valid is discussed by Kinsman (1965, ch.3.2). He defines two possible criteria for open water; the mathematician's condition where the wavelength must be less than twice the water depth and the oceanographer's condition where the wavelength must be less than four times the water depth. The latter condition implies a 5% error level which is quite adequate when one considers the majority of instruments used to measure ocean waves.

At the surface we may write down the kinematical boundary condition

$$\frac{\partial w}{\partial t} = - \left.\frac{\partial\Phi}{\partial z}\right|_{z=0}. \tag{2.18}$$

The problem may be divided naturally into two distinct regions 1 and 2 with different surface boundary conditions (fig.2.2).

Region 1

In region 1, $-\infty<x<0$, we assume a free surface so that Bernoulli's theorem provides a second boundary condition:

$$gw_1 = - \left.\frac{\partial\Phi_1}{\partial t}\right|_{z=0}, \tag{2.19}$$

where the subscript refers to the region and g is the acceleration due to gravity. Within region 1, therefore, we must satisfy Laplace's equation, the deep water condition and the two free surface conditions. A feasible solution is

$$\Phi_1 = (e^{ikx} + Re^{-ikx})\, e^{-kz} e^{-i\omega t}, \tag{2.20}$$

where R is now the reflection coefficient for amplitude, k is the wave number and ω is the circular frequency. Substitution into boundary conditions (2.18) and (2.19) leads to the well-known deep water dispersion equation

$$k = \frac{\omega^2}{g}. \tag{2.21}$$

Region 2

Provided that the waves are long when compared to the thickness of the sea ice we may assume that it suffers no submergence. Hence, in region 2, $0 \leq x < \infty$, we require an additional boundary condition along $z=0$. This boundary condition is provided by Bernoulli's theorem. Equation (2.15) may therefore be rewritten

$$\frac{3K^2 E^*(i\omega)h^3}{[9K - E^*(i\omega)][E^*(i\omega) + 3K]} \frac{\partial^4 w_2}{\partial x^4} - \rho h\omega^2 w_2 = -\rho'(g w_2 - i\omega \Phi_2|_{z=0}), \tag{2.22}$$

where ρ' is the density of sea water. There will be no change in frequency for an ocean swell impinging on the sea ice so that we may assume a solution of the form

$$\Phi_2 = (A_n e^{ik_n x} + B_n e^{-ik_n x})\, e^{-k_n z}\, e^{-i\omega t}, \tag{2.23}$$

where some summation is implicit. In this expression A_n and B_n are amplitude coefficients for the n th mode and k_n is the complex wave number associated with the n th mode.

Substitution into the boundary condition (2.22) yields the dispersion equation for region 2, a quintic polynomial in k_n:-

$$\frac{3K^2 E^*(i\omega)h^3}{[9K - E^*(i\omega)][E^*(i\omega) + 3K]} K_n^5 + (\rho' g - \rho h\omega^2) K_n - \rho'\omega^2 = 0. \tag{2.24}$$

Clearly, we must have boundedness as $z \to \infty$ so that any roots of this equation which have negative real parts are not permitted. Also, since the sea ice is assumed to extend from the origin to large x, we require boundedness as $x \to \infty$. Hence, we may restrict the solution (2.23) and write

$$\Phi_2 = \left[A_1 e^{ik_1 x} e^{-k_1 z} + A_2 e^{ik_2 x} e^{-k_2 z} + B_3 e^{-ik_3 x} e^{-k_3 z}\right] e^{-i\omega t}. \qquad (2.25)$$

Unlike the corresponding elastic theory there is no wave number which is purely real. All wave numbers have a non-zero imaginary part representing some attenuation of the flexural-gravity wave. Writing each wave number in terms of its component parts, we have

$$k_1 = \xi_1 + i\zeta_1, \quad k_2 = \xi_2 + i\zeta_2, \quad k_3 = \xi_3 - i\zeta_3, \qquad (2.26)$$

where ξ_n, ζ_n are real positive constants providing phase and attenuation information respectively.

At first sight, the third term in expression (2.25) appears to be physically unrealistic since the wave increases in amplitude as it propagates from large x to the ice edge. The wave may be put on more physical grounds, however, if it is decomposed into a decaying standing oscillation and a decaying wave propagating towards increasing x. Equation (2.25) therefore becomes

$$\Phi_2 = \Big\{ A_1 e^{i(\xi_1 x - \zeta_1 z)} e^{-(\zeta_1 x + \xi_1 z)} + A_2 e^{i(\xi_2 x - \zeta_2 z)} e^{-(\zeta_2 x + \xi_2 z)} + B_3 \left[2\cos(\xi_3 x - \zeta_3 z) - e^{i(\xi_3 x - \zeta_3 z)} \right] e^{-(\zeta_3 x + \xi_3 z)} \Big\} e^{-i\omega t}, \qquad \ldots(2.27)$$

where expressions (2.26) have been used to demonstrate the specific nature of the phase and attenuation constants. In the elastic case (Wadhams, 1973b), k_2 and k_3 turn out to be complex conjugate pairs so that expression (2.27) may be further simplified by merging the second and fourth terms. In the present case the second and fourth terms may be combined to produce a single term as an approximation only. The approximation is extremely good however

as may be seen by allowing ξ_3 and ζ_3 to be ξ_2 and ζ_2 plus a small quantity.

In order to solve the dispersion equation we require values for the material constants a_1, a_2, b_0, b_1 and the bulk modulus K. The former are provided by Tabata (1958a) as follows

$$a_1 = 0.4584\text{x}10^{-2}\ s^{-1},\quad a_2 = 0.2002\text{x}10^{-5}\ s^{-2},$$

$$b_0 = 0.4950\text{x}10^{9}\ Nm^{-2},\quad b_1 = 0.1130\text{x}10^{7}\ Nm^{-2}\ s^{-1}.$$

These values were obtained from the vertical loading test alone. Since the experiments were carried out over a range of temperatures, it is not simply a matter of averaging Tabata's values to provide the mean material constants. It is necessary to know something of the temperature behaviour of sea ice. This is discussed in Chapters 3 and 4 and will not be dealt with here. The values of a_1, a_2, b_0, b_1 chosen above, however, are consistent with those chosen later. Suitable trial values for the constant bulk modulus, K, must also be chosen in such a way that the term B_1, corresponding to the flexural rigidity, is not allowed to become negative. The dispersion equation may then be solved numerically to provide values for the complex wave numbers k_1, k_2 and k_3.

It is found that the three possible wave numbers represent a propagating wave with small attenuation together with two waves of greater attenuation which can exist only local to their point of generation. The former wave will be propagated far into the ice cover whereas the latter two waves will soon be attenuated so as to become unmeasurable. The three characteristic waves are seen for all reasonable values of K. In order to examine the effect of different constant bulk moduli on the solution, the theoretical wavelength in ice is plotted for each wave for various K (fig.2.3). The curves representing the two waves with large attenuation are superimposed in the lower diagram. The elastic bulk modulus is also shown. For the propagating wave and, to a lesser extent, the attenuated waves, the supposition that $K \rightarrow \infty$ seems reasonable for a 10 s wave. The approximation gets worse as the period decreases but even at 5 s the difference between the propagating wave at $K = 10^8$ and $K \rightarrow \infty$ is less than 5%.

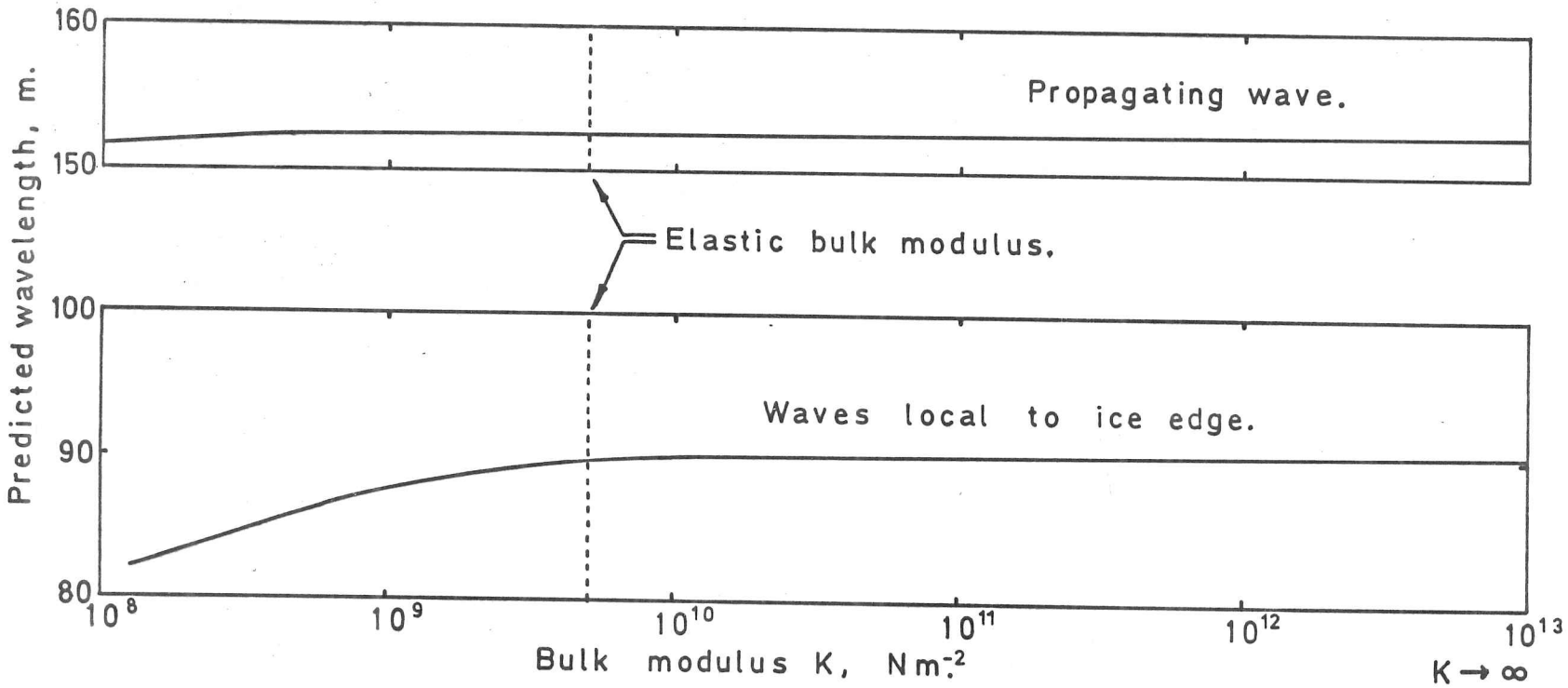

Fig. 2.3 The effect of a variety of constant bulk moduli on the predicted ice-coupled wavelengths for a 10 s wave in 1 m of sea ice. The elastic bulk modulus is also shown for comparison.

The imaginary parts of the complex wave numbers k_1, k_2 and k_3, representing the attenuation of the three possible flexural-gravity waves, are found to be slightly more dependent on the choice of the bulk modulus K. However, for k_1 there is still less than 5% deviation between the attenuation at the elastic bulk modulus and that at $K \to \infty$. For k_2 and k_3 the deviation is less than 1%. Bearing in mind the uncertainty in the value of the bulk modulus K, it therefore seems reasonable to choose $K \to \infty$ (Nevel, 1966, 1976; Squire and Allan, 1979). This reduces expression (2.14) for $B(i\omega)$ to

$$B_1^*(i\omega) = \frac{E^*(i\omega)h^3}{9} . \qquad (2.28)$$

Such a step imposes an additional condition on the complex Poisson's ratio, namely that ν is constant ($\nu = \frac{1}{2}$). In later chapters we shall tackle the analysis by assuming a constant Poisson's ratio at the outset.

Henceforth, the three possible flexural-gravity waves will be referred to by the subscript of their wave numbers. That is, wave 1 represents a wave with small attenuation which propagates far into the ice cover and waves 2 and 3 represent waves with relatively large attenuation which soon decay to unmeasurable proportions. We will consider wave 1 and waves 2 and 3 in turn for the case $K \to \infty$.

A graph of the wavelength against period for wave 1 (fig.2.4), shows the characteristic swing from a deep water dispersion relation for long waves to a dispersion curve which is controlled by the material properties of the floating sea ice for short waves. This behaviour is the origin of the term flexural-gravity waves. Such behaviour might indeed be expected since it is less likely that long waves will notice the effect of a thin cover of sea ice on the surface of deep water than short waves. The attenuation coefficient for wave 1 (fig.2.5), on the other hand, shows a marked decrease with increasing period once the period has exceeded some value. This implies that long waves will propagate much further than short

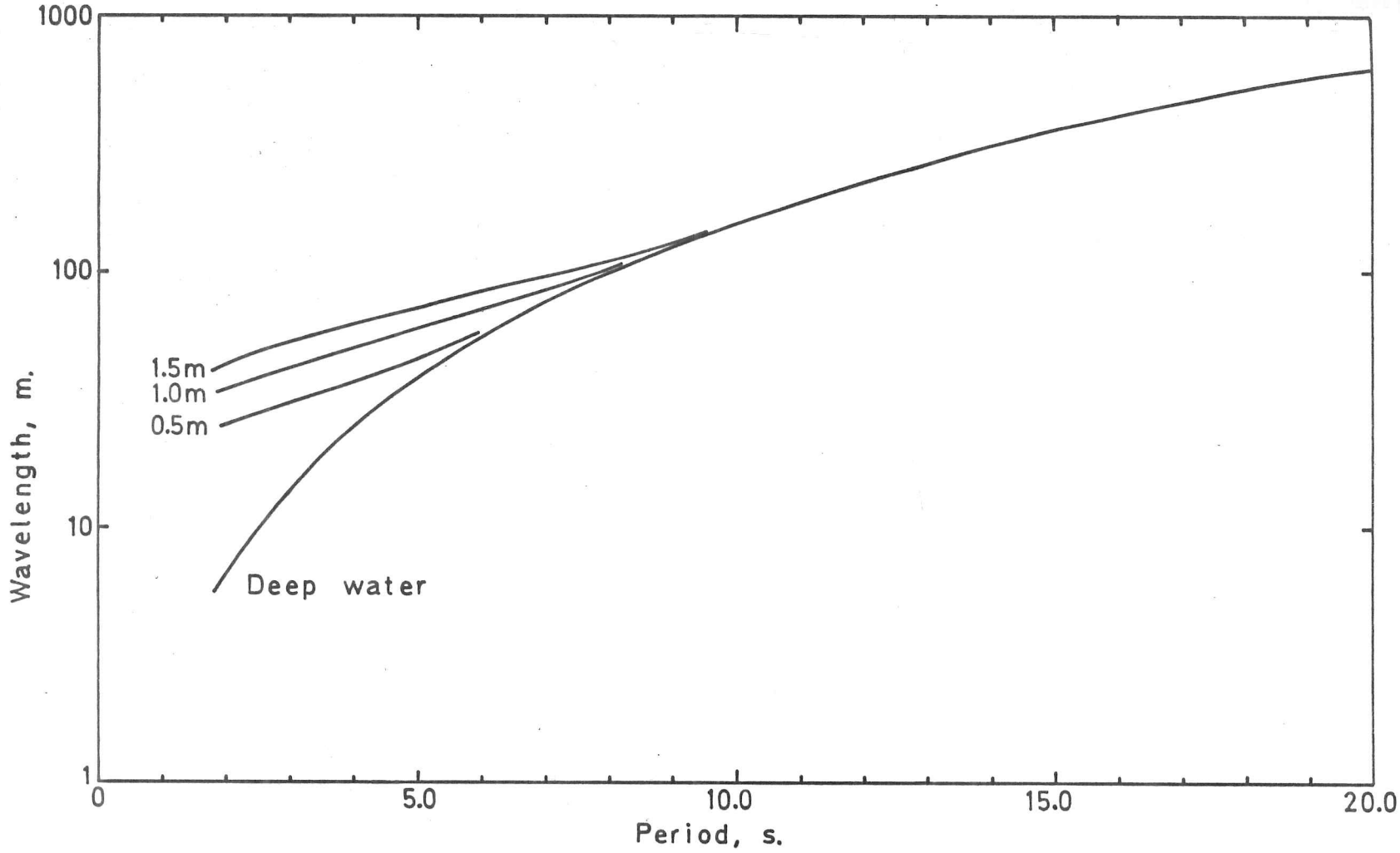

Fig. 2.4 The wavelength of the least attenuated flexural-gravity wave 1 as a function of period. Three ice thicknesses are shown and compared with the equivalent deep water curve.

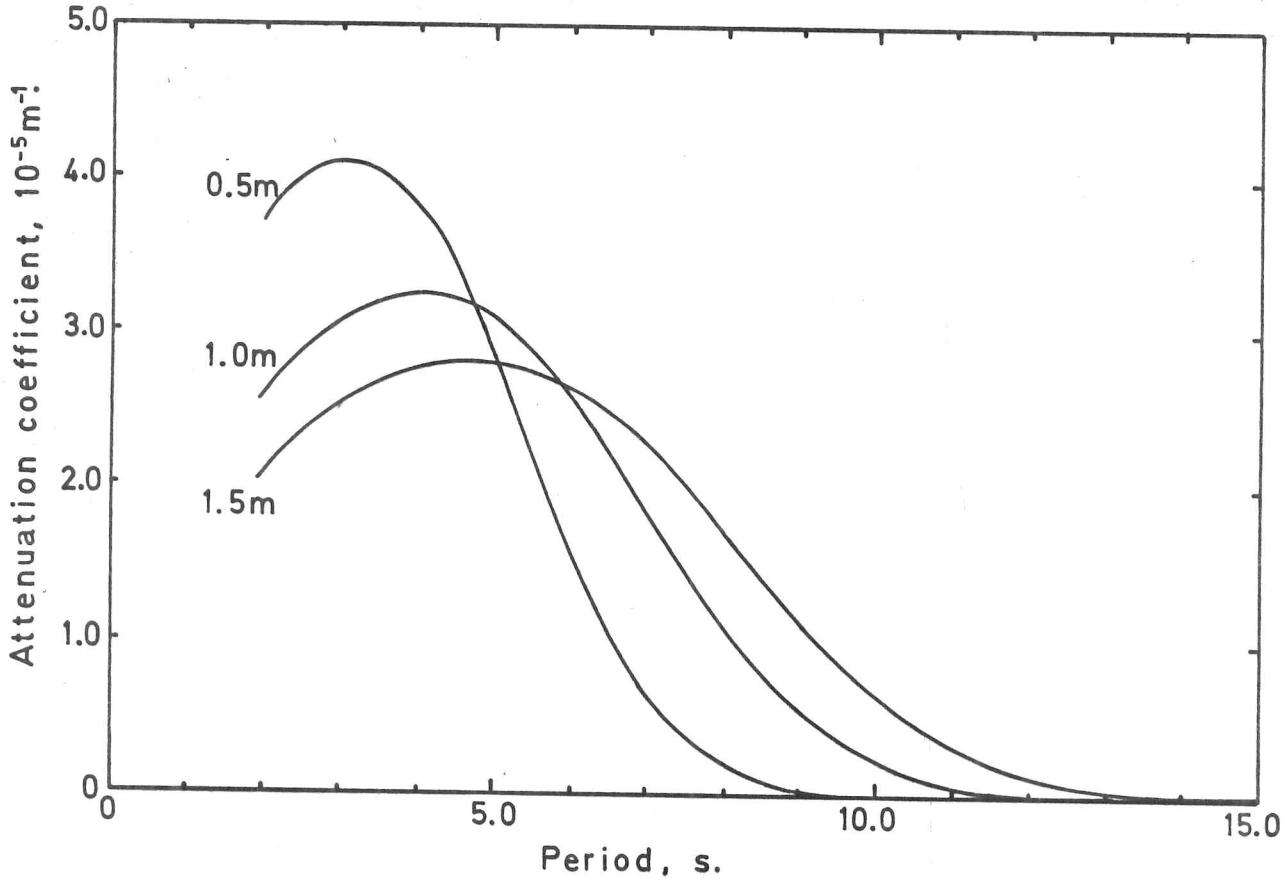

Fig. 2.5 The attenuation coefficient ζ_1 versus period for three sea ice thicknesses.

waves. Hence, at a given station on the ice one would expect to measure a skewed wave spectrum showing preference to long waves (other mechanisms leading to the same result will be discussed in Chapter 6). At the short period end of the curve the attenuation coefficient attains a maximum, the position of which is a function of the ice thickness. This maximum is to be expected since for high frequency waves the sea ice will behave as a floating elastic plate (Christensen, 1971, sect.1.6) so that attenuation must diminish with increasing frequency. The peak occurs at a higher period than might be expected which possibly demonstrates the inadequacy of available data. This point is discussed further in Appendix A. It must also be remembered that the analysis leading to these curves assumes isotropy, an assumption far from valid for floating sea ice.

In figures 2.6 and 2.7, respectively, we show the corresponding plots of wavelength and attenuation coefficient for waves 2 and 3. The wavelength shows a marked dependence on sea ice thickness but it is only for short waves that any significant dependence on period is apparent. For long waves, therefore, the wavelength may be assumed to be solely determined by the sea ice thickness. This may also be said of the attenuation coefficient for waves 2 and 3 (fig.2.7) since ζ_2 (or ζ_3) does not vary appreciably with period for long waves. For short waves, however, the attenuation coefficient increases rapidly as the period decreases. The waves show significant dependence on ice thickness over all periods with 0.5 m of ice cover offering more attenuation than 1.5 m.

2.4 Matching across Regions 1 and 2 and the Amplitude Ratios

So far we have not mentioned the interface x=0 between the two regions 1 and 2. We know that in region 1 the potential Φ_1 is given by expression (2.20) whereas in region 2, the potential Φ_2 is given by expression (2.25). In order to determine the values of the unknown constants R, A_1, A_2, B_3 and hence, the relative importance of each of the three waves, we must link these potentials across the boundary x=0. To do this we require four boundary conditions. Two of these conditions are provided by thin plate theory since the end x=0 is a free end. Hence, there can be no

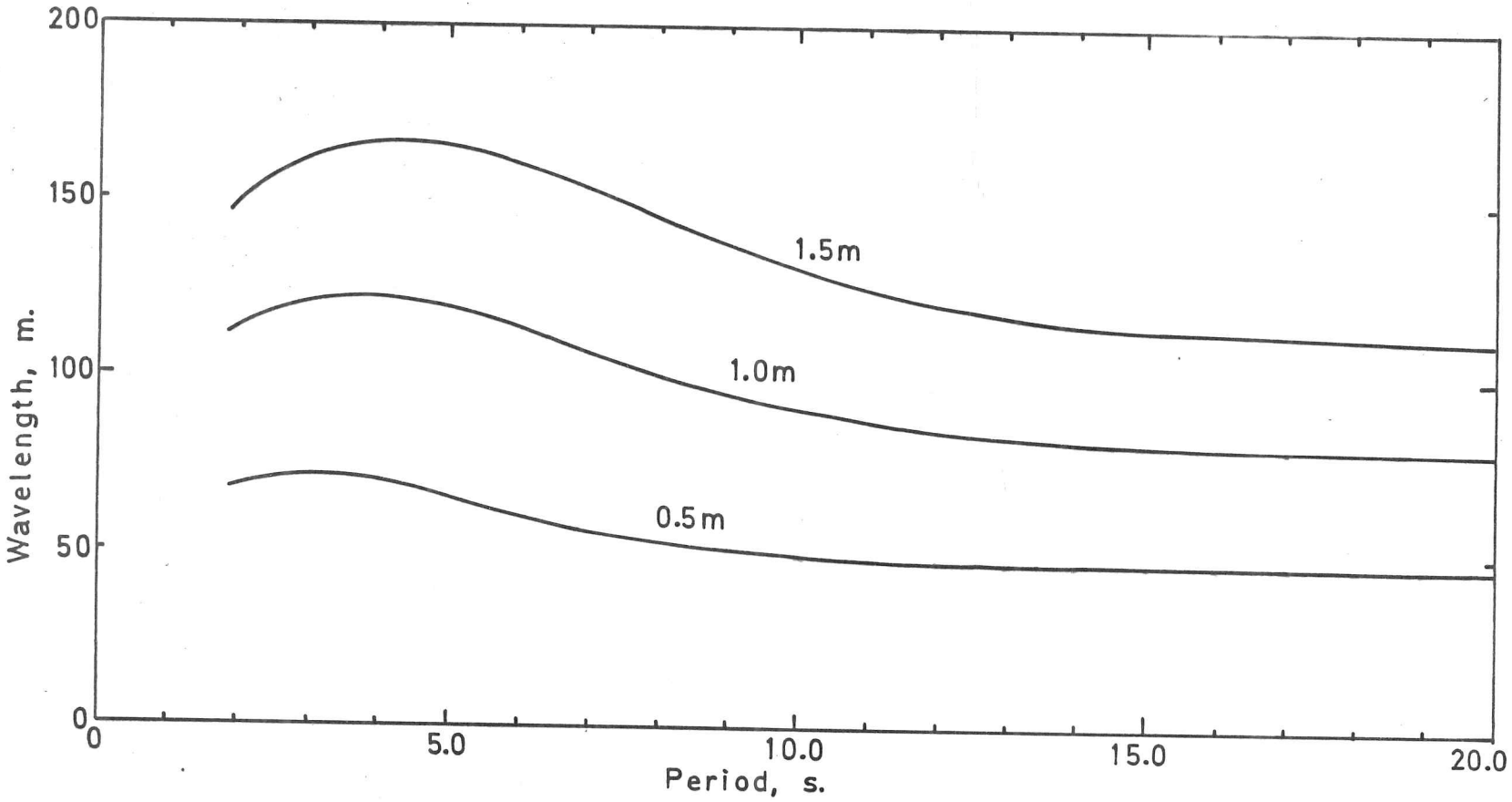

Fig. 2.6 Wavelength of waves 2 (or 3) as a function of period for various ice thicknesses.

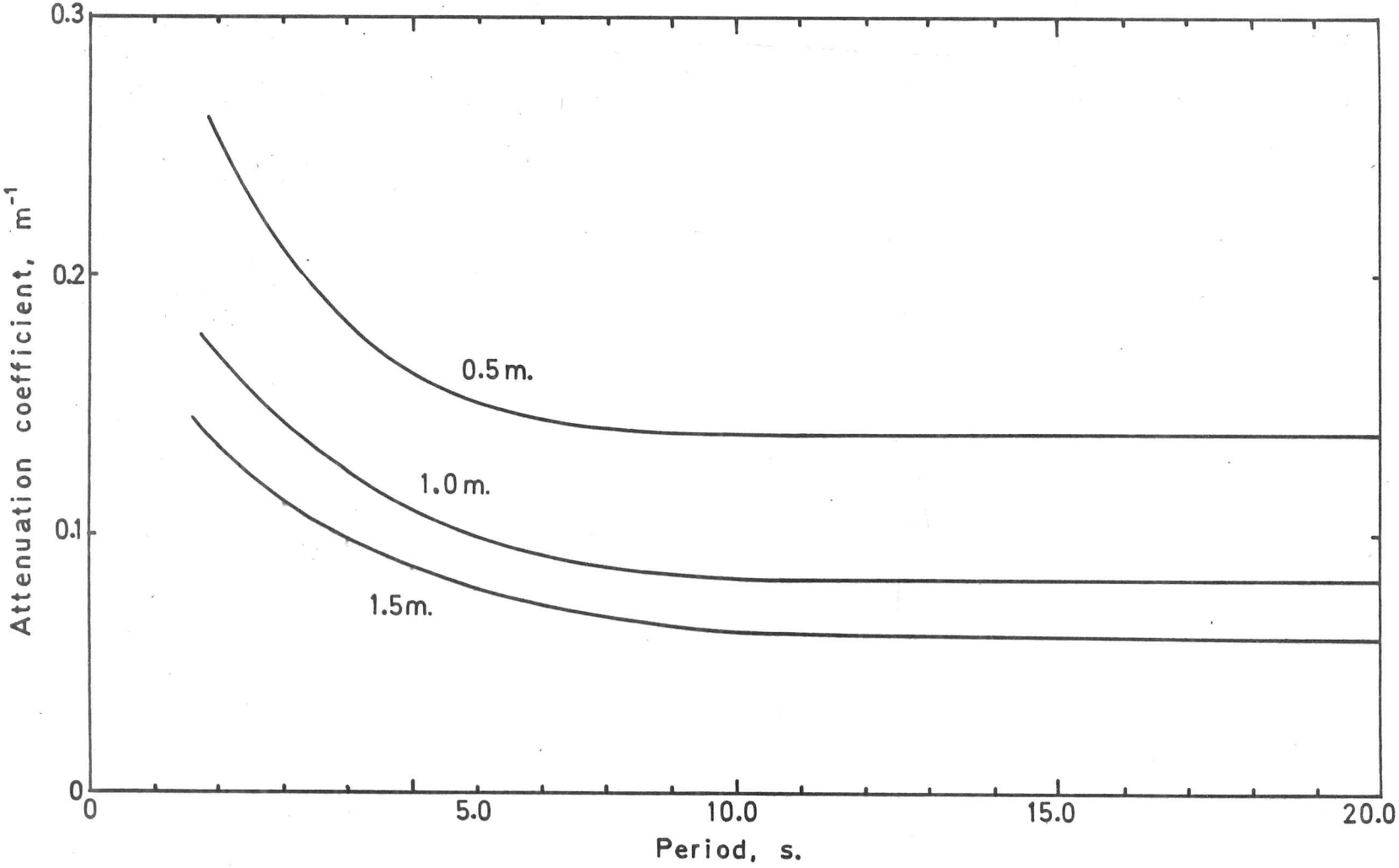

Fig. 2.7 The attenuation coefficient ζ_2(or ζ_3) versus period for three sea ice thicknesses.

bending moment or shear at x=0. That is

$$\frac{\partial^2 w_2}{\partial x^2} = 0\Big|_{x=0}, \quad \frac{\partial^3 w_2}{\partial x^3} = 0\Big|_{x=0}. \tag{2.29}$$

Two further conditions may be written down from the hydrodynamics, namely that the potentials Φ_1 and Φ_2 and their first derivatives with respect to x, $\partial\Phi_1/\partial x$ and $\partial\Phi_2/\partial x$ must match across x=0 for all z>0. Clearly these conditions cannot be satisfied with the existing expressions for Φ_1 and Φ_2 since k and k_1 (k_2, k_3) are not, in general, equivalent. This implies that the potentials Φ_1 and Φ_2 are an approximation to the true solution of the problem but to date the exact solution for deep water has not been found. Wadhams (1973b) discusses such an approximation in detail using the exact solution of a related problem (Ursell, 1947) and concludes that matching over z=0 gives a satisfactory approximation since most of the wave energy is near the surface. We therefore accept an impedance mismatch and link potentials over x=0, z=0. Our boundary conditions are therefore

$$\Phi_1 = \Phi_2\Big|_{x,z=0}, \quad \frac{\partial\Phi_1}{\partial x} = \frac{\partial\Phi_2}{\partial x}\Big|_{x,z=0}. \tag{2.30}$$

Hence, substitution of expressions (2.20) and (2.25) for the potentials Φ_1 and Φ_2 respectively into the boundary conditions (2.29) and (2.30) yields a system of four equations which may be solved numerically for the unknown R, A_1, A_2, B_3:

$$\left.\begin{aligned} 1 + R &= A_1 + A_2 + B_3, \\ k(1-R) &= k_1 A_1 + k_2 A_2 - k_3 B_3, \\ A_1 k_1^3 + A_2 k_2^3 + B_3 k_3^3 &= 0, \\ A_1 k_1^4 + A_2 k_2^4 - B_3 k_3^4 &= 0. \end{aligned}\right\} \tag{2.31}$$

In order to solve this system we split into real and imaginary parts and write as a single matrix equation

$$AX = Y. \tag{2.32}$$

To ensure that all terms in matrix A are approximately the same order of magnitude, a division by the modulus of k_1 is introduced,

so that A may be written

$$\begin{bmatrix}
-1 & 0 & 1 & 0 & 1 & 0 & 1 & 0 \\
0 & -1 & 0 & 1 & 0 & 1 & 0 & 1 \\
\frac{k}{|k_1|} & 0 & \mathrm{Re}\frac{k_1}{|k_1|} & -\mathrm{Im}\frac{k_1}{|k_1|} & \mathrm{Re}\frac{k_2}{|k_1|} & -\mathrm{Im}\frac{k_2}{|k_1|} & -\mathrm{Re}\frac{k_3}{|k_1|} & \mathrm{Im}\frac{k_3}{|k_1|} \\
0 & \frac{k}{|k_1|} & \mathrm{Im}\frac{k_1}{|k_1|} & \mathrm{Re}\frac{k_1}{|k_1|} & \mathrm{Im}\frac{k_2}{|k_1|} & \mathrm{Re}\frac{k_2}{|k_1|} & -\mathrm{Im}\frac{k_3}{|k_1|} & -\mathrm{Re}\frac{k_3}{|k_1|} \\
0 & 0 & \mathrm{Re}(\frac{k_1}{|k_1|})^3 & -\mathrm{Im}(\frac{k_1}{|k_1|})^3 & \mathrm{Re}(\frac{k_2}{|k_1|})^3 & -\mathrm{Im}(\frac{k_2}{|k_1|})^3 & \mathrm{Re}(\frac{k_3}{|k_1|})^3 & -\mathrm{Im}(\frac{k_3}{|k_1|})^3 \\
0 & 0 & \mathrm{Im}(\frac{k_1}{|k_1|})^3 & \mathrm{Re}(\frac{k_1}{|k_1|})^3 & \mathrm{Im}(\frac{k_2}{|k_1|})^3 & \mathrm{Re}(\frac{k_2}{|k_1|})^3 & \mathrm{Im}(\frac{k_3}{|k_1|})^3 & \mathrm{Re}(\frac{k_3}{|k_1|})^3 \\
0 & 0 & \mathrm{Re}(\frac{k_1}{|k_1|})^4 & -\mathrm{Im}(\frac{k_1}{|k_1|})^4 & \mathrm{Re}(\frac{k_2}{|k_1|})^4 & -\mathrm{Im}(\frac{k_2}{|k_1|})^4 & -\mathrm{Re}(\frac{k_3}{|k_1|})^4 & \mathrm{Im}(\frac{k_3}{|k_1|})^4 \\
0 & 0 & \mathrm{Im}(\frac{k_1}{|k_1|})^4 & \mathrm{Re}(\frac{k_1}{|k_1|})^4 & \mathrm{Im}(\frac{k_2}{|k_1|})^4 & \mathrm{Re}(\frac{k_2}{|k_1|})^4 & -\mathrm{Im}(\frac{k_3}{|k_1|})^4 & -\mathrm{Re}(\frac{k_3}{|k_1|})^4
\end{bmatrix} , \tag{2.33}$$

and the two column vectors X and Y are given by

$$X = \begin{bmatrix} R^r \\ R^i \\ A_1^{\,r} \\ A_1^{\,i} \\ A_2^{\,r} \\ A_2^{\,i} \\ B_3^{\,r} \\ B_3^{\,i} \end{bmatrix} , \quad Y = \begin{bmatrix} 1 \\ 0 \\ \frac{k}{|k_1|} \\ 0 \\ 0 \\ 0 \\ 0 \\ 0 \end{bmatrix} , \tag{2.34}$$

where the superscript denotes real or imaginary part in an obvious way.

In order to demonstrate how the incident energy at the ice edge is distributed between the three possible wave modes within the ice

cover, we introduce the amplitude ratio. This is defined for wave 1, as follows

$$\text{Amplitude ratio} = \frac{|k_1||A_1|}{k\sqrt{1-|R|^2}}\,, \qquad (2.35)$$

and similarly for waves 2 and 3. A comparison of the three amplitude ratios will therefore show the relative importance of each flexural-gravity wave near the ice edge. Figure 2.8 shows the three amplitude ratios plotted as functions of period for 1.0 m of sea ice. For short periods, the energy transmitted across the edge is divided, to the same order of magnitude, between the three possible wave solutions. However, it must be remembered that it is also for short periods that the attenuation of waves 2 and 3 is greatest. Hence, although a substantial fraction of the energy in an incident deep water wave is propagated under the ice as waves 2 and 3, the energy is dissipated within the ice very close to the ice edge. As the period of the incoming wave increases wave 1 begins to dominate and waves 2 and 3 become less significant. Thus although figure 2.7 shows a slightly decreased attenuation coefficient for waves 2 and 3 at longer periods, a small proportion of the incident wave energy excites these modes so that once again the waves can only be found local to the ice edge.

It is clear from figure 2.9 that ice thickness also plays an important role in determining the division of energy at the ice edge. For very thin ice, negligible energy is transmitted in the form of waves 2 and 3 and there is almost perfect transmission of energy across the edge into the propagating wave 1. For thicker ice, however, the respective amplitude ratios approach the same order of magnitude and all three waves become significant.

2.5 Summary

Throughout this chapter it has been assumed that the mechanical properties of floating sea ice may be adequately represented by use of a particular model from the theory of linear viscoelasticity. The mechanical analogy chosen, the Maxwell-Voigt model, was shown to describe the behaviour of sea ice in flexure by Tabata (1955,

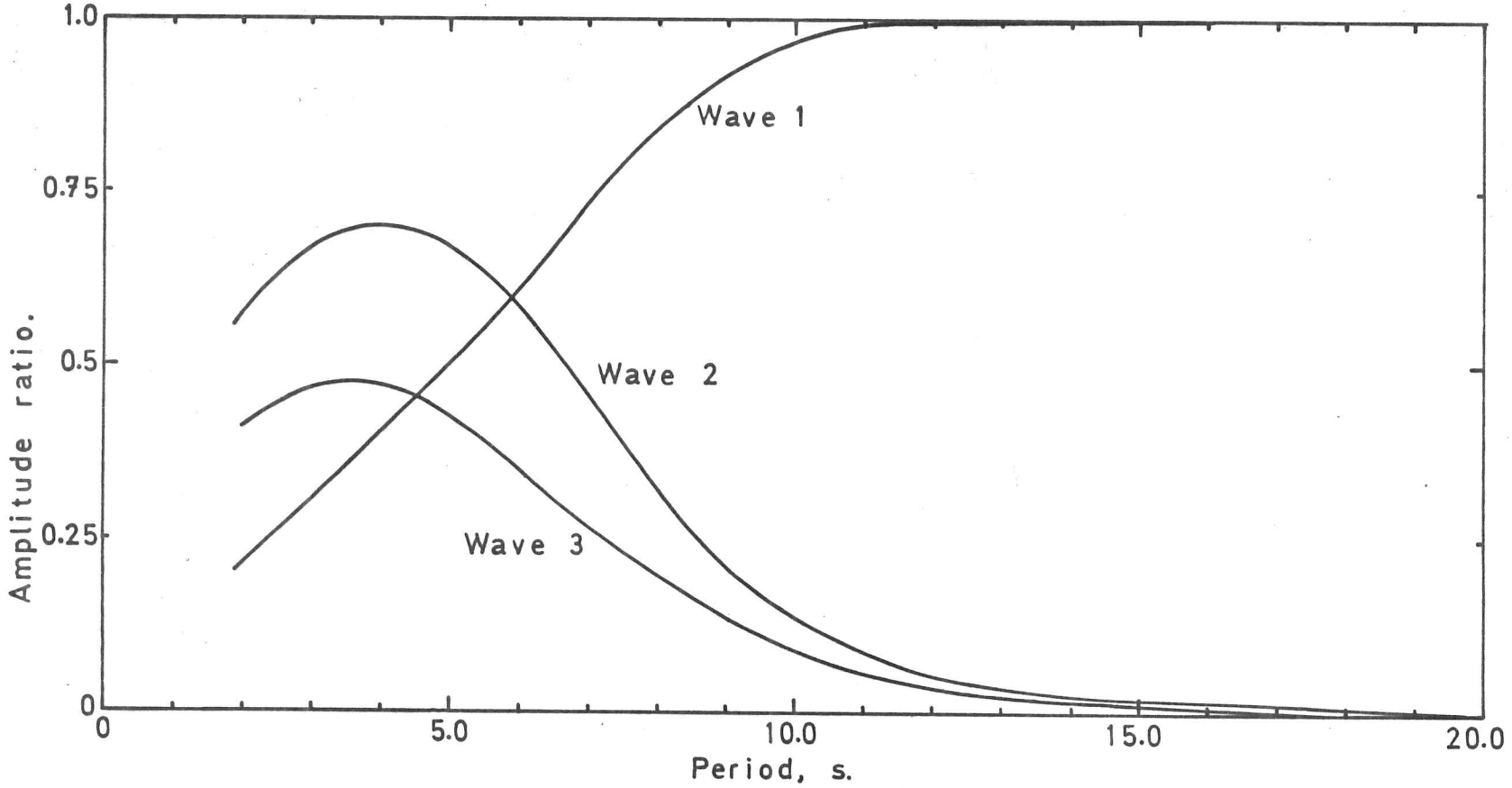

Fig. 2.8 The three amplitude ratios for 1.0 m of sea ice as a function of period.

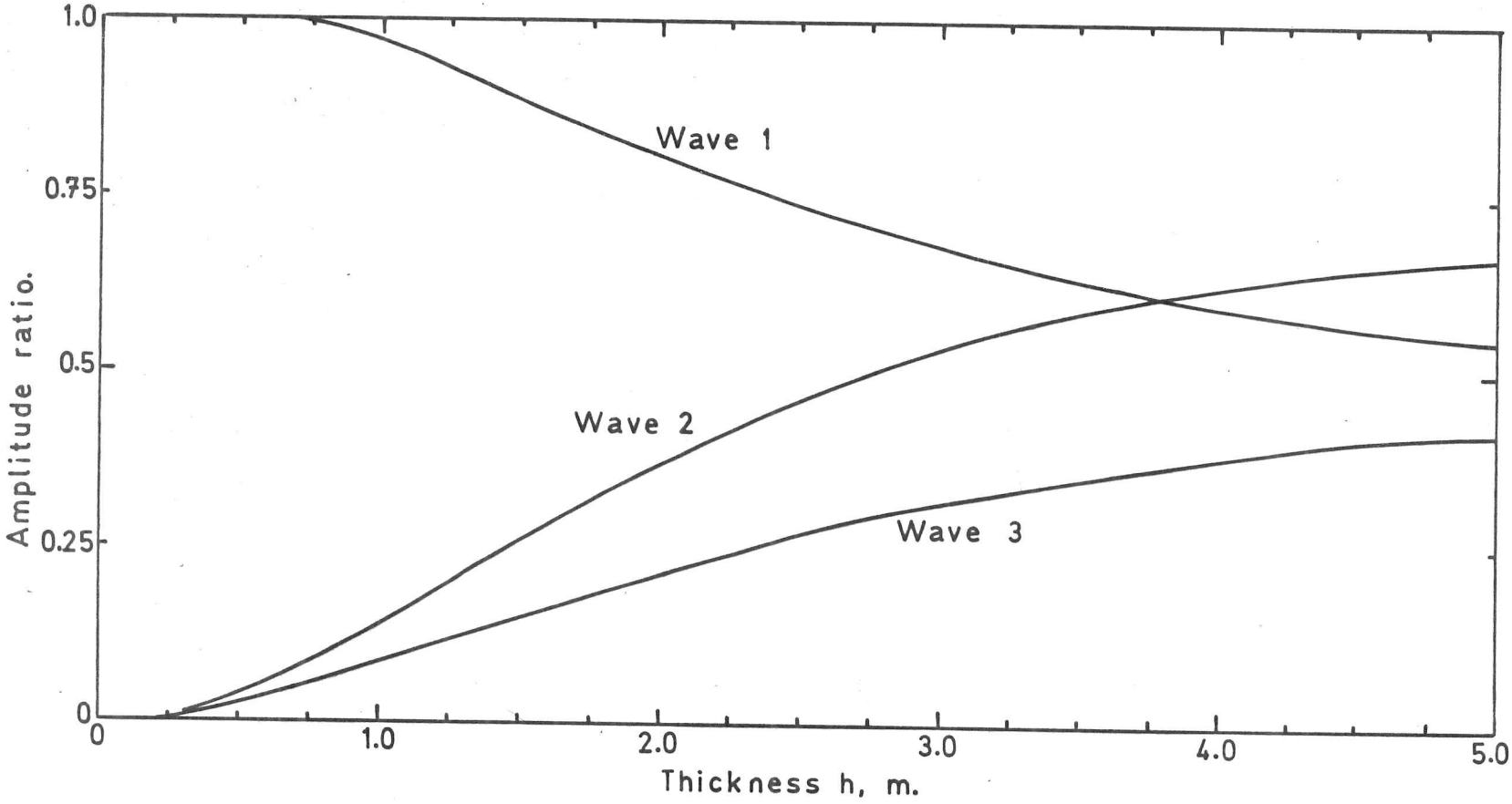

Fig. 2.9 The three amplitude ratios for a 10 s wave at various sea ice thicknesses.

1958a) in a series of experiments along the Japanese coast. With this model, it has been shown that a one-dimensional sea wave impinging on an ice edge will generate three types of wave within the ice cover; a propagating wave with small attenuation which can travel large distances within the ice and two waves which can exist only local to the ice edge.

The first wave has a dispersion relation for long periods which is approximately the same as for deep water. For short periods, however, the dispersion is governed by the material properties of the floating sea ice. The attenuation for this wave obeys the expected rule that long waves decay more slowly then short waves. We may therefore say that an incoming deep water wave of long period does not notice the effect of a thin cover of sea ice as much as a short wave.

The second two waves, which decay to negligible amplitude within metres from the ice edge, show dispersion and attenuation behaviour that significantly depend on period only for short periods. As the period of the incoming wave is increased the curves begin to flatten out until, at a position determined by the ice thickness, their gradient is negligible. These two waves are strictly approximations to the exact edge solution as can be seen if matching is attempted for all $z>0$. Matching is therefore carried out over $x=0$, $z=0$.

The division of energy at the edge into each of the three waves shows that, for thin ice, it is only for short periods that the second two waves are significant. For long periods, all the energy from an incoming swell will excite a wave of the first type. As the ice thickness increases, however, the significance of the local waves also increases so that for thick ice the energy is allotted with roughly the same order of magnitude among the three waves.

CHAPTER 3

THE THERMORHEOLOGICALLY SIMPLE VISCOELASTIC PLATE EQUATION

THE THERMORHEOLOGICALLY SIMPLE VISCOELASTIC PLATE EQUATIONS

3.1 Introduction

In the previous chapter and in Squire and Allan (1979) we discussed a first approach to the 'waves-in-ice' problem based on an extension of Hendrickson's analysis for an elastic plate into the theory of viscoelasticity. It was found that the major effect of including a viscosity term in the material behaviour of sea ice was to introduce some attenuation into the propagating wave of the corresponding elastic theory. This attenuation was small compared with that predicted by Wadhams (1973a) using a Glen flow law (Glen, 1955) to model the material's characteristics, but to date little empirical evidence is available to substantiate either theory. Both models do however show the characteristic decrease in the attenuation coefficient for swells as the period of the wave increases which has been observed to occur. Long waves have been observed under certain circumstances to penetrate through hundreds of kilometres of sea ice (Hunkins, 1962; LeSchack and Haubrich, 1964; LeSchack, 1964; LeSchack, 1965) though as Hunkins points out, the waves may possibly have been enhanced by wind energy. The advantage of the present author's approach is that the wave motion is dealt with directly, whereas the Wadhams (1973a) paper decouples the elastic effects from the rate of decay of energy. This implies that the former theory yields a complex wave number from which the dispersion and attenuation may be predicted directly, whereas the Wadhams paper yields a real wave number and then superposes some energy decay on that wave. Since the flow law for sea ice is unlikely to be the same as that for non-saline, polycrystalline ice and since the present author's approach exploits empirical sea ice data, the coupled viscoelastic approach will be used throughout. Such an analysis permits relatively easy extension into more complicated material properties.

The above theories both neglect any variation of the material properties of sea ice with direction and position. Clearly sea ice is not isotropic and homogeneous; it is a composite made up of pure ice, salts, brine and air, the position and quantity of which determine its viscoelastic behaviour. Sea ice is also subject to a very

pronounced temperature gradient across its thickness since at its underside the ice is at the freezing point of sea water whereas at the surface the temperature is controlled by climatic conditions. The freezing point of sea water is an approximately linear function of salinity (Lewis, 1971) for salinities up to about 50‰. We shall take a temperature of -1.8°C as the freezing point which corresponds to a salinity of about 33‰ though the specific value of the temperature is unimportant as far as the analysis is concerned. The vertical temperature gradient in sea ice leads one to the idea of modelling the material as an axially symmetric material with non-uniform properties in the direction of growth. The elastic analysis of such a material was originally carried out by Newman and Forray (1962) with particular application to the aerospace industry. It was later applied to floating ice by Kerr and Palmer (1970) based on a suggestion be Assur (1967) that the Young's modulus E should be allowed to vary with depth but Poisson's ratio ν should remain constant. Using a variational approach it was found that the equations for floating ice remained the same so long as a modified flexural rigidity D was defined where

$$D = \frac{1}{1-\nu^2}\int_{-\delta}^{h-\delta} z^2 E(z)\, dz \ , \qquad (3.1)$$

where h is the ice thickness and δ is the distance from the ice surface to the reference axis.

As mentioned earlier, the temperature gradient across the ice thickness plays a large part in determining the mechanical properties of sea ice. At a given temperature the proportion of ice, brine, and solid salts present is specified by the phase diagram (Assur, 1958; Weeks and Assur, 1967) so that a model of sea ice which included temperature as an explicit parameter might yield a closer approximation to the observed phenomenological response. The importance of including the thermodynamical state of the environment in any model of floating ice was recognised by Hutter (1973, 1975a) who used the method of Mindlin (1951) to derive a general system of temperature-dependent, linearly elastic equations permitting large displacements. The system of equations is extremely complicated however and without further approximations cannot be solved easily.

In a similar way, Hutter (1973, 1975b) has derived the corresponding system of viscoelastic equations with the hypothesis that sea ice is thermorheologically simple (Schwarzl and Staverman, 1952). This hypothesis has not been experimentally verified and no determination of the shift function for sea ice has yet been carried out. Once again the equations are extremely complex and solution to physical problems seems unlikely without further simplification. Williams (1976) uses essentially the same approach and solves a simplified thermoviscoelastic plate equation for the ice pressure on a circular pile using Neumann series from the theory of integral equations.

In this chapter we will derive the temperature-dependent linearly viscoelastic analogy to Mindlin's plate equation using certain assumptions thought to be reasonable for sea ice. Since we require to solve a propagating flexural wave problem, we do not need to permit large displacements so that our final equations will be completely linear. The Poisson's ratio of sea ice shows only a very weak dependence on temperature (Weeks and Assur, 1967) and Hutter (1975c, 1976) demonstrates by a very elegant method that its dependence may be neglected.

3.2 The Thermoviscoelastic Stress-Strain Relation

In order to simplify the analysis we will first consider a temperature-independent material behaviour. Then, assuming an isotropic, linearly viscoelastic stress-strain relation (c.f. generalised Hooke's law of linear, infinitesimal elasticity) we have

$$\sigma_{ij} = \delta_{ij}\lambda(t) \circ \varepsilon_{kk} + 2\mu(t) \circ \varepsilon_{ij} \,, \tag{3.2}$$

where $\lambda(t)$, $\mu(t)$ are called relaxation functions and describe the viscoelastic properties of the medium, δ_{ij} is the Kronecker delta and σ_{ij} , ε_{ij} are stress and strain respectively. The symbol $\circ$ (Williams, 1976) represents a functional operator defined as follows:

$$\mu \circ \varepsilon = \mu(0)\varepsilon(t) - \int_{-\infty}^{t} \varepsilon(\tau) \frac{d}{d\tau} \mu(t-\tau)\, d\tau \,, \tag{3.3}$$

where $\mu(t)$ belongs to H^1 (A function f belongs to H^N if f is defined on $(-\infty, \infty)$, f=0 on $(-\infty, 0)$ and f is continuous and N-times continuously

differentiable on $[0,\infty)$). Equation (3.2) represents an alternative (and more elegant) way of writing the stress-strain relation of Chapter 2. Anticipating the particular class of problems we wish to solve, we have extended the lower limit of integration in Williams' viscoelastic operator to take into account strains prior to t=0. If the strain $\varepsilon(t)$ also belongs to H^1 then an integration by parts yields the familiar operator due to Gurtin and Sternberg (1962):

$$\mu\circ\varepsilon = \mu(t)\varepsilon(0) + \int_0^t \mu(t-\tau)\frac{d\varepsilon}{d\tau}\,d\tau\,, \tag{3.4}$$

which is a standard definition of linear viscoelasticity.

Equation (3.2) may be decomposed into its hydrostatic and deviatoric parts according to the usual definitions of deviatoric stress and strain,

$$s = (3\lambda + 2\mu)\circ e\,, \qquad \sigma_{ij}' = 2\mu\circ\varepsilon_{ij}'\,, \tag{3.5}$$

where s, e are the hydrostatic components of stress and strain respectively and σ_{ij}', ε_{ij}' are the deviatoric components. Unfortunately, to date few experiments have been carried out to provide the exact form of the relaxation functions $\lambda(t)$ and $\mu(t)$.

Now for a uniaxial stress test we have only one component of stress σ, say, so that we may write

$$\sigma = E(t)\circ\varepsilon\,, \tag{3.6}$$

where $E(t)$ is the relaxation function corresponding to Young's modulus. Such a test can provide only one relaxation function and it is clear that we have insufficient information to evaluate both $\lambda(t)$ and $\mu(t)$ without a further assumption. We will assume that the viscoelastic Poisson's ratio $\nu(t)$, defined as minus the ratio of the time-dependent lateral strain to the constant axial strain under stress relaxation conditions, is a constant (Katona, 1974; Vaudrey and Katona, 1975; Nevel, 1976). We do not however insist that sea ice is incompressible under hydrostatic stress (Nevel, 1966; Kheisin, 1967; Squire and Allan, 1979). We may therefore write

$$\lambda(t) = \frac{2\nu}{1-2\nu}\,\mu(t) = \left\{\frac{\nu}{(1-2\nu)(1+\nu)}\right\}E(t)\,. \tag{3.7}$$

The assumption of constant Poisson's ratio therefore implies proportionality between all the usually defined relaxation functions. Also it is a necessary condition for a general separation of variables-type solution to exist except under very restricted conditions (Christensen, 1971, sect. 2.3).

Our original stress-strain relation (3.2) may be extended to include thermal effects by allowing the relaxation functions to become functions of absolute temperature $\vartheta(\underset{\sim}{x};t)$. Then so long as we retain our conditions of isotropy and constant Poisson's ratio (independent of both time and temperature as discussed earlier) and assume that the coefficient of linear thermal expansion α_0 is independent of temperature, we may write the stress-strain relation as (Williams, 1976)

$$\sigma_{ij} = \left(\frac{2\nu}{1-2\nu}\right)\delta_{ij}\,\mu(t,\vartheta)\circ\varepsilon_{kk} + 2\mu(t,\vartheta)\circ\varepsilon_{ij} - \frac{2\alpha_0(1+\nu)}{(1-2\nu)}\,\delta_{ij}\,\mu(t,\vartheta)\circ\vartheta'(x,t)\,, \tag{3.8}$$

where $\vartheta'(\underset{\sim}{x};t)$ represents the temperature difference between $\vartheta(\underset{\sim}{x};t)$ and some temperature where thermal strains vanish and the relaxation function $\mu(t,\vartheta)$ is formally allowed to include a dependence on temperature.

3.3 The Time-Temperature Shift Hypothesis

We have constructed a stress-strain relation (3.8) which allows the material's relaxation functions to depend on temperature, but as yet we have no idea what form the functional dependence takes. Considerable simplification is introduced if one assumes that sea ice exhibits the time-temperature equivalence characteristics often seen in the rheology of polymers (Christensen, 1971, sect. 3.6; Pipkin, 1972, ch. 6; Lockett, 1972, ch. 3, sect. 5). For such a material, the relaxation functions demonstrate translational invariance when plotted against ln t. This implies that the relaxation functions at any temperature may be obtained directly from those at some reference temperature by use of a shift function $\chi(\vartheta)$ which is a fundamental property of the material. We will refer to such behaviour subsequently as thermorheologically simple (Schwarzl and Staverman, 1952). Whether or not this hypothesis is valid for sea ice is questionable since to date no experiments have

been carried out to substantiate or disprove such a simplification or to find the shift function. We proceed to make such an assumption on the grounds that temperature is an extremely important parameter and should be included in any theory of flexure of sea ice. Hopefully theory will not predate experiment for too long.

For the problem we wish to solve we will not consider sea ice as a thermorheologically simple material in its most general functional form (Hutter, 1975b). Instead we will follow the analysis given by Morland and Lee (1960) and Muki and Sternberg (1961) where a reduced time ξ_t is defined such that

$$\xi_t(\underset{\sim}{x};t) = \int_0^t \chi\left[\vartheta(\underset{\sim}{x};s)\right] ds, \tag{3.9}$$

where the shift function $\chi(\vartheta)$ satisfies the conditions

$$\chi(\vartheta_0) = 1, \qquad \frac{d\chi}{d\vartheta} > 0. \tag{3.10}$$

Now a prerequisite of equation (3.8) was that the coefficient of linear thermal expansion α_0 was independent of temperature, a condition far from valid for floating sea ice (Anderson, 1960). We formally remove this restriction by allowing the temperature field $\vartheta'(\underset{\sim}{x};t)$ to be

$$\vartheta'(\underset{\sim}{x};t) = \frac{1}{\alpha_0}\int_{\vartheta_0}^{\vartheta(\underset{\sim}{x};t)} \alpha(s)\, ds, \quad \alpha_0 = \alpha(\vartheta_0). \tag{3.11}$$

Then the form of equation (3.8) remains the same with the operation $\mu\circ\varepsilon$ modified accordingly:

$$\mu\circ\varepsilon = \mu(0)\varepsilon(\underset{\sim}{x};t) - \int_{-\infty}^{t} \varepsilon(\underset{\sim}{x};\tau)\frac{\partial}{\partial\tau}\mu(\xi_t-\xi_\tau)\, d\tau, \tag{3.12}$$

where the subscript refers to the upper limit of integration in definition (3.9). Henceforth we shall neglect any dependence of the temperature field on horizontal coordinates, a valid assumption except near the ice edge.

For the specific problem of waves-in-ice it will be sufficient to neglect any dependence of the temperature field on time since

climatic conditions will be relatively slowly varying. Our thermo-rheologically simple behaviour therefore reduces to the constant temperature state case where the reduced time is now defined by

$$\xi_t = t\chi\left[\vartheta(z)\right]. \tag{3.13}$$

Hence, the operation $\mu \circ \varepsilon$ formally becomes

$$\mu\circ\varepsilon = \mu(0)\varepsilon(\underset{\sim}{x};t) - \int_{-\infty}^{t} \varepsilon(\underset{\sim}{x};\tau)\frac{\partial}{\partial\tau}\mu\left[\chi(\vartheta)(t-\tau)\right]d\tau\,, \tag{3.14}$$

However, in order to be as general as possible in the derivation of the plate equations we will retain the original definitions (3.9), (3.12) until we particularise the analysis to the specific problem.

Following the methods of Mindlin (1951), Newman and Forray (1962) and Hutter (1973, 1975a, 1975b) we note that the sea ice may be represented as a thin plate and define

$$\begin{aligned} M^{(m)}(t) &= \int_h z^m \mu\left[t, \vartheta(z;t)\right] dz\,, \\ \vartheta'(z;t) &= \sum_{m=0}^{\infty} z^m \theta^{(m)}(t)\,, \\ \varepsilon_{ij}(\underset{\sim}{x};t) &= \sum_{m=0}^{\infty} z^m E_{ij}^{(m)}(x,y;t), \\ \Sigma_{ij}^{(m)}(x,y;t) &= \int_h z^m \sigma_{ij}(\underset{\sim}{x};t)\,dz. \end{aligned} \tag{3.15}$$

so that multiplying (3.8) by z^m and integrating over the thickness of the plate gives

$$\Sigma_{ij}^{(m)} = 2\sum_{n=0}^{\infty}\left\{ M^{(m+n)}\circ E_{ij}^{(n)} + \delta_{ij}\left[\left(\frac{\nu}{1-2\nu}\right)M^{(m+n)}\circ E_{kk}^{(n)} - \frac{\alpha_0(1+\nu)}{(1-2\nu)} M^{(m+n)}\circ \theta^{(n)}\right]\right\}. \tag{3.16}$$

This equation represents the macroscopic thermoviscoelastic stress-strain relation. Although we began the analysis with an isotropic

stress-strain law we have now introduced a dependence on z through the temperature so that we have the desired axially symmetric model with non-uniform properties in the z-direction.

3.4 The Constitutive Equations

We seek a set of temperature-dependent viscoelastic constitutive equations for the non-zero membrane forces, transverse shear forces and bending and twisting moments where, following Hutter (1973) we define Membrane forces:

$$N_x = \Sigma_{11}^{(0)}, \quad N_{xy} = \Sigma_{12}^{(0)}, \quad N_y = \Sigma_{22}^{(0)}, \tag{3.17}$$

Transverse shear forces:

$$Q_x = \Sigma_{13}^{(0)}, \quad Q_y = \Sigma_{23}^{(0)}. \tag{3.18}$$

Bending and twisting moments:

$$M_x = \Sigma_{11}^{(1)}, \quad M_{xy} = \Sigma_{12}^{(1)}, \quad M_y = \Sigma_{22}^{(1)}. \tag{3.19}$$

All other stress resultants will be assumed to be zero. For the wave problem we wish to solve it may be sufficient to neglect the transverse shear forces but we will retain these terms here for completeness.

Equation (3.16) may be expanded explicitly. Retaining terms up to and including $O(1)$, write

$$a = \frac{\nu}{1-2\nu}, \quad b = -\alpha_0 \left(\frac{1+\nu}{1-2\nu}\right), \tag{3.20}$$

then,

$$\left.\begin{aligned}
N_x &= 2\left\{M^{(0)} \circ \left[E_{11}^{(0)} + aE_{kk}^{(0)} + b\theta^{(0)}\right] \right. \\
&\qquad \left. + M^{(1)} \circ \left[E_{11}^{(1)} + aE_{kk}^{(1)} + b\theta^{(1)}\right]\right\}, \\
N_{xy} &= 2\left\{M^{(0)} \circ E_{12}^{(0)} + M^{(1)} \circ E_{12}^{(1)}\right\}, \\
N_y &= 2\left\{M^{(0)} \circ \left[E_{22}^{(0)} + aE_{kk}^{(0)} + b\theta^{(0)}\right] \right. \\
&\qquad \left. + M^{(1)} \circ \left[E_{22}^{(1)} + aE_{kk}^{(1)} + b\theta^{(1)}\right]\right\},
\end{aligned}\right\} \tag{3.21}$$

$$\left.\begin{aligned} Q_x &= 2\left\{M^{(0)} \circ E_{13}^{(0)} + M^{(1)} \circ E_{13}^{(1)}\right\}, \\ Q_y &= 2\left\{M^{(0)} \circ E_{23}^{(0)} + M^{(1)} \circ E_{23}^{(1)}\right\}, \end{aligned}\right\} \quad (3.22)$$

$$\left.\begin{aligned} M_x &= 2\left\{M^{(1)} \circ \left[E_{11}^{(0)} + aE_{kk}^{(0)} + b\theta^{(0)}\right] \right. \\ &\qquad \left. + M^{(2)} \circ \left[E_{11}^{(1)} + aE_{kk}^{(1)} + b\theta^{(1)}\right]\right\}, \\ M_{xy} &= 2\left\{M^{(1)} \circ E_{12}^{(0)} + M^{(2)} \circ E_{12}^{(1)}\right\}, \\ M_y &= 2\left\{M^{(1)} \circ \left[E_{22}^{(0)} + aE_{kk}^{(0)} + b\theta^{(0)}\right] \right. \\ &\qquad \left. M^{(2)} \circ \left[E_{22}^{(1)} + aE_{kk}^{(1)} + b\theta^{(1)}\right]\right\}. \end{aligned}\right\} \quad (3.23)$$

We also have

$$\left.\begin{aligned} \Sigma_{33}^{(0)} &= 2\left\{M^{(0)} \circ \left[E_{33}^{(0)} + aE_{kk}^{(0)} + b\theta^{(0)}\right] \right. \\ &\qquad \left. + M^{(1)} \circ \left[E_{33}^{(1)} + aE_{kk}^{(1)} + b\theta^{(1)}\right]\right\} = 0, \\ \Sigma_{33}^{(1)} &= 2\left\{M^{(1)} \circ \left[E_{33}^{(0)} + aE_{kk}^{(0)} + b\theta^{(0)}\right] \right. \\ &\qquad \left. + M^{(2)} \circ \left[E_{33}^{(1)} + aE_{kk}^{(1)} + b\theta^{(1)}\right]\right\} = 0, \end{aligned}\right\} \quad (3.24)$$

and,

$$\left.\begin{aligned} \Sigma_{13}^{(1)} &= 2\left\{M^{(1)} \circ E_{13}^{(0)} + M^{(2)} \circ E_{13}^{(1)}\right\} = 0, \\ \Sigma_{23}^{(1)} &= 2\left\{M^{(1)} \circ E_{23}^{(0)} + M^{(2)} \circ E_{23}^{(1)}\right\} = 0. \end{aligned}\right\} \quad (3.25)$$

Equations (3.24) and (3.25) provide a means of eliminating the unwanted terms $E_{33}^{(0)}$, $E_{33}^{(1)}$, $E_{13}^{(1)}$, $E_{23}^{(1)}$ from equations (3.21), (3.22) and (3.23). To achieve this end it is necessary to define a relaxation function $\left[M^{(i)}\right]^{-1}$ which when operating on $M^{(i)} \circ (.)$ produces $I \circ (.)$ where I is the identity relaxation function which maps the argument (.) onto itself. We call the relaxation function $\left[M^{(i)}\right]^{-1}$ the inverse of under the operation $\circ$. The

constitutive equations may then be written

$$\left.\begin{aligned} N_x &= \frac{2}{1-\nu}\Big\{M^{(0)}\circ\Big[E_{11}^{(0)} + \nu E_{22}^{(0)} - \alpha_0(1+\nu)\theta^{(0)}\Big] \\ &\qquad + M^{(1)}\circ\Big[E_{11}^{(1)} + \nu E_{22}^{(1)} - \alpha_0(1+\nu)\theta^{(1)}\Big]\Big\}, \\ N_{xy} &= 2\Big\{M^{(0)}\circ E_{12}^{(0)} + M^{(1)}\circ E_{12}^{(1)}\Big\}, \\ N_y &= \frac{2}{1-\nu}\Big\{M^{(0)}\circ\Big[\nu E_{11}^{(0)} + E_{22}^{(0)} - \alpha_0(1+\nu)\theta^{(0)}\Big] \\ &\qquad + M^{(1)}\circ\Big[\nu E_{11}^{(1)} + E_{22}^{(1)} - \alpha_0(1+\nu)\theta^{(1)}\Big]\Big\}, \end{aligned}\right\} \quad (3.26)$$

$$\left.\begin{aligned} Q_x &= 2\Gamma\circ E_{13}^{(0)}, \\ Q_y &= 2\Gamma\circ E_{23}^{(0)}, \end{aligned}\right\} \quad (3.27)$$

$$\left.\begin{aligned} M_x &= \frac{2}{1-\nu}\Big\{M^{(1)}\circ\Big[E_{11}^{(0)} + \nu E_{22}^{(0)} - \alpha_0(1+\nu)\theta^{(0)}\Big] \\ &\qquad + M^{(2)}\circ\Big[E_{11}^{(1)} + \nu E_{22}^{(1)} - \alpha_0(1+\nu)\theta^{(1)}\Big]\Big\}, \\ M_{xy} &= 2\Big\{M^{(1)}\circ E_{12}^{(0)} + M^{(2)}\circ E_{12}^{(1)}\Big\}, \\ M_y &= \frac{2}{1-\nu}\Big\{M^{(1)}\circ\Big[\nu E_{11}^{(0)} + E_{22}^{(0)} - \alpha_0(1+\nu)\theta^{(0)}\Big] \\ &\qquad + M^{(2)}\circ\Big[\nu E_{11}^{(1)} + E_{22}^{(1)} - \alpha_0(1+\nu)\theta^{(1)}\Big]\Big\}, \end{aligned}\right\} \quad (3.28)$$

where Γ is another relaxation function defined by the relation

$$\Gamma \equiv M^{(0)} - M^{(1)}\circ\left[M^{(2)}\right]^{-1}\circ M^{(1)}, \quad (3.29)$$

the operation $\circ$ being carried out from right to left. It will be shown later that the relaxation functions are in some way commutative so that this restriction may be lifted.

3.5 The Strain-Displacement Relations and the Equations of Motion

For the simple temperature dependence that we have considered, it is only the viscoelastic constitutive equations which differ from those of the corresponding theory of infinitesimal elasticity and all other governing equations follow directly from linear elasticity with the

understanding that all variables are time dependent. Following the previous discussion we will write the displacement u_i as a power series in z expanded about z=0:

$$u_i(x;t) = \sum_{m=0}^{\infty} z^m u_i^{(m)}(x,y;t). \tag{3.30}$$

The usual definition of infinitesimal strain,

$$\varepsilon_{ij} = \frac{1}{2}(u_{i,j} + u_{j,i}), \tag{3.31}$$

may be written in a form to explicitly demonstrate differentiation by z:

$$\varepsilon_{ij} = \frac{1}{2}(u_{i,\alpha}\delta_{\alpha j} + u_{j,\alpha}\delta_{\alpha i} + u_{i,3}\delta_{3j} + u_{j,3}\delta_{3i}), \tag{3.32}$$

so that from (3.30) we may write

$$E_{ij}^{(m)} = \frac{1}{2}\left[(u_{i,\alpha}^{(m)}\delta_{\alpha j} + u_{j,\alpha}^{(m)}\delta_{\alpha i}) + (m+1)(u_i^{(m+1)}\delta_{3j} + u_j^{(m+1)}\delta_{3i})\right] \tag{3.33}$$

Hence, writing relevant strains explicitly up to O(1) we have

$$E_{\alpha\beta}^{(0)} = \frac{1}{2}(u_{\alpha,\beta}^{(0)} + u_{\beta,\alpha}^{(0)}), \quad E_{\alpha 3}^{(0)} = \frac{1}{2}(u_{3,\alpha}^{(0)} + u_{\alpha}^{(1)}),$$
$$E_{\alpha\beta}^{(1)} = \frac{1}{2}(u_{\alpha,\beta}^{(1)} + u_{\beta,\alpha}^{(1)}). \tag{3.34}$$

In order to simplify the subsequent work we will adopt the following notation

$$u_i^{(0)} = (u, v, w), \quad u_i^{(1)} = (\varphi, \psi, \chi), \tag{3.35}$$

then equations (3.34) become

$$E_{11}^{(0)} = \frac{\partial u}{\partial x}, \quad E_{22}^{(0)} = \frac{\partial v}{\partial y}, \quad E_{12}^{(0)} = \frac{1}{2}\left(\frac{\partial u}{\partial y} + \frac{\partial v}{\partial x}\right),$$
$$E_{13}^{(0)} = \frac{1}{2}\left(\frac{\partial w}{\partial x} + \varphi\right), \quad E_{23}^{(0)} = \frac{1}{2}\left(\frac{\partial w}{\partial y} + \psi\right), \tag{3.36}$$
$$E_{11}^{(1)} = \frac{\partial \varphi}{\partial x}, \quad E_{22}^{(1)} = \frac{\partial \psi}{\partial y}, \quad E_{12}^{(1)} = \frac{1}{2}\left(\frac{\partial \varphi}{\partial y} + \frac{\partial \psi}{\partial x}\right).$$

We now turn our attention to the derivation of the equations of motion for which we will use direct integration of the equation for balance of linear momentum across the thickness of the sea ice (fig. 3.1). The momentum equation is

$$\sigma_{ij,j} + f_i = \rho \frac{\partial^2 u_i}{\partial t^2} \quad , \tag{3.37}$$

where f_i are the body forces per unit volume and ρ is the mass density of sea ice. We do not permit any wind or current coupling at the upper and lower surfaces of the sea ice so that we may define a surface load of order m as

$$S_i^{(m)} = \sigma_{i3} z^m \Big|_{\text{Upper}}^{\text{Lower}} \quad , \tag{3.38}$$

With the introduction of two further definitions for the body force of order m and the acceleration resultant of order m respectively

$$F_i^{(m)} = \int_h z^m f_i \, dz \quad , \quad \frac{\partial^2 U_i}{\partial t^2}^{(m)} = \sum_{n=0}^{\infty} I^{(m+n)} \frac{\partial^2 u_i}{\partial t^2}^{(n)} \quad , \tag{3.39}$$

where $I^{(m)} = \int_h z^m dz$ is the m th moment of inertia, we may multiply equation (3.37) by z^m and integrate across the plate to obtain

$$\rho \frac{\partial^2 U_i}{\partial t^2}^{(m)} = \Sigma_{i\alpha,\alpha}^{(m)} - m\Sigma_{i3}^{(m-1)} + (S_i^{(m)} + F_i^{(m)}). \tag{3.40}$$

Now since we have not permitted any transverse surface forces we may write

$$S_i^{(m)} + F_i^{(m)} = q\delta_{i3} \quad , \tag{3.41}$$

so that the equation of motion becomes

$$\rho \frac{\partial^2 U_i}{\partial t^2}^{(m)} = \Sigma_{i\alpha,\alpha}^{(m)} - m\Sigma_{i3}^{(m-1)} + q\delta_{i3} \, . \tag{3.42}$$

In expanding this equation explicitly up to $0(1)$ terms we note that we have not yet defined the position of our coordinate system relative to the plate. It is usual in works where the material parameters are allowed to vary through the plate thickness (Kerr and Palmer, 1970; Williams, 1976; Hutter, 1973, 1975a) to define

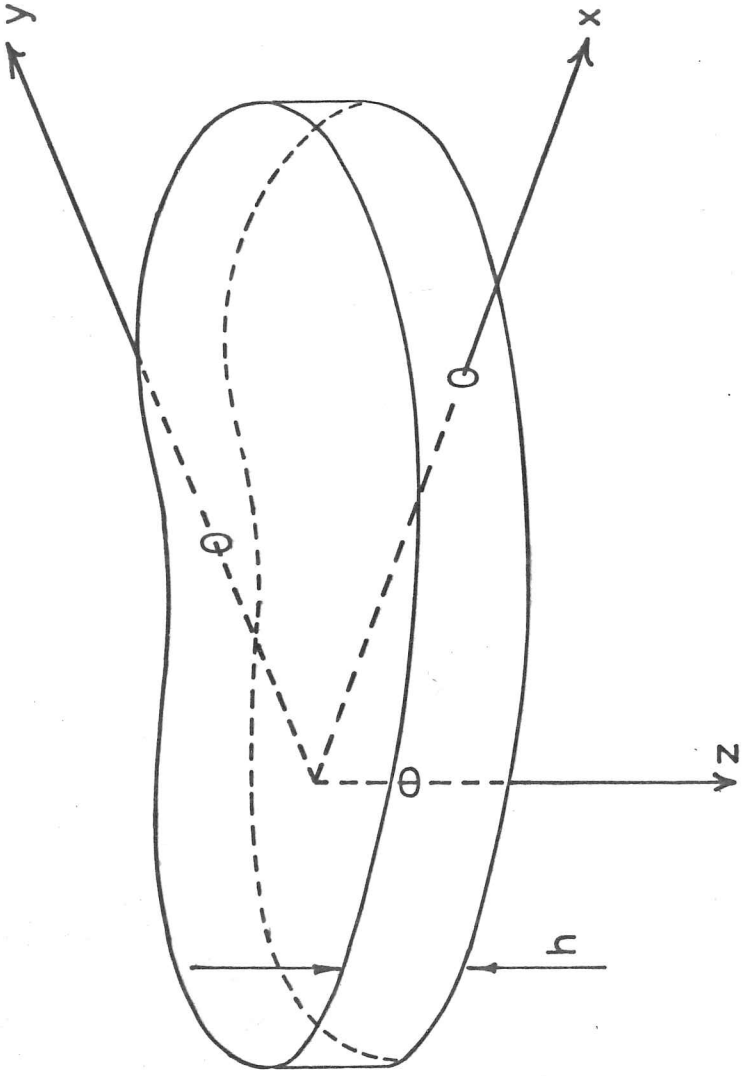

Fig. 3.1 The co-ordinate system for the plate equation.

the reference (x,y) plane by an equation of the form

$$\int_{-\delta}^{h-\delta} z\lambda(z)dz = 0 . \tag{3.43}$$

With the introduction of viscoelasticity and temperature dependence, the position of the reference plane becomes more difficult to define. Williams (1976) defines δ by the relation

$$\int_{-\delta}^{h-\delta} z\,\mu\left[0, \vartheta(z;t)\right] dz = 0, \tag{3.44}$$

and this is criticised by Hutter (1977) for imposing unrealistic restrictions on the temperature distribution. Hutter defines his reference plane to coincide with the middle plane of the plate. However, for the thermorheologically simple viscoelastic stress-strain law that Hutter uses, Williams' condition sets exactly the same reference plane since condition (3.44) reduces to

$$\int_{-\delta}^{h-\delta} z\,\mu(0)dz = 0 . \tag{3.45}$$

To be consistent we shall adopt the middle plane as our reference (x,y) plane so that in all subsequent analysis $\delta=h/2$. Such a choice of reference plane is invalid for materials which are not thermorheologically simple. For more general temperature-dependent behaviour, relation (3.44) as suggested by Williams must be used. With $\delta=h/2$, $I^{(1)}$ vanishes and we may write the equations of motion explicitly to to O(1) as

$$\left.\begin{aligned}
\rho h\frac{\partial^2 u}{\partial t^2} &= \frac{\partial N_x}{\partial x} + \frac{\partial N_{xy}}{\partial y} , \\
\rho h\frac{\partial^2 v}{\partial t^2} &= \frac{\partial N_{xy}}{\partial x} + \frac{\partial N_y}{\partial y} , \\
\rho h\frac{\partial^2 w}{\partial t^2} &= \frac{\partial Q_x}{\partial x} + \frac{\partial Q_y}{\partial y} + q , \\
\frac{\rho h^3}{12}\frac{\partial^2 \varphi}{\partial t^2} &= \frac{\partial M_x}{\partial x} + \frac{\partial M_{xy}}{\partial y} - Q_x , \\
\frac{\rho h^3}{12}\frac{\partial^2 \psi}{\partial t^2} &= \frac{\partial M_{xy}}{\partial x} + \frac{\partial M_y}{\partial y} - Q_y .
\end{aligned}\right\} \tag{3.46}$$

Equations (3.46) represent a system of equations of motion which complement the strain-displacement relations and the thermo-rheologically simple constitutive equations.

3.6 The Compatibility Conditions

The compatibility conditions may be written down directly from Mindlin (1951) as

$$\begin{aligned} &\frac{\partial^2}{\partial y^2} E_{11}^{(0)} + \frac{\partial^2}{\partial x^2} E_{22}^{(0)} - 2\frac{\partial^2}{\partial x \partial y} E_{12}^{(0)} = 0 , \\ &\left(\frac{\partial}{\partial y} E_{11}^{(1)} - \frac{\partial}{\partial x} E_{12}^{(1)}\right) = \frac{\partial}{\partial x}\left(\frac{\partial}{\partial y} E_{13}^{(0)} - \frac{\partial}{\partial x} E_{23}^{(0)}\right), \\ &\left(\frac{\partial}{\partial x} E_{22}^{(1)} - \frac{\partial}{\partial y} E_{12}^{(1)}\right) = \frac{\partial}{\partial y}\left(\frac{\partial}{\partial x} E_{23}^{(0)} - \frac{\partial}{\partial y} E_{13}^{(0)}\right). \end{aligned} \tag{3.47}$$

Another equation which will prove useful in the subsequent analysis may be found by elimination of terms of order zero from the last two equations. That is

$$\frac{\partial^2}{\partial y^2} E_{11}^{(1)} + \frac{\partial^2}{\partial x^2} E_{22}^{(1)} - 2\frac{\partial^2}{\partial x \partial y} E_{12}^{(1)} = 0 . \tag{3.48}$$

These equations are necessary to ensure single valuedness of the kinematical parameters.

3.7 The Plate Equation for Flexure

We require to find a single equation for the vertical displacement w which may be solved for the particular problem of flexural-gravity waves propagating through sea ice. To this end we define the quantities Φ and Ψ as follows:

$$\Phi = \frac{\partial u}{\partial x} + \frac{\partial v}{\partial y} , \qquad \Psi = \frac{\partial \varphi}{\partial x} + \frac{\partial \psi}{\partial y} . \tag{3.49}$$

By use of the constitutive equations (3.26) and the strain-displacement relations (3.36), equations (3.46a) and (3.46b) may be combined to give a single equation in Φ and Ψ.

$$\rho h \frac{\partial^2 \Phi}{\partial t^2} = \frac{2}{1-\nu}\left[M^{(0)} \circ \nabla^2 \Phi + M^{(1)} \circ \nabla^2 \Psi\right] . \tag{3.50}$$

In a similar way we may simplify equations (3.46d) and (3.46e) to obtain a single equation in Φ, Ψ and w,

$$\frac{\rho h^3}{12}\frac{\partial^2\Psi}{\partial t^2} = \frac{2}{1-\nu}\left[M^{(1)} \circ \nabla^2 \Phi + M^{(2)} \circ \nabla^2 \Psi \right] - \Gamma \circ (\Psi + \nabla^2 w). \tag{3.51}$$

Equation (3.46c) may also be written in terms of w and Ψ using the constitutive equations (3.27),

$$\rho h \frac{\partial^2 w}{\partial t^2} = q + \Gamma \circ (\nabla^2 w + \Psi). \tag{3.52}$$

We now have a simplified system of three equations in the unknowns Φ, Ψ and w. It is certainly a feasible proposition to eliminate Φ and Ψ to obtain a single equation in w though the algebra is lengthy and the resulting equation in w is complicated. However since we are only concerned with the flexural bending of sea ice sheets we will neglect the horizontal accelerations. That is

$$\frac{\partial^2 u}{\partial t^2} = \frac{\partial^2 v}{\partial t^2} = 0 , \tag{3.53}$$

so that equation (3.50) becomes

$$M^{(0)} \circ \nabla^2 \Phi = - M^{(1)} \circ \nabla^2 \Psi . \tag{3.54}$$

The only other occurrence of Φ is in equation (3.51) so we write

$$M^{(1)} \circ \nabla^2 \Phi = -M^{(1)} \circ \left\{ \left[M^{(0)} \right]^{-1} \circ (M^{(1)} \circ \Psi) \right\} , \tag{3.55}$$

where the relaxation function $\left[M^{(0)}\right]^{-1}$ is the inverse of $M^{(0)}$ under the operation $\circ$. Substitution into equation (3.51) therefore gives

$$\frac{\rho h^3}{12}\frac{\partial^2\Psi}{\partial t^2} = \frac{2}{1-\nu} (\Pi \circ \nabla^2 \Psi) - \Gamma \circ (\nabla^2 w + \Psi), \tag{3.56}$$

where

$$\Pi \equiv M^{(2)} - M^{(1)} \circ \left[M^{(0)}\right]^{-1} \circ M^{(1)} . \tag{3.57}$$

In order to proceed we require two conditions to be upheld; commutability between consecutive relaxation functions operating on some parameter and interchangeability between differentiation with respect to time and the operator $\circ$. The former is proved without restriction in the class of thermorheologically simple materials defined by (3.9), (3.10) and (3.12) in Appendix B. The latter unfortunately is not true generally (Appendix C) and we are forced to limit the applicability of the derived equations of motion to temperature fields which do not vary with time. With this in mind, we may operate on equation (3.56) with $\Gamma \circ$ and use equation (3.52) to give the final equation for the deflection w.

$$\left[\left(\frac{2}{1-\nu}\right)\Pi \circ \nabla^2 - \frac{\rho h^3}{12}\frac{\partial^2}{\partial t^2}\right]\left[\Gamma \circ \nabla^2 - \rho h \frac{\partial^2}{\partial t^2}\right]w + \rho h \Gamma \circ \frac{\partial^2 w}{\partial t^2}$$

$$= \left[\Gamma \circ + \frac{\rho h^3}{12}\frac{\partial^2}{\partial t^2} - \left(\frac{2}{1-\nu}\right)\Pi \circ \nabla^2\right] q , \tag{3.58}$$

This equation is the temperature dependent, linearly viscoelastic equivalent to Mindlin's final equation for an elastic plate including the effects of rotatory inertia and transverse shear (Mindlin, 1951).

If we restrict the relaxation moduli to be both time and temperature independent then

$$\Gamma \equiv \mu h , \quad \Pi \equiv \frac{\mu h^3}{12} , \tag{3.59}$$

which produces the elastic equation of motion as in Mindlin's paper with $\varkappa = 1$.

The viscoelastic equation may be simplified by neglection of rotatory inertia, transverse shear or both rotatory inertia and

transverse shear leading to the following three equations respectively,

$$\left(\frac{2}{1-\nu}\right)\Pi\circ\left[\Gamma\circ\nabla^2 - \rho h\frac{\partial^2}{\partial t^2}\right]\nabla^2 w + \rho h\Gamma\circ\frac{\partial^2 w}{\partial t^2} = \left[\Gamma\circ - \left(\frac{2}{1-\nu}\right)\Pi\circ\nabla^2\right]q \ , \tag{3.60}$$

$$\left[\left(\frac{2}{1-\nu}\right)\Pi\circ\nabla^2 - \frac{\rho h^3}{12}\frac{\partial^2}{\partial t^2}\right]\nabla^2 w + \rho h\frac{\partial^2 w}{\partial t^2} = q \ , \tag{3.61}$$

$$\boxed{\left(\frac{2}{1-\nu}\right)\Pi\circ\nabla^4 w + \rho h\frac{\partial^2 w}{\partial t^2} = q \ .} \tag{3.62}$$

The last equation bears a remarkable similarity to the usual equation of motion for a linearly elastic plate on an elastic foundation (Timoshenko and Woinowsky-Krieger, 1959, sect.59).

It is interesting to note that, for the case of flexural bending where the horizontal accelerations may be neglected, the equations of motion for the membrane forces (3.46a) and (3.46b) may be satisfied identically with the introduction of a stress function defined as follows:

$$N_x = \frac{\partial^2 F}{\partial y^2} \ , \quad N_{xy} = -\frac{\partial^2 F}{\partial x \partial y} \ , \quad N_y = \frac{\partial^2 F}{\partial x^2} \tag{3.63}$$

It only remains to find an equation for the stress function F. Using equation (3.26) we may write

$$\left.\begin{aligned} N_x - \nu N_y &= 2(1+\nu)\left\{M^{(0)}\circ\left[E_{11}^{(0)} - \alpha_0\theta^{(0)}\right] + M^{(1)}\circ\left[E_{11}^{(1)} - \alpha_0\theta^{(1)}\right]\right\}, \\ N_y - \nu N_x &= 2(1+\nu)\left\{M^{(0)}\circ\left[E_{22}^{(0)} - \alpha_0\theta^{(0)}\right] + M^{(1)}\circ\left[E_{22}^{(1)} - \alpha_0\theta^{(1)}\right]\right\}, \\ N_{xy} &= 2\left\{M^{(0)}\circ E_{12}^{(0)} + M^{(1)}\circ E_{12}^{(1)}\right\}. \end{aligned}\right\} \quad \ldots(3.64)$$

Hence, anticipating the form of the equations of compatibility (3.47a) and (3.48) we write

$$\begin{aligned} &\frac{\partial^2 N_x}{\partial y^2} + \frac{\partial^2 N_y}{\partial x^2} - \nu\left(\frac{\partial^2 N_x}{\partial x^2} + \frac{\partial^2 N_y}{\partial y^2}\right) - 2(1+\nu)\frac{\partial^2 N_{xy}}{\partial x\,\partial y} \\ &2(1+\nu)\left\{M^{(0)}\circ\left(\frac{\partial^2 E_{11}^{(0)}}{\partial y^2} + \frac{\partial^2 E_{22}^{(0)}}{\partial x^2} - 2\frac{\partial^2 E_{12}^{(0)}}{\partial x\,\partial y}\right)\right. \\ &\qquad \left. + M^{(1)}\circ\left(\frac{\partial^2 E_{11}^{(1)}}{\partial y^2} + \frac{\partial^2 E_{22}^{(1)}}{\partial x^2} - 2\frac{\partial^2 E_{12}^{(1)}}{\partial x\,\partial y}\right)\right\}. \end{aligned} \quad (3.65)$$

Substitution for N_x, N_{xy}, N_y from equation (3.63) therefore yields the final equation for the stress function F.

$$\nabla^4 F = 0. \quad (3.66)$$

This is the familiar biharmonic equation which often occurs in the theory of linear plane-strain elasticity.

3.8 Summary

In this chapter we have derived an equation of motion for flexure of sea ice allowing the material properties to be both viscoelastic and temperature dependent. To achieve this end it was necessary to make certain assumptions regarding the nature of floating sea ice. It was assumed that the relaxation function corresponding to Poisson's ratio is constant, that sea ice is thermorheologically simple and that the problem we wish to solve may be successfully modelled by a linear theory. These conditions specialise the validity of the plate equation to floating sea ice under a certain restricted set of phenomenological conditions and even then ice as a thermorheologically simple material with a constant temperature

history is clearly an approximation not based on any experimentally verified facts. This may also be said of constant Poisson's ratio for although Hutter (1975c, 1976) has established that the temperature dependence is insignificant, it is an approximation to assume independence of time. The authenticity of these assumptions for the particular problem of flexural-gravity waves propagating in fast ice can only be established by experiment and such experiments pose serious operational problems.

CHAPTER 4

THE TEMPERATURE DEPENDENT FLEXURAL-GRAVITY WAVE

THE TEMPERATURE DEPENDENT FLEXURAL-GRAVITY WAVE

4.1 Introduction

In the previous chapter we derived the thermoviscoelastic equation of motion for the deflection w of a thin sheet of sea ice in flexure assuming that sea ice is thermorheologically simple. This represents a generalization of the viscoelastic plate equation derived by Biot (1955) to include a temperature gradient through the plate thickness. The more general equation also reduces to the plate equation of Chapter 2 if transverse shear, rotatory inertia and temperature effects are neglected. Whether or not it is valid to neglect these terms will be discussed for the particular case of flexural-gravity waves propagating under a sea ice cover. Comparing with the corresponding elastic theory (Mindlin, 1951), however, we suspect that the former two effects may be neglected for wave periods of the order of one second and above. Also since a change in temperature for a thermorheologically simple material influences the viscous properties (Hunter, 1961), it might be expected that the attenuation coefficient for the wave would be a function of temperature as well as ice thickness. With this in mind we shall consider two cases; a temperature dependent equation of motion with no shear or rotatory inertia effects (3.62) and the complete equation of motion (3.58). Before proceeding however we require to know more about the effect of temperature on the material properties.

With the assumption of sea ice as a thermorheologically simple material, the dependence of the relaxation functions on temperature is governed by a shift function $\chi(\vartheta)$ which must be determined experimentally for the material. Such experiments have not yet been carried out for sea ice so that it is necessary to devise a suitable shift function. This implies that we have replaced the ice sheet with a material which has certain temperature properties which we believe to be close to those of sea ice. However, an experimentally derived shift function for sea ice may be employed at a later date with little modification.

4.2 The Shift Function and Temperature Field through the Ice Sheet

We define a shift function $\chi(\vartheta)$ only over the range of temperatures likely to be encountered so that we are not limited by the restriction that $\chi(\vartheta) \to 0$ as $\vartheta \to 0°A$ (Schwarzl and Staverman, 1952). We therefore choose the shift function according to three criteria:

(i) As the temperature decreases sea ice becomes less likely to flow.

(ii) As the temperature increases towards the melting point, its ability to flow increases until at the melting point it becomes a Newtonian fluid.

(iii) The dependence of the shift function on temperature decreases away from the melting point.

These conditions may be expressed in an alternative form with the introduction of the relaxation time for the material. Then, as the temperature tends to large negative, the relaxation times tends to large positive; as the temperature tends to the melting point, the relaxation time tends to zero; the derivative of the relaxation time with respect to temperature becomes negatively larger as the temperature tends to the melting point.

A simple shift function which satisfies all these conditions is the parabola,

$$\chi(\vartheta) = \sqrt{\frac{\vartheta_L - \vartheta_0}{\vartheta_L - \vartheta}}\,, \tag{4.1}$$

where ϑ_0 is some reference temperature and ϑ_L represents the melting point of sea ice (the temperature at the underside of the ice). This function satisfies conditions (3.10) provided we restrict to the positive root.

It was necessary in the derivation of the general plate equation of motion (3.58) to assume that the temperature field was independent of time and that any dependence on horizontal coordinates could be neglected. No explicit dependence on the vertical coordinate was given however. We shall assume forthwith that the temperature

gradient across the sea ice is linear (see Appendix A), so that

$$\vartheta = \left(\frac{\vartheta_L + \vartheta_U}{2}\right) + z\left(\frac{\vartheta_L - \vartheta_U}{h}\right), \tag{4.2}$$

where ϑ_U is the surface temperature. Hence from (4.1),

$$\chi(\vartheta) = \sqrt{\frac{2(\vartheta_L - \vartheta_0)}{(\vartheta_L - \vartheta_U)(1 - \frac{2z}{h})}}\,. \tag{4.3}$$

Equation (4.3) therefore enables us to find the value of the relaxation times and hence the relaxation functions at positions through the ice sheet.

4.3 The Equivalence of the Relaxation Functions and the Complex Modulus

It is usual in problems where the stress and strain vary sinusoidally with time to work solely in terms of the complex modulus (Flügge, 1975, ch.5), one of the several equivalent functions which may be used to describe a viscoelastic material. To avoid prematurely restricting the analysis to periodic problems alone, we shall consider two possible formulations; the relaxation function and the complex modulus. For completeness, we shall demonstrate the association between these two functions for the case where temperature is included in a thermorheologically simple sense.

The relaxation function for constant temperature states may in general be written as the sum of a constant term and a term which decays to zero at large times. That is

$$\mu\left[\chi(\vartheta)t\right] = \mathring{\mu} + \tilde{\mu}\left[\chi(\vartheta)t\right], \quad \tilde{\mu}\left[\chi(\vartheta)t\right] \longrightarrow 0 \quad t \longrightarrow \infty. \tag{4.4}$$

Then, for a periodic strain of circular frequency ω, we may write

$$\varepsilon(x;t) = \mathring{\varepsilon}(x)\, e^{-i\omega t}, \tag{4.5}$$

so that the operation $\mu \circ \varepsilon$ becomes

$$\mu \circ (\mathring{\varepsilon}\, e^{-i\omega t}) = \mathring{\mu}\mathring{\varepsilon}\, e^{-i\omega t} + \tilde{\mu}(0)\mathring{\varepsilon}\, e^{-i\omega t} - \int_{-\infty}^{t} \mathring{\varepsilon}\, e^{-i\omega t} \frac{\partial}{\partial \tau} \tilde{\mu}\left[\chi(\vartheta)(t-\tau)\right] d\tau\,. \tag{4.6}$$

An integration by parts and a change of variable, $\eta = t-\tau$, yields

$$\mu \circ (\mathring{\varepsilon} e^{-i\omega t}) = \left[\left\{ \mathring{\mu} + \omega \int_0^\infty \tilde{\mu}\left[\chi(\vartheta)\eta\right] \sin \omega\eta \, d\eta \right\} - i\left\{ \omega \int_0^\infty \tilde{\mu}\left[\chi(\vartheta)\eta\right] \cos \omega\eta \, d\eta \right\} \right] \mathring{\varepsilon} e^{-i\omega t}. \quad \ldots(4.7)$$

With the substitution $t = \chi(\vartheta)\eta$ we may therefore write

$$\mu \circ (\mathring{\varepsilon} e^{-i\omega t}) = \mu^* \left[i\left\{ \frac{\omega}{\chi(\vartheta)} \right\} \right] \mathring{\varepsilon} e^{-i\omega t} = \left[\mu_1\left\{ \frac{\omega}{\chi(\vartheta)} \right\} - i\mu_2\left\{ \frac{\omega}{\chi(\vartheta)} \right\} \right] \mathring{\varepsilon} e^{-i\omega t}, \quad (4.8)$$

where

$$\left.\begin{aligned} \mu_1\left\{ \frac{\omega}{\chi(\vartheta)} \right\} &= \mathring{\mu} + \frac{\omega}{\chi(\vartheta)} \int_0^\infty \tilde{\mu}(t) \sin \frac{\omega t}{\chi(\vartheta)} \, dt, \\ \mu_2\left\{ \frac{\omega}{\chi(\vartheta)} \right\} &= \frac{\omega}{\chi(\vartheta)} \int_0^\infty \tilde{\mu}(t) \cos \frac{\omega t}{\chi(\vartheta)} \, dt. \end{aligned}\right\} \quad (4.9)$$

The functions $\mu^*(.)$, $\mu_1(.)$ and $\mu_2(.)$ are referred to as the complex shear modulus, the storage modulus and the loss modulus respectively. It should be noted that for reasons of consistency, the modulus defined above is the complex conjugate of that defined in Flugge (1975). We have therefore shown that, for a periodic strain, the operation $\mu \circ \varepsilon$ is equivalent to multiplication by a complex function of frequency and temperature.

Equations (4.9) may be inverted to give the relaxation function in terms of the storage modulus by formally recognising the integrals as Fourier sine and cosine transformations respectively (Chirgwin and Plumpton, 1969, sect.4.2). Then with the observation that

$$\frac{2}{\pi} \int_0^\infty \frac{1}{\omega} \sin \frac{\omega t}{\chi(\vartheta)} \, d\omega = 1, \quad (4.10)$$

(Chirgwin and Plumpton, 1969, sect.4.2) we may write

$$\mu\left[\chi(\vartheta)t\right] = \frac{2}{\pi}\int_0^\infty \mu_1\left[\frac{\omega}{\chi(\vartheta)}\right]\sin\omega t\ \frac{d\omega}{\omega}\ , \qquad (4.11)$$

or equivalently,

$$\mu\left[\chi(\vartheta)t\right] = \frac{2}{\pi}\int_0^\infty \mu_1(\omega)\sin\left[\chi(\vartheta)\omega t\right]\frac{d\omega}{\omega} \qquad (4.12)$$

Hence, we see from equations (4.9), (4.11) and (4.12) that the isothermal equations linking the relaxation function and the complex modulus may be employed for thermorheologically simple materials at constant temperature states provided the frequency is modified accordingly.

4.4 The Sea Ice Model

As mentioned in Chapter 2, the only data currently available on the viscoelastic properties of sea ice (Tabata, 1955, 1958a, 1958b) model the material as a Maxwell-Voigt spring-dashpot system (fig.4.1). The data are certainly inadequate and hopefully experiments will be carried out in the next few years to correct this. However, since it is common practice to represent the relaxation functions as a sum of exponentials, an alternative relaxation function may be employed with little difficulty. We therefore model the viscoelastic Young's modulus with a Maxwell-Voigt system characterised by the differential equation

$$\left(\frac{\partial^2}{\partial t^2} + a_1\frac{\partial}{\partial t} + a_2\right)\sigma = \left(b_0\frac{\partial^2}{\partial t^2} + b_1\frac{\partial}{\partial t}\right)\varepsilon. \qquad (4.13)$$

With the understanding that the stresses and strains are periodic in time, we may write down the corresponding temperature-independent storage modulus

$$E_1(\omega) = \frac{b_0\omega^4 + (a_1b_1 - a_2b_0)\omega^2}{\omega^4 + (a_1^2 - 2a_2)\omega + a_2^2}\ . \qquad (4.14)$$

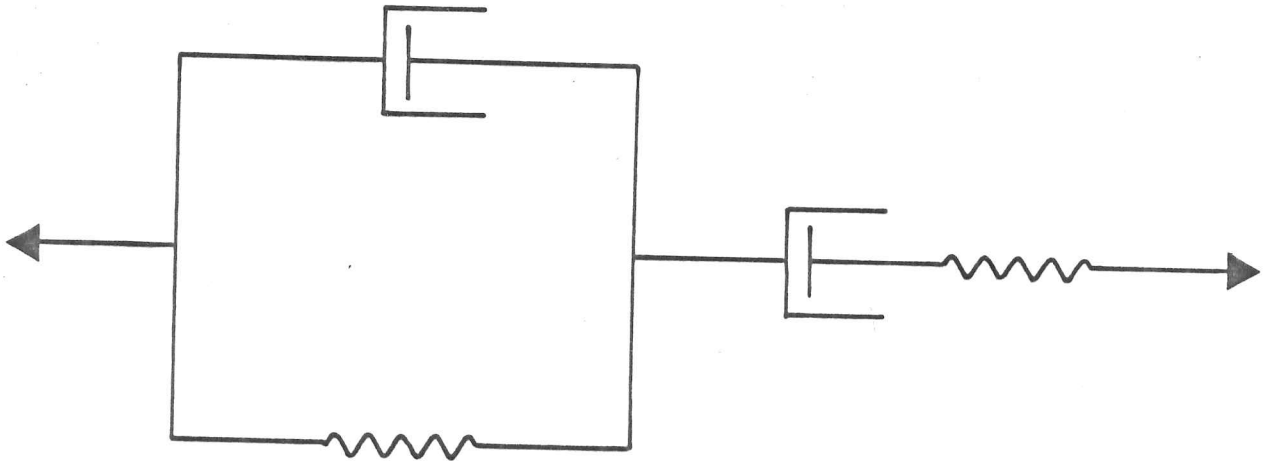

Fig. 4.1 Maxwell-Voigt spring-dashpot sea ice model.

By way of illustration we shall use equation (4.11) to derive the associated temperature dependent relaxation function $E[\chi(\vartheta)t]$. Substituting (4.14) into (4.11) and writing $\eta=wt$ we obtain

$$E\left[\chi(\vartheta)t\right] = \frac{2}{\pi}\int_0^\infty \frac{[b_1\eta^2 + (a_1b_1 - a_2b_0)t^2\chi^2(\vartheta)]\,\eta\sin\eta}{\eta^4 + (a_1^2 - 2a_2)\eta^2t^2\chi^2(\vartheta) + a_2^2t^4\chi^4(\vartheta)}\,d\eta. \qquad (4.15)$$

Since the integrand is even we may integrate over $(-\infty, \infty)$ and introduce an additional odd imaginary term without affecting the result. So that

$$E\left[\chi(\vartheta)t\right] = -\frac{i}{\pi}\int_{-\infty}^{\infty} \frac{b_0\eta^2 + (a_1b_2 - a_2b_0)t^2\chi^2(\vartheta)\;\eta e^{i\eta}}{\eta^4 + (a_1^2 - 2a_2)\eta^2t^2\chi^2(\vartheta) + a_2t^4\chi^4(\vartheta)}\,d\eta. \qquad (4.16)$$

By writing this expression in partial fraction form,

$$E\left[\chi(\vartheta)t\right] = -\frac{i}{\pi}\int_{-\infty}^{\infty}\left[\frac{E_1\eta}{\eta^2 + s_1^2t^2\chi^2(\vartheta)} - \frac{E_2\eta}{\eta^2 + s_2^2t^2\chi^2(\vartheta)}\right]e^{i\eta}d\eta, \qquad (4.17)$$

we may integrate using contour integration (Jeffreys and Jeffreys, 1972, ch.12) and obtain

$$E\left[\chi(\vartheta)t\right] = E_1e^{-s_1\chi(\vartheta)t} - E_2e^{-s_2\chi(\vartheta)t}, \qquad (4.18)$$

where

$$E_{1,2} = \frac{b_0s_{1,2} - b_1}{\sqrt{a_1^2 - 4a_2}}, \quad s_{1,2} = \frac{1}{2}(a_1 \pm \sqrt{a_1^2 - 4a_2}). \qquad (4.19)$$

This may be expressed in a neater form by defining a temperature dependent relaxation time for each exponential. In which case,

$$E\left[\chi(\vartheta)t\right] = E_1e^{-t/t_1(\vartheta)} - E_2e^{-t/t_2(\vartheta)}. \qquad (4.20)$$

This form for the relaxation function will be consistently used in the subsequent analysis. Clearly the inclusion of a constant or additional exponential terms in equation (4.20) would pose no problems should a better mechanical analogy for sea ice than the Maxwell-Voigt model be found. It is important to note that for a thermorheologically simple material, the temperature dependence

enters through the relaxation time alone. This provides a simple method of determining whether a material is thermorheologically simple if the mechanical analogy is known in advance since the constants E_1 and E_2 should be independent of temperature. Tabata's data show too much scatter to conclusively prove the desired result.

The relaxation function (4.20) may also be derived for non-periodic strains belonging to H^1 by use of the convolution theorem of Laplace transforms (Dettman, 1970, ch.9).

4.5 Evaluation of the Relaxation Functions $M^{(0)}$, $M^{(1)}$ and $M^{(2)}$

The general equation for the deflection w, (3.58), contains two related relaxation functions, Γ and Π. These functions may be written in terms of $M^{(0)}$, $M^{(1)}$ and $M^{(2)}$ defined by equation (3.15a) as

$$\left.\begin{aligned} \Gamma &\equiv M^{(0)} - M^{(1)} \circ \left[M^{(2)}\right]^{-1} \circ M^{(1)} , \\ \Pi &\equiv M^{(2)} - M^{(1)} \circ \left[M^{(0)}\right]^{-1} \circ M^{(1)} . \end{aligned}\right\} \tag{4.21}$$

It is not strictly necessary to evaluate the $M^{(i)}$ explicitly since for the periodic case we need only their Fourier transforms and for the non-periodic case, their Laplace transforms. However for the particular temperature dependence we have chosen, the integrals reduce to standard forms so we shall evaluate $M^{(0)}$, $M^{(1)}$ and $M^{(2)}$ for completeness. From equations (3.7) and (4.20), the form of the relaxation function $\mu\left[\chi(\vartheta)t\right]$ is

$$\mu\left[\chi(\vartheta)t\right] = \mu_1 e^{-t/t_1(\vartheta)} - \mu_2 e^{-t/t_2(\vartheta)} . \tag{4.22}$$

Hence, with the shift function discussed in Section 4.2 we may write

$$\left.\begin{aligned} M^{(0)} &= \int_{-h/2}^{h/2} \mu_1 \exp\left\{\frac{-t'}{\sqrt{(1 - 2z/h)/2}}\right\} dz + \ldots , \\ M^{(1)} &= \int_{-h/2}^{h/2} \mu_1 z \exp\left\{\frac{-t'}{\sqrt{(1 - 2z/h)/2}}\right\} dz + \ldots , \\ M^{(2)} &= \int_{-h/2}^{h/2} \mu_1 z^2 \exp\left\{\frac{-t'}{\sqrt{(1 - 2z/h)/2}}\right\} dz + \ldots , \end{aligned}\right\} \tag{4.23}$$

where t' is now a non-dimensional time and we have omitted the second exponential term for reasons of brevity. Explicitly,

$$t' = ts_1 \sqrt{\left| \frac{\vartheta_L - \vartheta_0}{\vartheta_L - \vartheta_U} \right|} \quad , \tag{4.24}$$

and we may define an equivalent non-dimensional time for the second exponential. In all cases t' is strictly greater than zero. With the substitution

$$u = \frac{t'}{\sqrt{(1 - 2z/h)/2}} \quad , \tag{4.25}$$

equations (4.23) reduce to standard forms. That is,

$$\left.\begin{aligned} M^{(0)} &= 2\int_{t'}^{\infty} \mu_1 h t'^2 \frac{e^{-u}}{u^3}\, du + \ldots , \\ M^{(1)} &= \int_{t'}^{\infty} \mu_1 h^2 t'^2 \left(1 - \frac{2t'^2}{u^2}\right) \frac{e^{-u}}{u^3}\, du + \ldots , \\ M^{(2)} &= \frac{1}{2}\int_{t'}^{\infty} \mu_1 h^3 t'^2 \left(1 - \frac{2t'^2}{u^2}\right) \frac{e^{-u}}{u^3}\, du + \ldots \end{aligned}\right\} \tag{4.26}$$

Hence, from Gradshteyn and Ryzhik (1965, sect.3.381, eq.6) we may finally write

$$\left.\begin{aligned} M^{(0)} &= 2\mu_1 h (t')^{1/2} e^{-t'/2} W_{-3/2,-1}(t') + \ldots , \\ M^{(1)} &= \mu_1 h^2 (t')^{1/2} e^{-t'/2} \left\{ W_{-3/2,-1}(t') - 2t' W_{-5/2,-2}(t') \right\} + \ldots , \\ M^{(2)} &= \frac{1}{2}\mu_1 h^3 (t')^{1/2} e^{-t'/2} \left\{ W_{-3/2,-1}(t') \right. \\ &\qquad \left. - 4t' W_{-5/2,-2}(t') + 4t'^2 W_{-7/2,-3}(t') \right\} + \ldots , \end{aligned}\right\} \tag{4.27}$$

where $W_{a,b}(.)$ represent Whittaker functions (Spain and Smith, 1970, sect.7.7). In the limit of large times the Whittaker functions tend to zero exponentially so that $M^{(0)}, M^{(1)}, M^{(2)} \to 0$ as $t \to \infty$. For small times we may write the Whittaker functions in terms of

Kummer's functions to obtain the values of the relaxation functions $M^{(i)}$ to zeroth order (Abramowitz and Stegun, 1965, eq.13.1.33, 13.5.12). This yields the corresponding elastic moduli

$$M^{(0)} = h(\mu_1 - \mu_2), \quad M^{(1)} = 0, \quad M^{(2)} = \frac{h^3}{12}(\mu_1 - \mu_2). \tag{4.28}$$

4.6 The Transforms of the Relaxation Functions Γ and Π

We have shown that for periodic strains, the operation $\mu \circ \varepsilon$ reduces to multiplication by a complex modulus found by use of Fourier sine and cosine transforms. For non-periodic strains belonging to H^1, solution is through the theory of Laplace transforms. Despite the complicated form of the equations (4.27), it is possible to determine both the Fourier and Laplace transforms by a change in the order of integration.

Periodic Problems

If we denote the storage and loss moduli corresponding to $M^{(i)}$ by $\varpi_1^{(i)}$ and $\varpi_2^{(i)}$ respectively, then from equations (4.9), (4.22) and (4.23) we may write expressions for $\varpi_1^{(0)}$ and $\varpi_2^{(0)}$ as follows:

$$\left.\begin{aligned} \varpi_1^{(0)} &= \omega \int_0^{\infty} \sin \omega t \, dt \int_{-h/2}^{h/2} \mu_1 e^{-t/t_1} \, dz + \ldots, \\ \varpi_2^{(0)} &= \omega \int_0^{\infty} \cos \omega t \, dt \int_{-h/2}^{h/2} \mu_1 e^{-t/t_1} \, dz + \ldots \end{aligned}\right\} \tag{4.29}$$

where t_1 is a function of z. For the Maxwell-Voigt model the constant term $\overset{\circ}{\mu}$ in equation (4.9) is zero. Similar equations may also be written down for other relevant $\varpi^{(i)}$. With a change in the order of integration, equations (4.29) reduce to standard Fourier sine and cosine transforms which may be evaluated provided $t_1 \geq 0$, as

$$\left.\begin{aligned} \varpi_1^{(0)} &= \mu_1 \omega \int_{-h/2}^{h/2} \frac{\omega}{\omega^2 + t_1^{-2}} \, dz + \ldots, \\ \varpi_2^{(0)} &= \mu_1 \omega \int_{-h/2}^{h/2} \frac{(1/t_1)}{\omega^2 + t_1^{-2}} \, dz + \ldots \end{aligned}\right\} \tag{4.30}$$

Substituting $u=1/t_1$ and then $\omega\tan\theta=u$ yields expressions for $\varpi_1^{(0)}$ and $\varpi_2^{(0)}$ which are analytically integrable. That is

$$\left.\begin{aligned}\varpi_1^{(0)} &= \frac{2\mu h c_1^2}{\omega^2}\int_{\theta_1}^{\frac{\pi}{2}} \frac{d\theta}{\tan^3\theta} + \ldots,\\ \varpi_2^{(0)} &= \frac{2\mu h c_1^2}{\omega^2}\int_{\theta_1}^{\frac{\pi}{2}} \frac{d\theta}{\tan^2\theta} + \ldots,\end{aligned}\right\} \qquad (4.31)$$

where,

$$\tan\theta = \frac{c_1}{\omega}, \quad c_1 = s_1\sqrt{\frac{\vartheta_L-\vartheta_0}{\vartheta_L-\vartheta_U}}. \qquad (4.32)$$

Hence, the integrals may be evaluated to give

$$\left.\begin{aligned}\varpi_1^{(0)} &= \frac{\mu_1 h c_1^2}{\omega^2}\left[\frac{\omega^2}{c_1^2} - \ln\left(\frac{\omega^2+c_1^2}{c_1^2}\right)\right] + \ldots,\\ \varpi_2^{(0)} &= \frac{\mu_1 h c_1^2}{\omega^2}\left[2\left(\tan^{-1}\frac{c_1}{\omega} + \frac{\omega}{c_1}\right) - \pi\right] + \ldots\end{aligned}\right\} \qquad (4.33)$$

Following exactly the same method the explicit forms of $\varpi^{(1)}$ and $\varpi^{(2)}$ may also be written down

$$\left.\begin{aligned}\varpi_1^{(1)} &= \frac{\mu_1 h^2 c_1^2}{2\omega^2}\left[\left\{\frac{\omega^2}{c_1^2} - \ln\left(\frac{\omega^2+c_1^2}{c_1^2}\right)\right\}\left(1+\frac{2c_1^2}{\omega^2}\right) - \frac{\omega^2}{c_1^2}\right] + \ldots,\\ \varpi_2^{(1)} &= \frac{\mu_1 h^2 c_1^2}{2\omega^2}\left[\left\{2\left(\tan^{-1}\frac{c}{\omega} + \frac{\omega}{c_1}\right) - \pi\right\}\left(1+\frac{2c_1^2}{\omega^2}\right) - \frac{4\omega}{3c_1}\right] + \ldots,\end{aligned}\right\} \qquad \ldots(4.34)$$

and,

$$\left.\begin{aligned}\varpi_1^{(2)} &= \frac{\mu_1 h^3 c_1^2}{4\omega^2}\left[\left\{\frac{\omega^2}{c_1^2} - \ln\left(\frac{\omega^2+c_1^2}{c_1^2}\right)\right\}\left(1+\frac{2c_1^2}{\omega^2}\right)^2 - \frac{2\omega^2}{3c_1^2}\left(1+\frac{3c_1^2}{\omega^2}\right)\right] + \ldots,\\ \varpi_2^{(2)} &= \frac{\mu_1 h^3 c_1^2}{4\omega^2}\left[\left\{2\left(\tan^{-1}\frac{c_1}{\omega} + \frac{\omega}{c_1}\right) - \pi\right\}\left(1+\frac{2c_1^2}{\omega^2}\right)^2 - \frac{16\omega}{15c_1}\left(1+\frac{5c_1^2}{2\omega^2}\right)\right] + \ldots\end{aligned}\right\} \qquad (4.35)$$

For the case of $c_1 \to 0$ (and c_2 corresponding to the second suppressed term) the respective relaxation times, $t_1(\vartheta)$, $t_2(\vartheta) \to \infty$ so that the material tends to behave elastically. That is, from Abramowitz and Stegun (1965, eq.4.1.30, 4.4.42),

$$\left.\begin{aligned} &\mathrm{Im}_1^{(0)} \to h(\mu_1 - \mu_2), \quad \mathrm{Im}_1^{(1)} \to 0, \quad \mathrm{Im}_1^{(2)} \to \frac{h^3}{12}(\mu_1 - \mu_2), \\ &\mathrm{Im}_2^{(0)}, \quad \mathrm{Im}_2^{(1)}, \quad \mathrm{Im}_2^{(2)} \to 0, \end{aligned}\right\} \quad (4.36)$$

so that,

$$\Gamma \to h(\mu_1 - \mu_2), \quad \Pi \to \frac{h^3}{12}(\mu_1 - \mu_2). \quad (4.37)$$

Now c_1, c_2 are inversely proportional to the square root of the difference of the surface and underside temperatures of the sea ice, ϑ_U and ϑ_L respectively. Hence as ϑ_U tends to ϑ_L, c_1 and $c_2 \to \infty$. But as c_1, $c_2 \to \infty$ (Abramowitz and Stegun, 1965, eq.4.1.24, 4.4.42), the values of the storage and loss moduli to order ω tend to

$$\begin{aligned} &\mathrm{Im}_1^{(0)}, \quad \mathrm{Im}_1^{(1)}, \quad \mathrm{Im}_1^{(2)} \to 0, \\ &\mathrm{Im}_2^{(0)}, \quad \mathrm{Im}_2^{(1)}, \quad \mathrm{Im}_2^{(2)} \to 0\left(\frac{\omega}{c_1}\right) + \ldots \end{aligned} \quad (4.38)$$

Hence, the storage moduli for Γ and Π tend to zero and the loss moduli tend to $\eta\omega$ and $\eta'\omega$, respectively, where η and η' are small parameters. It is interesting to note that the storage and loss moduli for a viscous fluid are zero and $\eta\omega$ respectively, so that very close to the melting point, the sea ice is behaving as a Newtonian fluid with low viscosity, that is, the sea ice is melting.

Equivalently it can be shown that for very fast processes ($\omega \to \infty$) the material behaves elastically and for very slow processes ($\omega \to 0$) the material behaves as a Newtonian fluid with low viscosity. This statement is more general than is indicated here. The former behaviour is the basis of high frequency wave experiments to evaluate elastic moduli.

Non-Periodic Problems

Denote the one-sided Laplace transform defined in the usual way (Dettman, 1970, ch.9) by a bar, then from equations (4.22) and (4.23) we may write

$$\overline{M^{(0)}(s)} = \int_0^\infty e^{-st}\,dt \int_{-h/2}^{h/2} \mu_1 e^{-t/t_1}\,dz + \ldots, \qquad (4.39)$$

so that a change in the order of integration produces

$$\overline{M^{(0)}(s)} = \mu_1 \int_{-h/2}^{h/2} \frac{dz}{s + (1/t_1)} + \ldots, \quad s + \frac{1}{t_1} > 0. \qquad (4.40)$$

Following the equivalent periodic analysis, the substitution $u=1/t$ gives

$$\overline{M^{(0)}(s)} = 2\mu_1 h c_1^2 \int_{c_1}^\infty \frac{du}{u^3(u+s)} + \ldots, \qquad (4.41)$$

which may be integrated using partial fractions to finally give

$$\overline{M^{(0)}(s)} = 2\mu_1 h c_1^2 \left\{ \frac{1}{s^3} \ln\left(\frac{c_1+s}{c_1}\right) + \frac{1}{c_1 s^2} - \frac{1}{2c_1^2 s} \right\} + \ldots, \qquad (4.42)$$

In a similar way the Laplace transforms of $M^{(1)}$ and $M^{(2)}$ may be derived

$$\left.\begin{aligned} \overline{M^{(1)}(s)} &= \mu_1 h^2 c_1^2 \left\{ \frac{1}{s^3} \ln\left(\frac{c_1+s}{c_1}\right)\left(1 - \frac{2c_1^2}{s^2}\right) + \frac{2c_1}{s^4} - \frac{1}{s^3} - \frac{1}{3c_1 s^2} \right\} + \ldots, \\ \overline{M^{(2)}(s)} &= \frac{\mu_1 h^3 c_1^2}{2} \left\{ \frac{1}{s^3} \ln\left(\frac{c_1+s}{c_1}\right)\left(1 - \frac{2c_1^2}{s^2}\right)^2 - \frac{4c_1^3}{s^6} + \frac{2c_1^2}{s^5} \right. \\ &\qquad \left. + \frac{8c_1}{3s^4} - \frac{1}{s^3} - \frac{7}{15c_1 s^2} + \frac{1}{6c_1^2 s} \right\} + \ldots \end{aligned}\right\} \qquad (4.43)$$

Hence, the relevant transforms determining the solution for two types of problem have been evaluated; the periodic case and the case where the strain is non-periodic and begins at t=0.

4.7 The Wave Solution neglecting Rotatory Inertia and Transverse Shear

We now restrict the analysis to the problem we have set ourselves

to solve; the propagation of flexural-gravity waves along the interface between floating sea ice and water. With the assumption that the ice edge is a long way from the origin of coordinates, we may align the x-axis with the axis of propagation of the wave. In this case, equation (3.62) for the deflection w neglecting rotatory inertia and transverse shear becomes

$$\left(\frac{2}{1-\nu}\right)\Pi \circ \frac{\partial^4 w}{\partial x^4} + \rho h \frac{\partial^2 w}{\partial t^2} = q \,, \tag{4.44}$$

so that with the usual boundary conditions for a plate on deep water (Chapter 2), we may write equation (4.44) as

$$\left(\frac{2}{1-\nu}\right)\Pi \circ \frac{\partial^4 w}{\partial x^4} + \rho' g w + \rho h \frac{\partial^2 w}{\partial t^2} + \frac{\rho'}{k}\frac{\partial^2 w}{\partial t^2} = 0, \tag{4.45}$$

where k is the wave number and ρ' is the density of sea water. A corresponding analysis may be carried out if the underlying water is assumed to be shallow. Hence, denoting the complex modulus corresponding to the relaxation function Π by Π^*, equation (4.45) reduces to the dispersion equation for k,

$$\left(\frac{2}{1-\nu}\right)\Pi^* k^5 + (\rho' g - \rho h \omega^2)k - \rho' \omega^2 = 0. \tag{4.46}$$

This dispersion equation, a quintic polynomial in k, is strikingly similar to the temperature independent equation of Chapter 2. Since we know Π in terms of $M^{(0)}$, $M^{(1)}$, $M^{(2)}$ and we have found the necessary complex moduli, it is a simple matter to find Π^* and hence solve the dispersion equation numerically for k. To achieve this end we use Tabata's Maxwell-Voigt data for the viscoelastic Young's modulus with reference temperature ϑ_0 taken at the temperature for which the relaxation times were measured (-3.0°C).

The dispersion equation again permits five possible values for the complex wave number, three of which satisfy conditions of boundedness (the boundary conditions are discussed more fully in Chapter 2). Hence, with the assumption that the waves propagate in the same direction, the displacement is made up of three components:- a wave with slight attenuation corresponding to the

propagating wave of the equivalent elastic theory (Wadhams, 1973b) and a pair of waves with substantial attenuation which can exist only local to their point of generation. If the flexural-gravity waves are due to an ocean swell impinging on to sea ice from the open ocean, we need consider only the former wave so long as we are not too close to the ice edge.

Adopting the same notation as in Chapter 2, we may write the three possible wave numbers as

$$k_1 = \xi_1 + i\zeta_1, \quad k_2 = \xi_2 + i\zeta_2, \quad k_3 = \xi_3 - i\zeta_3, \tag{4.47}$$

where ξ_i, ζ_i are real positive constants which provide phase and attenuation information respectively. Then, without confusion, a wave may be referred to by using the subscript of its wave number. The corresponding wavelengths and attenuation coefficients are denoted by λ_i and α_i in the obvious way. It is found that at any particular surface temperature, ϑ_U, the complex wave numbers k_1, k_2 and k_3 behave in much the same way as for the temperature independent case. A graph of wavelength λ_1 against period at some particular surface temperature for various sea ice thicknesses (fig.4.2) shows the same characteristic shape as the simpler model of Chapter 2. In fact the temperature dependence of λ_1 is negligible for temperatures not too close to -1.8°C so that the particular surface temperature chosen in unimportant. The curves therefore exactly coincide with the wavelengths predicted for the temperature independent case provided similar material properties are chosen. Hence, if sea ice behaves as a thermorheologically simple material, a temperature independent model is adequate to predict the wavelength λ_1 as a function of period.

The attenuation coefficient α_1 as a function of period however is clearly dependent on temperature as can be seen in figures 4.3. Figures 4.3a, b, c and d illustrate the attenuation coefficient at three ice thicknesses for surface temperatures of -5°C, -10°C, -20°C and -50°C respectively. The effect of temperature appears to be to shift the curves vertically in such a way that the attenuation coefficient decreases significantly with temperature.

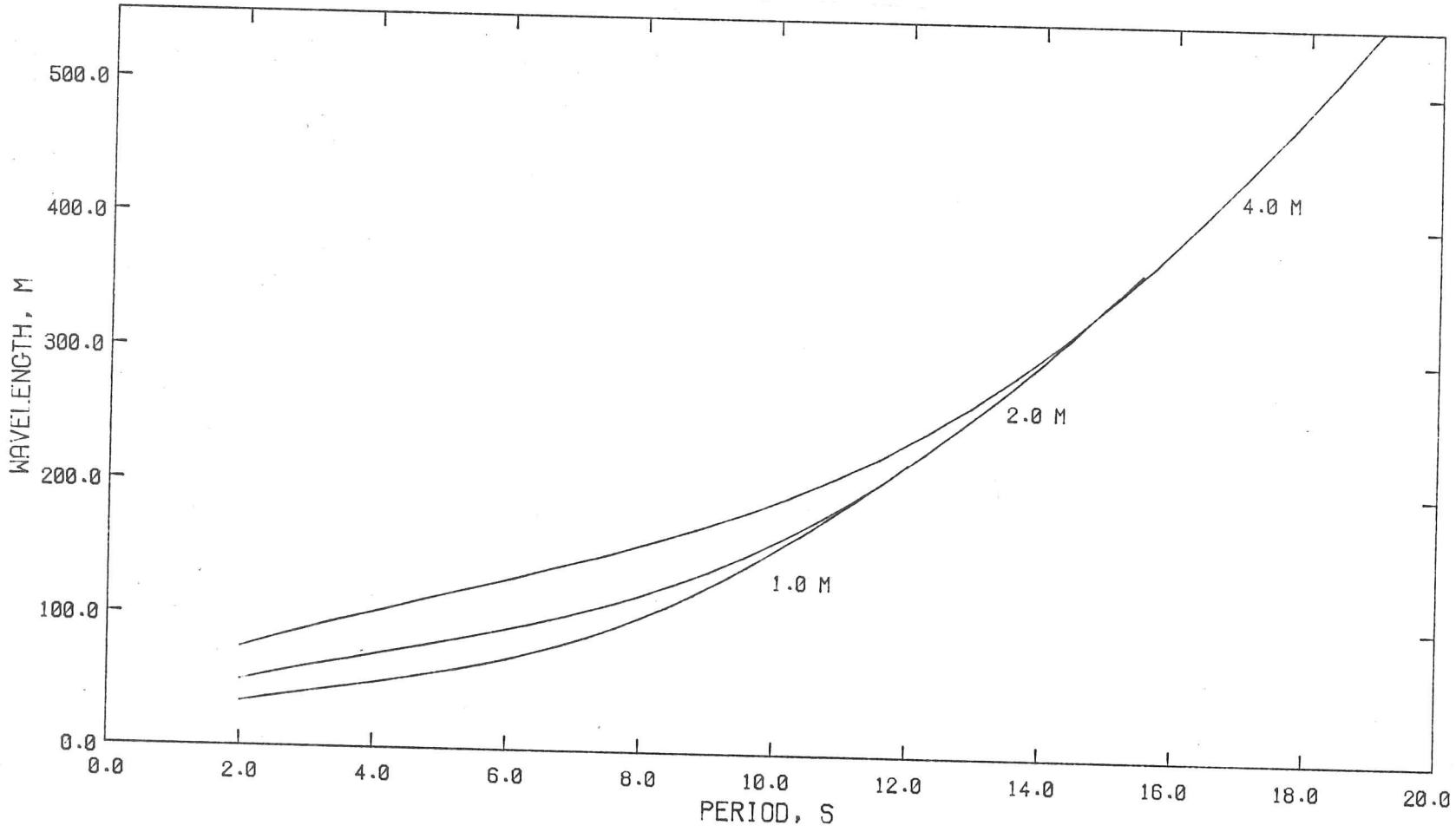

Fig. 4.2 Ice-coupled wavelengths at three ice thicknesses.

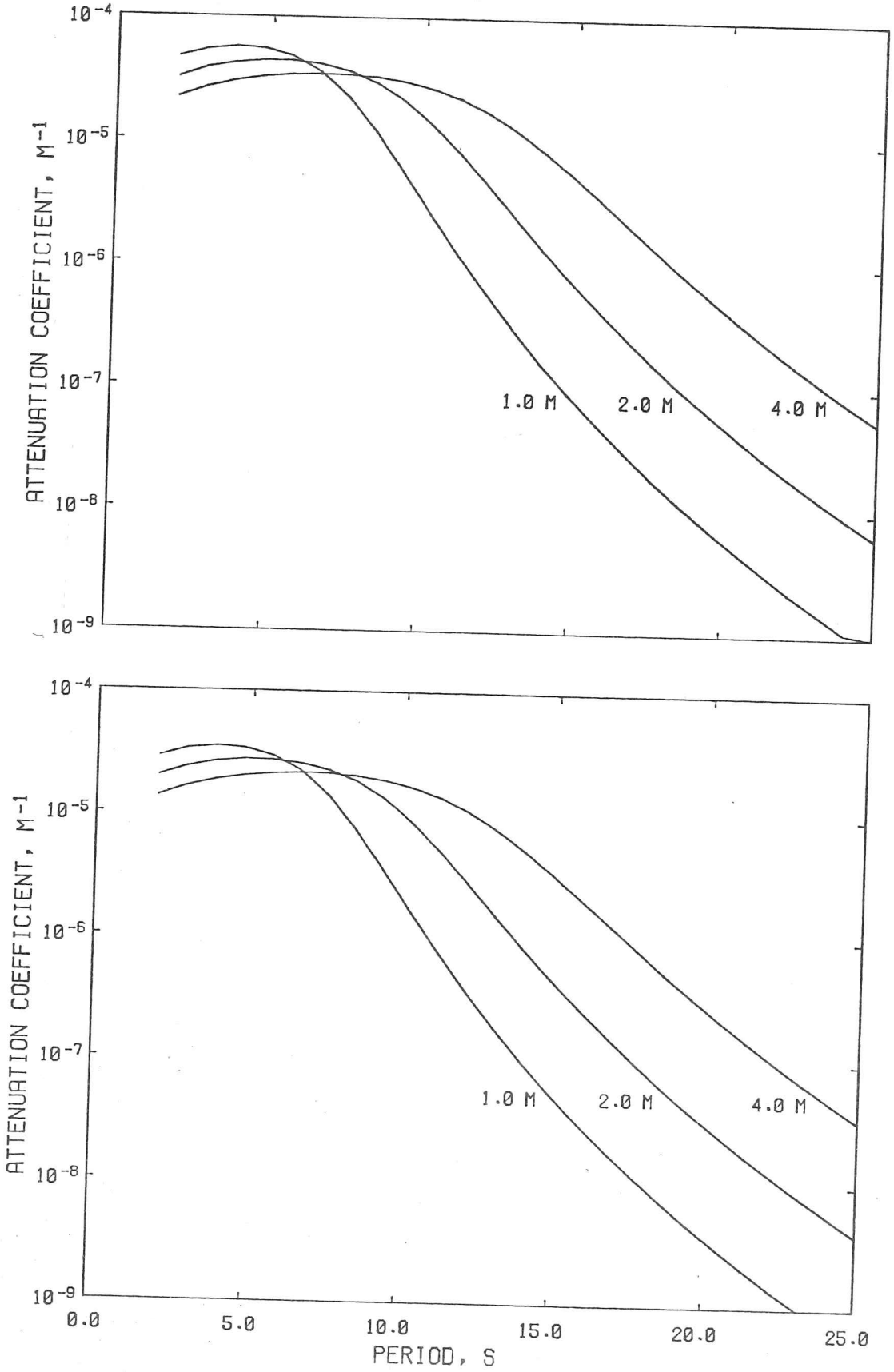

Fig. 4.3a,b The attenuation coefficient for three ice thicknesses at surface temperatures of -5°C and -10°C.

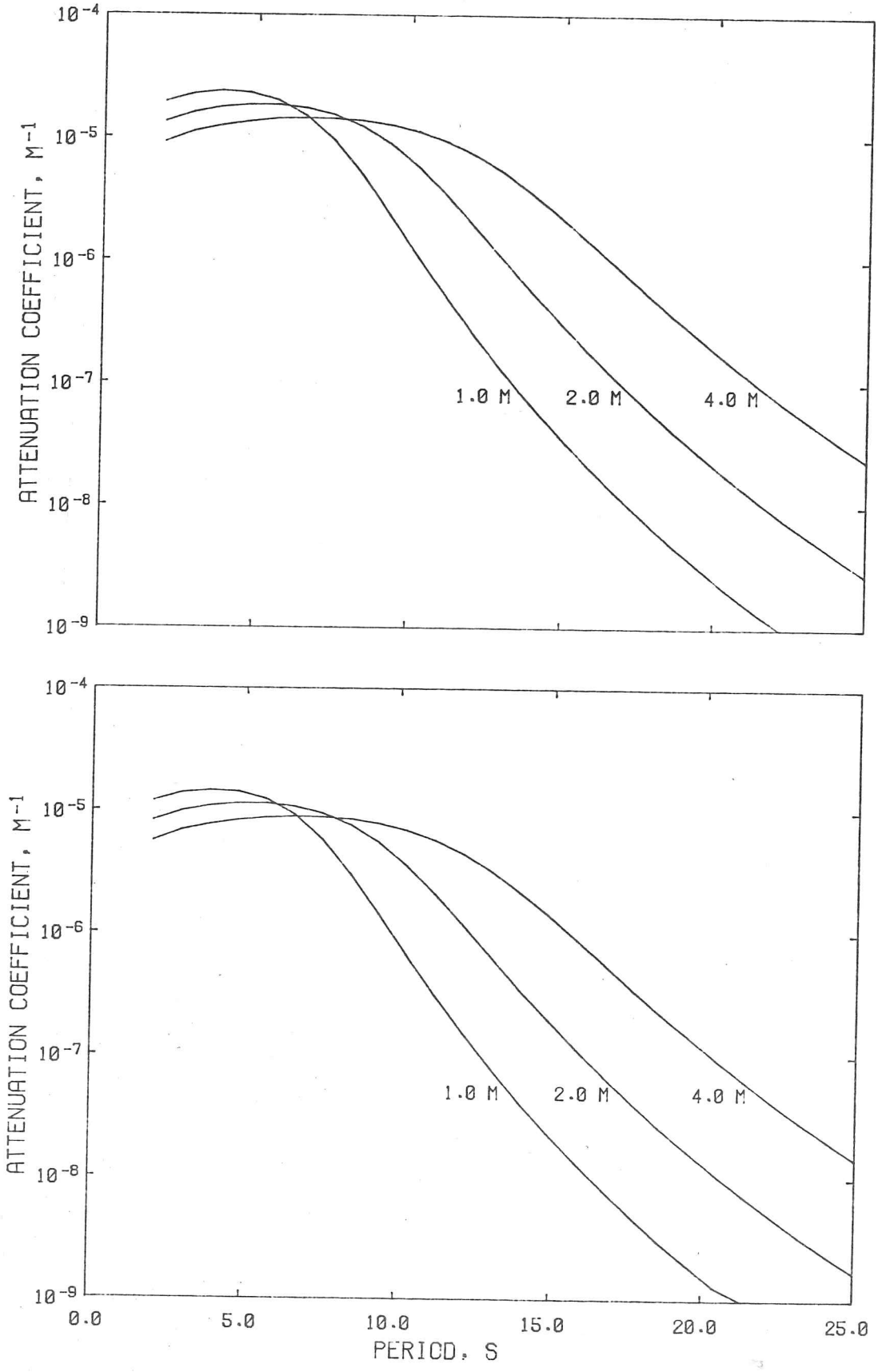

Fig. 4.3c,d The attenuation coefficient for three ice thicknesses at surface temperatures of -20°C and -50°C.

A graph of the attenuation coefficient against the difference of the surface and under-ice temperatures plotted on logarithmic axes for an ice thickness of 1 m is shown in figure 4.4. The linearity of the curves is striking indicating that a power law relation of the form

$$\alpha_1 = c(\vartheta_L - \vartheta_U)^a \qquad (4.48)$$

exists for surface temperatures not too close to -1.8°C. A linear regression analysis over a range of surface temperatures from -2.1°C to large negative on the theoretically derived points gave a value of $a = -0.5$ independent of both period and ice thickness. The standard errors in this regression were of the order of 10^{-3} and decreased with increasing circular frequency ω. Clearly from figure 4.5 showing the behaviour of α_1 for different ice thicknesses at constant period, the parameter C in expression (4.48) is a function of both frequency and ice thickness. Hence we may write

$$\alpha_1 = \frac{c(\omega,h)}{\sqrt{\vartheta_L - \vartheta_U}} \,. \qquad (4.49)$$

Using the results of the linear regression analysis, the behaviour of the parameter $C(\omega, h)$ as a function of circular frequency ω and the ice thickness h may be plotted (fig.4.6). Hence, given a surface temperature and the value of C for a particular ice thickness, it is a simple matter to employ equation (4.49) to find the attenuation coefficient at some wave period. This provides an <u>in situ</u> method of verifying the hypothesis of sea ice as a thermorheologically simple material with the assumed shift function. Such an experiment would measure the attenuation coefficient for different wave periods as a function of temperature.

So far we have not mentioned temperatures very close to the melting point of sea ice, that is, when $\vartheta_U \to \vartheta_L$. In this case we look at the asymptotic expansion as $c_1, c_2 \to \infty$ (eq.4.38). To first order therefore, the storage modulus vanishes and the loss modulus is very small. Hence by expanding the wave number as an

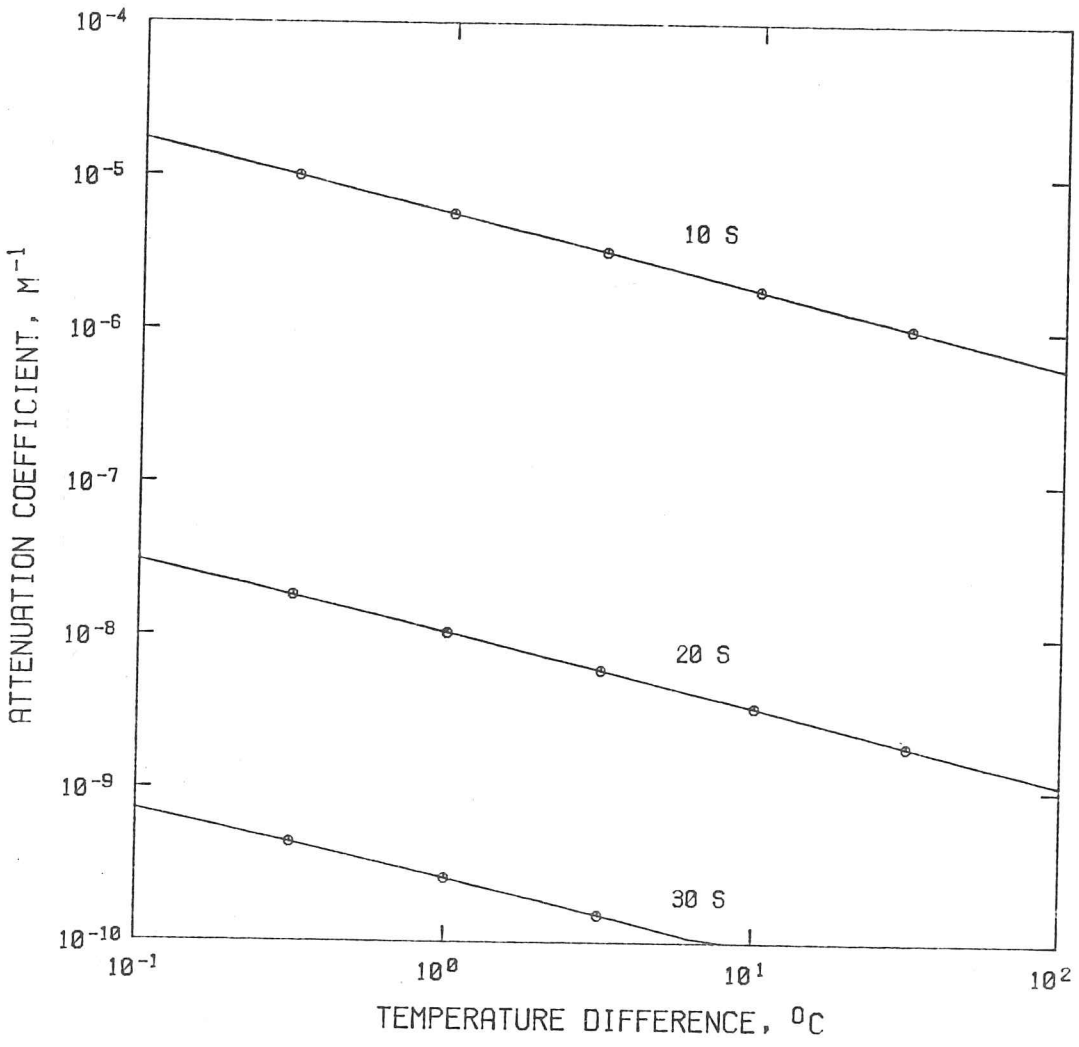

Fig. 4.4 The attenuation coefficient as a function of temperature difference, $\vartheta_L - \vartheta_U$, for 1 m of sea ice at three different periods.

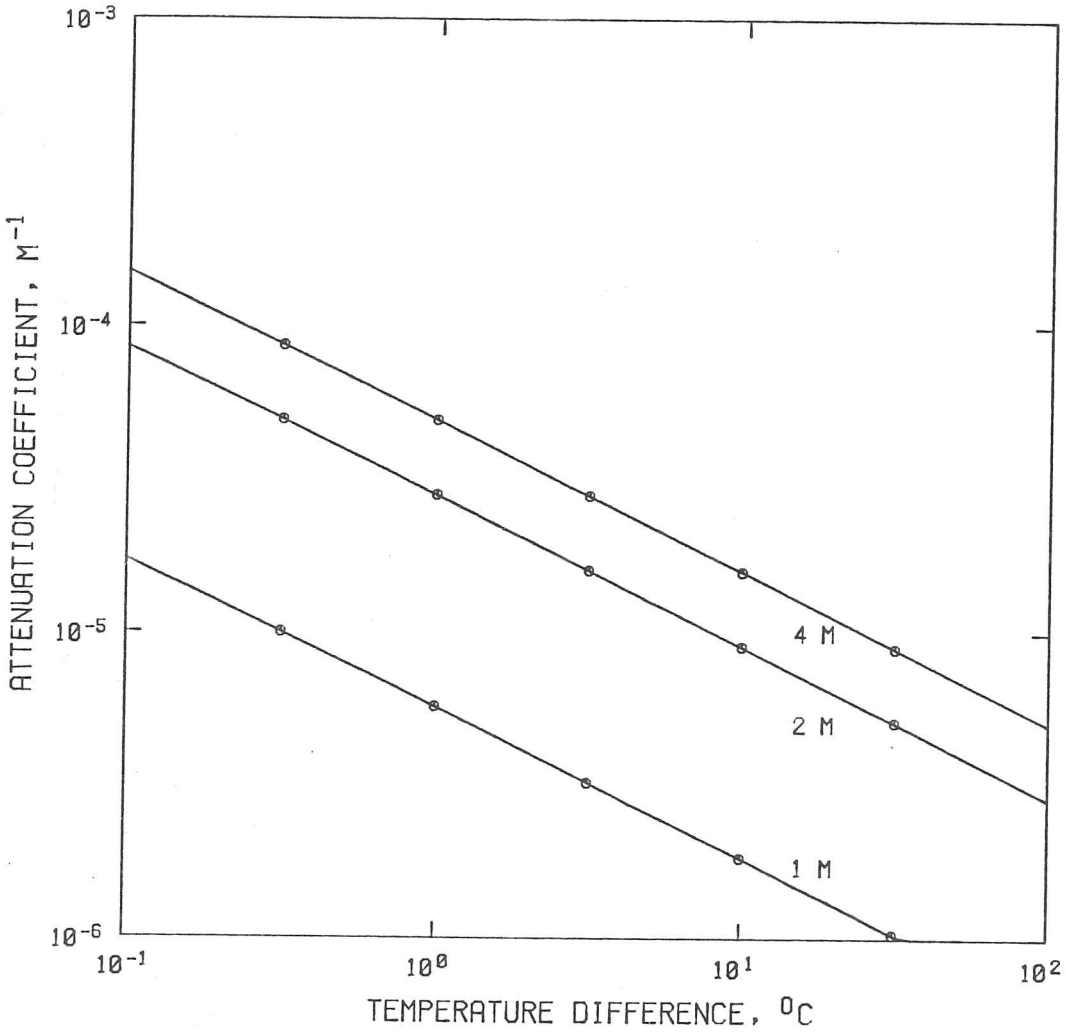

Fig. 4.5 The attenuation coefficient as a function of temperature difference, $\vartheta_L - \vartheta_U$, for a 10 s wave at various thicknesses of sea ice.

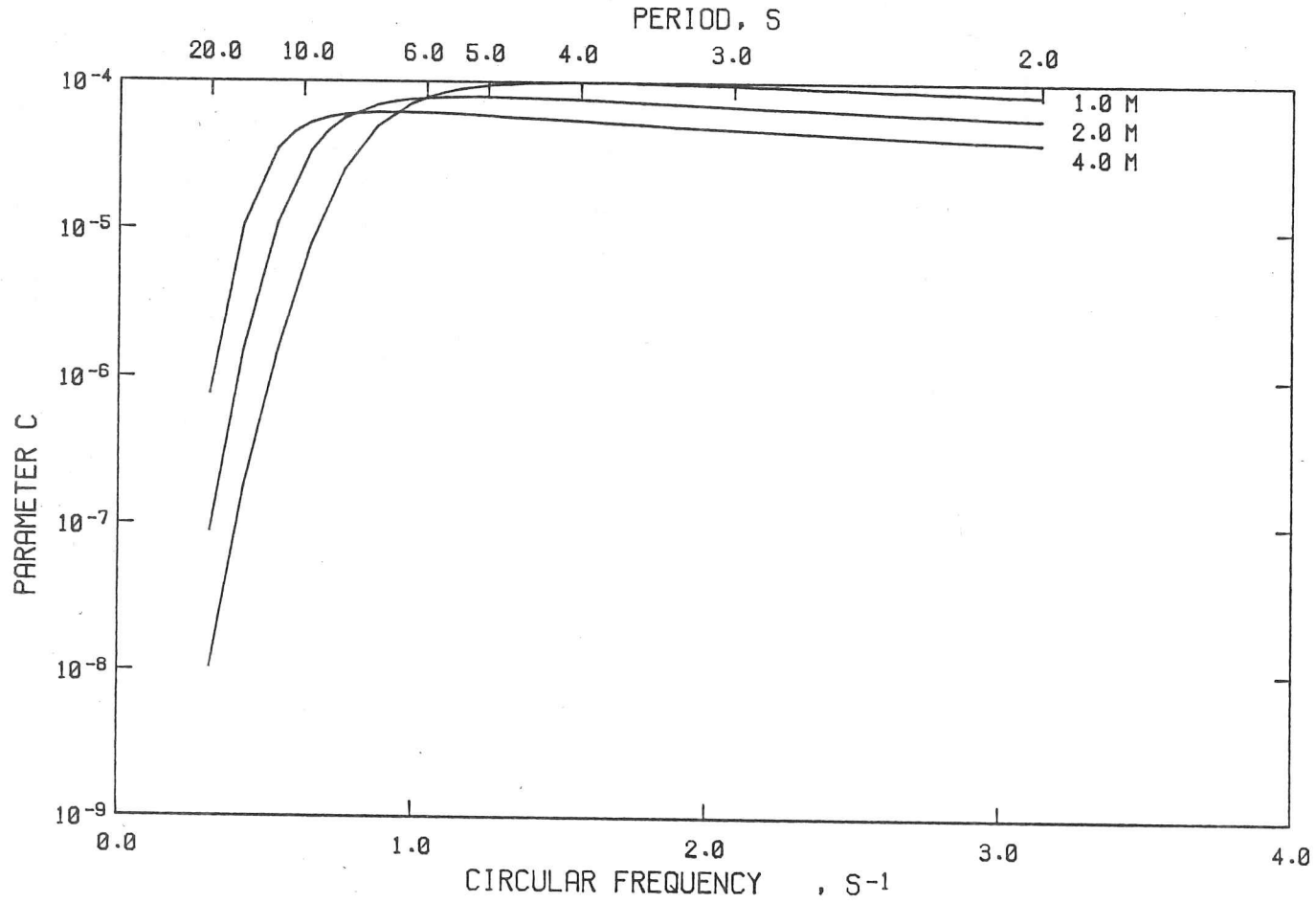

Fig. 4.6 The behaviour of parameter $c(\omega, h)$ at three ice thicknesses.

asymptotic expansion it is easy to show by substitution into equation (4.46) that the attenuation is very small. The sea ice then effectively behaves as a continuous medium composed of a dense cover of small non-interacting mass points (Weitz and Keller, 1950; Peters, 1950; Keller and Weitz, 1953) if this slight attenuation is neglected.

It therefore seems that the validity of equation (4.49) is limited to temperatures not too close to the melting point since this equation implies an increase in the attenuation coefficient α_1 with surface temperature. Hence, α_1 increases to a maximum for surface temperatures close to the melting point and then decreases to zero at the melting point. The position of this maximum is determined by the properties of the material, the wave period and the sea ice thickness. Preliminary results from laboratory controlled experiments to measure wave decay in frazil ice indicate the expected large values for the attenuation coefficient at temperatures close to the freezing point of water (S. Martin, personal communication, 1978).

As well as the propagating wave discussed above, we noted earlier the existence of two waves which are important close to their point of generation but decay within a few hundred metres so as to become unmeasurable. Since we are mainly concerned in this chapter with waves which propagate far into the sea ice cover, we shall consider these waves only briefly. It is interesting however to compare the temperature dependence of wave numbers k_2 and k_3 with those of the propagating wave. It is found that the wave numbers k_2 and k_3 are only slightly dependent on temperature. This dependence is negligible when compared with that of the attenuation coefficient α_1.

The model for floating sea ice that we have chosen therefore predicts three wave solutions; a propagating wave with the temperature dependence entering only through some small decay rate and two waves with substantial attenuation which may essentially be regarded as being temperature independent. Clearly, in looking

at waves far from an ice edge, the surface temperature is an extremely important parameter which cannot be overlooked. Any experiment which hopes to gain some insight into the physical behaviour of sea ice by measuring rates of decay of ocean waves must therefore monitor local air and sea temperatures continuously in addition to parameters such as ice thickness and wave period.

In the above analysis we have made no simplifying assumptions concerning the relative magnitudes of $M^{(0)}$, $M^{(1)}$ and $M^{(2)}$. One might suspect, looking at their behaviour for small argument (4.28), that $M^{(1)}$ is small compared to $M^{(0)}$ and $M^{(2)}$ and might be neglected (Hutter, 1973). This yields a considerably simplified system of equations which may be solved in a similar way. However, a comparison of wave numbers produced as solutions from the respective dispersion equations shows that such an approximation is reasonable only for characteristics controlled by the elastic properties. We shall therefore retain the former solutions.

4.8 The Wave Solution including Rotatory Inertia and Transverse Shear

Until now we have not used the most general equation for the displacement w as derived in Chapter 3. Instead a simpler equation was employed neglecting the effects of rotatory inertia and transverse shear. Such effects were found to be important in the corresponding elastic theory (Mindlin, 1951) only for waves of high frequency or for thick plates so that their neglect seems reasonable given the range of sea ice thicknesses and wave periods likely to be encountered. We might therefore expect the wavelength predicted by the dispersion equation neglecting rotatory inertia and transverse shear to become less accurate as wave period decreased or sea ice thickness increased. The attenuation coefficient, however, has not yet been discussed and no intuitive argument based on the corresponding elastic theory can yield information as to its behaviour. With this in mind it is necessary to solve the flexural wave problem for the more general equation including rotatory inertia and transverse shear in order to find where the simpler model becomes inadequate.

We rewrite the relevant equations here for convenience. The equation for the displacement w (3.58) may be written

$$\left[\frac{2}{1-\nu}\Pi\circ\nabla^2-\frac{\rho h^3}{12}\frac{\partial^2}{\partial t^2}\right]\left[\Gamma\circ\nabla^2-\rho h\frac{\partial^2}{\partial t^2}\right]w$$
$$+\rho h\Gamma\circ\frac{\partial^2 w}{\partial t^2}=\left[\frac{\rho h^3}{12}\frac{\partial^2}{\partial t^2}+\Gamma\circ-\frac{2}{1-\nu}\Pi\circ\nabla^2\right]q, \qquad (4.50)$$

where

$$\left.\begin{aligned}\Pi &\equiv M^{(2)}-M^{(1)}\circ\left[M^{(0)}\right]^{-1}\circ M^{(1)},\\ \Gamma &\equiv M^{(0)}-M^{(1)}\circ\left[M^{(2)}\right]^{-1}\circ M^{(1)}.\end{aligned}\right\} \qquad (4.51)$$

The expression for q may also be written down as before

$$q=-\rho'\left(gw+\frac{1}{k}\frac{\partial^2 w}{\partial t^2}\right). \qquad (4.52)$$

Denoting the complex moduli of Π and Γ by Π^* and Γ^* respectively and assuming that the displacement w may be written as the sum of wave modes of the form $e^{\pm i(kx-\omega t)}$, a substitution into equation (4.50) yields the dispersion equation

$$\frac{2}{1-\nu}\Pi^*\Gamma^*k^5+\left[\frac{2}{1-\nu}\Pi^*(\rho'g-\rho h\omega^2)-\frac{\rho h^3}{12}\Gamma^*\omega^2\right]k^3$$
$$-\frac{2}{1-\nu}\rho'\Pi^*\omega^2+\left[(\rho'g-\rho h\omega^2)\left(\Gamma^*-\frac{\rho h^3}{12}\omega^2\right)\right]k \qquad (4.53)$$
$$-\rho'\omega^2\left(\Gamma^*-\frac{\rho h^3}{12}\omega^2\right)=0.$$

This equation, though somewhat more complicated than its equivalent when rotatory inertia and transverse shear are neglected, may be solved in exactly the same way. Certain roots may be rejected on the grounds of boundedness (see Chapter 2) leaving three relevant wave numbers denoted by k_1, k_2 and k_3 as before (eq.4.47).

Numerical values of the wave numbers k_1, k_2 and k_3 exhibit exactly the same behaviour as regards period, ice thickness and temperature as did the simpler model. In fact the two models differ significantly

only for high frequency waves or unrealistically thick sea ice. Since high frequency flexural oscillations of sea ice are unlikely to occur by natural means and average sea ice thicknesses greater than 5 m are unusual, the model neglecting rotatory inertia and transverse shear is adequate.

With the introduction of rotatory inertia and transverse shear one is tempted to extend the possible application of our solution somewhat further. Two possible questions arise; can the wave period be decreased so that we may look at high frequency waves, can the ice thickness be increased to cope with oscillation of glacier tongues due to ocean waves? We will answer each question in turn.

Because of the small amount of energy at the high frequency end of a typical open ocean wave spectrum (Bretschneider, 1963; Pierson and Moskowitz, 1964), high frequency flexural oscillations would be of artificial origin. Such waves have been studied in detail for thin lake ice (Ewing *et al*, 1934; Ewing and Crary, 1934; Press *et al*, 1951) using an elastic analysis neglecting rotatory inertia and transverse shear but including the compressibility of water. Good agreement was obtained using arrays of geophones to measure displacements due to explosion-generated waves up to frequencies of approximately 100 Hz. The present model includes the added sophistications of rotatory inertia and transverse shear and a very small temperature dependent attenuation. It does not take into account the compressibility of the underlying water. Anticipating the type of experiment likely to be carried out to measure high frequency ice-coupled flexural waves, it is unlikely that the very slight attenuation coefficients predicted could be measured. A better theoretical treatment would take into account the compressibility of the water and rotatory inertia and transverse shear but neglect any viscous properties of sea ice. The replacement of the equation of flexure used by Ewing and Crary (1934) by that of Mindlin (1951) would pose no serious problems.

The present theory may certainly be extended to cope with oscillations of glacier tongues due to ocean waves but we are limited

by some of our original assumptions. It is unlikely, for instance, that an ice tongue some 200 m thick should have a linear temperature distribution in the vertical direction. Also, given the length of waves likely to be encountered and the large proportion of ice submerged or possibly grounded, a cantilever beam analysis in shallow water might be more appropriate. The related problem of calving of ice bergs by glacier tongues has been discussed in detail by Holdsworth (1969, 1971, 1974) but until recently little data were available on flexural waves. Data collected on the Erebus ice tongue and surrounding sea ice (Goodman, D.J., personal communication, 1978) are currently being spectrally analysed and promise some interesting results. Goodman hopes to derive a transfer function from his data which will show how wave energy in the sea ice couples with the ice tongue. It is felt that discussion of flexural waves in extremely thick sea ice should be postponed until such an analysis has been completed.

4.9 Summary

In this chapter we have derived a deep water solution for flexural-gravity waves propagating under a temperature dependent sea ice sheet of constant thickness. Because of the lack of experimental data, it was necessary to assume certain reasonable material characteristics. A Maxwell-Voigt spring-dashpot system was chosen to represent the sea ice with temperature dependence entering through a parabolic shifting of properties relative to some datum temperature. Such a choice is not important in itself since any linear viscoelastic law (not necessarily a mechanical analogy) and any temperature shifting function may be chosen. One is limited solely by the ability to solve the subsequent mathematics. With the model chosen, relevant complex moduli and Laplace transforms were evaluated. Two solutions were then considered; a solution neglecting rotatory inertia and transverse shear and a solution including these effects. It was found that the former solution was adequate for reasonable sea ice thicknesses and wave periods likely to be encountered in nature. The difference between the two theories is only significant for artificially generated seismic flexural waves or ice shelves.

The inclusion of temperature in a model of waves-in-ice was found to be extremely important only as far as the attenuation coefficient of the propagating wave was concerned. A power law reflecting the shift function chosen was found to fit the temperature dependence with negligible error for physically measurable temperatures. High attenuation was found at temperatures close to the melting point. The wavelength and phase velocity (Lorrain and Carson, 1970, app.E) for the propagating wave was found to show negligible dependence on temperature.

The results of this chapter clearly demonstrate that any experiment designed to measure the decay of flexural gravity waves with distance due to viscous losses in sea ice must measure a surface temperature at each recording site. If sea ice does behave as a thermorheologically simple material, then effects depending on elastic properties may be regarded as independent of temperature.

CHAPTER 5

EXPERIMENTS TO MEASURE ICE COUPLED WAVES

EXPERIMENTS TO MEASURE ICE COUPLED WAVES

5.1 Introduction

The preceding chapters have discussed two possible theoretical models for modelling the flexural behaviour of floating sea ice:- a temperature independent formulation where any change in the material properties through the ice is neglected; and a thermorheologically simple formulation where such effects are included. Both models assume a linear viscoelastic phenomenological response calling on the early work of Tabata (1955a, 1958a) to provide some of the necessary empirical data. Unfortunately, since sea ice is a composite with properties which depend on both the conditions under which it is formed and the conditions of the day, it is questionable whether data measured locally on one ice sheet may be applied to that ice sheet as a whole or, worse, to other ice sheets with totally different growth histories. Further, when the simple viscoelastic formulation is extended to cope with the more realistic situation of an anisotropic ice sheet whose temperature gradient is significant in the vertical direction, no progress can be made mathematically without additional assumptions. The first of these, that sea ice is thermorheologically simple, could be tested experimentally and would make the second assumption unnecessary by providing an empirically derived shift function. Given no such shift function however, it has been assumed parabolic.

The original purpose of setting up equations for the flexure of a cover of floating sea ice was to consider the effect of such a cover on an impinging ocean swell. Observations have shown the existence of flexural waves in ice with periods of the same order of magnitude as incident open water waves but the nature of the coupling between the forcing and the effect or indeed, the nature of the ice-coupled wave, is unclear. Few experiments have been carried out with any previous theoretical work available to dictate those parameters which should be measured so that the theoretical solutions to this problem found in earlier chapters lead to a series of questions which may only be answered by *in situ* experiments.

A series of experiments to measure flexural-gravity waves at sites situated on floating sea ice was initiated in February, 1977. All experiments were carried out near Twillingate, Newfoundland (fig.5.1) since this area provided readily accessible floating fast ice so that logistic expenses could be minimized. The operation formed part of a joint venture between C-CORE, Memorial University of Newfoundland and the Scott Polar Research Institute, Cambridge to look at various properties of sea ice. Problems included the physical properties of sea ice (Lau and Rossiter, 1978), the impulse radar sounding of sea ice (Rossiter et al, 1977) and the measurement of flexural-gravity waves in ice using strainmeters (Squire and Allan, 1979; Allan and Squire, 1978; Squire, 1978).

Two types of strainmeter were used in the wave experiments and both are discussed briefly below. A more complete account of each instrument may be found in Allan and Windsor, 1977 and Goodman, 1977 respectively. It should be remembered that both types of strainmeter measure the extension in their gauge length. To convert to strain the record must be calibrated and divided by the gauge length.

The C-CORE Wire Strainmeter

This instrument is a modified version of a strainmeter designed and built at the Department of Geodesy and Geophysics, University of Cambridge for the purpose of measuring earth tides (King and Bilham, 1973). The modifications carried out were aimed at adapting the instrument for use on sea ice. They were prompted by work on fast ice at Bylot Sound, Thule, Greenland (Goodman et al, 1975) and Point Amour, Labrador (Allan, 1975).

Each strainmeter may be divided into three component parts; the active unit, the reference wire and the range-reset mechanism. The active unit (fig.5.2) incorporates an L.V.D.T. (linear variable differential transformer) with a core mounted on a lever suspended by invar flexure pivot hinges. The invar reference wire is tensioned to 5 N by a weight attached to the lever. Invar is used to minimize fluctuations in the length due to local temperature

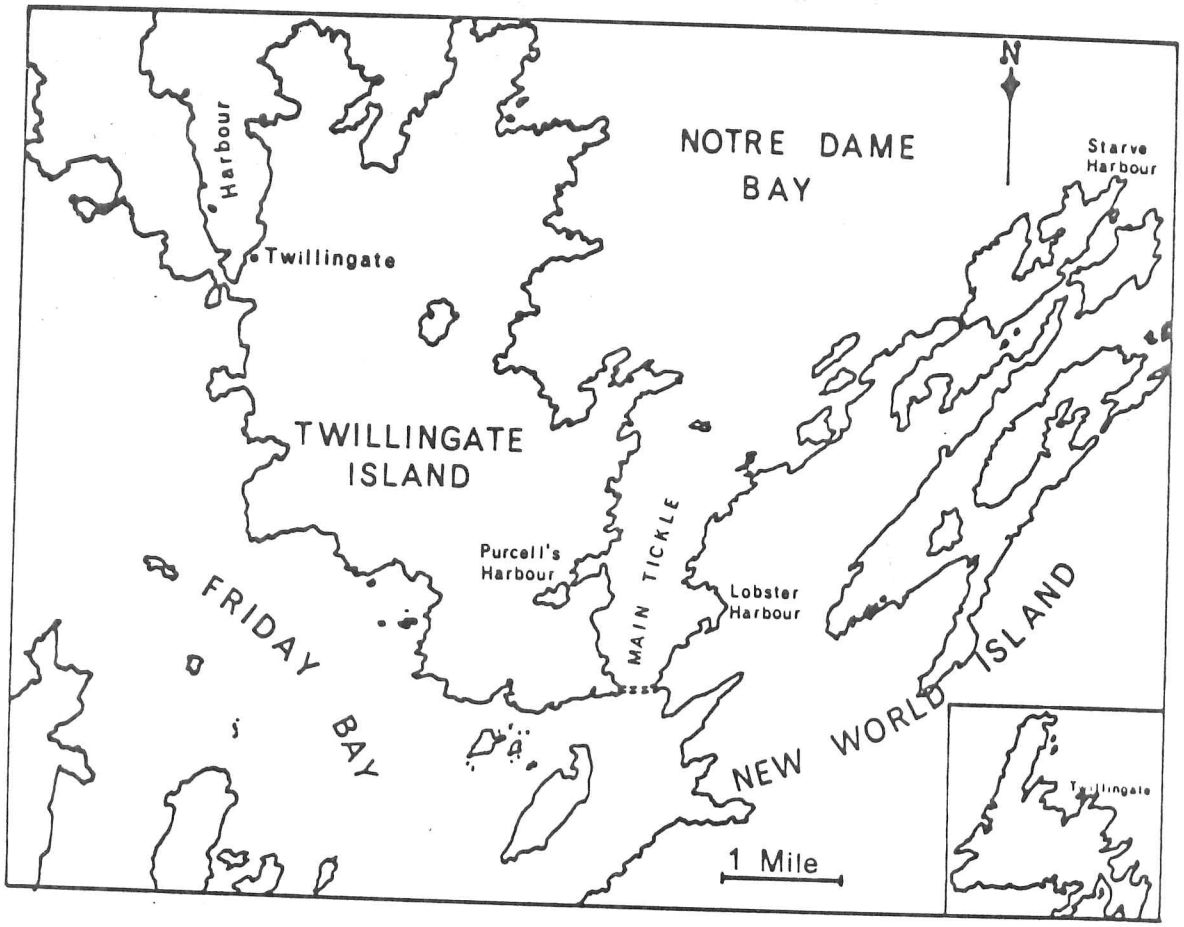

Fig. 5.1 Twillingate Island and New World Island. Inset shows location relative to Newfoundland.

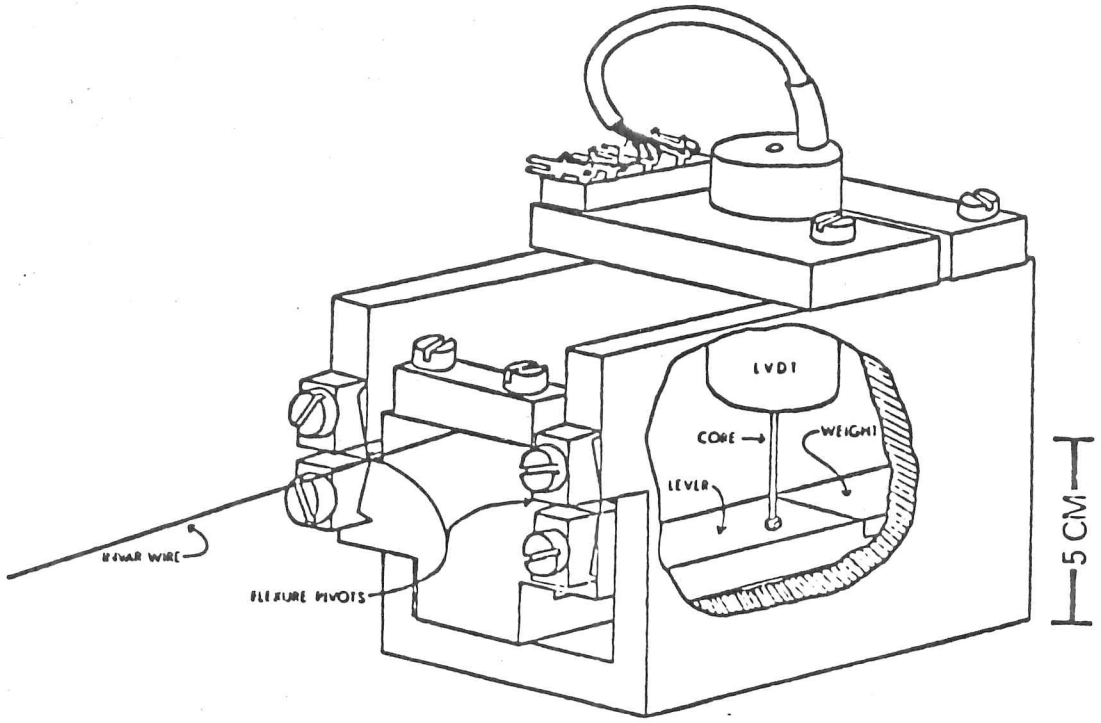

Fig. 5.2 The active unit of C-CORE strainmeter.

changes. Figure 5.3 shows the range-reset mechanism whereby the range of the instrument is increased from 0.05 mm to 5 mm by firing a small servo motor which drives a screw to return the L.V.D.T. core back to its centre position. The motor is fired when the strain causes the transducer to exceed its range. The instrument is accompanied by an electronics package which provides amplification and the limit detection and control for the servo motor. In cases where the environment is particularly severe or there is a danger of loss of instrument, an expendable 8-channel telemetry system may be used to transmit data back to a field laboratory.

The S.P.R.I. Rod Strainmeter

The rod strainmeter was developed by Dougal Goodman of the Cavendish Laboratory, Cambridge University using the experience gained with both the early development of the wire strainmeter and preliminary experiments with a prototype rod strainmeter in Greenland, 1974. The accompanying electronics package was developed with close collaboration between the Department of Geodesy and Geophysics and the Scott Polar Research Institute, University of Cambridge (Goodman and Neal, 1977).

The principle of the rod strainmeter is simpler than the wire strainmeter since the transducer is mounted horizontally so that no lever is required to turn the motion through ninety degrees. The core is fixed directly to a one metre rod of invar so that when strain occurs, the rod pushes or pulls the core out of the transducer body. Range-reset is in this case achieved by driving the entire transducer assembly horizontally independent of the core. Problems in the prototype instrument concerning lateral movement of the core within the transducer body were successfully overcome in the present design by setting the core between two sets of three steel springs mounted at right angles.

The Location

The choice of a suitable experimental site to measure the interaction of ocean swell with sea ice was based on several

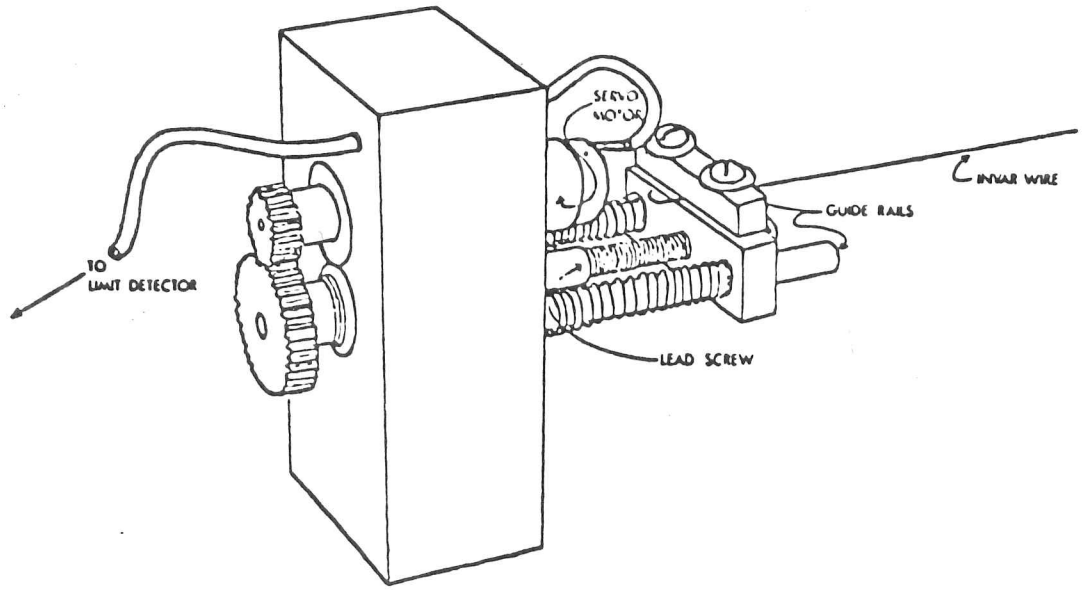

Fig. 5.3 The range reset mechanism of C-CORE strainmeter.

criteria. The sea ice needed to be as close to semi-infinite as possible so that from a logistics point of view, fast ice was chosen. It needed to be as smooth as possible since thin plate theory contains as a variable the cube of the plate thickness (Timoshenko and Woinowsky-Krieger, 1959) so that any variations would be amplified considerably. The ice chosen had to be reasonably safe but open to the North Atlantic so as to receive waves of measurable amplitude. It is clear from a map of the Twillingate area (fig.5.1) that there are several suitable bays on the northern side of Twillingate Island and on the adjacent New World Island. Tentatively, Twillingate Harbour had been chosen during the previous summer as a suitable site but it was now clearly unsuitable since the ice was cracked and uneven. It proved difficult to find smooth, safe ice on Twillingate Island and the eventual choice was Starve Harbour, a north-east-facing bay on New World Island (fig.5.4).

Starve Harbour is a small community on Salt Harbour Island about 10 miles from Twillingate. The bay opens on to the North Atlantic so that it receives a reasonable swell but because of a small island in its mouth, the fast ice had not broken up in the early stages of growth and was a smooth sheet of sea ice of thickness approximately 28 cm. There was a clear ice edge about 50 m to the landward side of this island beyond which the ice was made up of rafted wave-broken ice cakes and small floes which moved to-and-fro with the incoming swell. Later in the season the fast ice reached a thickness of approximately 50 cm and extended to the other side of the island making it much more difficult to define a clear edge. A chart of the local area shows Starve Harbour to vary between 20 m and 30 m in depth though a shoal of only 5 m in depth was observed in one localized area. Starve Harbour therefore provided a suitable, though far from ideal, site for the first part of the season where the majority of the experiments were carried out using the newly developed rod strainmeter.

Early in March it was decided to relocate the site for a new series of experiments to measure the phase of the incoming flexural wave and look at effects local to the ice edge. These experiments

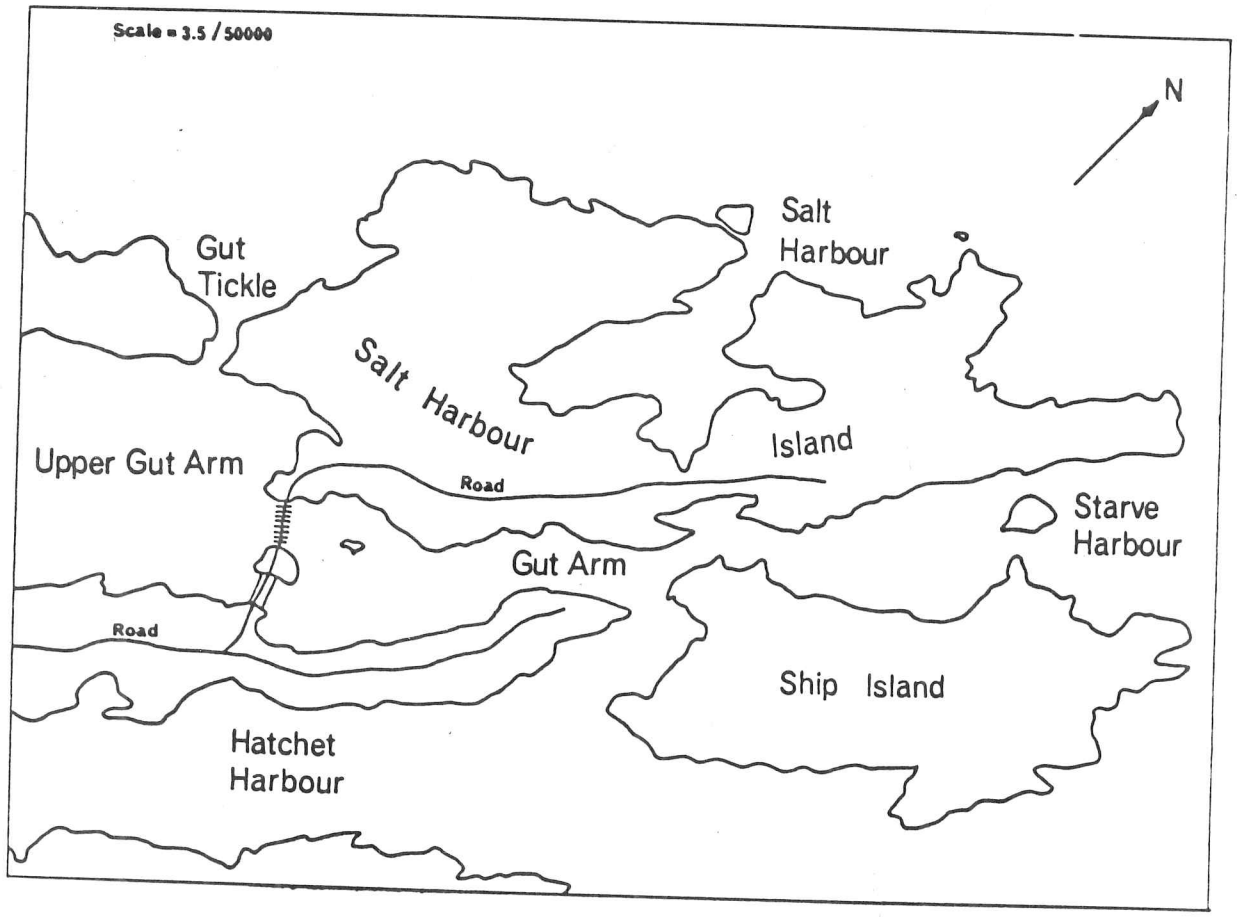

Fig. 5.4 Starve Harbour and surrounding islands.

were to be carried out using C-CORE strainmeters and the newly developed telemetry system. The site chosen was Main Tickle (fig.5.1), a north-facing, deep water strait between Notre Dame Bay and Friday Bay. A causeway joining Twillingate Island to New World Island modifies the oceanography of the area however and effectively creates a deep bay. Ice in Main Tickle extended from the causeway as far as Purcell's Harbour and was made up of a large area of smooth ice of about 50 cm thickness though close to the edge the ice became much rougher. Unfortunately a storm broke up much of the ice sheet before the instruments could be deployed and a new edge formed across from Lobster Harbour. The remaining experiments were carried out on this ice.

The remaining chapter will be divided into three discrete sections, a discussion of some additional observations gained from one of the experiments and a summary. Each section will discuss a single experiment, its associated theory and the data processing. The sections are arranged such that there is a natural development in the data processing rather than in the order in which the experiments were carried out. All data processing was carried out on a Hewlett Packard, 5451B Fourier Analyser using systems programs written by the author.

5.2 Power Spectral Density and Relative Power Between Instruments

Theory

We suppose that the strain $\varepsilon(t)$ experienced at the surface of floating sea ice is an example of a random process. Then, for an ensemble of floating ice sheets under the same physical and meteorological conditions, strain records $\varepsilon_r(t)$ taken simultaneously at the same point on each ice sheet will not be identical or closely similar in nature. Such an assumption is reasonable for strains due to naturally generated flexural-gravity waves propagating along the interface between the ice and water (Squire and Allan, 1979). Further we assume that the random process is both stationary and ergodic. That is to say, the statistical properties of the ensemble do not change with time and a single

sample strain record characterizes the ensemble statistically.

For a random process it is not possible to define a Fourier transform in the usual way, namely

$$\mathcal{F}\{\varepsilon(t)\} = \int_{-\infty}^{\infty} \varepsilon(t) e^{-i2\pi ft}\, dt, \tag{5.1}$$

since such a process cannot satisfy the conditions of absolute integrability. In this and subsequent equations $\mathcal{F}\{.\}$ denotes the Fourier transform and f $(=\omega/2\pi)$ is the frequency.

The sample function $\varepsilon_T(t)$, however, is of finite duration. Specifically,

$$\varepsilon_T(t) = \begin{cases} \varepsilon(t), & -T \leqslant t \leqslant T, \\ 0, & |t| > T. \end{cases} \tag{5.2}$$

This satisfies the condition for integrable square functions, that is

$$\int_{-\infty}^{\infty} |\varepsilon_T(t)|^2 dt < \infty, \tag{5.3}$$

so that the Fourier transform may be defined as

$$\mathcal{F}\{\varepsilon_T(t)\} = \int_{-\infty}^{\infty} \varepsilon_T(t) e^{-i2\pi ft}\, dt, \tag{5.4}$$

and will exist for all $T<\infty$.

From Parseval's theorem (Lathi, 1965, ch.2), we may write

$$\int_{-\infty}^{\infty} \varepsilon_T^2(t)\, dt = \int_{-\infty}^{\infty} |\mathcal{F}\{\varepsilon_T(t)\}|^2\, df. \tag{5.5}$$

It is not possible to allow $T\rightarrow\infty$ since $\mathcal{F}\{\varepsilon_T(t)\}$ is then not defined. However the expected value of $(|\mathcal{F}\{\varepsilon_T(t)\}|^2)/2T$ does exist so that

$$E\left[\frac{1}{2T}\int_{-\infty}^{\infty} \varepsilon_T^2(t)\, dt\right] = E\left[\frac{1}{2T}\int_{-\infty}^{\infty} |\mathcal{F}\{\varepsilon(t)\}|^2\, df\right], \tag{5.6}$$

where $E[.]$ denotes the expected value.

Hence

$$\overline{\varepsilon^2} = \int_{-\infty}^{\infty} \underset{T\to\infty}{\text{Limit}} \frac{E[|\mathcal{F}\{\varepsilon_T(t)\}|^2]\,df}{2T} , \qquad (5.7)$$

since the process is stationary and ergodic. The integrand in this expression is called the two-sided power spectral density. If we restrict the frequency to positive values then we may define the more usual one-sided power spectral density as

$$G(f) = 2 \underset{T\to\infty}{\text{Limit}} \left[\frac{E[|\mathcal{F}\{\varepsilon_T(t)\}|^2]}{2T} \right] . \qquad (5.8)$$

Returning to the particular problem of flexural oscillations induced by ocean waves, we note that the assumption of stationary statistics is valid only for timescales which are not too long. On the other hand, a single sample will produce a power spectral density with a standard error of unity (Wadhams, 1973b) so that it is clear that some averaging is necessary. Two possibilities arise; averaging between a number of power spectral densities taken over short sections of data or frequency averaging over a single power spectral density representing a longer section of data. The author has chosen the former approach since the software was readily available at C-CORE. The latter method is recognized as being less likely to introduce errors since the effect of the window function is minimized. It should be borne in mind, however, that the difference between the two resulting power spectral densities is much less than their standard errors. It is clear then that we have two opposing aims; to average as much as possible but also to retain stationarity. For the present analysis, each power spectral density was derived from twelve blocks of data of 320 s duration. There is no hard-and-fast rule however and these values were chosen from the wave conditions at the time of recording the data.

Experiment

Three strainmeters 1, 2 and 3 were deployed in a straight line

on fast ice at Main Tickle, Twillingate (fig.5.1) with the purpose of monitoring the local strain field around an ice edge as a function of distance from that edge. Instrument separations of 10 m (and later 5 m) were chosen with strainmeter 1 positioned as close to the edge as possible. The experiment was allowed to run for about fifteen hours during which time any changes in the local oceanographic conditions could be observed in the strain records of individual instruments.

The Analysis

The fifteen hours of recorded data were divided into blocks of 320 s duration, calibrated and converted to strain by division by the gauge length of the instrument (2 m). In this form a running average power spectral density program could be applied to the data over sets of twelve blocks so that the fractional error in any magnitude was $1/\sqrt{12}$. Typical spectra are shown in figure 5.5 for each of the three strainmeters. Each power spectral density shows clear peaks around periods of 6.4 s, 11.0 s and 13.3 s with most of the energy at the short period. These spectra represent the strain field soon after the instruments had been set up. Subsequent spectra show a gradual widening of the peak around 6.4 s and gradual decrease in the magnitude by approximately one order. This change reflected the onset of a storm blowing from the east across the bay.

The sample power spectral densities shown in figure 5.5 indicate that the power density at a particular frequency changes as the wave penetrates the ice cover. Further, the way in which it changes is a function of frequency. In order to study this effect in more detail we must find the root-mean-square (R.M.S.) strain associated with a particular peak in the spectrum. This may be found by integration of the spectra over selected bandwidths and then taking the square root. A bandwidth of 5/320 Hz was used in the present analysis. The total R.M.S. strain in the spectrum may be found in a similar way by integrating between the limits of zero Hertz and the maximum frequency in the band and then square rooting. A brief look at the power spectral densities showed significant energy

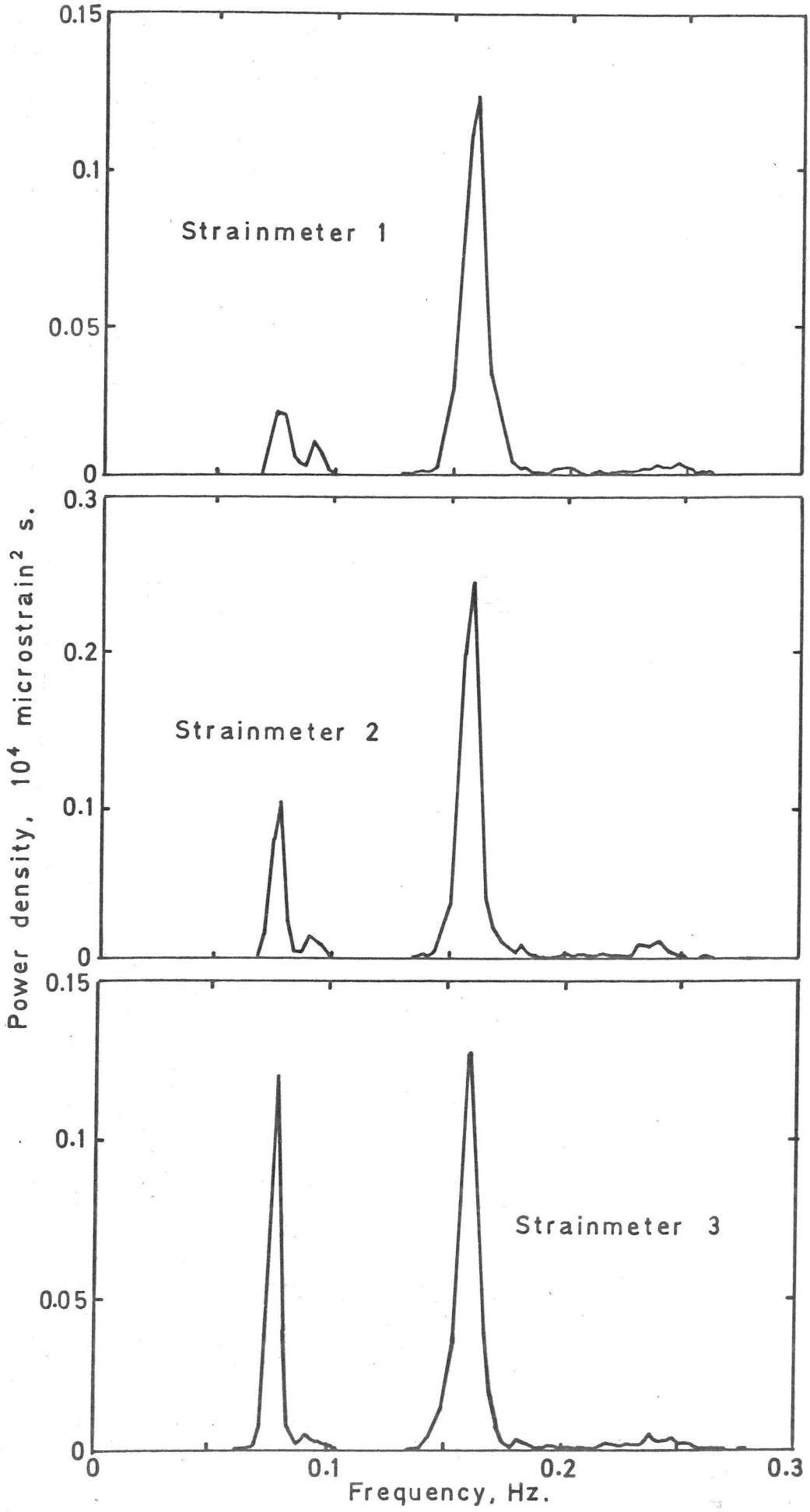

Fig. 5.5 Typical power spectral densities for strainmeters deployed at edge, 10 m back from edge, and 20 m back from edge.

around 5.82 s, 6.53 s, 11.03 s and 13.33 s so it is the strain centred at these periods and the total strain which are shown in figure 5.6.

Bearing in mind that the instruments are deployed at 10 m intervals back from the edge, the curves show a distinct change in magnitude with distance from the edge. The curves representing total R.M.S. strain show an increase and then decrease with distance from the edge whereas the curves representing strain around a particular frequency behave in a manner which depends on that frequency. This may be seen more clearly in figure 5.7 where the fractional change between strainmeters 1 and 2, and then 1 and 3 is considered. In figure 5.7a, all the curves are clustered between 1.0 and 2.0 indicating an increase in the R.M.S. strain. In figure 5.7b, however, most of the curves lie between 0 and 1.0 indicating a decrease in strain. The exception is the long wave which appears to show hardly any change in magnitude. As might be expected, the scatter in the curve increases as the original strain magnitudes decreases. The means and variances over the entire experiment are presented in Table 5.1.

2/1	1	2	3	4	5
Mean	1.24	1.13	1.20	1.24	1.55
Variance	0.02	0.01	0.02	0.01	0.08

3/1	1	2	3	4	5
Mean	1.00	0.89	0.78	0.85	1.57
Variance	0.02	0.00	0.03	0.02	0.12

Table 5.1 The means and variances for fractional changes in R.M.S. strain relative to the edge strainmeter.

In interpreting the data it must be remembered that the infinitesimal strain at a free edge is zero. The non-zero strain magnitude seen in the power spectral densities of strainmeter 1 are therefore due to the finite length of the instrument.

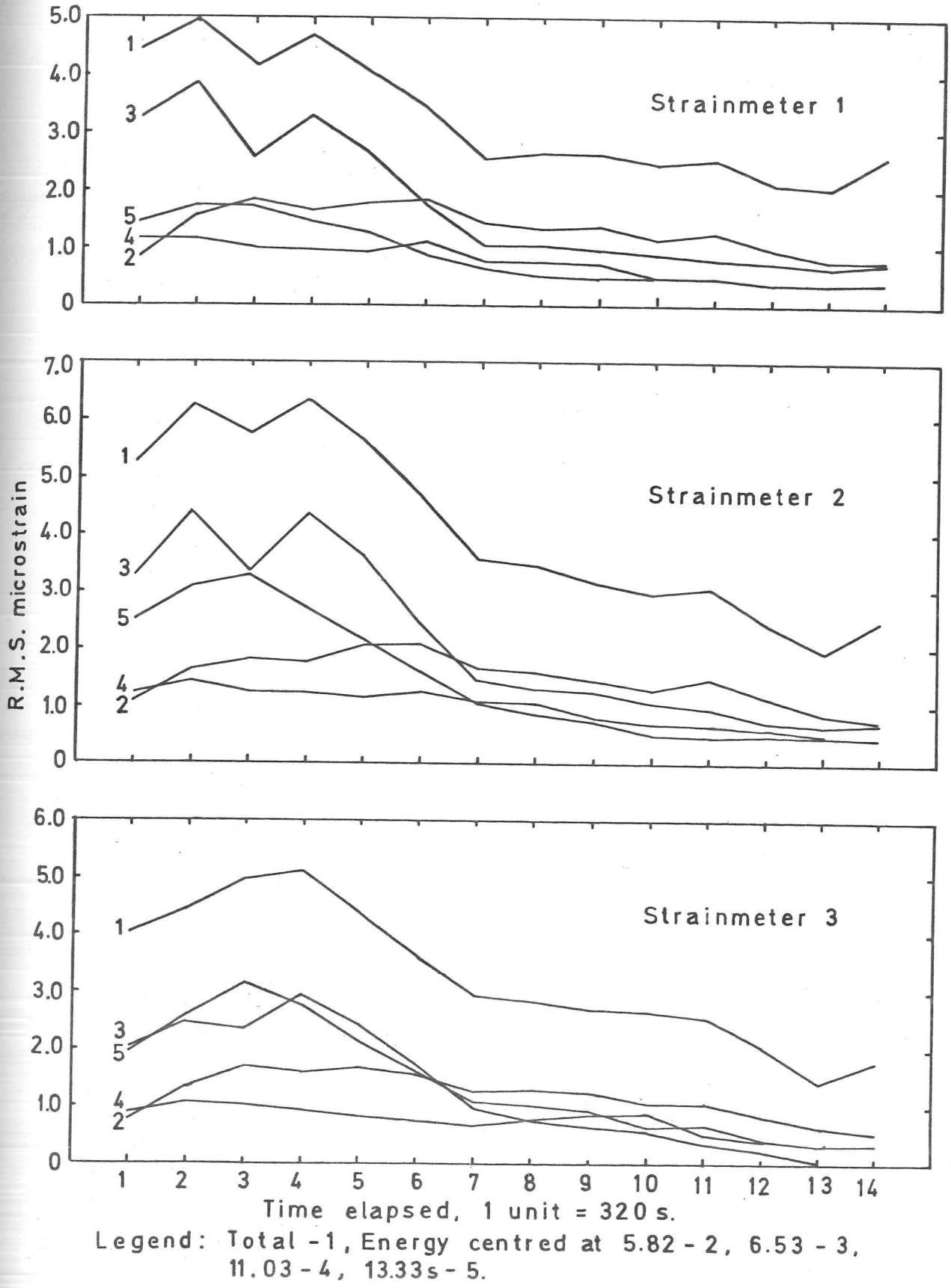

Fig. 5.6 The R.M.S. strain as measured by strainmeters 1, 2 and 3 for significant magnitudes in the respective power spectral densities.

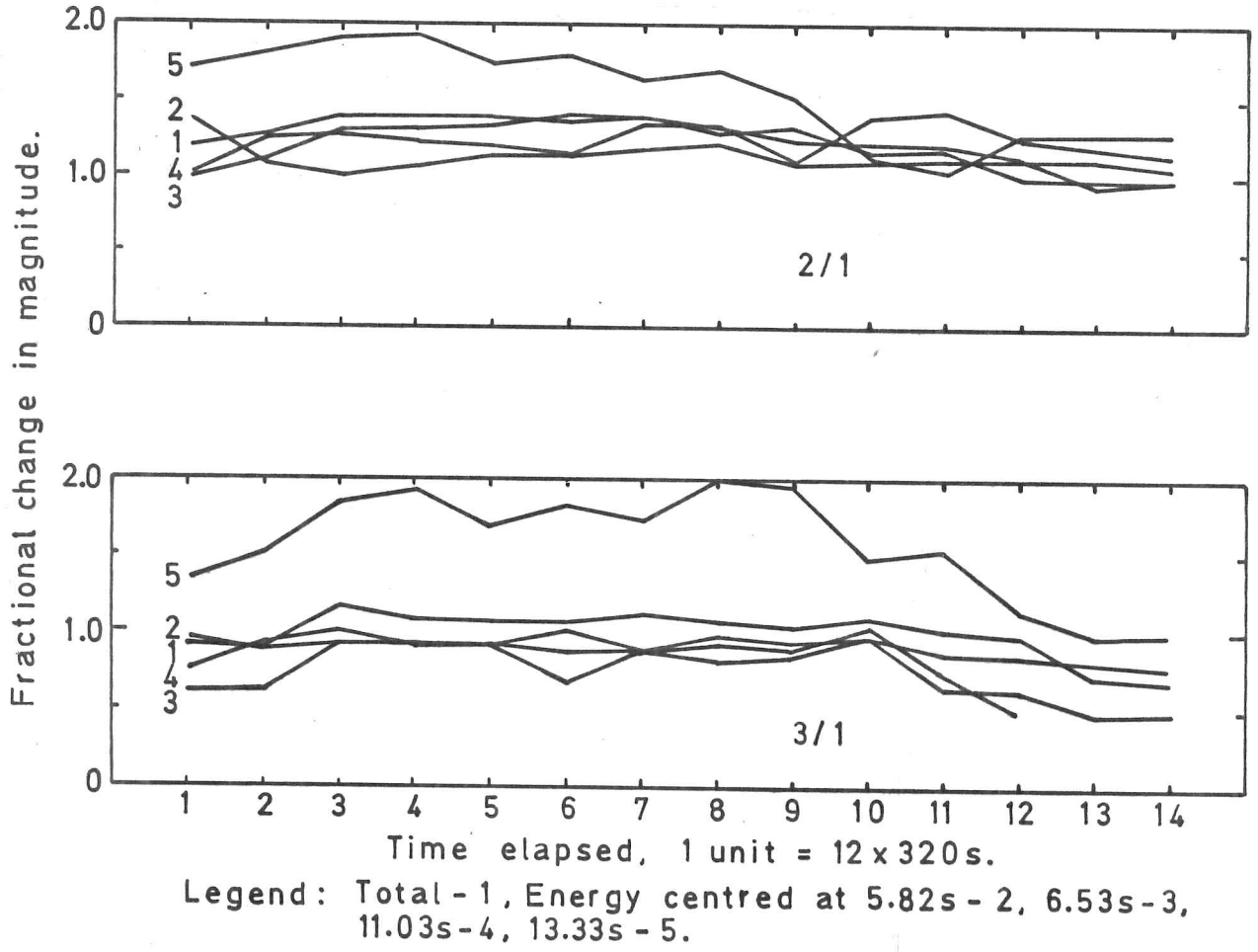

Fig. 5.7 The fractional change in R.M.S. strain between strainmeters 1 and 2, and 1 and 3 for significant magnitudes in the respective power spectral densities.

5.3 The Phase Change between Strainmeters and the Dispersive Properties of Sea Ice

Theory

The theoretical models discussed in earlier chapters have shown that the propagating ice-coupled flexural-gravity wave with least attenuation has a wave number whose real part may be assumed to be independent of surface temperature. We have hence been able to plot graphs of the expected wavelength in various thicknesses of sea ice as a function of period. Given an instrument, therefore, which is capable of measuring the strain due to these flexural-gravity waves at the ice surface, we are in a position to check these curves empirically. This is the purpose of the present experiment.

Consider the change in phase between two sites, x_1 and x_2, of known separation, sufficiently distant from the ice edge to neglect any effects due to local waves generated near the edge. A wave-generated displacement propagating between the two sites may then be assumed to be made up of a superposition of wave modes of the type

$$w = A \cos 2\pi\left(\frac{x}{\lambda} - ft\right), \tag{5.9}$$

where A is the amplitude, λ is the wavelength and other terms are as defined earlier. Any attenuation may be neglected so long as x_1 and x_2 are close together (a necessary condition also for a phase-type experiment). The phase change between x_1 and x_2 is therefore

$$\frac{2\pi}{\lambda}(x_2 - x_1), \tag{5.10}$$

so that given $(x_2 - x_1)$ and that it is possible to measure the phase change experimentally, we may find the wavelength λ for the wave mode. Hence, for a displacement made up of a superposition of such wave modes, we may find the wavelength as a function of frequency.

Experiment

Three strainmeters were deployed at 10 m intervals along a 358° line on fast ice at Main Tickle (fig.5.8). The aim of the experiment was to measure the phase change discussed above for the ice-coupled flexural-gravity wave spectrum. For an *in situ* experiment the forcing is not a single sinusoidal oscillation but a superposition of incident wave energies. It was therefore hoped to take advantage of this and, depending on the oceanographic conditions of the day, measure the wavelength for a variety of wave periods. Only those components of the spectrum with significant wave energy could be considered so it was impossible to predict in advance which frequencies would be present. Since three instruments were used, separations of both 10 m and 20 m were available. Both these distances are less than the smallest wavelength likely to be encountered so that any ambiguity in distinguishing consecutive cycles of the same wave is resolved.

The Analysis

Three possible methods of analysis were considered (Allan and Squire, 1978):- the cross correlation; the phase spectrum; and the frequency response function (or more generally, the transfer function). The cross correlation proved to be difficult to interpret for all but the simplest of strain records. The phase spectrum method was slow and also carried with it large statistical errors. The method finally adopted was that of the frequency response function and the associated coherence function (Bendat and Piersol, 1971). This approach is often used in engineering applications to compare the input and output of a "black-box system".

Given signals from two strainmeters 1 and 2, say, at a known separation we define the frequency response function, H(f), as

$$H(f) = \frac{G_{12}(f)}{G_{11}(f)} \quad , \tag{5.11}$$

where G_{12} is the cross power spectral density between strainmeters 1

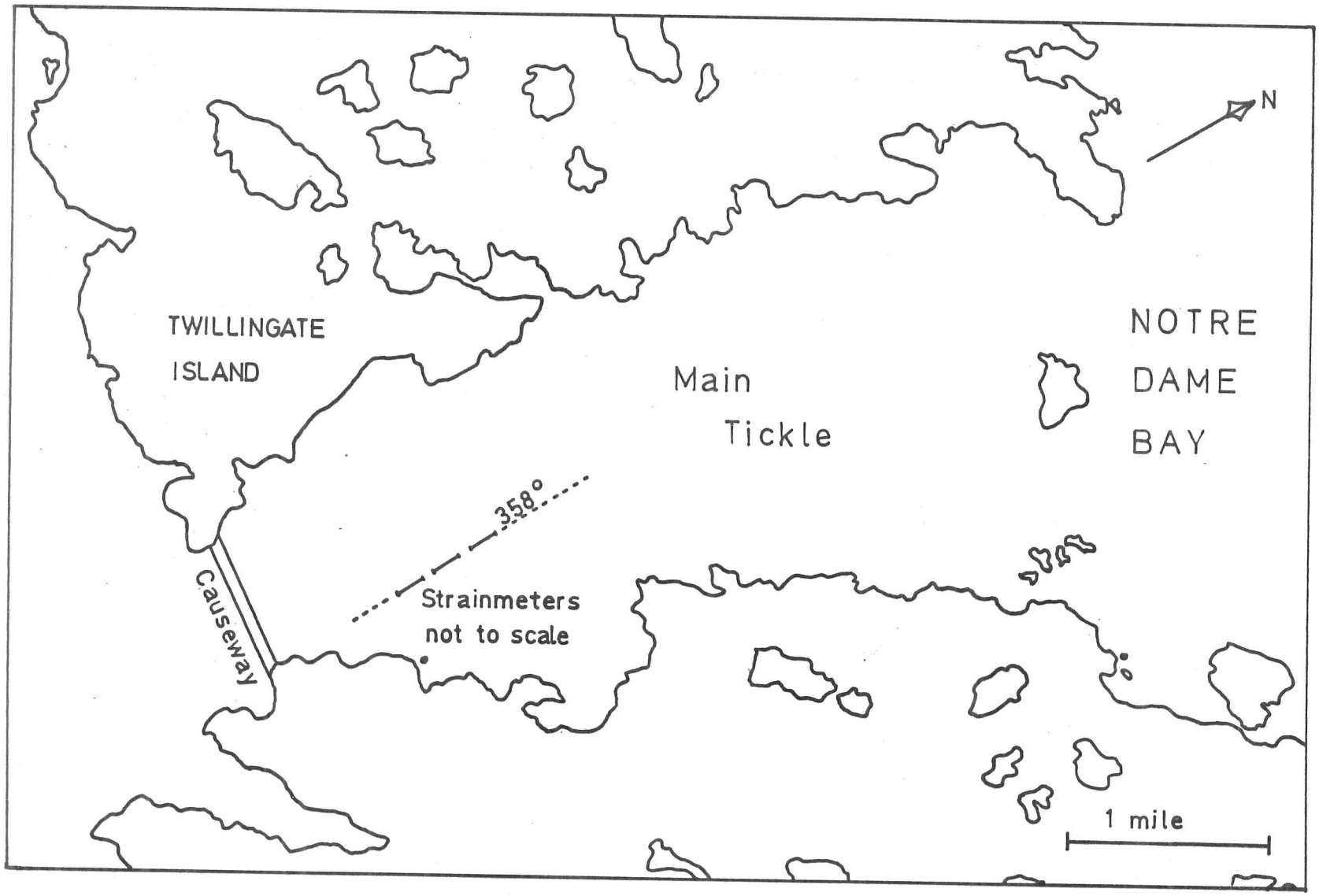

Fig. 5.8 Main Tickle showing layout of strainmeters.

and 2, and G_{11} is the auto power spectral density for strainmeter 1. The frequency response function is in general a complex quantity containing both magnitude and phase information. These are referred to as the gain factor and the phase factor respectively. Writing the frequency response function an alternative way, namely the ratio of the Fourier transforms of signals 1 and 2, it is clear that the gain factor represents the change in amplitude between signals 1 and 2, and the phase factor, their change of phase. We therefore have a method by which to determine the phase change between two strainmeters, Averaging was carried out over approximately one hour, a reasonable time given the meteorological conditions over the duration of the experiment.

A measure of the validity of the frequency response function is provided by the coherence function, $\gamma_{12}^2(f)$, defined as

$$\gamma_{12}^2(f) = \frac{|G_{12}(f)|^2}{G_{11}(f)G_{22}(f)} , \qquad (5.12)$$

where G_{22} is the auto power spectral density for strainmeter 2. The function represents a measure of the degree of similarity between two signals and affords some measure of confidence in the associated frequency response function.

Using this approach the wavelength for a variety of periods, corresponding to a minimum coherence of 0.96, were chosen for both 10 m and 20 m separation (fig.5.9). Within the standard error the experimental data do not differ significantly from the theoretical curves and do not show a bias to either side. A chi-squared test

$$\chi^2 = \sum^{n} \frac{(\lambda_o - \lambda_t)^2}{\lambda_t} , \qquad (5.13)$$

where λ_o is the observed wavelength, λ_t is the theoretical wavelength and n is the number of samples, gave values for χ^2/n of 7.99, 12.15 and 16.97 for 0.5 m, 1.0 m of ice and the deep water wave respectively. A thickness of approximately 0.5 m was measured over the experimental site agreeing with the lowest chi-squared value.

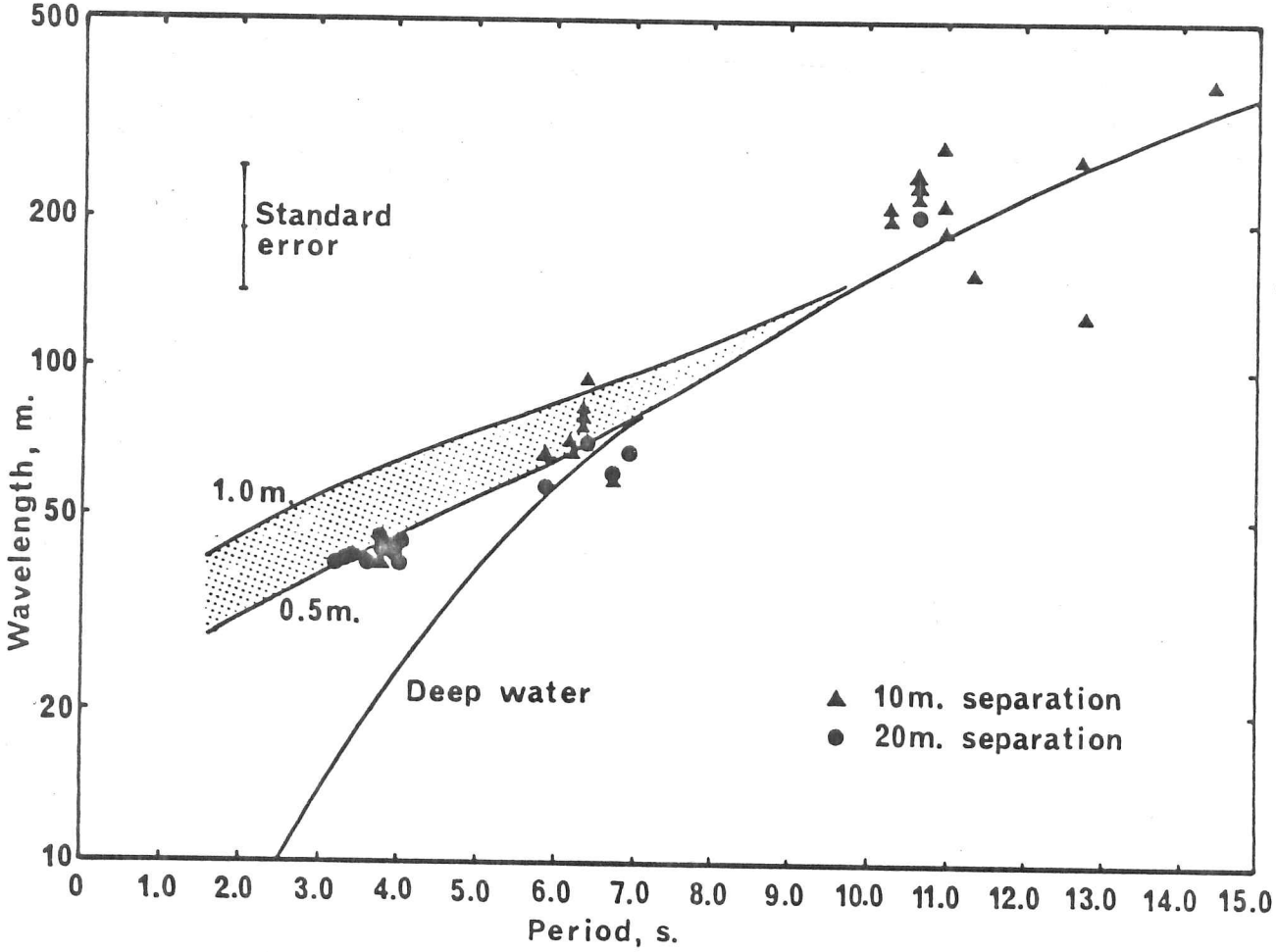

Fig. 5.9 Comparison of measured wavelength with that predicted by the theory of Chapter 2.

5.4 The Attenuation of Flexural-Gravity Waves by Sea Ice

Theory

In the previous section we have described an experiment to measure the wavelength in ice as a function of period and compare the values obtained with those predicted by the theory. The wavelength is derived directly from the real part of the complex wave number. The imaginary part, on the other hand, represents attenuation in the ice coupled wave. We have shown theoretically that the attenuation depends significantly on the surface temperature of the sea ice so that no experiment to measure attenuation can yield meaningful results unless accompanied by surface temperature data and preferably a continuous temperature profile through the ice sheet.

Suppose we consider a single monochromatic flexural-gravity wave propagating between two points 1 and 2, say, on the ice sheet. Then, the displacement due to that wave may be written

$$w = A e^{-bx} \cos(ax - 2\pi f t), \tag{5.14}$$

where a and b are the real and imaginary parts of the complex wave number respective ($a=\xi_1$, $b=\zeta_1$). Hence, the change in magnitude between points 1 and 2 is determined by the ratio

$$e^{-b(x_1 - x_2)}, \tag{5.15}$$

where x_1 and x_2 represent distance from the ice edge in the obvious way. With a suitably large, continuous ice sheet, therefore, the change in displacement amplitude between the two sites located on the ice may be found and the attenuation coefficient b for that frequency, evaluated.

Experiment

At first sight an experiment to measure the attenuation of waves by fast ice does not appear at all involved. However, such an experiment has never been successfully carried out for naturally-generated waves. Since the attenuation provides information on the viscous properties of ice, it is unlikely that such a key experiment would be overlooked so that one must assume that it

presents hidden difficulties. The problem lies in locating a large enough sheet of uncracked sea ice where instruments may be deployed with sufficient separation to measure the slight attenuation. Instruments should be separated by at least 1 km, and even with this separation an assumed attenuation coefficient of $b=10^{-5}$ yields a magnitude change of only 1%, better than the calibration of most instruments. This does not preclude separations less than 1 km so long as the experiment is designed to measure waves with large attenuation rates, namely with periods less than 10 s. With this in mind the Twillingate area was thoroughly surveyed for suitable fast ice.

Most bays around Twillingate contained insufficient or badly cracked sea ice in early February. Starve Harbour (fig.5.10) was eventually chosen for its smooth sheet of ice but the bay was not nearly long enough, too shallow and had an island in its mouth which had a diffusing effect on the incoming swell. This was the only available, readily accessible fast ice however.

A 32° line was surveyed on the ice and three S.P.R.I. rod strainmeters deployed at 150 m intervals beginning as close to the edge as possible (fig.5.10). The experiment was aimed at both providing a field test for the newly developed rod strainmeter and trying to measure the attenuation coefficient. In addition, a thermister probe was frozen into the sea ice and a strainmeter deployed parallel to the ice edge about half-way down the bay. These instruments monitored the temperature profile at 10 cm intervals through the ice (appendix A) and measured the long-term strain respectively.

The Analysis

In any real situation the strain experienced at the surface of an ice sheet due to incident ocean waves will not be a single monochromatic wave but a complicated superposition of wave energies. A method of analysis is therefore required which can decouple these component energies and compare magnitude at two sites. The gain factor of the frequency response function (sect.5.3) may be used

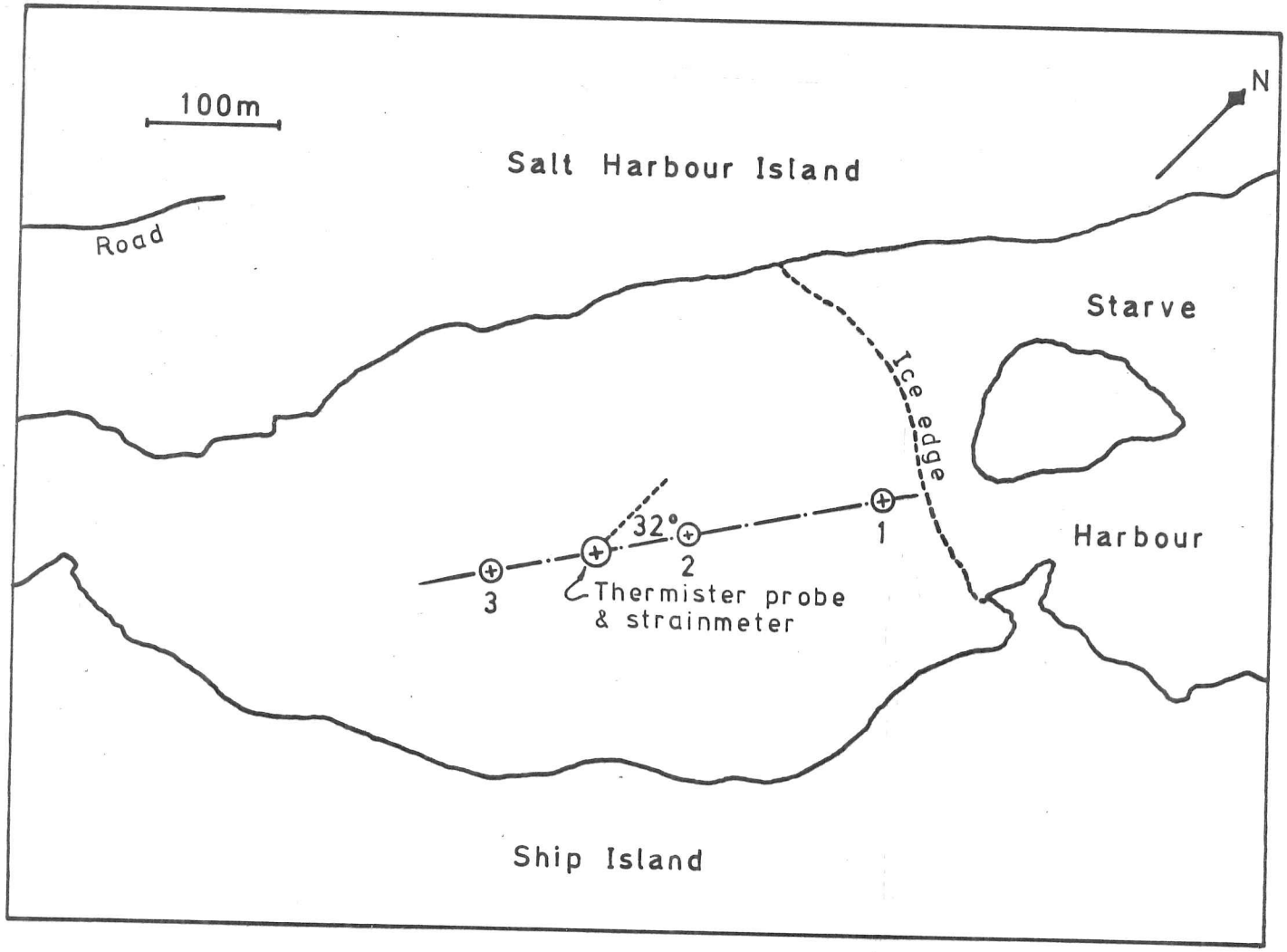

Fig. 5.10 Starve Harbour showing positions of three strainmeters 1, 2 and 3, and thermistor probe with laterally deployed strainmeter.

in this way. Since no phase information is required we may consider only relative magnitude and write

$$G_{22}(f) = |H(f)|^2 G_{11}(f), \qquad (5.16)$$

where $|H(f)|$ is the magnitude of the frequency response function (the gain factor) and G_{11}, G_{22} are as defined earlier. It should be emphasized that expression (5.16) contains no information about the phase change. If such information is required then the more general expression (5.11) involving cross power spectral density must be used.

Each averaged power spectral density was derived from approximately 45 minutes of strain data (the maximum allowed by the recording system before resetting). In all of the data there was very little long wave activity and the spectra showed most of the energy to be between three and ten seconds. The frequency response functions showed a decrease in strain at the centre strainmeter and then an increase at strainmeter 3. The reliability of these results is questionable however since the coherence over the entire range of periods was very low. The data is presented in full in Allan and Squire (1978).

It seems clear that two factors are influencing the ice-coupled waves; the shallow water in the bay and the island in its mouth. The waves will "feel bottom" and so any analysis in this thesis is not applicable. The island will cause diffraction effects which will make an experiment to measure attenuation difficult to interpret.

5.5 The Incident Amplitude Spectrum: Additional Observations from Section 5.2

The arrangement of instruments discussed in section 5.2 lends itself to another interpretation based on a combination of theory and experiment.

In chapter 2 we were able to calculate theoretically how the energy in an incident wave of given period would be distributed

among the three transmitted waves and the reflected wave at the ice edge. With this division of energy we may find the displacement, and hence surface strain (Allan and Squire, 1978), due to the superposed transmitted waves propagating into the ice cover. The infinitesimal surface strains may then be combined along the length of an imaginary instrument deployed at some point on the surface of the ice to provide the equivalent finite strain as experienced by that instrument. This strain will be a function of distance from the ice edge due to the presence of both local edge waves and attenuation. We have therefore found the strain as measured by a strainmeter situated on the ice sheet as a function of period. This strain is relative to an incident wave of unit amplitude.

It is unfortunate that no wave rider buoy data are available to compare the theoretical and observed energy distributions across the edge. However, we do have the strain field measured as a function of distance from the ice edge as discussed in section 5.2. Hence, since we have assumed linearity with an incident wave of amplitude unity in our theoretical calculations, the ratio (observed strain/theoretical strain) will give some indication of the incident wave amplitude spectrum. Clearly such a method can only provide an approximation to the incident spectrum because of the inherent simplifications in the theory. However, the similarity of the predicted open water spectrum from three strainmeters situated at 5 m, 10 m and 15 m from the ice edge is striking. Figure 5.11 shows open water amplitude spectra at approximately one hour intervals and in each, the three predicted spectra do not significantly differ from one another.

All the spectra show the same characteristic shape and reflect the observed oceanographic conditions at the time of the experiment, i.e. small amplitude, locally generated sea waves with no long period component. The 5 m curve is consistently of larger magnitude than the 10 m and 15 m curves, possibly due to the local edge effects.

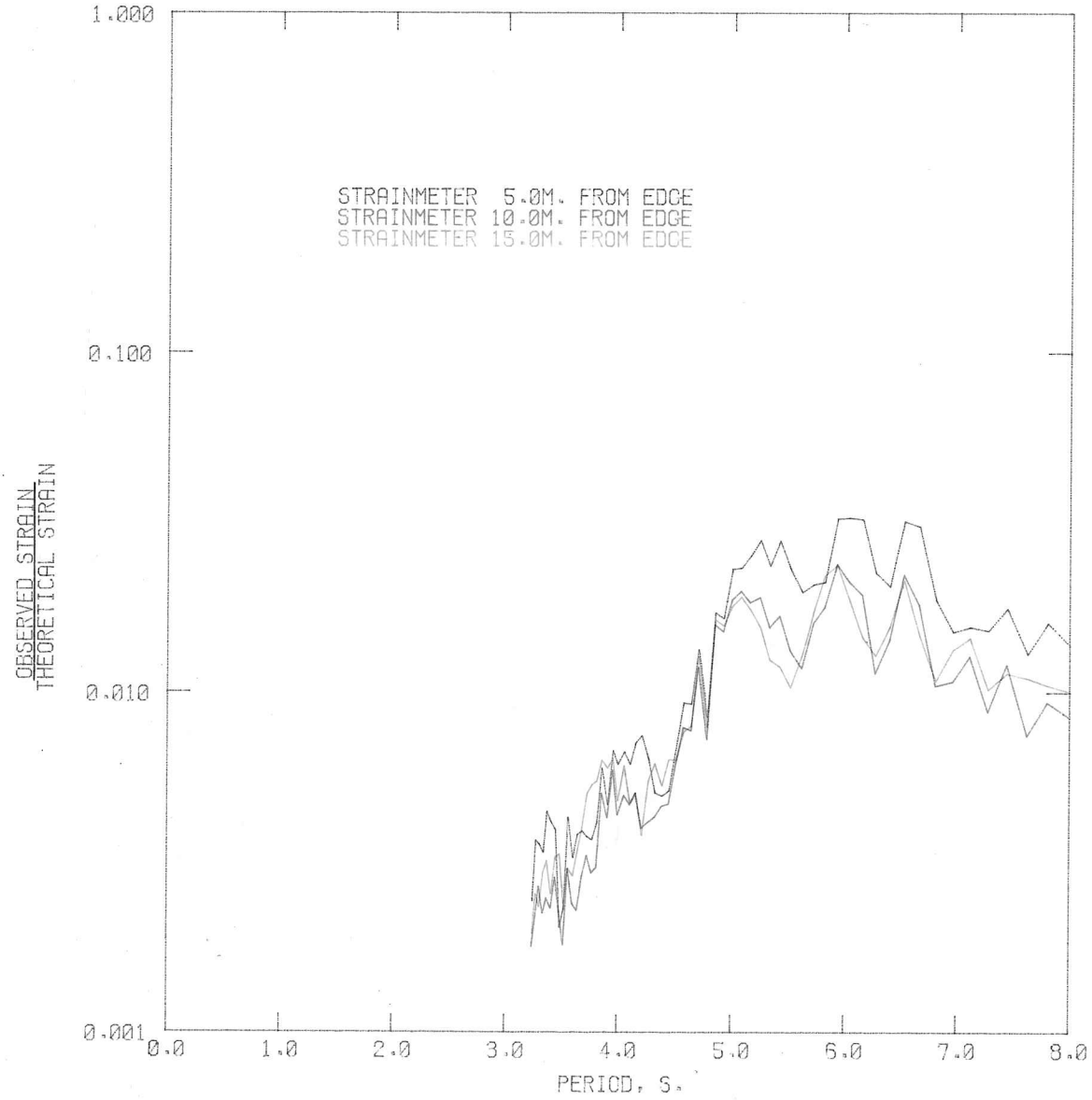

FIG. 5.11A RATIO OF OBSERVED TO THEORETICAL STRAIN AS A FUNCTION OF PERIOD. CURVE REPRESENTS A SEMI-QUANTITATIVE APPROACH TO EVALUATING THE INCIDENT AMPLITUDE SPECTRUM.

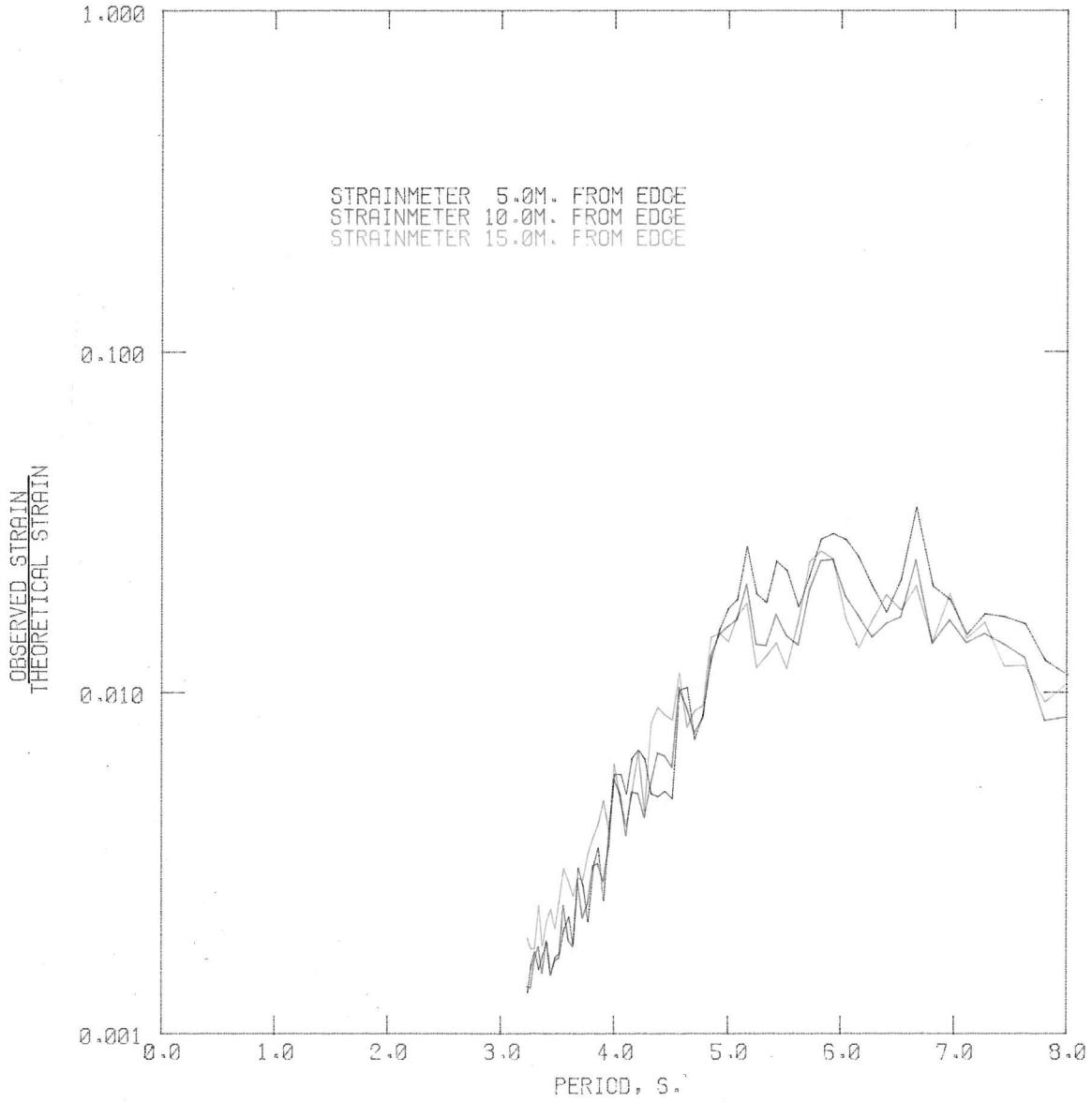

FIG. 5.11B RATIO OF OBSERVED TO THEORETICAL STRAIN AS A FUNCTION OF PERIOD. CURVE REPRESENTS A SEMI-QUANTITATIVE APPROACH TO EVALUATING THE INCIDENT AMPLITUDE SPECTRUM.

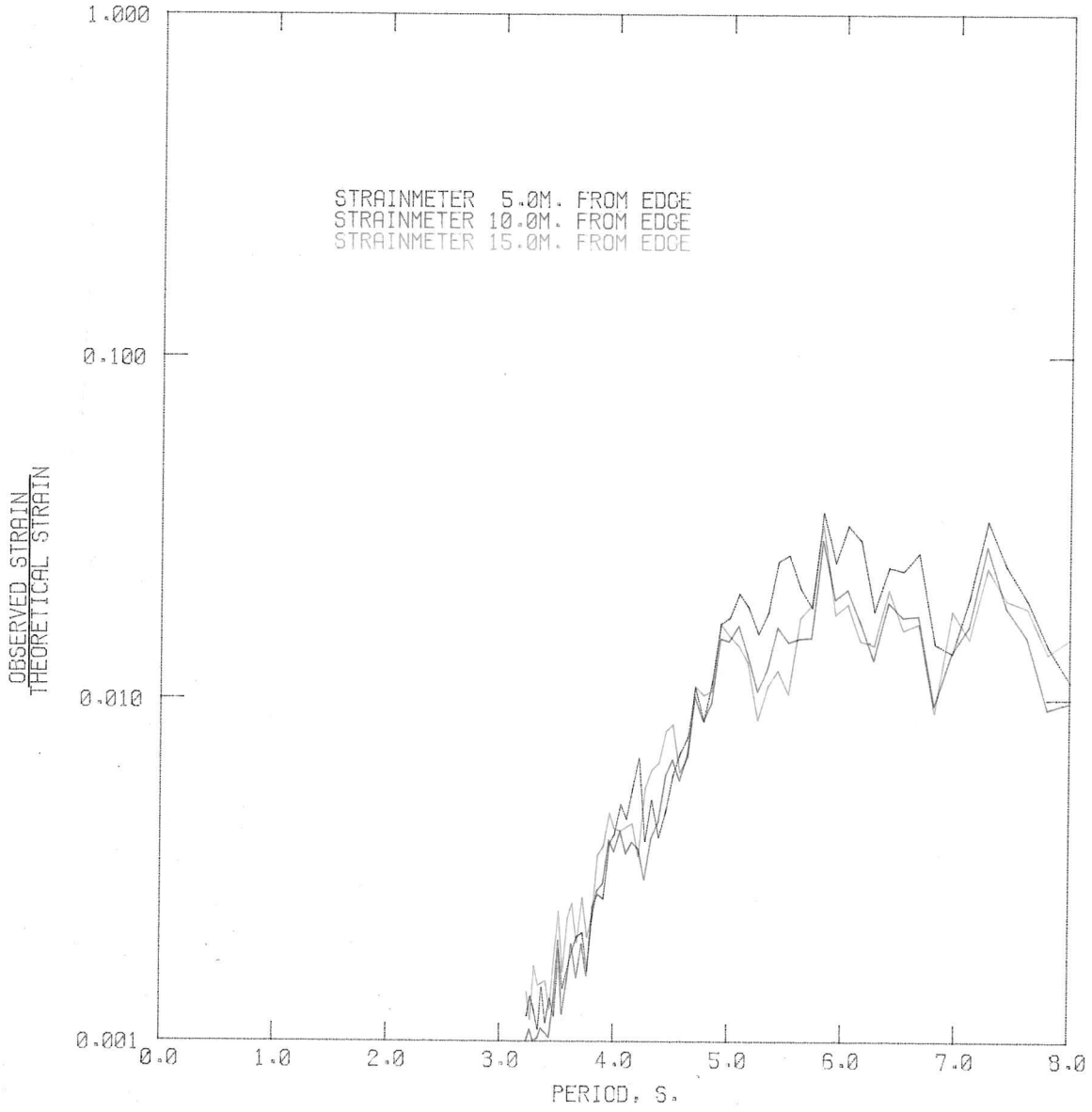

FIG. 5.11C RATIO OF OBSERVED TO THEORETICAL STRAIN AS A FUNCTION OF PERIOD. CURVE REPRESENTS A SEMI-QUANTITATIVE APPROACH TO EVALUATING THE INCIDENT AMPLITUDE SPECTRUM.

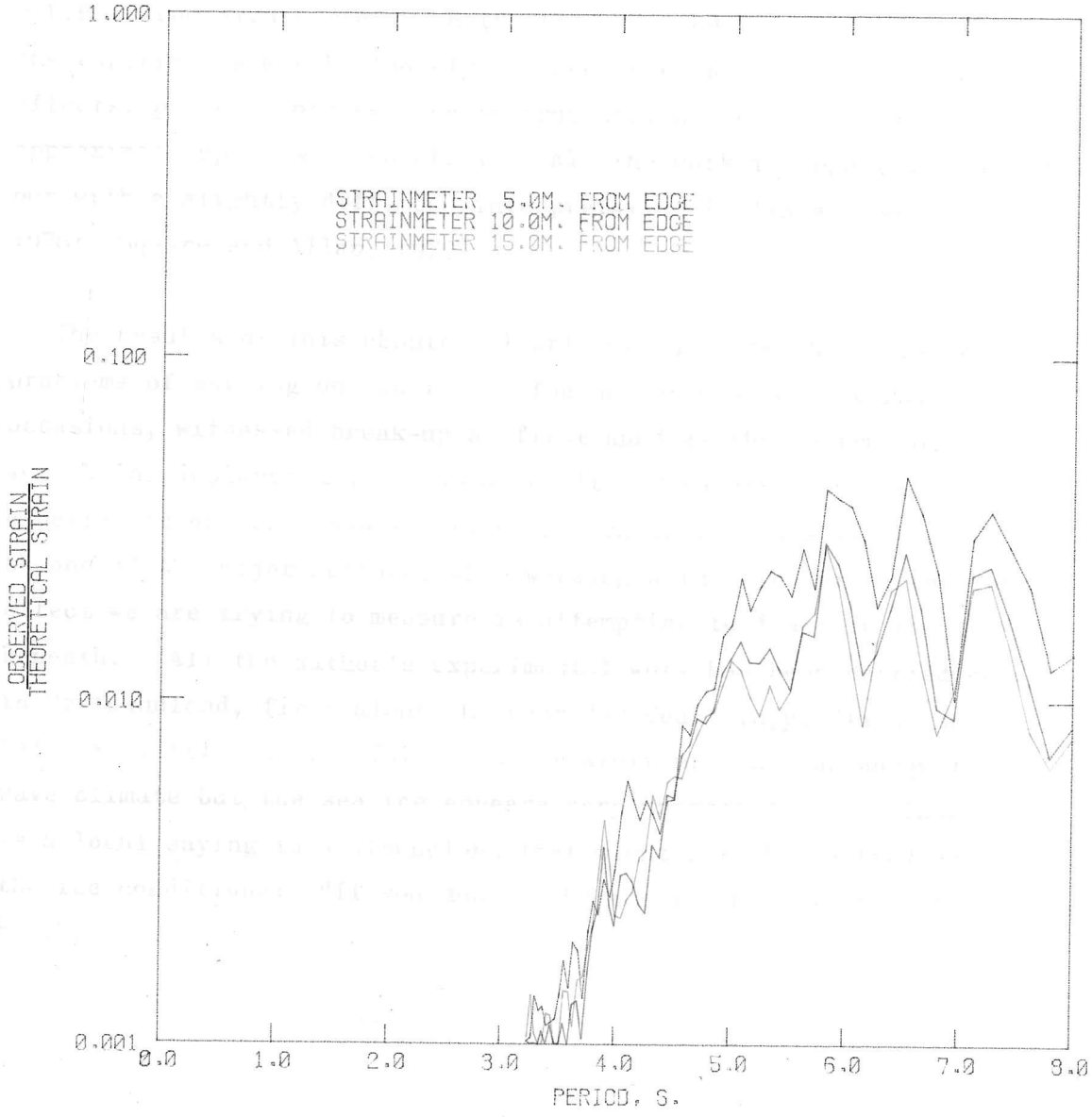

FIG. 5.11D RATIO OF OBSERVED TO THEORETICAL STRAIN AS A FUNCTION OF PERIOD. CURVE REPRESENTS A SEMI-QUANTITATIVE APPROACH TO EVALUATING THE INCIDENT AMPLITUDE SPECTRUM.

5.6 Summary

In this chapter we have discussed a series of experiments carried out in and around the Twillingate area of Newfoundland in February 1976 to measure flexural-gravity waves in sea ice. The wave experiment formed a small part of a larger project organized by C-CORE, Memorial University of Newfoundland to look at various problems relating to sea ice. Two types of strainmeter were used to detect the wave motion; the C-CORE wire strainmeter and the S.P.R.I. rod strainmeter. Both are discussed briefly in the text. The experiments may be loosely grouped into four sections: edge effects, phase change between instruments, attenuation and the approximate open water spectrum. All the work is reported elsewhere but with a slightly different interpretation (Allan and Squire, 1978; Squire and Allan, 1979).

The results of this chapter clearly demonstrate the logistic problems of working on sea ice. The author has, on several occasions, witnessed break-up at first hand as the instruments were being deployed and has as a result had to carry out the experiments on less than satisfactory sea ice. This will always be one of the major setbacks when working with waves since the very effect we are trying to measure is attempting to fracture the ice beneath. All the author's experimental work has been carried out in Newfoundland, first along the Labrador Coast (appendix A) and later at Twillingate. This area certainly provides an adequate wave climate but the sea ice appears very unpredictable. There is a local saying in Newfoundland that might well be applied to the ice conditions: "If you don't like the weather, wait half an hour".

CHAPTER 6

MULTIDIRECTIONAL WAVES AND THE USE OF STRAIN ROSETTES

MULTIDIRECTIONAL WAVES AND THE USE OF STRAIN ROSETTES

6.1 Introduction

Experiments to measure flexural-gravity waves in sea ice have shown the presence of significant energy at more than one period so that a monochromatic sine wave analysis falls short of reality. Thus an instrument located on the ice will experience a complicated motion determined by the superposition of all the individual wave energies in the spectrum. If this spectrum is one-dimensional and is propagating perpendicular to the ice edge then it is a relatively simple matter to decide upon the orientation of an array of instruments. However it is unlikely that both these conditions would be fulfilled in nature. In general, if one assumes that the ice-coupled waves are generated by incident open water swells, both conditions should be relaxed to allow for the possibility of directional spectra (Longuet-Higgins et al, 1963; Barnett and Wilkerson, 1967) whose principal directions are not necessarily normal to the ice edge. With the inclusion of oblique incidence, a more detailed understanding of the resulting ice-coupled waves is necessary. Clearly, since the edge represents an interface between two media of different characteristic wave number, some law of refraction equivalent to Snell's law in optics must exist at the edge. This law will provide the angles of transmission for the three possible wave modes discussed in chapter 2. Since some attenuation is present for all three ice-coupled waves, refraction at the ice edge will be governed by a complex Snell's law and the waves will not be simple propagating waves with decay as was the case for normal incidence. Instead they will be inhomogeneous plane waves (Budden, 1961, sect.4.7) so that their surfaces of constant amplitude and surfaces of constant phase do not coincide.

The inclusion of oblique incidence and, more generally directional spectra, at the ice edge leads one to a far more complicated situation than might have first been expected. Given that the effect of an incident spectrum is to be measured at some site within the ice cover, how should instruments be deployed so as to eliminate any directional uncertainty? This question is raised in the latter

part of the chapter.

6.2 Oblique Incidence

Following chapter 2 we consider two regions occupying $-\infty<x<0$ and $0\leqslant x<\infty$ representing open water and ice-covered water respectively. The potentials within those regions will be denoted by Φ_1 and Φ_2. To allow for obliquely incident ocean waves, each region is assumed three dimensional with the y-axis along the ice edge. Then, if for brevity we discuss waves only at the surface (remembering the problems of matching potentials at all depths), we may write the open water surface potential as

$$\Phi_1^s = \left(e^{ik(x\cos\theta+y\sin\theta)} + Re^{-ik(x\cos\theta-y\sin\theta)}\right)e^{-i\omega t}, \tag{6.1}$$

where θ is the angle of incidence and the superscript s implies at the surface. Similarly within the ice cover

$$\Phi_2^s = \left(A_1 e^{ik_1(x\cos\theta_1+y\sin\theta_1)} + A_2 e^{ik_2(x\cos\theta_2+y\sin\theta_2)} + B_3 e^{-ik_3(x\cos\theta_3-y\sin\theta_3)}\right)e^{-i\omega t}, \tag{6.2}$$

where θ_1, θ_2, θ_3 are the respective angles of refraction for the three possible wave modes. Matching the surface potentials across $x=0$ for all y yields expressions linking the angles of refraction and incidence (Heading, 1964, ch.5). For example

$$\sin\theta_1 = \frac{k}{k_1}\sin\theta. \tag{6.3}$$

However, it must be remembered that k_n is complex so that θ_1 is not an angle of refraction in the strict sense. For completeness, a discussion of the refracted waves will be given here though the analysis parallels that for refraction of electromagnetic waves at a good conductor.

As before, if $k_1 = \xi_1 + i\zeta_1$, then

$$\sin\theta_1 = \frac{\xi_1 - i\zeta_1}{(\xi_1^2+\zeta_1^2)}\,k\sin\theta. \tag{6.4}$$

In order to express cos θ_1 simply, we write

$$\cos\theta_1 = q e^{i\gamma}, \tag{6.5}$$

where q and γ are real. Then,

$$\left.\begin{aligned} q^2\cos 2\gamma &= 1 - \frac{k^2(\xi_1^2 - \zeta_1^2)\sin^2\theta}{(\xi_1^2 + \zeta_1^2)^2}, \\ q^2\sin 2\gamma &= \frac{2\xi_1\zeta_1 k^2\sin^2\theta}{(\xi_1^2 + \zeta_1^2)^2}. \end{aligned}\right\} \tag{6.6}$$

Hence, the ice-coupled wave may be written

$$A_1 e^{-xq(\zeta_1\cos\gamma + \xi_1\sin\gamma)} e^{i[xq(\xi_1\cos\gamma - \zeta_1\sin\gamma) + yk\sin\theta - \omega t]}. \tag{6.7}$$

We see that the surfaces of constant amplitude are planes parallel to the ice edge and the surfaces of constant phase are given by

$$yk\sin\theta + xq(\xi_1\cos\gamma - \zeta_1\sin\gamma) = \text{Constant}. \tag{6.8}$$

These represent planes with their normals inclined at an angle θ' to the normal at the ice edge where θ' is given by

$$\text{Tan}\,\theta' = \frac{k\sin\theta}{q(\xi_1\cos\gamma - \zeta_1\sin\gamma)}. \tag{6.9}$$

Clearly then, the surfaces of constant amplitude and phase are inclined at some angle to one another. Waves of this type are called inhomogeneous and are discussed fully in Budden (1961). If the direction of propagation is defined as that perpendicular to the planes of constant phase so that θ' represents the angle of transmission, we may define a real wave number $k_1(\theta)$ which is a function of the incident angle of attack as follows

$$k_1(\theta) = \sqrt{k^2\sin^2\theta + q^2(\xi_1\cos\gamma - \zeta_1\sin\gamma)^2} \tag{6.10}$$

Then, from equation (6.9) a refraction law may be written down corresponding to Snell's law:

$$\sin\theta' = \frac{k}{k_1(\theta)}\sin\theta. \tag{6.11}$$

This expression reduces to (6.3) when $\zeta_1 = 0$. For normal incidence

expression (6.7) reduces to that for a simple propagating wave with decay in the direction of propagation.

6.3 The Quasi-Critical Angle

In the previous section we have shown that the direction of propagation of the ice-coupled wave is prescribed by a modified Snell's law where the wave number in ice is a function of the angle of incidence. It is natural to ask if the angle θ' is always defined as less than ninety degrees or, equivalently, does a critical angle exist. Such a condition could exist if the right-hand side of equation (6.11) became greater than unity. That is,

$$k\sin\theta > k_1(\theta). \tag{6.12}$$

However, we have defined q, γ as real and ξ_1, ζ_1 as real and positive so that this inequality can never be satisfied.

If $\xi_1>0$, $\zeta_1=0$ then attenuation is negligible and the planes of constant amplitude and phase coincide. In this case a critical angle can exist depending on the relative magnitudes of the wave numbers outside and inside the ice cover. Loosely, it may be said that waves of short period are more likely to be totally reflected than long waves. This is shown schematically in figure 6.1 where the upper diagram (fig.6.1a) represents the case $k>\xi_1$ and the lower diagram (fig.6.1b), the case $k<\xi_1$.

If $\xi_1=0$, $\zeta_1>0$, an unrealistic condition in the present case, all transmitted waves propagate along the interface between the two media and there is no penetration. In this case the planes of constant amplitude and phase are at right angles.

Returning to the case at hand we see that within the ice cover we have three possible wave numbers, each with some non-zero imaginary part. This implies that the ice-coupled waves will always be inhomogeneous (except at normal incidence) and no real critical angle exist. However, we know that the imaginary part of $k_1(=\zeta_1)$ is very small so that the wave corresponding to this wave number

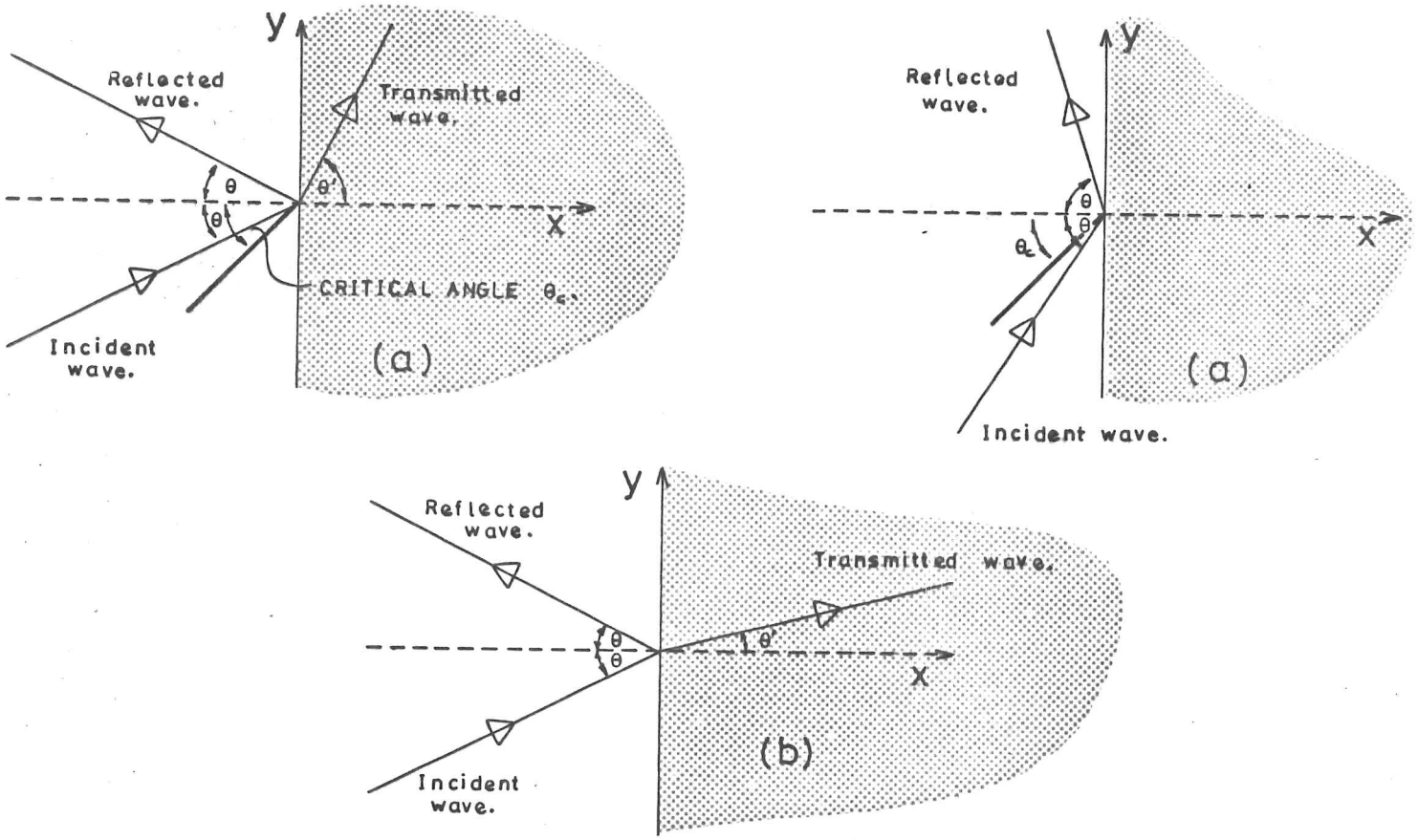

Fig. 6.1 The two regimes for transmission of an obliquely incident ocean wave; (a) period<critical period, (b) period>critical period.

will "almost be homogeneous" and a critical angle "almost exist". The effect of this small attenuation may be seen more clearly by assuming only one transmitted wave, then the modulus of the reflection coefficient will demonstrate whether or not a critical angle situation can arise. The two curves in figure 6.2 represent (schematically) the two cases of zero attenuation where $\zeta_1=0$ and small attenuation where $0<\zeta_1\ll 1$. The effect of non-zero ζ_1 is therefore to smooth the curve for $\zeta_1=0$ so that strictly a critical angle may not be defined. However, we may define a quasi-critical angle such that either the modulus of the reflection coefficient is very close to unity or the maximum gradient of the modulus is extrapolated to cross the $|R|=1$ line. Other possible criteria could also be considered.

6.4 Matching across the Ice Edge for Oblique Incidence

In chapter 2 we solved for the unknown coefficients R, A_1, A_2 and B_3 by matching potentials and velocities across x=0 and assuming zero bending moment and shear at the ice edge. In principle, a similar system of equations may be written down and solved in the present case where the coefficients are functions of incident angle Θ. We will consider each boundary condition in turn:

(i) $\Phi_1 = \Phi_2\big|_{\substack{x=0\\z=0}}$. Since this condition is true for all y, expressions linking angles of refraction with angle of incidence may be written down (e.g. equation 6.3):

$$k\sin\theta = k_1\sin\theta_1 = k_2\sin\theta_2 = k_3\sin\theta_3 . \qquad (6.13)$$

Also, we have

$$1 + R = A_1 + A_2 + B_3 . \qquad (6.14)$$

(ii) $\dfrac{\partial\Phi_1}{\partial x} = \dfrac{\partial\Phi_2}{\partial x}\Big|_{\substack{x=0\\z=0}}$. This yields a second equation

$$k\cos\theta(1-R) = A_1k_1\cos\theta_1 + A_2k_2\cos\theta_2 - B_3k_3\cos\theta_3 . \qquad (6.15)$$

(iii) Zero bending moment. The simple one-dimensional free edge boundary condition of chapter 2 must now be extended to cope with a two-dimensional thin plate. In this case the boundary condition is

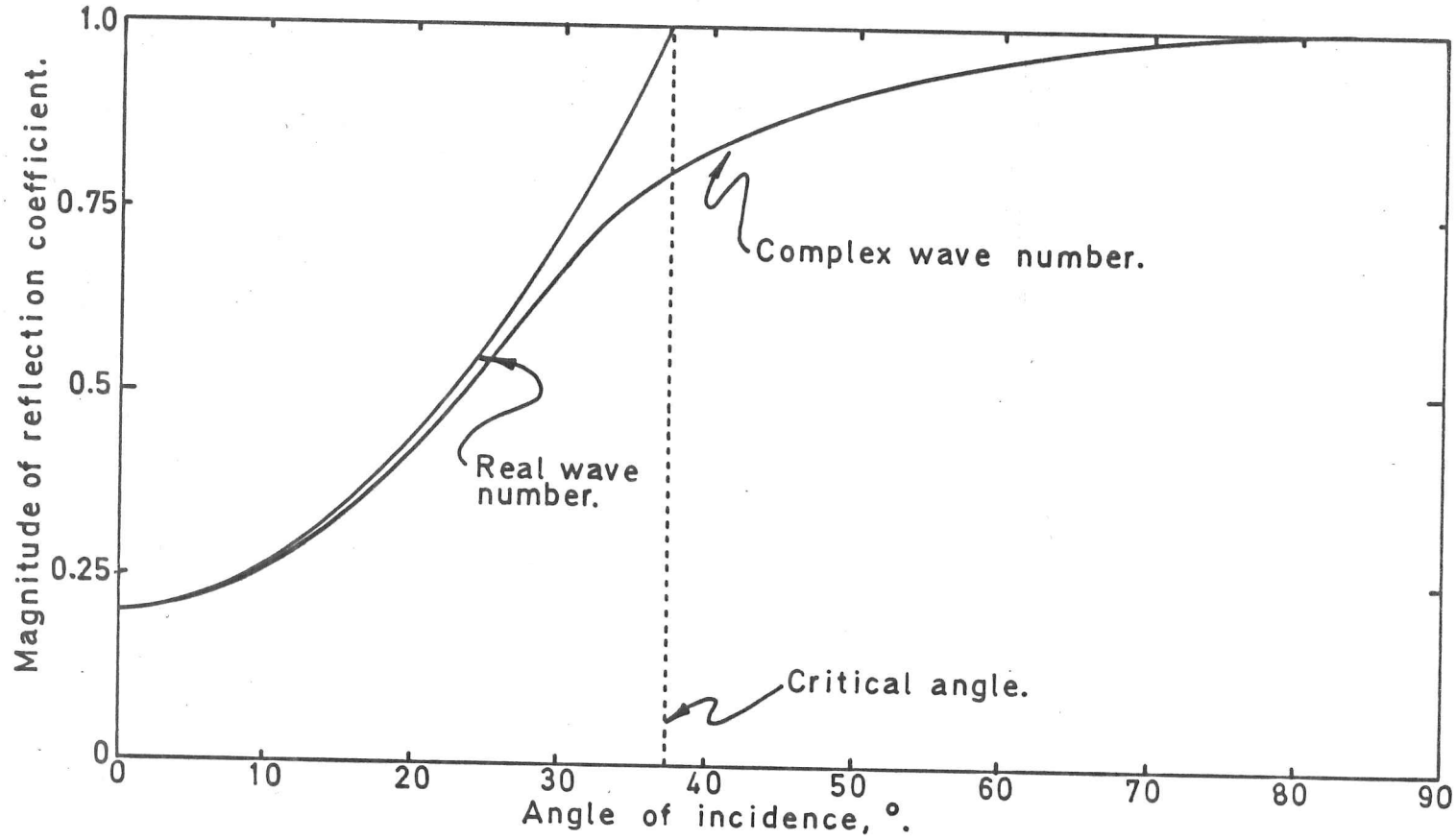

Fig. 6.2 Sketch showing effect of allowing wave number to have small imaginary part on magnitude of reflection coefficient.

$$\frac{\partial^2 w_2}{\partial x^2} + \nu \frac{\partial^2 w_2}{\partial y^2} = 0, \tag{6.16}$$

(Graff, 1975, sect.4.2.2) so long as Poisson's ratio is constant. Hence,

$$A_1 k_1^3(\cos^2\theta_1 + \nu\sin^2\theta_1) + A_2 k_2^3(\cos^2\theta_2 + \nu\sin^2\theta_2) + B_3 k_3^3(\cos^2\theta_3 + \nu\sin^2\theta_3) = 0. \tag{6.17}$$

(iv) Zero shear. In this case the two-dimensional edge boundary condition is

$$\frac{\partial^3 w_2}{\partial x^3} + (2-\nu)\frac{\partial^3 w_2}{\partial x \partial y^2} = 0, \tag{6.18}$$

so that a substitution for w_2 provides the final equation

$$A_1 k_1^4 \cos\theta\left[\cos^2\theta_1 + (2-\nu)\sin^2\theta_1\right] + A_2 k_2^4 \cos\theta\left[\cos^2\theta_2 + (2-\nu)\sin^2\theta_2\right] - B_3 k_3^4 \cos\theta\left[\cos^2\theta_3 + (2-\nu)\sin^2\theta_3\right] = 0. \tag{6.19}$$

Equations (6.13), (6.14), (6.15), (6.17) and (6.19) may be solved numerically for R, A_1, A_2, B_3 as functions of angle of incidence.

Figure 6.3 shows a three-dimensional graph of the magnitude of R as a function of both wave period and angle of incidence in 1 m of sea ice. There is a clear dependence of critical angle on period with longer waves more likely to be transmitted than short waves. Angles of incidence very close to 90° are considered though strictly at 90° there is no reflection so that the reflection coefficient cannot be defined. A graph corresponding to figure 2.8 is shown in figure 6.4 for an angle of incidence of 45° and an ice thickness of 1.0 m. The graph shows the division of energy at the ice edge between the three possible wave modes. For small periods negligible

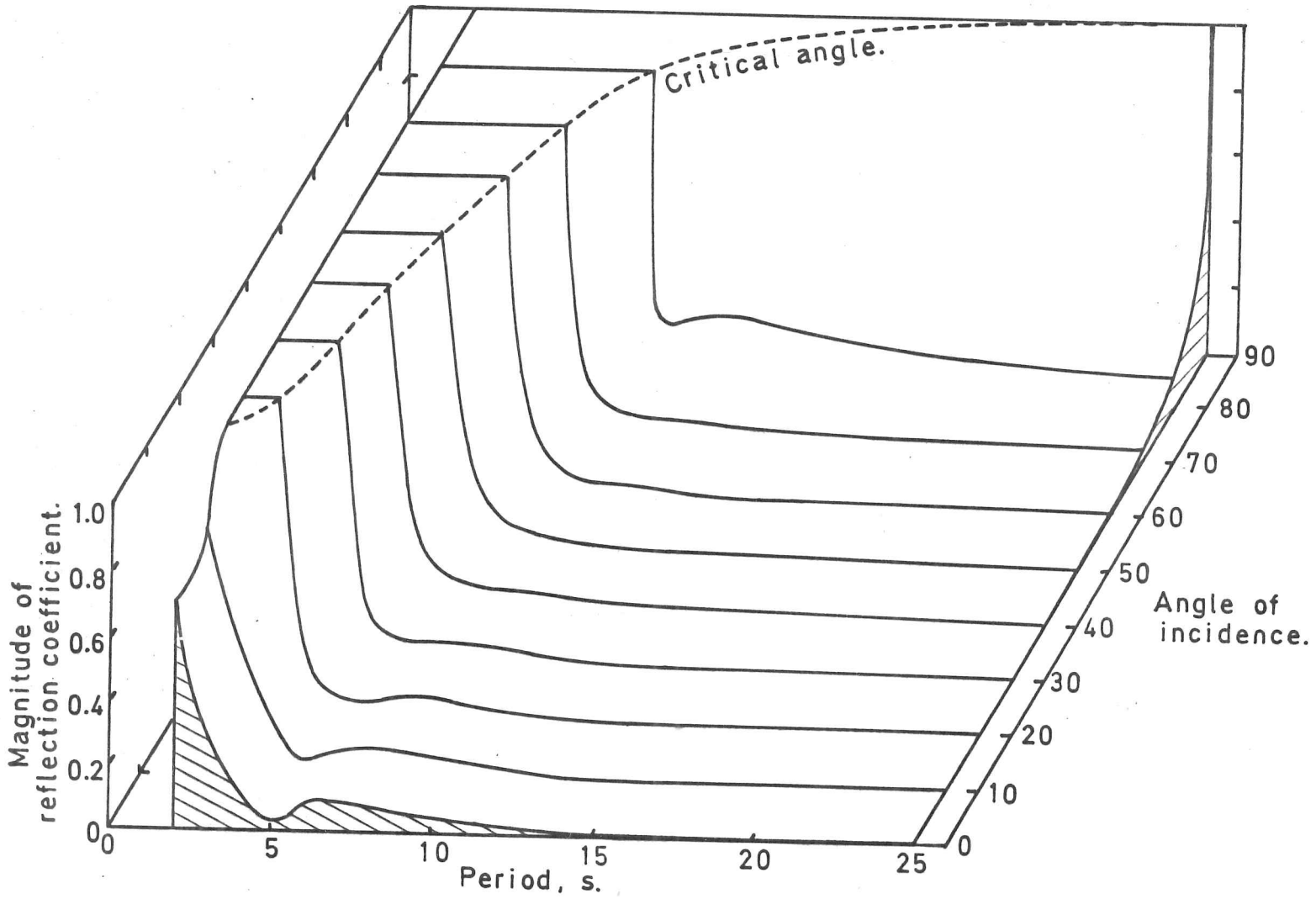

Fig. 6.3 Three-dimensional graph showing dependence of reflection coefficient on both wave period and angle of incidence. The critical angle is shown.

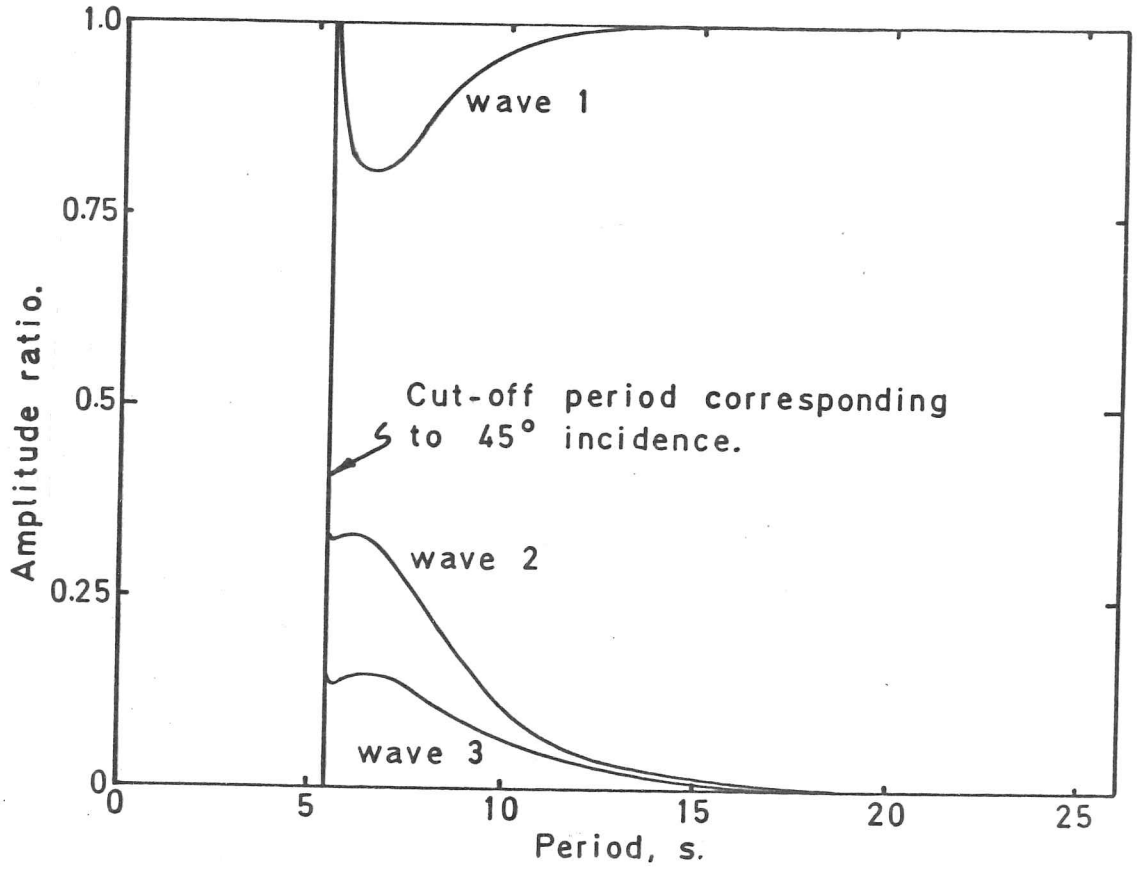

Fig. 6.4 The energy distribution at the ice edge for the three possible ice-coupled waves. Ice thickness is 1.0 m, angle of incidence is 45°.

energy is transmitted since 45° incidence exceeds the critical incidence. For longer periods, the curves show a similar structure to those at normal incidence.

6.5 Discussion

It is clear that the existence of a non-zero imaginary part in the wave numbers of all three ice-coupled waves complicates any analysis concerned with oblique incidence. An open water wave impinging at other than normal incidence will give rise to inhomogeneous plane waves within the ice cover with the angle between the planes of constant amplitude and plans of constant phase, an increasing function of angle of incidence. That is, as the angle of incidence increases the waves become "more inhomogeneous". The degree of inhomogeneity in the transmitted wave also depends on the wave period. For long periods the angle of transmission for the least attenuated wave (wave 1) increases from 0° at normal incidence to just less than the angle of incidence for sea waves impinging at large angles. For short waves, however, the angle of transmission rapidly increases to close to 90° for relatively small angles of incidence. Waves 2 and 3 are "almost homogeneous" for long periods but for short periods their angle of transmission increases rapidly with angle of incidence.

The attenuation rate for each of the three transmitted waves is also an increasing function of angle of incidence though the dependence is almost insignificant for waves 2 and 3. For wave 1 on the other hand, the attenuation coefficient at small periods can change rapidly by several orders of magnitude as the angle of incidence varies from 0° to 90°. The attenuation coefficient at longer periods shows a more gradual increase as the incident angle is increased. Since attenuation now depends on the direction of propagation of an ice-coupled wave we see that the directional character of the wave spectrum will change with distance from the ice edge. In particular we may say that the inhomogeneity decreases as we travel further from the edge. Far into the ice cover, therefore, the precise nature of the open water spectrum will have less significance since the intervening sea ice will have acted to

collimate the local spectrum normal to the ice edge.

The reflection coefficient at the ice edge and the three transmission coefficients within the ice cover are also functions of the angle of incidence and the wave period. Incident open water waves with periods in excess of approximately 20 s are transmitted as wave 1 with negligible reflection for all but very large angles of incidence (~90°). Shorter waves, however, may generate waves of type 2 and 3 as well as type 1 within the ice cover. The reflection coefficient for short waves is also significantly larger and, depending on the period, allows the existence of total reflection at the ice edge. The angle for which total reflection first occurs (critical angle) has been shown to be an increasing function of wave period (fig.6.3) so that there will be a natural selection at the ice edge in favour of small angles of incidence and long waves.

The effect of an ice cover on an impinging directional open water spectrum may therefore be separated into two distinct actions; to collimate the spectrum normal to the ice edge and to preferentially select long waves. There will be two factors favouring collimation; the critical angle and the tendency for inhomogeneity to decrease with distance. There will be three factors favouring long waves; a critical angle which is larger for short waves, and reflection and attenuation coefficients which decrease with increasing period. Far into the ice cover one would therefore expect to find only long homogeneous plane waves propagating perpendicular to the ice edge.

The presence of a critical angle also implies that wave activity just outside an ice edge will be much greater than within the ice cover. Waves of short period would be totally reflected for all angles except those close to normal incidence. Thus a wave-rider-buoy deployed on the seaward side of an ice edge would be expected to produce a power spectral density showing considerably more short wave activity than one deployed within ice covered water. Unfortunately, we do not have such data recorded simultaneously. However, Dr Peter Wadhams has kindly provided two spectra recorded

off the east coast of Newfoundland during a field season in February-March, 1978. Figure 6.5a shows an open water spectrum and figure 6.5b, a spectrum recorded between ice floes in a region of almost complete ice cover. The vertical axes represent power density in m^2sx10^4 and the horizontal axes, frequency in Hz. Though the spectra cannot strictly be compared since they were not recorded at the same time, they are strikingly dissimilar. The open water shows significant energy over a broad range from about 3 s to 20 s. The spectrum recorded within the ice cover on the other hand shows a distinct peak between 10 s and 20 s and no short wave activity. The difference between the spectra could certainly be attributed to a change in wave conditions between the times of recording but the narrowness of the latter spectrum is so conspicuous that some angular selection is possibly occurring at the ice edge. Both spectra show peaks at around 12.5 s.

6.6 The Use of Strain Rosettes

Often, if one is working close to a clearly defined, compacted ice edge, it is reasonable for a short term experiment, to align instruments according to an incoming swell. Well into the ice cover, however, the location and direction of the ice edge is seldom known so that since the wave motion is often physically imperceptible, it is necessary to locate the direction of propagation for significant wave energies. This involves the deployment of instruments in a so-called rosette (three instruments placed at a known angle to one another). A variety of rosette configurations may be used which are discussed fully in the engineering literature (see for example Meier, 1950; Holister, 1967). The configuration chosen for the present analysis and in Squire (1978) is that of the delta rosette where the three instruments are aligned at 120° to one another. This is chosen because one has no idea at the outset of an experiment about the directional nature of the flexural-gravity spectrum. The precise configuration chosen is unimportant since a modification of the subsequent analysis to another type of rosette will produce similar effects. The instruments used were 2 m gauge length strainmeters belonging to C-CORE, Memorial University of Newfoundland.

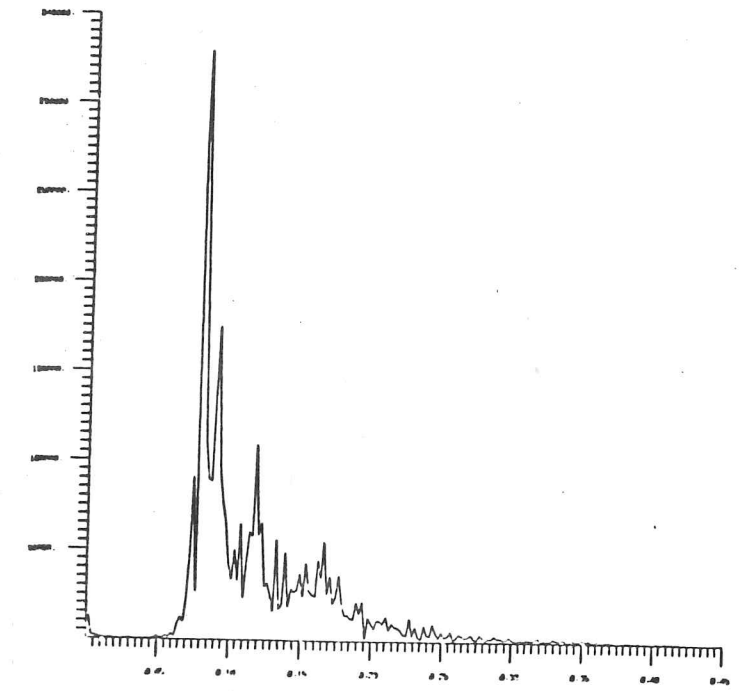

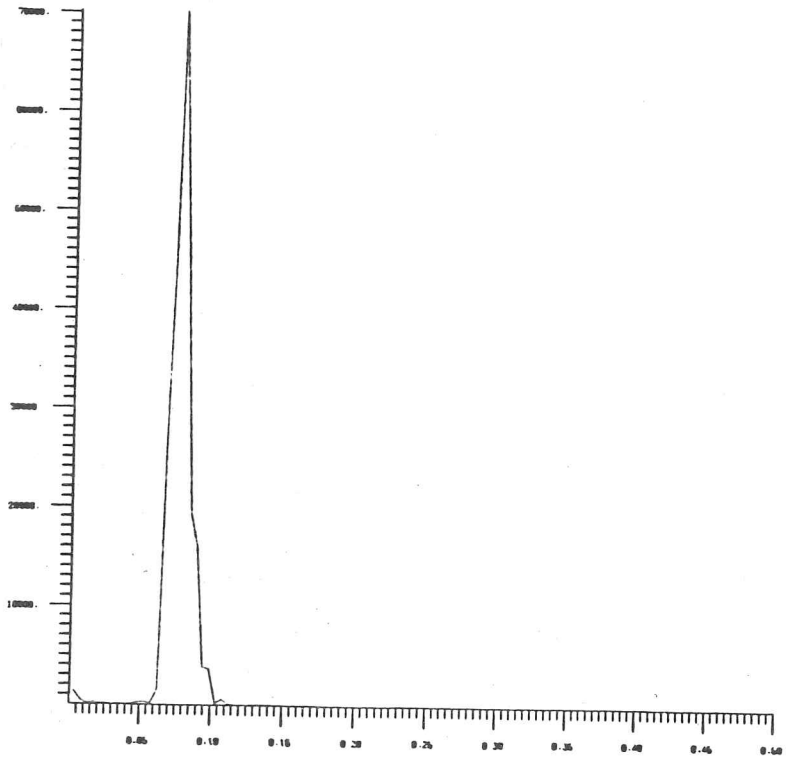

Fig. 6.5 Two power spectral densities recorded a) outside the ice cover, and b) within the ice cover, respectively

Strain gauges and strain gauge rosettes are very often employed to evaluate the principal strains and directions of the axes of principal strain for problems in experimental mechanical engineering. These gauges are considerably smaller than 2 m gauge length but the effect they are trying to measure is also correspondingly smaller. Hence, problems encountered with strain gauges will also occur with strainmeters, and vice versa. Many such problems are directly attributable to the gauge length of the instrument. Consider, for example, a rectangular strain pulse propagating past a strain gauge. Three different effects will be observed depending on the ratio of the pulse length to the gauge length. In each case the output-pulse from the strain gauge is distorted. As the pulse length decreases relative to the gauge length this distortion becomes progressively worse. This effect is discussed in detail by Murphy et al (1957) and Dove and Adams (1964, sect.4.2k).

Another problem related to the gauge length of an instrument is discussed by Dally and Riley (1965, sect.15.4). This concerns the measurement of strain at a point on a standing sinusoidal strain wave. Dally and Riley show that large errors may ensue if one simply assumes that the gauge reads the strain at its midpoint since a strain gauge will measure the average strain over its length.

In this chapter we discuss another source of error which results from the measurement of a propagating strain wave by a rosette of three gauges. The method of rosette analysis though well established in engineering is rarely applied to measure the effects of a propagating wave and it was felt that a simple theoretical model might yield some unexpected results. To avoid unnecessary complication a two-dimensional, linearly elastic, thin plate formulation is used throughout and deep water is assumed. Such an analysis predicts a dispersion equation which permits a propagating wave. It is this wave which is used as input to the strain rosette.

6.7 The Dispersion Equation

We consider an experimental site to be situated on the ice surface

far from open water. To a first approximation the flexural oscillations of sea ice due to ocean swell may be modelled by a thin elastic sheet on deep water. Then noting the co-ordinate system shown in figure 6.6, we may write down an equation for the vertical displacement $w(x,y,t)$ as follows:

$$D\nabla^4 w + \rho h \frac{\partial^2 w}{\partial t^2} = P(x,y;t), \tag{6.20}$$

where, ∇^4 is the usual two-dimensional biharmonic operator, $P(x,y,t)$ is the pressure exerted on the ice by the underlying water, $D = h^3E/12(1-\nu^2)$ is the flexural rigidity of the ice, ν is Poisson's ratio, E is Young's modulus, ρ is the density of sea ice and h is the ice thickness. Values of $E = 6.0\text{x}10$ N m^{-2}, $\nu = 0.3$, $\rho = 9.225$ Kg m^{-3} were chosen as typical of sea ice.

If the hydrodynamics are assumed to be linear and irrotational throughout the fluid we may define a velocity potential Φ such that at every point, Laplace's equation

$$\frac{\partial^2 \Phi}{\partial x^2} + \frac{\partial^2 \Phi}{\partial y^2} + \frac{\partial^2 \Phi}{\partial z^2} = 0, \tag{6.21}$$

is satisfied (Stoker, 1957). Hence, applying the pressure equation (Chapter 2) at the ice/water interface, we may write equation (6.20) as

$$D\nabla^4 w + \rho h \frac{\partial^2 w}{\partial t^2} = \rho' \left(\frac{\partial \Phi}{\partial t}\bigg|_{\text{Interface.}} + gw \right), \tag{6.22}$$

where ρ' is the density of the underlying water. The relation between the velocity potential Φ and the displacement w is provided by the kinematical boundary condition at the interface:

$$\frac{\partial w}{\partial t} = -\frac{\partial \Phi}{\partial z}\bigg|_{\text{Interface.}}. \tag{6.23}$$

We assume the usual two-dimensional, deep water wave expression for Φ and write the displacement w as

$$w = \exp\left[i \left\{ k(\underline{n}.\underline{r}) - \omega t \right\} \right], \tag{6.24}$$

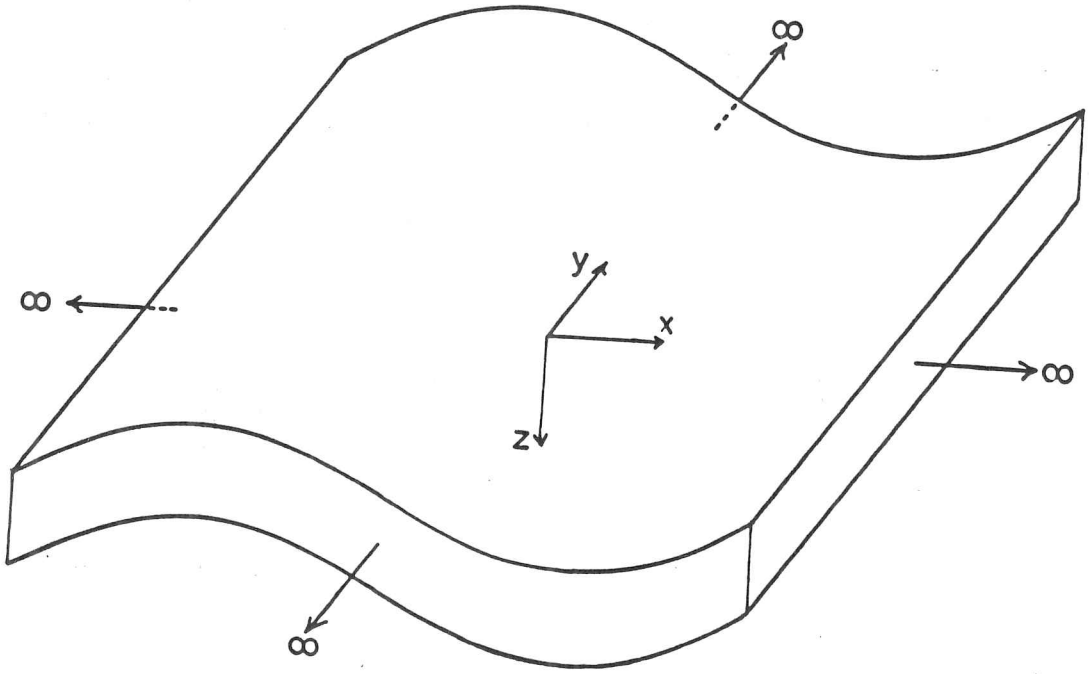

Fig. 6.6 Schematic diagram of wave in ice showing co-ordinate system.

where k is now the wave number in the ice cover and $n = (\cos\alpha, \sin\alpha)$. This represents a plane wave front propagating in a direction α to the normal at the ice edge (fig.6.7). Substitution into equation (6.22) gives the required dispersion equation, a quintic in k:

$$Dk^5 + (\rho' g - \rho h \omega^2)k - \rho' \omega^2 = 0 . \qquad (6.25)$$

We will only concern ourselves with roots of this equation which are purely real. Such a root does not exist for the corresponding viscoelastic analysis but the imaginary part of the wave number is small enough to be neglected. With this restriction we have limited ourselves to being far from the ice edge.

6.8 Principal Axes

From Graff (1975, sect.4.2) we may write down expressions for the infinitestimal strain at the surface of the sea ice in terms of the vertical displacement of the ice sheet

$$\varepsilon_{xx} = \frac{-h}{2}\frac{\partial^2 w}{\partial x^2}, \quad \varepsilon_{xy} = \frac{-h}{2}\frac{\partial^2 w}{\partial x \partial y}, \quad \varepsilon_{yy} = \frac{-h}{2}\frac{\partial^2 w}{\partial y^2} . \qquad (6.26)$$

In these expressions we have adopted the mathematical rather than the engineering definition of shear strain. Engineers would tend to use a value twice that defined here. Substituting expression (6.24) into (6.26) we may therefore write

$$\left.\begin{aligned} \varepsilon_{xx} &= \tfrac{1}{2} h l^2 k^2 w, \\ \varepsilon_{xy} &= \tfrac{1}{2} h lm k^2 w, \\ \varepsilon_{yy} &= \tfrac{1}{2} h m^2 k^2 w. \end{aligned}\right\} \qquad (6.27)$$

Hence, we have found the two-dimensional components of strain referred to the co-ordinate system shown in figure 6.6 in terms of the displacement w. But, from Jaeger (1956, sect.10) we may write the strain in some arbitrary direction β as

$$\varepsilon_\beta = \varepsilon_{xx}\cos^2\beta + 2\varepsilon_{xy}\sin\beta\cos\beta + \varepsilon_{yy}\sin^2\beta, \qquad (6.28)$$

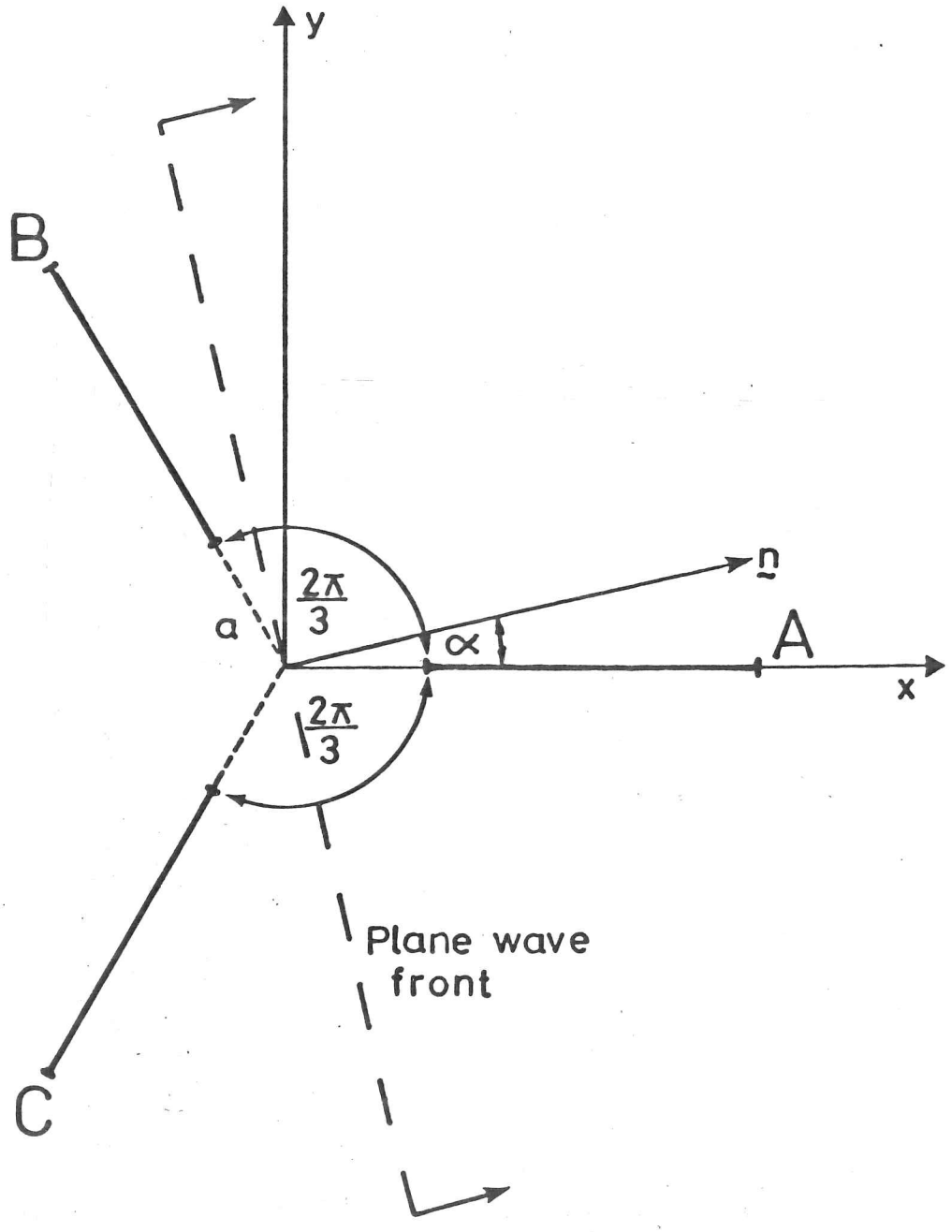

Fig. 6.7 Plane wave front impinging on a delta rosette ABC with separation parameter a.

so that substituting for ε_{xx}, ε_{xy} and ε_{yy} from equations (6.27) gives

$$\varepsilon_\beta = \tfrac{1}{2}hk^2w\cos^2(\alpha-\beta). \qquad (6.29)$$

Hence, in directions A, B, C (fig.6.7), the respective infinitestimal strains are

$$\left.\begin{aligned}\varepsilon_A &= \tfrac{1}{2}hwk^2\cos^2\alpha,\\ \varepsilon_B &= \tfrac{1}{2}hwk^2\cos^2(\alpha-\tfrac{2\pi}{3}),\\ \varepsilon_C &= \tfrac{1}{2}hwk^2\cos^2(\alpha+\tfrac{2\pi}{3}).\end{aligned}\right\} \qquad (6.30)$$

The directions A, B and C are now considered to theoretically represent the instruments of a 120° delta rosette. Each such instrument is supposed of gauge length 2 m, corresponding to the strainmeter used in the experimental section. In any realistic experiment some radial separation of the strainmeters is inevitable. We therefore introduce a separation parameter a, measured from the origin to the nearest end of the strainmeters (fig.6.7). A value of a=-1.0 m will thus position the strainmeters in a star configuration.

Given a wave impinging from some arbitrary direction α, it is possible to calculate the infinitestimal surface strain for any point along each instrument of the delta rosette. The compounded effect of the infinitesimal strain, as measured by an individual instrument, may therefore be found. The strainmeter will not measure the strain at its midpoint but the average strain over its gauge length. It is at this point that the effect of separation is introduced.

So far we have theoretically considered a propagating strain wave impinging on a delta rosette and have calculated the strain that each instrument will record. We will now seemingly reverse the process and attempt to predict the original wave from the strain records provided by those instruments. Such an analysis may at first sight appear circuitous but it must be remembered that a separation parameter a has been introduced.

Given three strains on a delta rosette ε_A, ε_B and ε_C, we may locate the axes of principal strain and compute the principal strains ε_1 and ε_2 as follows

$$\left.\begin{aligned} \varepsilon_A &= \tfrac{1}{2}(\varepsilon_1+\varepsilon_2) + \tfrac{1}{2}(\varepsilon_1-\varepsilon_2)\cos 2\alpha', \\ \varepsilon_B &= \tfrac{1}{2}(\varepsilon_1+\varepsilon_2) + \tfrac{1}{2}(\varepsilon_1-\varepsilon_2)\cos 2(\alpha'+\tfrac{2\pi}{3}), \\ \varepsilon_C &= \tfrac{1}{2}(\varepsilon_1+\varepsilon_2) + \tfrac{1}{2}(\varepsilon_1-\varepsilon_2)\cos 2(\alpha+\tfrac{2\pi}{3}), \end{aligned}\right\} \qquad (6.31)$$

where α' is the angle between the axes of principal strain and strainmeter A of the delta rosette. After some algebra these equations lead to

$$\left.\begin{aligned} \varepsilon_1+\varepsilon_2 &= \tfrac{2}{3}(\varepsilon_A+\varepsilon_B+\varepsilon_C), \\ \varepsilon_1-\varepsilon_2 &= \pm\tfrac{4}{3}(\varepsilon_A^2+\varepsilon_B^2+\varepsilon_C^2-\varepsilon_A\varepsilon_B-\varepsilon_B\varepsilon_C-\varepsilon_C\varepsilon_A)^{1/2}, \\ \operatorname{Tan} 2\alpha' &= \frac{\sqrt{3}(\varepsilon_B-\varepsilon_C)}{2\varepsilon_A-\varepsilon_B-\varepsilon_C}. \end{aligned}\right\} \qquad (6.32)$$

The condition $|\varepsilon_1| \geq |\varepsilon_2|$ fixes the sign of $\varepsilon_1-\varepsilon_2$ so that any ambiguity in the angle α' may be resolved.

Given the incident flexural wave of known period and angle of attack α, it is therefore possible to compare the expected surface strain and angle α with that predicted by the delta rosette. The difference of the true and predicted values for surface strain and direction will demonstrate the validity of using a strain gauge rosette for the particular application of a propagating strain wave. A look at the percentage error in the surface strain as the wave passes the delta rosette (fig.6.8) illustrates clearly that unsuitably large errors may result. The predicted angle α' for various angles of attack (fig.6.9) shows similarly unsatisfactory results. In both figures a choice of a = 0.0 m has been adopted. This is the minimum possible a if overlapping of the instruments is not allowed. Errors become substantially worse if values of a greater than 0.0 m are chosen. If overlapping is allowed then a choice of a < 0.0 m will decrease the error correspondingly. An absolutely correct prediction of the surface strain and direction

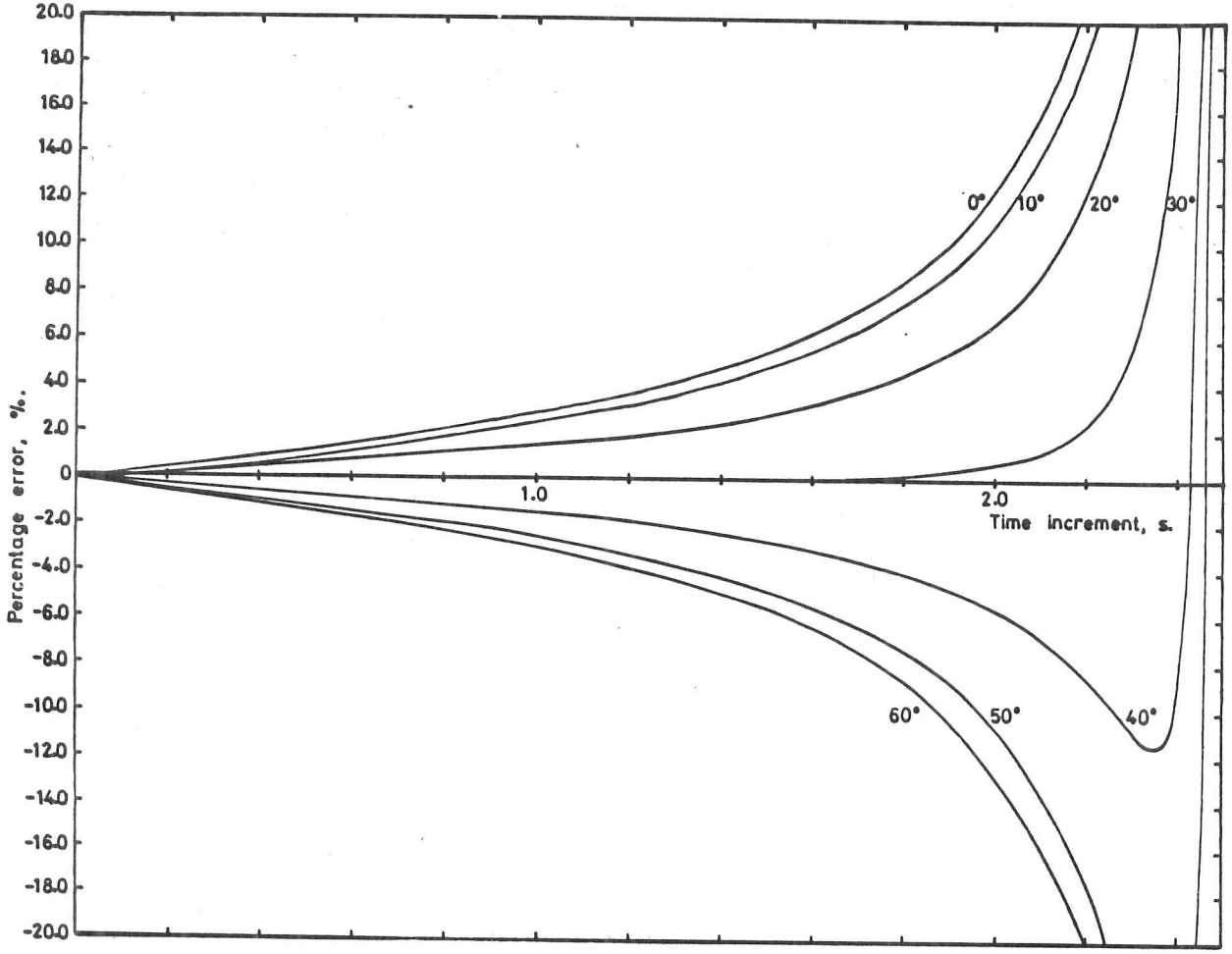

Fig. 6.8 Percentage error of strain measured by delta rosette as compared with single strainmeter in direction of impinging wave as a function of time increment for various angles of attack. Wave period is 10 s, separation parameter a=0.0 m.

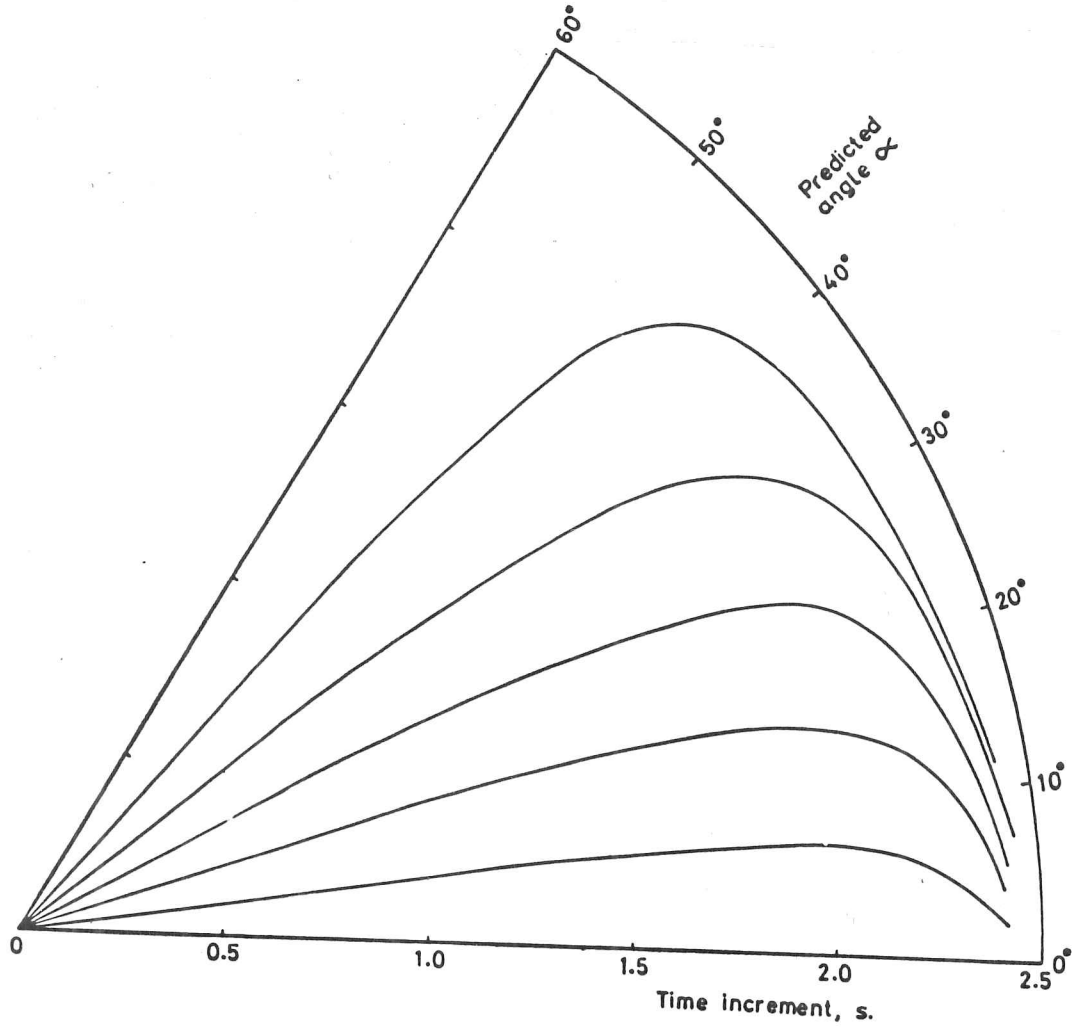

Fig. 6.9 Predicted angle α as measured by delta rosette as a function of time increment for various angles of attack. Wave period is 10 s, separation parameter a=0.0 m.

is only obtained if the instruments are positioned in a star configuration with a = -1.0 m. Such a configuration is hard to achieve in practice without a specially constructed set of meters, and has never as yet been employed.

The observed difference between input to the strain rosette and its output may be explained if one imagines oneself to be moving at the same velocity as the wave. As the wave propagates past the strain rosette, each instrument will sample a different part of its cycle due to their physical separation. The simplest example to consider is a wave whose direction of propagation is along the axis of one of the strainmeters, say in a direction $\alpha = 0^{\circ}$. Then strainmeters OB and OC will always experience a slight phase lag from strainmeter OA. An extreme case is when the strain measured on OB and OC vanishes. Then the strain measured by OA will not be zero and will give rise to a false principal strain in the y-direction. In this case the directions of the axes of principal strain will be correctly predicted. Waves whose paths do not coincide with the axis of a strainmeter, however, will produce errors in both the predicted directions and the principal strain values.

In order to demonstrate the use of strain rosettes to determine characteristics for propagating strain waves, we have for brevity assumed a monochromatic wave of known direction. Such a forcing is unrealistic for waves-in-ice and one might encounter a sea made up of waves and swell of many periods from several directions. The errors then become so unpredictable that continuous computation in the time domain is not a viable method for evaluating the direction of wave propagation and associated principal strains. Experiments with a simple one-dimensional Bretschneider spectrum (Bretschneider, 1963) showed large errors in the predicted angle of attack for all separations a not equal to -1.0 m. If a = -1.0 m, the direction and principal strains were correctly predicted.

6.9 Frequency-Domain Analysis

We have shown theoretically in the preceding analysis that a monochromatic sine wave propagating past a strain rosette will give rise to unavoidable errors due to a frequency-dependent phase lag between instruments. Clearly then, given the complexity of a typical ocean wave spectrum, an alternative method to time series analysis must be found. One such method is by transformation of the strain into frequency space. The method is demonstrated with data obtained on fast ice in Notre Dame Bay, Newfoundland. All data processing was carried out using the Hewlett-Packard 5451B Fourier Analyser system located at Memorial University of Newfoundland.

A running-power spectral density was computed for each strainmeter in the rosette every five minutes over the several hours of wave data. From each power spectral density a root-mean-square strain about some centre frequency was found by integration over a small frequency bandwidth. The bandwidth chosen was 5/320 Hz. There were clear peaks at 6 s and 13 s and it was the strains corresponding to these peaks which were used in the principal axes calculation. Figures 6.10 and 6.11 show the variation of the orientation of the axes of principal strain and the principal strains for the long- and short-period wave components as a function of elapsed time for the recorded ten hours of data.

The mean and standard deviation of the orientation angle weighted with respect to the larger principal strain were found for both components. The respective means were 2.4° and -13.6° with standard deviations of 7.8° and 7.3°. A Student's t-test gave independent distributions with better than 99.9% confidence indicating that the wave components were propagating in different directions and had originated from different sources. Observed wave directions over the duration of the experiment agreed with those predicted by the rosette.

At a particular location on the sea ice, the orientation of the axes of principal strain at any instant in time will depend on both

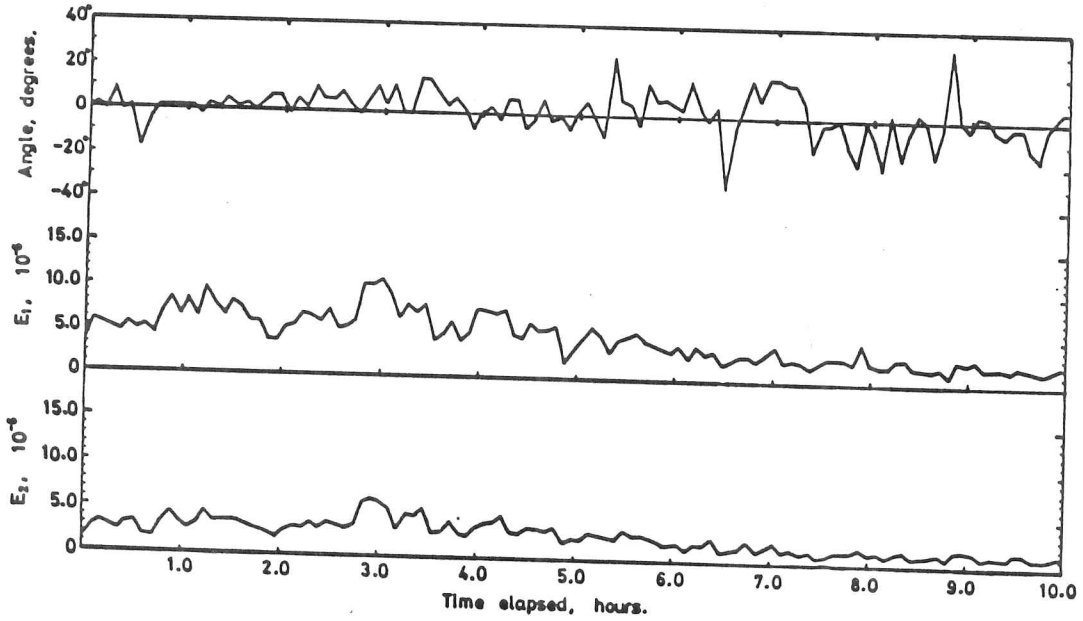

Fig. 6.10 Variation of orientation of principal axes of strain and principal strains for long-period component over 10 hours.

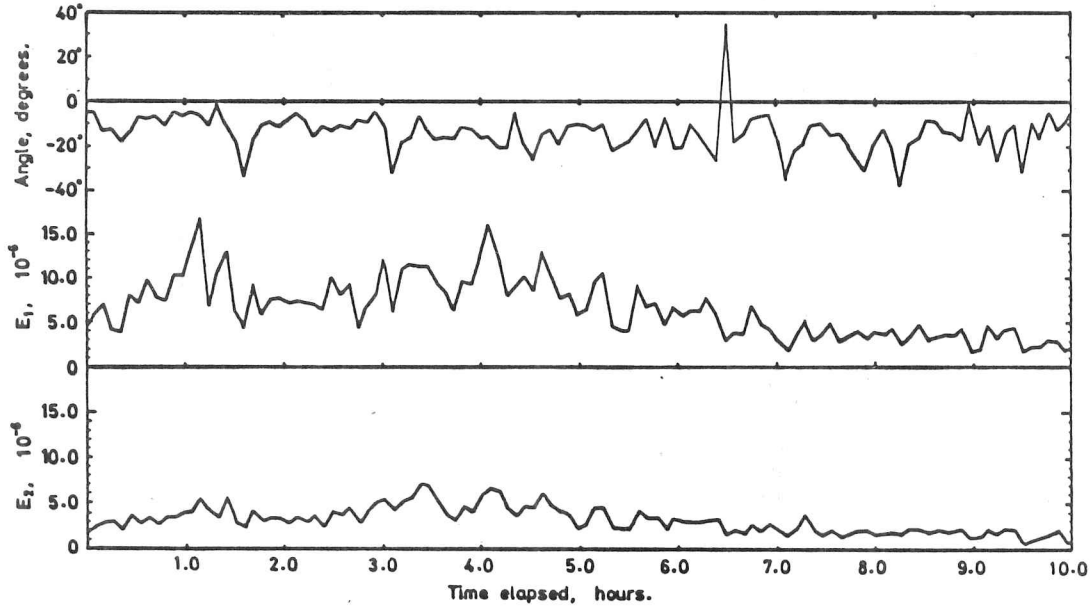

Fig. 6.11 Variation of orientation of principal axes of strain and principal strains for short-period component over 10 hours.

the amplitude and direction of the individual energies in the flexural wave spectrum. A predominant swell normal to the ice edge will generate a flexural wave travelling in the same direction. Waves impinging from other directions will interfere with the basic wave to produce a swing in the principal axes. This mechanism is a possible explanation for the parallel cracks which often form at an angle to the apparent incident swell during the wave break-up of sea ice. It also hints that a relationship between crack spacing and incident wavelength might be considerably more complicated than was first imagined.

6.10 Summary

We have extended the simple one-dimensional analysis of earlier chapters to allow for the possibility of waves impinging on an ice edge at other than normal incidence or, more generally, directional open water spectra. We have found that due to the presence of some attenuation in the wave numbers of all ice-coupled waves, their surfaces of constant phase and surfaces of constant amplitude do not coincide. The ice-coupled waves are therefore inhomogeneous. However, the functional dependence of the attenuation on angle of incidence is such that the inhomogeneity decreases with distance from the ice edge. The possibility of a critical angle is also discussed and it is found that particularly for short periods, total reflection can indeed occur for open water waves which have quite small angles of incidence. No critical angle exists for waves above a certain period so that long waves impinging at any angle will always generate ice-coupled waves.

In the second part of the chapter we have discussed the effect of the small but finite separation of the gauges in a strain rosette on the measurement of a propagating strain wave. The effect of this separation is to introduce a frequency-dependent phase difference between the gauges which gives rise to unsatisfactorily large errors in the subsequent analysis. These errors may be removed by superposition of the instruments to form a star configuration but such a rosette is physically unrealistic. Since most strain rosettes used at present in both mechanical and ice engineering do suffer

from some small gauge separation, it is essential to take this into account when measuring propagating cyclic strains.

The random nature of the forcing in geophysical applications makes it impossible to eliminate errors if the principal axes method is used in the time domain. It is therefore essential to employ frequency domain analysis for the treatment of data obtained by strainmeter rosettes.

CHAPTER 7

EXPERIMENTS AT STRATHCONA SOUND

EXPERIMENTS AT STRATHCONA SOUND

7.1 Introduction

The presence of flexural-gravity waves in sea ice has been established both theoretically and empirically in earlier chapters. Theoretically, it has been shown that the complex wave numbers associated with the wave modes in a linear theory are functions of both the material properties of the sea ice and the kinematics of the underlying water. That is to say that both the dispersive behaviour and the attenuation are prescribed by the adopted phenomenological model. The displacement due to such waves at any position on the surface of floating ice is therefore prescribed by three factors: the ice; the water; and the mode of generation. Experimentally, waves of this type have been observed close to large expanses of open water and their presence has been attributed to incident open water waves propagating beneath the ice cover. In this chapter, prompted by data obtained at Strathcona Sound, Baffin Island during Spring 1976 (Allan, 1976), we pose the question "Can flexural-gravity waves in sea ice be generated by mechanisms other than incident ocean waves?"

Strathcona Sound is a narrow fjord at the north-west end of Baffin Island. Its mouth opens on to Admiralty Inlet, a deep north-east facing bay adjoining Lancaster Sound (fig.7.1). The fjord is approximately 35 km long and at its mouth measures about 8 km across. About 20 km from the mouth a wharf comprised of three gravel-filled cells connected by a rock-filled apron to the shore has been constructed. The cells stand about 75 m off-shore in about 12 m of water. The wharf is shown in the insert of figure 7.2 and is discussed more fully in Frederking and Sinha (1977) with reference to its instrumentation with pressure transducers and strain gauges during Winter, 1975-1976. This formed part of a program by the Division of Building Research at the National Research Council in Ottawa to determine ice forces on off-shore structures.

In addition to wharf instrumentation it was felt that an analysis

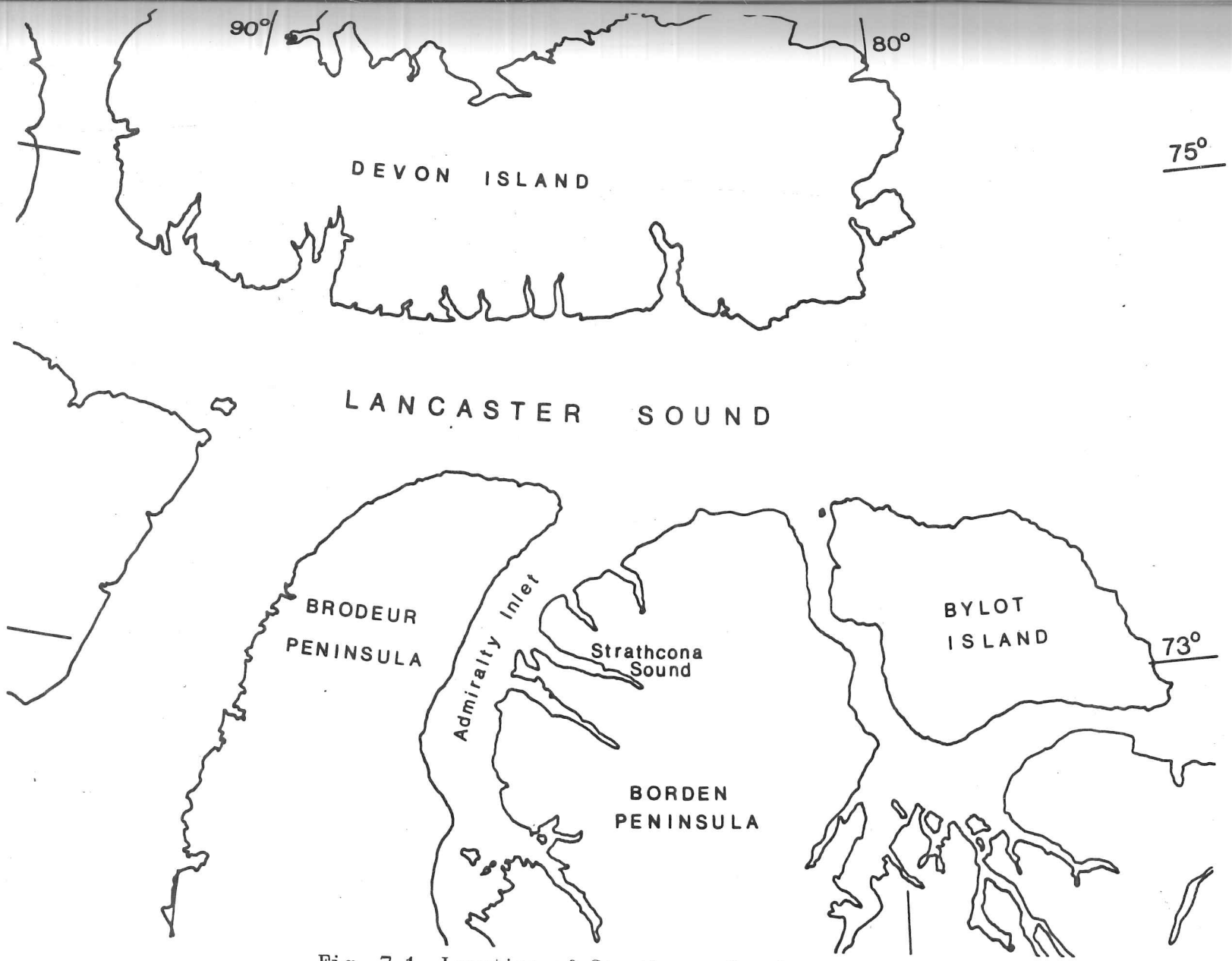

Fig. 7.1 Location of Strathcona Sound showing surrounding islands.

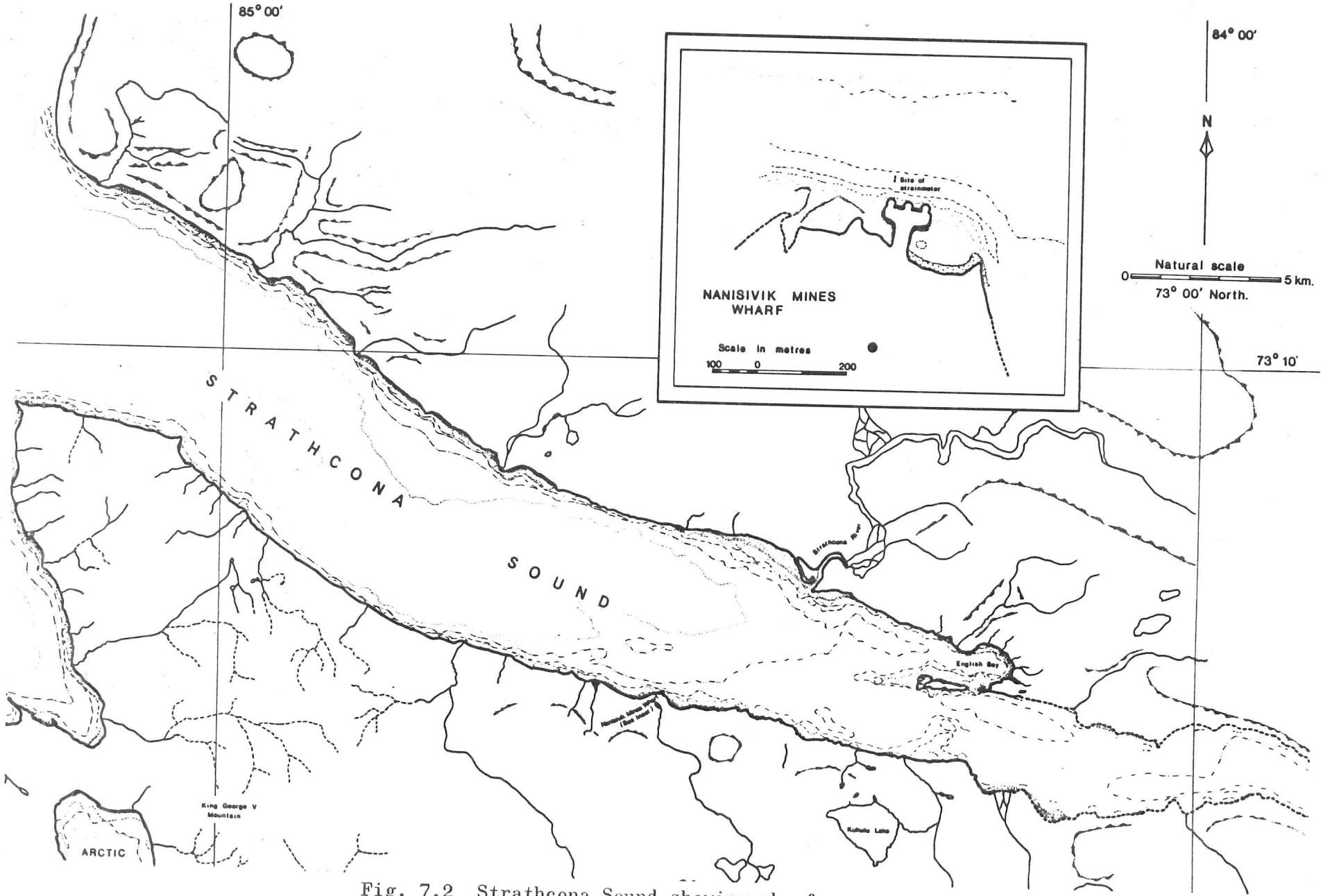

Fig. 7.2 Strathcona Sound showing wharf.

of the strain field around the wharf would provide valuable information towards the understanding of the stress processes at the ice/wharf interface. For this reason a linear array of three strainmeters was deployed on the surrounding sea ice. The ice around the cell formed three distinct regions: an active zone of width about 12 m consisting of very thick ice; an intermediate zone of width about 13 m; and a natural ice zone of ice thickness about 1.7 m which extended across the Sound. The strainmeters were positioned, one per zone, so as to extend radially from one of the three cells in a normal direction to the shore. The data discussed in this chapter were obtained from the strainmeter positioned farthest from the shore within the natural ice zone. We will not discuss results obtained relating to forces on the wharf but will report on some additional interesting observations which are significant to this thesis. The account will not be mathematical since insufficient data is available to prove or disprove any theory. Instead, the processed data will be presented and several possible mechanisms discussed by which such observations could occur. It is left to the reader to form his own conclusions.

7.2 The Wave Structure of the Strain Data

In order to ensure a good bond between the strainmeters and the underlying sea ice, a small area of surface snow was cleared before the instruments were deployed. The strainmeters were then encapsulated within their heavy plastic covers and the surface snow replaced so as to reduce to a minimum any direct coupling by the wind. Soon after the strainmeters were deployed a north-easterly wind of about 30 knots began to blow. The wind continued from the evening of the 18th May, through the 19th until, on the 20th, the storm subsided. Throughout the storm all three strainmeters continued to record.

On the morning of the 19th the ice at the wharf was observed to be moving to-and-fro with a period of about 30 s. This oscillation could also be seen on the meters registering the output from the instruments on the ice. The oscillations represented a cyclic

flexing of the ice by the underlying water. Such waves are commonplace in areas close to open water but were unexpected in the present situation. The data were recorded on a Racal Store 4 F.M. tape recorder for subsequent processing back in the laboratory.

The data from the strainmeter located on natural ice were digitised on the Hewlett Packard 5451B Fourier Analyser situated at Memorial University in Newfoundland. A preliminary analysis in the frequency domain revealed the presence of significant wave energy but it was felt that a larger computer was required to enable a more sophisticated numerical analysis to be carried out. The digitised data were therefore transferred via paper tape to the I.B.M. 370/165 at Cambridge University. A calibrated time-series plot of the data is shown in figure 7.3. The time-series shows a clear wave-like structure with the expected period of about 30 s. There is a significant trend which may be attributed to tide and a long wave of between 200 and 300 s which probably represents a seiche. A rough order of magnitude calculation based on the distance across the Sound shows the period of the long wave to be in good agreement with the fundamental seiche frequency.

The wave character of the strain record is seen more clearly in figure 7.4. These figures represent power spectral densities over blocks of about forty minutes. Each pair represents an unsmoothed and frequency averaged spectrum respectively. The spectra show significant energy in the band 25 s to 50 s with negligible energy for periods less than 10 s. Within that band the structure of the spectra remains the same though slight changes in the relative magnitudes are observed. At the 50 s end of the band the magnitude decreases and then increases again for the longer periods. This represents the long wave energy component in the record. Given the length of the time series considered however, no quantative interpretation of these long period waves is justified.

7.3 Discussion of Possible Mechanisms

The discussion will be divided into a number of subsections

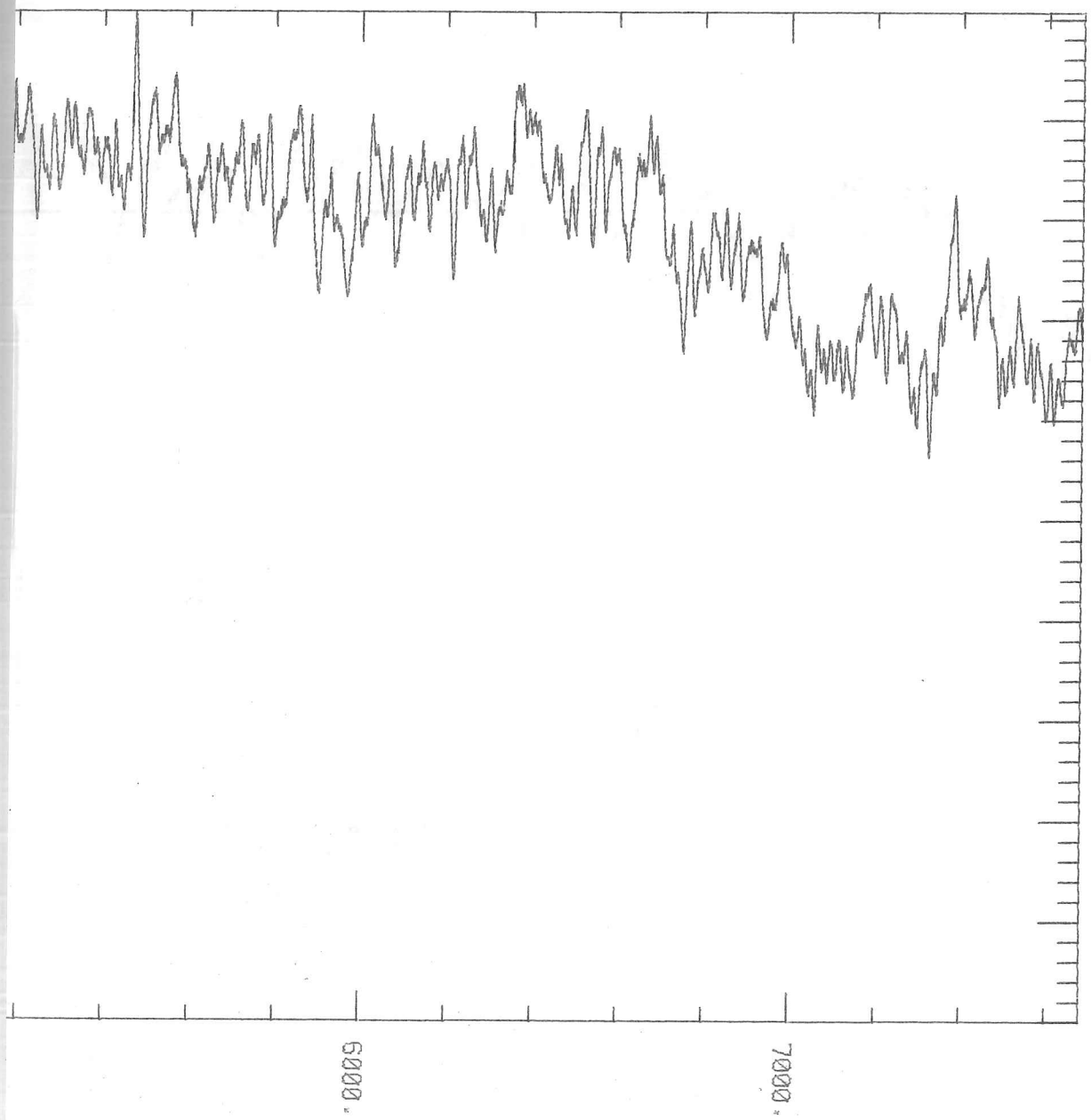

Fig. 7.3 Time series measured at Strathcona Sound.

5000
6000
7000

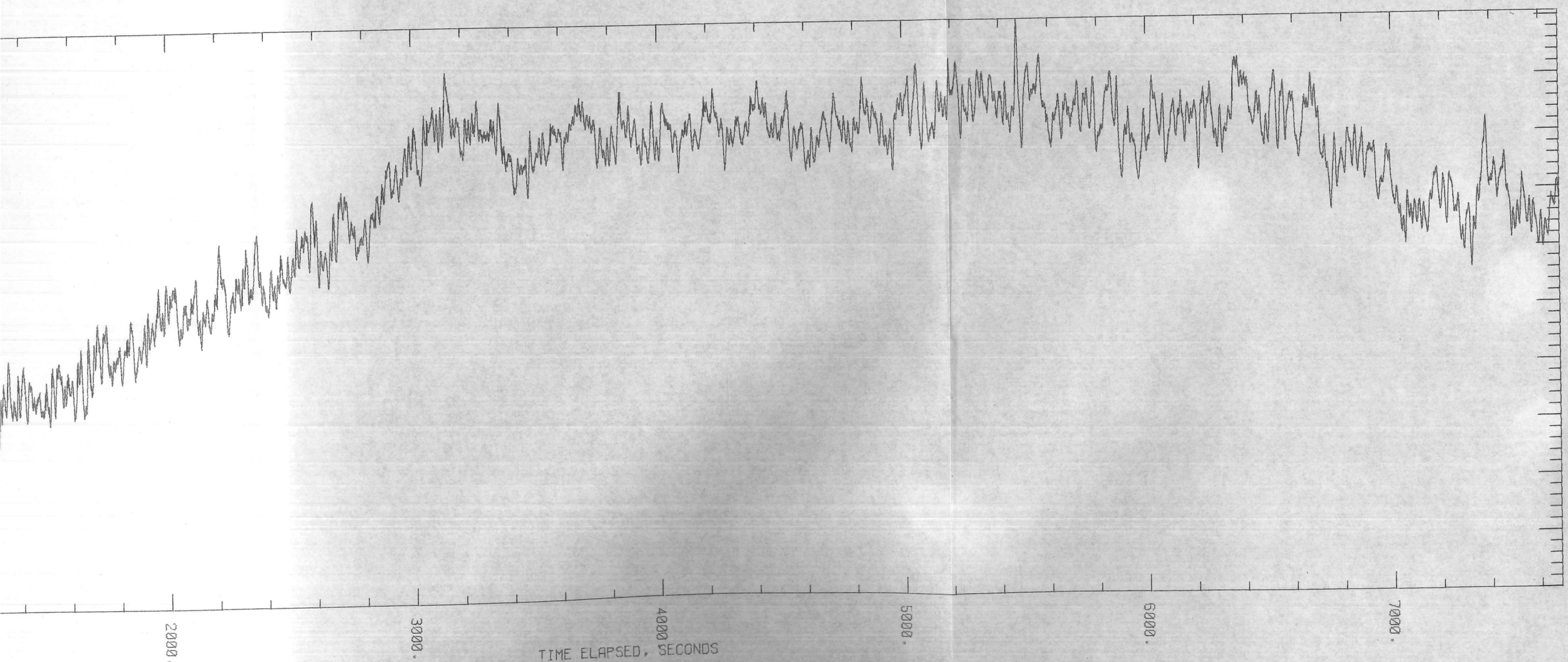

cona Sound.

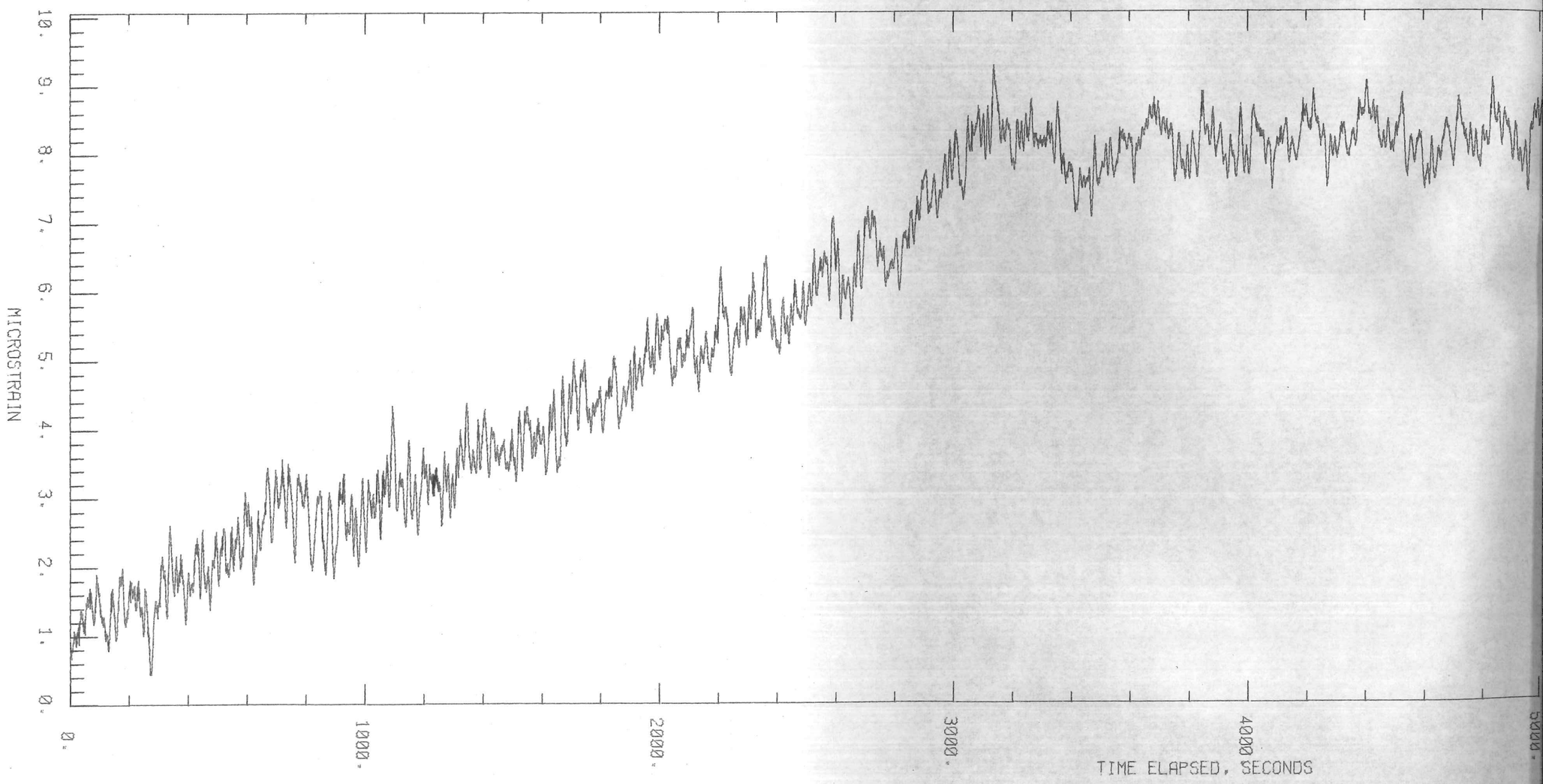

Fig. 7.3 Time series measured at Strathcona Sound.

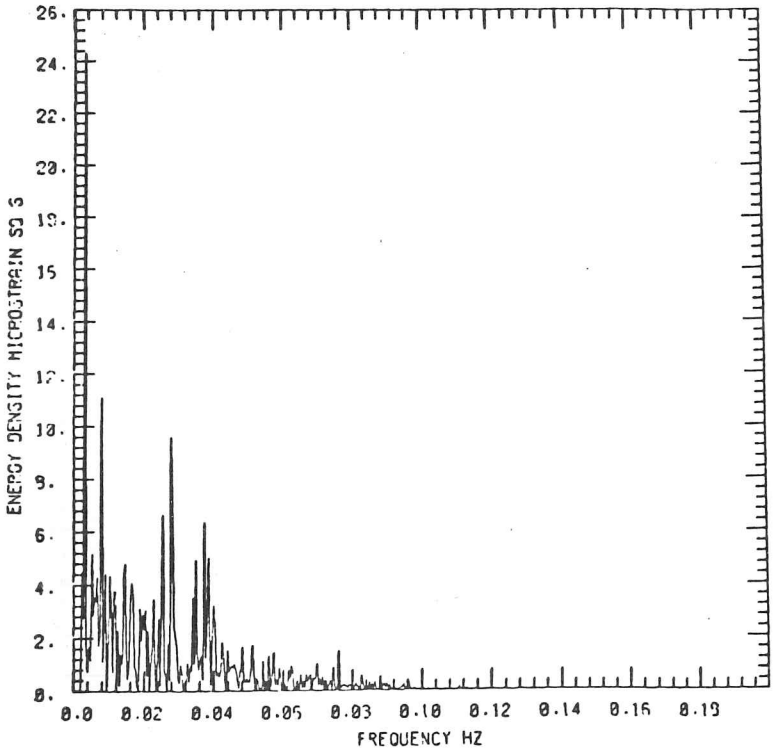

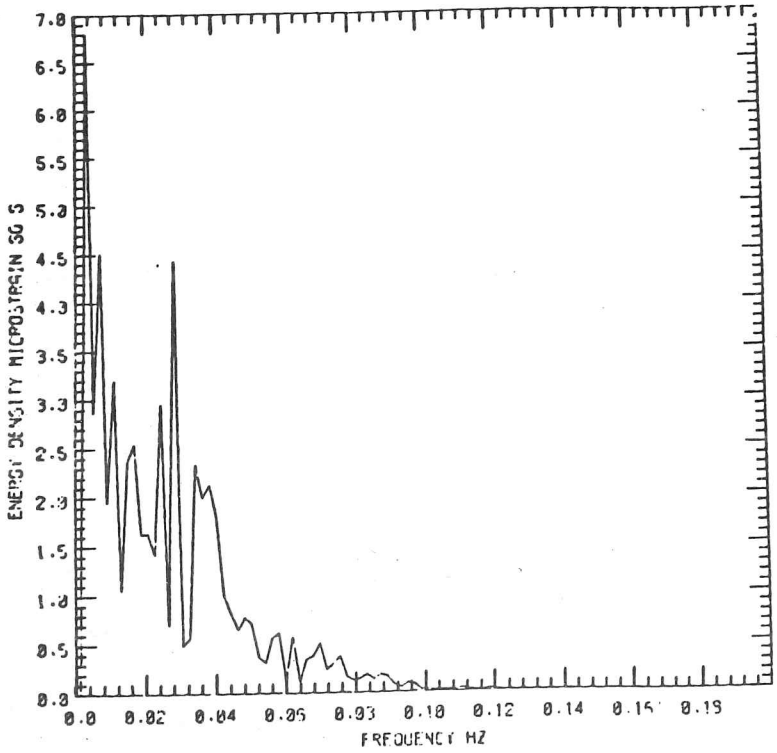

Fig. 7.4a Unsmoothed and frequency averaged spectra from Strathcona Sound strainmeter.

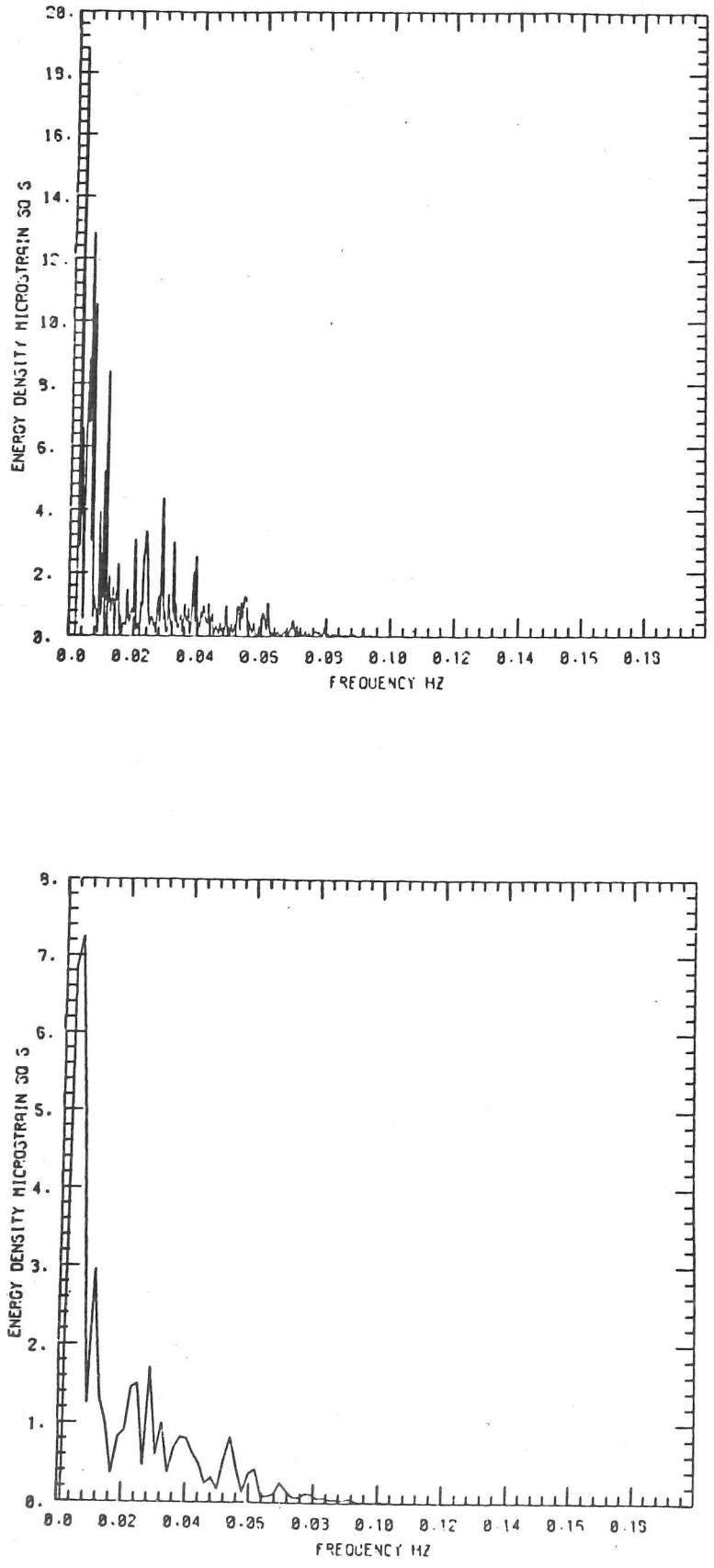

Fig. 7.4b Unsmoothed and frequency averaged spectra from Strathcona Sound strainmeter.

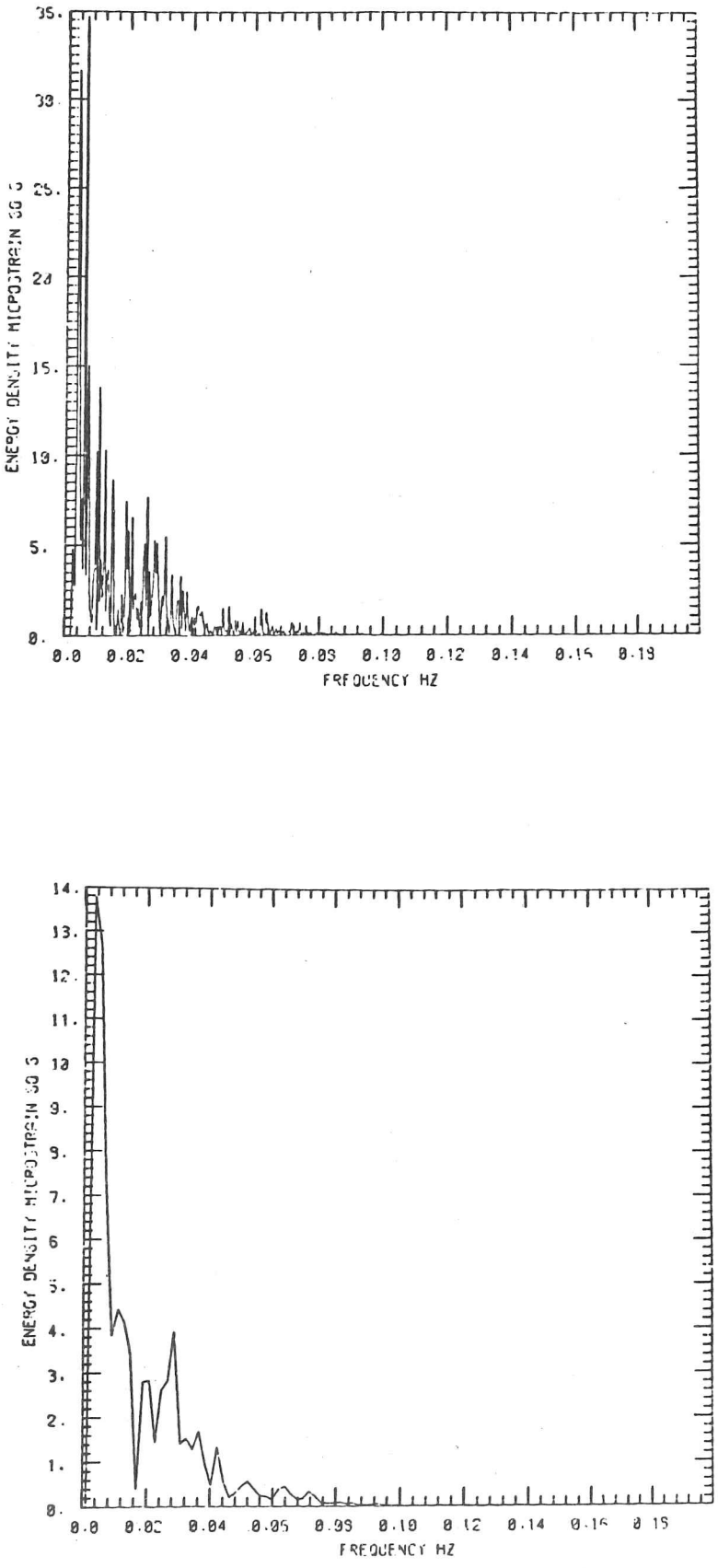

Fig. 7.4c Unsmoothed and frequency averaged spectra from Strathcona Sound strainmeter.

each considering a different mechanism by which the waves observed at Strathcona Sound could be generated.

Waves Generated in the Davis Strait

The spectra observed near the wharf in Strathcona Sound show little energy at periods less than 25 s. This type of spectrum might be expected for waves impinging on to the ice cover from the open ocean if the instruments were far enough from the ice edge. Clearly the location of the wharf satisfies this criterion. However it must be remembered that Strathcona Sound, Admiralty Inlet and much of Lancaster Sound were ice covered at the time of the experiment. Swells generated in the Davis Strait would therefore be required to travel quite a circuitous route as ice-coupled waves before finally reaching the wharf at Strathcona Sound. Further, if the spectrum is generated in the Davis Strait and all the short period energy is damped out during its passage through the ice, then the energy at 25-50 s should still be no greater than the energy in this frequency band observed in the open sea. The measured strains are of sufficiently large amplitude (0.1-1.0 microstrain) that the open water swells would require an extremely long fetch to reach the necessary magnitudes. Also the strainmeters were deployed with their axes across the Sound so that flexural waves propagating parallel to the coast would need to suffer significant refraction to produce the observed strains.

Edge Waves

D.A. Huntley (personal communication, 1977) suggested that the waves in Strathcona Sound could possibly be attributed to either progressive or standing, ice-coupled edge waves. Such waves are well discussed in the literature for open water (Bowen and Inman, 1971; Guza and Davis, 1974; Huntley, 1976) and may be thought of as longshore periodic wave motions whose amplitude is a decaying function of distance from the shore. The present author was unable to find any evidence for such waves in ice-covered water however. We shall assume that such waves can exist and suppose that the periodic surface strain measured at Strathcona Sound may

be attributed to their presence.

Since the strainmeters are deployed with their axes across the Sound they will record a wave motion which depends only on the rate of decay of the edge wave with distance from the shore. This may be seen more clearly in figure 7.5. For a standing edge wave, a strainmeter deployed as shown will register extension or compression depending on whether the ice profile is convex- or concave-up. A rough order of magnitude calculation may be carried out by assuming that the decay curve fits the profile for shallow, ice-free water and the ice represents a thin, inextensible layer on the surface. Then, in the concave-up position, the profile $w(x)$ is given by

$$\left.\begin{aligned} w(x) &= A_n L_n(2kx) e^{-kx}, \\ \left(\frac{2\pi}{T}\right)^2 &= gk(2n+1)\beta. \end{aligned}\right\} \qquad (7.1)$$

In these expressions, k is the longshore wave number, T is the period, A_n is the amplitude, β is the beach slope, x is the off-shore coordinate, g is the acceleration due to gravity and n is the edge wave mode number. The function $L_n(.)$ represents the Laguerre polynomial of order n. If we consider only the zeroth order then expressions (7.1) reduce to

$$\left.\begin{aligned} w(x) &= A_0 e^{-kx}, \\ \left(\frac{2\pi}{T}\right)^2 &= gk\beta. \end{aligned}\right\} \qquad (7.2)$$

The calculation now proceeds as follows: For a particular value of A_0 the x value corresponding to the strainmeter position is used to find the radius of curvature. Since the instruments are of short gauge length, the curvature along the strainmeter is assumed to be independent of x so that the chord length may be found easily. The theoretical strain experienced by the instrument may therefore be tabulated as a function of amplitude for various wave periods.

The above calculation was carried out for the present data and it was found that unrealistically large amplitudes A_0 (of the order of 10 m and above) would be necessary to achieve the measured

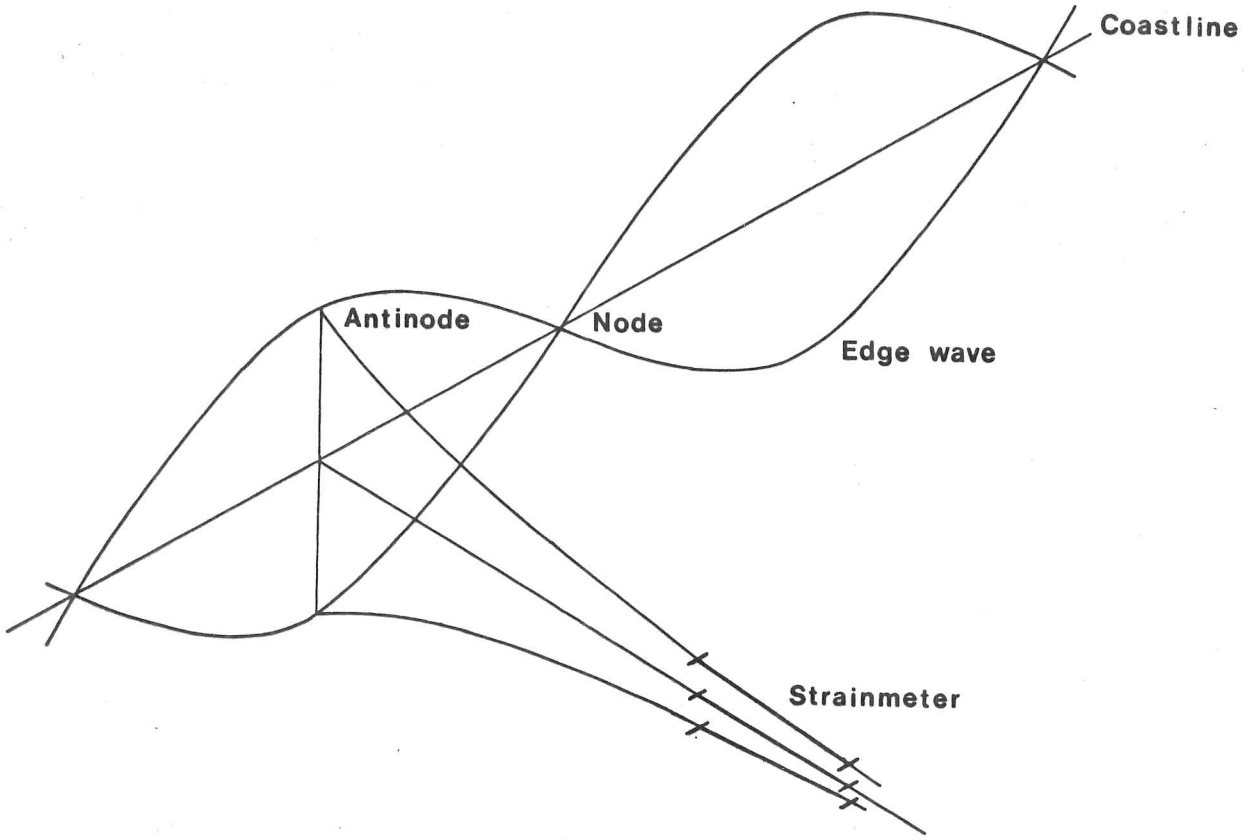

Fig. 7.5 Schematic representation of standing edge wave showing position of strainmeter relative to coast.

strains. Similar results were obtained for edge wave modes of higher order.

These calculations, though far from conclusive, demonstrate that the measured surface strains are unlikely to have been due to edge waves.

Wind Generation of Ice-Coupled Waves

Since the wave activity in Strathcona Sound appears to be linked with the onset of a storm, the possibility of generation of flexural-gravity waves by wind must be considered. Hunkins (1962) proposes such a mechanism for observations obtained at four U.S. drifting research stations in the Arctic Ocean. He found a continuous vertical oscillation in the period range 15 to 60 s using seismometers and gravimeters and attempted to correlate the wave amplitude with wind velocity. Correlation was notable only for wind speeds in excess of 10 or 12 ms^{-1}. Hunkins proposes that this represents a threshold speed and that efficient excitation of waves in ice-covered waters cannot occur at wind speeds less than this critical value. Observations carried out by LeSchack (1964) using gravimeters show the same continuous vertical oscillation of the ice cover. He concludes that the motion is due to both waves travelling from the open ocean and generation (or enhancement) of ice-coupled waves. Recent experimental work by Kiviniemi (1975) on ice in Pyhäjärvi Lake, Finland, also demonstrates the existence of wind-generated, ice-coupled waves. Using gravimeters and levelling instruments, Kiviniemi measured periods of about 15 s in thicknesses of ice between 20 and 35 cm over a wind speed range of 0.4–14 ms^{-1}. The wave and wind directions did not necessarily coincide.

Mills (1969) discusses wave generation by wind theoretically by considering a line pressure impulse moving over the ice surface. He shows the existence of a critical velocity at which the nature of the resulting solution for the deflection changes. For subcritical velocities the solution is characterized by a single

wavelength and attenuation coefficient which both decrease as the velocity tends to its critical value. For supercritical velocities however, the solution is made up of two wavelengths, one increasing, and the other decreasing as the velocity increases. The critical velocity corresponds to the minimum phase velocity. In a later paper Mills (1972) considers the problem more generally by assuming a travelling forcing effect of oscillating strength. Mills shows the significance of minimum group velocity and minimum phase velocity in determining the type of solutions generated. The frequency of oscillation is also critical.

For completeness, the present author has calculated expressions for both the phase and group velocities for an elastic plate on a fluid foundation of finite depth. The phase velocity c is given by

$$\left.\begin{aligned} c^2 &= \frac{\lambda g}{2\pi}\left[\frac{1 + (2\pi F/\lambda^4 g)}{\coth(\frac{2\pi D}{\lambda}) + \frac{G}{\lambda}}\right], \\ F &= \frac{2\pi^3 h^3 E}{3(1-\nu^2)\rho'}, \quad G = \frac{2\pi h \rho}{\rho'}. \end{aligned}\right\} \tag{7.3}$$

The group velocity U is given by

$$U = \frac{c}{2}\left[\frac{\coth(\frac{2\pi D}{\lambda}) + (\frac{2\pi D}{\lambda})\operatorname{cosech}^2(\frac{2\pi D}{\lambda}) + \frac{4F}{\lambda^3 c^2}}{\coth(\frac{2\pi D}{\lambda}) + \frac{G}{\lambda}}\right] \tag{7.4}$$

In the above equations, λ is the wavelength and D is the depth. All other parameters are defined earlier. Both these expressions have a minimum which depends on the water depth D and the ice thickness h. As depth increases the minimum phase velocity increases asymptotically to its value for deep water. The minimum group velocity however, reaches a maximum and then begins to decrease to the deep water value. The period at which the minima occur decreases with increasing water depth. As ice thickness increases the minimum in both the phase and group velocity occurs at larger periods and their magnitude increases.

Since the wave of minimum group velocity radiating from a

disturbance is associated with a relatively small energy decay, the behaviour of the group velocity curves is critical in determining dominant waves generated by moving pressure fluctuations. Unfortunately in Strathcona Sound the available wave data are insufficient to draw any quantative conclusions. The depth and geometry will play an important role in determining the dominant waves in a given situation. The maximum in the minimum group velocity at a particular depth may also be significant. In Strathcona Sound this would occur at a water depth of about 40 m and correspond to a period of about 17 s.

The wave spectrum at a given situation on the ice in Strathcona Sound might also be influenced by wind-induced seiche harmonics. Preferential coupling across the entire Sound could possibly cause a resonance at certain harmonics of the fundamental seiche frequency. Clearly this problem requires numerical work suited only to Strathcona Sound and will not be tackled here.

Non-Linear Effects and Surf-Beat

Very little can be said in this section due to both the extreme lack of data and the complexity of any non-linear theory which includes floating ice. Waves with the periods observed could certainly be generated by non-linear interaction between short period waves and long waves to form surf-beat but we still require a mechanism for the short waves. Perhaps the spectra observed at Strathcona Sound do indeed represent surf-beat where the shorter waves are generated by wind and the longer are natural oscillations within the Sound.

7.4 Summary

In this chapter we have presented some additional data showing flexural-gravity waves in sea ice. The data show significant energy between the periods 25 and 50 s. Several possible generating mechanisms have been discussed though few conclusions may be drawn because of the lack of data. The author feels that the oscillations are in part, if not entirely, due to wind coupling

with ice though it is left to the reader to form his own conclusions. It is hoped that further experiments in this field may be carried out in the near future using lake ice so that no swell-induced waves will be present.

CHAPTER 8

CONCLUSION AND OBSERVATIONS RELATING TO THE WAVE BREAK-UP OF SEA ICE

CONCLUSION AND OBSERVATIONS RELATING TO THE WAVE BREAK-UP OF SEA ICE

8.1 Summary

This brief section is included in order to reiterate some of the conclusions drawn in earlier chapters.

It was assumed in chapter 2 that the mechanical behaviour of sea ice in flexure may be represented by a thin, viscoelastic sheet whose properties are uniform through its thickness. This model was used to study the effect of waves impinging from an open water region ($x<0$) on to a semi-infinite cover of sea ice ($x\geq 0$). A monochromatic deep water wave at normal incidence was shown to generate a displacement within the ice cover which could be represented approximately by the superposition of three ice-coupled, flexural wave modes. The dispersion properties of the first of these three waves were similar to those of deep water waves at long periods but were dominated by the sea ice at shorter periods. The attenuation coefficient for this wave also depended on period and showed a gradual decrease as the wave period increased. The second and third waves, on the other hand, were determined by an attenuation coefficient and wavelength which, for all but very short waves, showed negligible dependence on period. These waves were attenuated much more rapidly than the corresponding wave of the first type so that, taking into account the respective transmission coefficients for the three waves, it is unlikely that they are significant after the first 50 m or so. They may, however, be critical in determining the wave break-up of fast ice. This is discussed further in section 8.2.

One of the limitations of chapter 2 which is clearly significant for sea ice, was the assumption that the properties did not vary through its thickness. In order to remove this restriction while still retaining some degree of mathematical tractability, a plate equation was derived in chapter 3 which allowed the viscoelastic model to be temperature dependent. Unfortunately, a single equation

equivalent to that used in chapter 2 could not be written down in general, and it was necessary to assume a steady temperature distribution through the ice cover. Further, the derived plate equations were only valid for materials which are thermorheologically simple. That is, the viscoelastic moduli at any temperature may be found directly from those at some reference temperature by using a shift function which is a fundamental property of the material.

By assuming a linear temperature gradient through the ice sheet and a reasonable, though not empirical, shift function, the plate equations of chapter 3 were shown to permit propagating, ice-coupled, flexural waves. A discussion of these waves was provided in chapter 4 where, rather than considering a semi-infinite ice cover, the ice was assumed to be infinite in extent. The inclusion of temperature had negligible effect on the wavelength of the ice-coupled waves but was critical in determining their attenuation coefficients. Rotatory inertia and transverse shear were shown to have little effect except for unrealistically thick sea ice or artificially generated high frequency flexural oscillations.

In chapter 5, a summary was given of preliminary, field experiments carried out by the author to measure flexural-gravity waves in sea ice. The data were recorded using strainmeters deployed on the surface of fast ice in Newfoundland. Subsequent data processing revealed the presence of significant wave energy within the ice cover and allowed the author to measure the wavelength at certain periods. Good agreement with the theory was found. Further observations relating to waves near the ice edge, attenuation, and the incident open water spectrum were also discussed.

The important generalization to three-dimensionality was made in chapter 6 where obliquely incident deep water waves were considered. It was shown that waves of this type can give rise to inhomogeneous flexural waves within the ice cover so long as their angle of incidence is less than some critical angle. Total reflection occurred at angles of incidence greater than the critical angle and this possibly accounts for the unexpectedly severe wave activity

on the open water side of an ice edge (P. Wadhams, personal communication, 1978).

The second part of chapter 6 was included to demonstrate an unexpected problem that the author experienced while measuring directional surface strain fields on fast ice. It was found that large errors may result from attempting to use a standard rosette analysis for measuring propagating cyclic strains. A simple theoretical model showed that instrument separation was critical and that, in a physically realizable rosette, the errors were unavoidable without frequency domain analysis.

Chapter 7 was, in many ways, an adjunct to the rest of the thesis since the conclusions reached were purely speculative. Nevertheless the observations are considered to be extremely significant because they possibly represent a different mechanism for the generation of ice-coupled waves. Due to insufficient data, no positive conclusions were reached though certain generating mechanisms were tentatively rejected.

8.2 Wave Break-up of Fast Ice in Newfoundland

No discussion of ice-coupled waves in fast ice off the Newfoundland coast is complete without some brief mention of wave break-up. This occurs whenever the incident sea has sufficient intensity to fracture the ice. The pattern always seems to be the same. Parallel cracks appear roughly perpendicular to the predominant sea swell so as to form long strips of ice independent of the main ice sheet. Each strip then rotates in turn on the wavefield, breaks up along its length and the resulting angular cakes float clear. In this way several hundred metres of smooth fast ice can become independently floating ice floes and cakes in less than an hour.

Examination of both the remaining ice after break-up and photographs of the dispersed floes (see plates 3 and 4) shows that crack separation is remarkably consistent. This hints that the

break-up has been determined by the wave characteristics of the incident sea rather than any imperfections in the original ice sheet. In all cases observed the crack separation has been of the order of 20 m though the open water conditions have appeared to be totally different in each case. This suggests that perhaps the crack separation is only weakly dependent on the period of the incident sea waves. That is, the dispersive properties of the fracturing oscillation are such that the wavelength does not change significantly with period. The common factor in all cases however has been an ice thickness between 40 and 50 cm.

This section may well have been called "future work", for the author does not propose to solve the question of wave break-up. However, the observation that crack separation is consistent in similar thicknesses of sea ice for different incident seas, is believed to be extremely relevant. Figure 2.6 indicates that the two waves which can exist only locally to the ice edge may play an important role. Field work being carried out off the east coast of Greenland at the present time has enabled direct measurements to be made of the surface strain at the moment of break-up. It is hoped that subsequent data processing will provide both the magnitude and period of the fracturing strain field, and an additional measure of the crack separation.

8.3 Further Work

Finally, we collect together some of the many suggestions for further work which have appeared in this thesis:

(i) The thermoviscoelastic model. Experimental verification that sea ice may be modelled as a thermorheologically simple material is required. Such an experiment would provide more data for (or against) the Maxwell-Voigt mechanical analogy and would yield an empirically derived shift function. A more realistic theoretical description of sea ice might then proceed along the lines of chapter 3. The author cannot see an easy way of removing the assumption of a steady temperature distribution though the brief

discussion on temperature in Appendix A shows that this is a good approximation.

(ii) A brine volume model. An extension to section (i) might be to use brine volume rather than temperature in a theoretical model of sea ice. Such a model would require experimental determination of the viscoelastic moduli as functions of brine volume, and a knowledge of the brine volume distribution through the sea ice.

(iii) Experiments. Further experiments with strainmeters are required to measure the dispersive characteristics of the ice-coupled waves and their attenuation as a function of distance from the ice edge. The experiments should be backed-up with an extensive programme to measure local physical properties. Also data are required from strainmeters deployed on lake ice to determine whether wind-coupling is a possible generating mechanism for flexural waves in ice.

(iv) Wave break-up. An extension to section 8.2 is required. The author believes that the major factor which controls the crack separation is ice thickness. An experiment could easily be carried out to test this hypothesis.

APPENDIX A

THE SEA ICE MODEL

THE SEA ICE MODEL

A.1 Introduction

The assumption of a linear viscoelastic formulation for the behaviour of sea ice requires that some particular relaxation function be chosen to solve problems. This relaxation function and its associated complex modulus may only be determined by experiment and one would expect that no such function exists which adequately represents sea ice under all circumstances. Although by no means necessary, we have used a mechanical analogy to model the visco-elastic properties for the particular example of sea ice in flexure. The analogy we have chosen is that of a Maxwell unit in series with a Voigt unit as shown in figure 2.1. The data for the individual elements in this model were provided by Tabata (1958a) who measured flexural bending of sea ice beams. In this, and a later paper by Tabata in Japanese (Tabata, 1958b), the Maxwell-Voigt model provides good agreement with experiment. There was, however, much scatter in the values obtained for the spring and dashpot constants and their orders of magnitude were questionable.

The two Young's moduli were found to be smaller than expected by an order of magntude and the two viscosities larger by approximately the same amount. These discrepancies may possibly be explained by the variability of sea ice as a material; perhaps the sea ice tested by Tabata in Japan was not representative of sea ice in general. Certainly sea ice along the Labrador coast of Newfoundland shows marked differences from Arctic sea ice in both its crystal structure and its material properties.

A.2 The Variability of Sea Ice (Newfoundland, 1976)

Newfoundland sea ice rarely shows the columnar structure often seen in the Arctic; it tends to show a polycrystalline structure throughout its thickness. This is believed to be due to the conditions under which it is formed. A. Allan (personal communication, 1977) proposes that wave climate plays an important role. Storms incident on the Newfoundland coast will "churn-up" freshly grown frazil ice between ice floes to form an abnormally

thick soupy mass which will solidify into a polycrystalline composite. Two cores taken by the author from first year ice in the Strait of Belle Isle in February, 1976 substantiate this argument. Plate 5 shows typical Newfoundland sea ice whereas plate 6 shows Newfoundland sea ice obtained from a particularly sheltered area nearby where growth was undisturbed. Each photograph within the plates represents a horizontal section taken at 10 cm intervals down the core. Using a sledge microtome the sections were honed to optimum thickness for photography through crossed polaroids and a 1 cm graticule. The length of each core was approximately 60 cm. Clearly then, as far as crystal structure is concerned, sea ice is an extremely variable material. Cores taken within tens of metres of one another may show an entirely different composition when viewed through crossed polaroids.

In addition to its crystal structure, other factors may influence the mechanical properties of sea ice. A parameter often used in this connection is the porosity or volume of void within the ice (Schwarz and Weeks, 1977). If the volume of air within the sea ice is assumed small when compared with the brine volume then the porosity may be regarded as being wholly due to the brine volume. The brine volume may be derived from the salinity and temperature profiles across the ice thickness using the empirical relations derived by Frankenstein and Garner (1967).

Profiles of temperature, salinity and density were constructed from ice samples obtained in the Strait of Belle Isle. From the first two profiles, the brine volume variation through the ice thickness could therefore be calculated. Each profile was constructed from measurements made at approximately the same air temperature as quickly as possible after the core had been removed from the ice sheet. Figure A.1 shows typical profiles through 55 cm of ice cover. For most of the cores examined the salinity curve showed the characteristic C-shape observed by Weeks and Lee (1958, 1962). The large salinity at the surface of the sea ice is attributable to the fast growth velocity during the early stages of formation (Weeks and Lofgren, 1967). One would therefore expect the salinity to decrease substantially for the first 20 cm. Below that, the

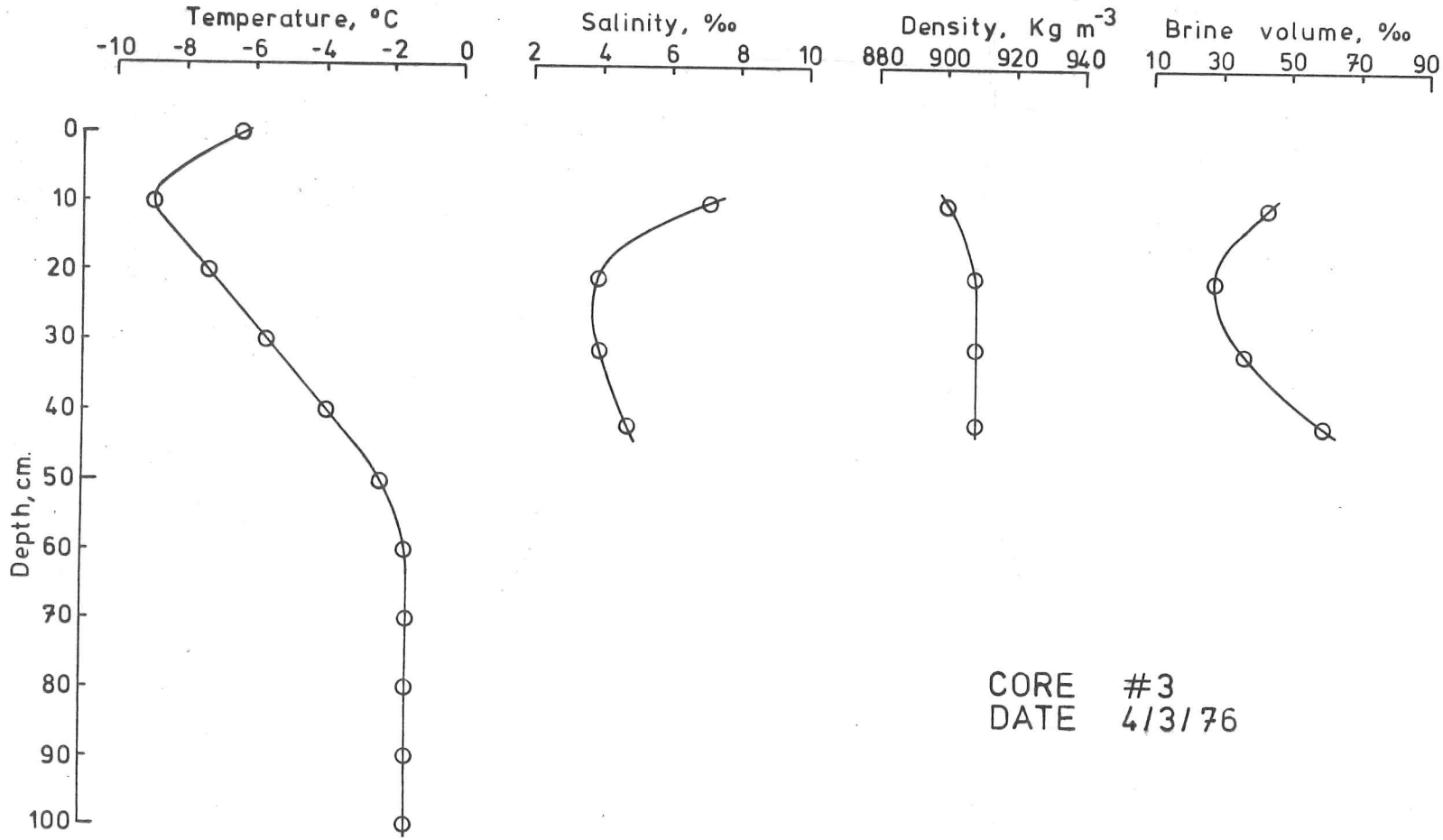

Fig. A.1 Temperature, salinity, density and brine volume profiles through an ice core.

salinity gradually increases again due to the underlying sea water tending to fill brine channels under hydrostatic equilibrium. This explanation over-simplifies many of the more subtle effects encountered in growing sea ice concerned with brine drainage features and brine cell migration. We shall not discuss such effects here; the interested reader is referred to Weeks (1966) and Eide and Martin (1975).

Density data for all the cores obtained are presented in figure A.2. Clearly the data is extremely scattered and there does not appear to be any systematic variation in density through the ice sheet. Density values below 850 Kg m^{-3} may be attributed to layers of air bubbles in the core. Weeks and Lee (1958) observed similar scatter for cores obtained at Hopedale in Labrador and noted a general decrease in density with age of the ice sheet. Unfortunately, density measurements could not be made over a sufficient time-scale to observe this effect in the present data due to an early break-up. The density data are presented here only for completeness. In order to obtain a meaningful profile of density as a function of depth in the sea ice sheet, each density reading must be corrected for both salinity and temperature (Anderson, 1960).

The temperature data in figure A.1 were obtained using a thermistor probe, designed and built by Terry Ridings of C-CORE, Memorial University of Newfoundland. The probe was frozen into the sea ice early in the season and daily readings were taken at the same time as the ice cores were removed for analysis. The particular profile shown in figure A.1 shows sea ice which has not yet reached equilibrium. If the boundary conditions remain the same, the effect of the surface temperature will slowly propagate through the ice at a rate controlled by the thermal diffusivity of the material. The shape of the steady state curve will depend on the thermal conductivity (Doronin and Kheisin, 1977, ch.5); a constant thermal conductivity yielding a linear temperature profile. A linear temperature profile has been used consistently in the temperature dependent ice sheet model of chapter 4. This is shown

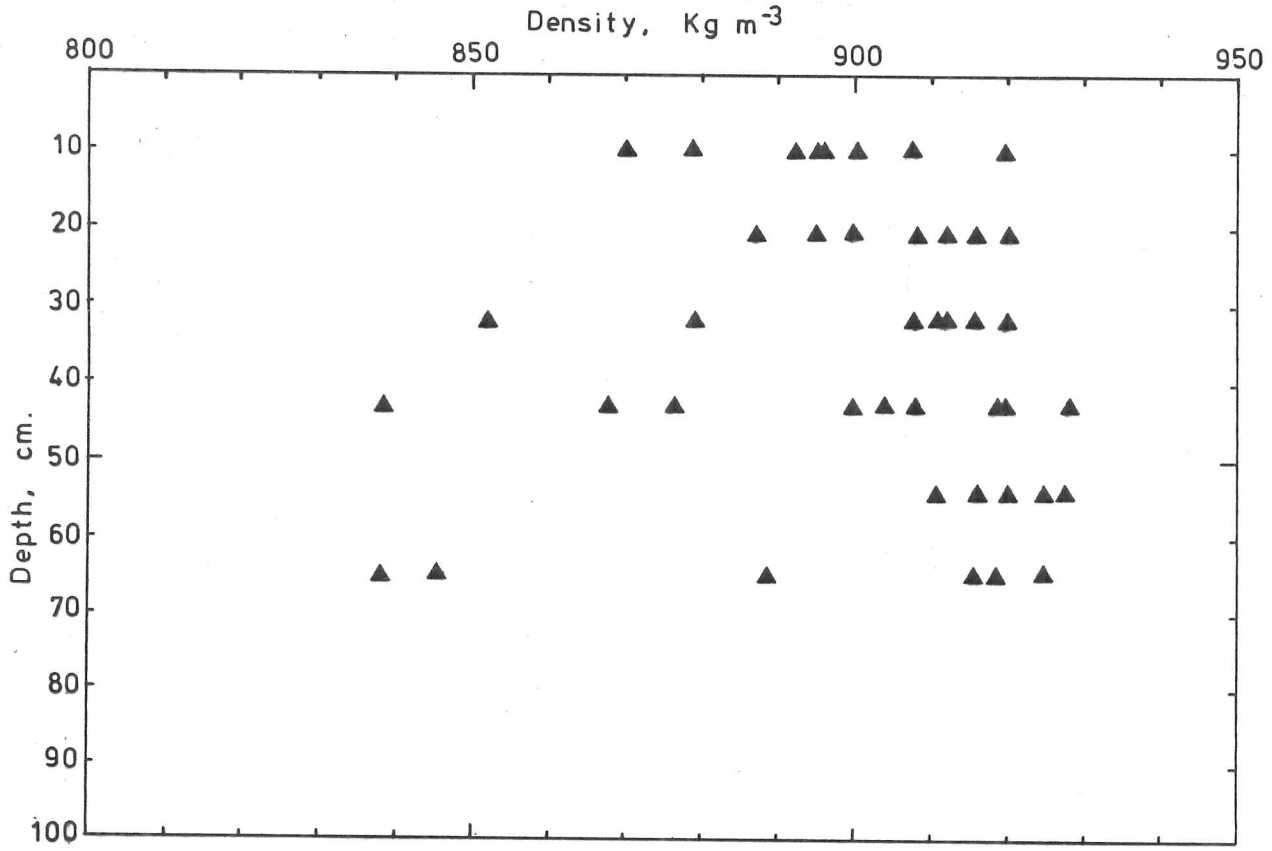

Fig. A.2 Scatter diagram for density profile through the ice sheet.

to be a reasonable approximation for floating sea ice in the three dimensional evolutionary temperature profiles shown in figure A.3. The figure shows a series of daily temperature profiles taken over three-and-a-half weeks. The gaps represent days when storms prevented any measurements being taken. Fluctuations in the surface temperature show as a saw-tooth in the direction of time at depth zero whereas the equivalent fluctuation at depth 100 cm is approximately constant since the thermistor probe is well into the underlying sea water. Each daily profile consists of a linear portion within the sea water and an approximately linear portion of different gradient through the sea ice. The location of this change in gradient therefore reflects the ice thickness and the growth of the ice with time is clearly seen.

An alternative presentation for the temperature profile through an ice sheet is shown in figure A.4. This data was obtained the following year from a thermistor probe frozen into sea ice at Starve Harbour, near Twillingate, Newfoundland. The method of sampling had been improved from the previous year and a chart recorder automatically recorded a profile through the ice every hour. There is a five minute time lag between sampling of individual thermistors in the probe and the temperature records of each depth have been shifted in time accordingly. By tracing certain surface temperature features through the ice, an approximate value for the average thermal diffusivity between the surface thermistor and any other thermistor in the probe may be found. Such problems are discussed fully in Carslaw and Jaeger (1973, chap.3).

In the above discussion experimental results obtained in Newfoundland have been used to demonstrate the considerable variability of sea ice and show the behaviour of some important parameters. These parameters were obtained from cores withdrawn from the floating ice sheet in the usual way. It is important to note however that the material properties should strictly be measured <u>in situ</u>, an extremely difficult task for all but the temperature profile. Although the cores were analysed as quickly as possible after withdrawal from the ice sheet, some brine drainage

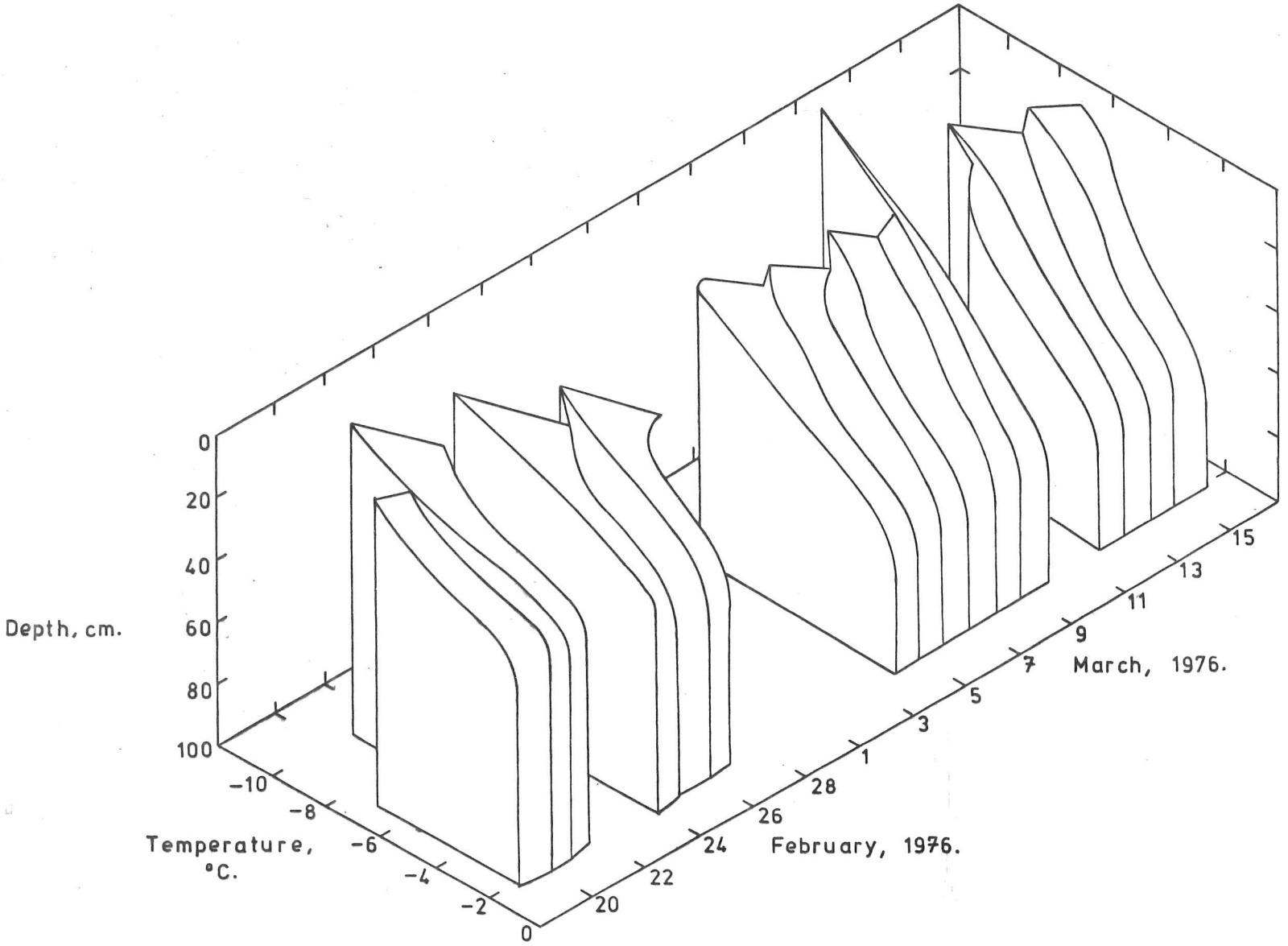

Fig. A.3 Three-dimensional evolution of temperature through a sea ice sheet.

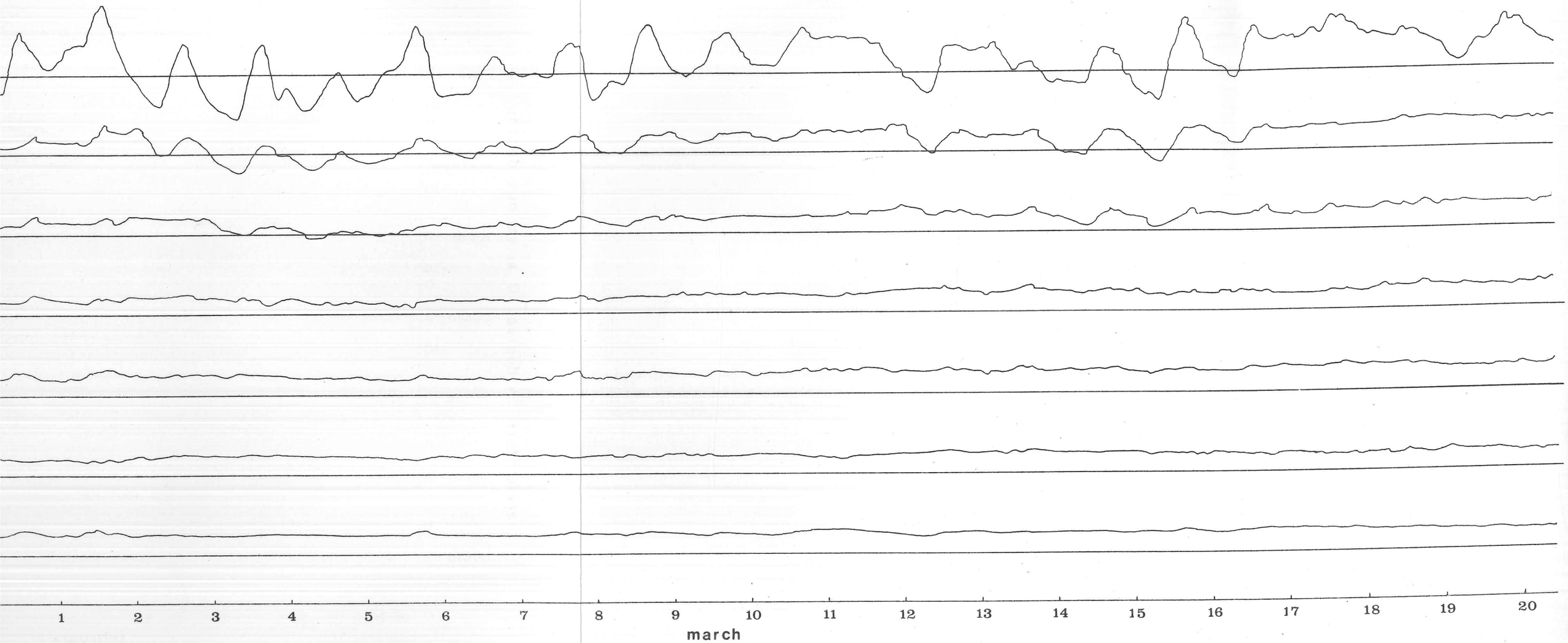
1
2
3
4
5
6
7
8
9
10
11
12
13
14
15
16
17
18
19
20
march
time elapsed (date & hour)

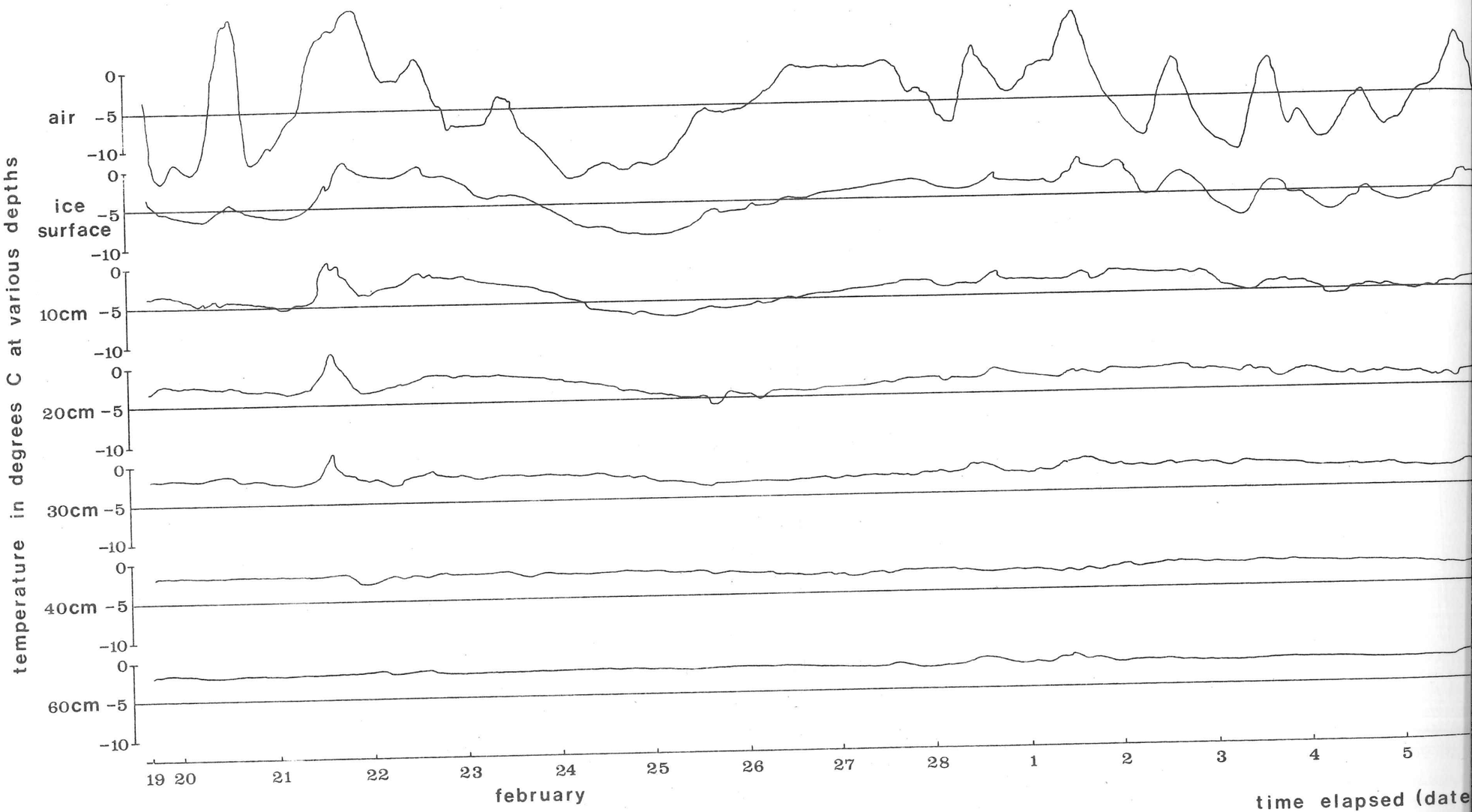
temperature in degrees C at various depths
air
ice surface
10cm
20cm
30cm
40cm
60cm
0
-5
-10
19 20
21
22
23
24
25
26
27
28
1
2
3
4
5
february
time elapsed (date

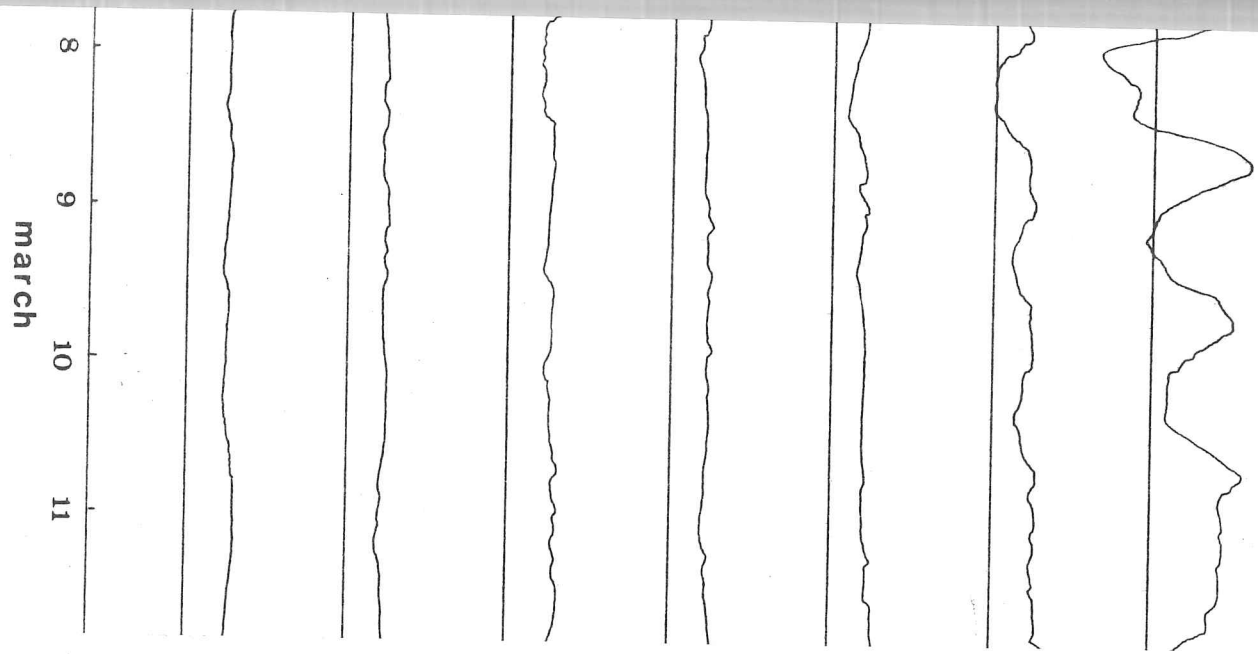

Fig. A.4 Temperature profile through sea ice at Starve Harbour.

is inevitable since the ice sheet is in hydrostatic equilibrium. As soon as the core is removed, a distinct change in shade takes place as the brine flows under gravity down brine channels into the underlying sea water. Such a change was also obtained in laboratory grown sea ice at temperatures as low as -30°C. It therefore seems that any estimates of salinity and hence brine volume obtained from cores will considerably underestimate the *in situ* value. Unfortunately, since the amount of brine present in the sea ice due to hydrostatic pressure is a function of the distribution and size of brine drainage channels, no correction may be applied to yield *in situ* brine volume profiles.

A.3 A Further Discussion of Temperature

With the uncertainty of the magnitude and shape of the *in situ* salinity and density profiles through sea ice and the considerable dependence of brine volume on temperature, the first improvement to an isotropic model of sea ice would be a model with a realistic temperature profile. Such a formulation could draw upon the literature of both ice engineering and the polymer sciences. In the previous section we decided that a linear temperature profile would provide a good approximation to floating sea ice but we still have no idea how the mechanical properties depend on temperature. Since the necessary experiments on sea ice have not been carried out it was necessary to make certain assumptions regarding this temperature dependence. Sea ice was assumed to be thermorheologically simple (Schwarzl and Staverman, 1952) with a parabolic shift function. Such a choice is discussed in chapter 4 from a mathematical point of view. The only experimental study which might provide an empirically derived shift function for sea ice discusses the internal friction (Tabata, 1959).

In terms of the parameters used in this thesis, internal friction is defined as

$$\frac{\text{loss modulus}}{\text{storage modulus}} \qquad \text{(A.1)}$$

and is usually denoted by $\tan \delta$. Tabata measured the internal

friction of sea ice by the lateral vibration method. In this method a small sample of material is made to resonate by some external forcing. After some time the forcing is removed and the oscillations allowed to decay naturally. From the decay rate, the internal friction may be found. This technique to determine the viscoelastic properties of a material does not work for long time-scales. Unfortunately in dealing with floating sea ice, it is precisely those time-scales that we are interested in. Hence, on this scale, it is impossible to test whether sea ice satisfies a certain viscoelastic model by the lateral vibration method alone. For this reason we chose the in situ bending beam tests of Tabata (1958) rather than the lateral vibration tests of Tabata (1959) as our model of sea ice. Once again it is clear that considerably more in situ experimental work must be carried out on sea ice before we can even begin to understand its complex material properties.

In the 1959 paper, Tabata shows the internal friction as a function of temperature. His figure 6 is presented here for convenience as figure A.5. In that paper he also derives the Young's modulus and, tentatively assuming a Maxwell model, the internal viscosity of sea ice. If we compare these values with those of Tabata (1958) we find inconsistencies. This leads to a difference of several orders of magnitude if the internal friction, as calculated from the 1958 paper, is compared with figure A.5. It is this reason that prevents a shift function being derived from Tabata (1959). If, however, frequency and temperature data from that paper are used with the chosen parabolic shift function, the internal friction curves show exactly the same shape as those of figure A.5. Qualitatively we may therefore say that our hypothetical shift function is physically reasonable.

D.J. Goodman (personal communication, 1978) has pointed out that the functional dependence of creep on temperature for non-saline, polycrystalline ice is known to be of the form:

$$\exp\left(\frac{Q}{RT}\right), \qquad \text{(A.2)}$$

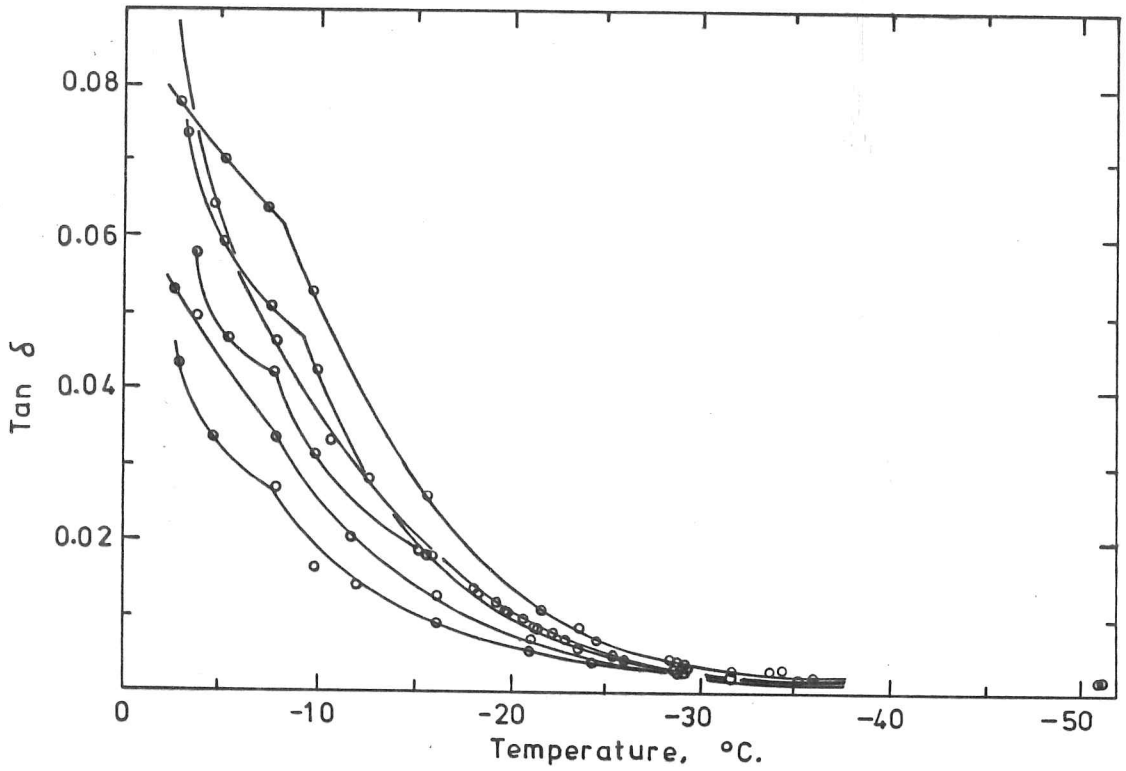

Fig. A.5 The relationship between tan δ and temperature for granular ice (after Tabata, 1959).

where Q is the activation energy, R is the gas constant and T is the temperature in °A. This expression may be justified on a microscopic scale (Goodman, 1977). However, it is important to note that sea ice material is known to behave quite differently from non-saline ice under a change of temperature. The presence of large quantities of unfrozen brine and air in any sample of sea ice affect its thermal properties considerably. This is clearly seen if one compares Hobbs (1974, chap.5) with Anderson (1960). In addition, although the activation energy for non-saline ice has been measured several times, little experimental work has been carried out in this respect on sea ice.

A survey of the current literature revealed a paper by Nakaya and Muguruma (1962) discussing the physical properties of old sea ice. Strictly, old sea ice is an entirely different material from the first year ice of Newfoundland since brine volume decreases with age. Indeed Inuits recognize old sea ice as a fresh water source. Nakaya and Muguguma show that an exponential relationship between viscosity and temperature is satisfactory in the range -3°C to -18°C. However very few data points are available. For temperatures above -3°C no data exist, for temperatures below -18°C an exponential increase seems too fast. Unfortunately, since the underside of floating sea ice is at its melting point, a knowledge of the dependence of creep on temperatures above -3°C is essential. As Glen (1955) points out in his experimental study of non-saline polycrystalline ice, local melting on an appreciable scale would upset the foundations on which the exponential law is based. Given first year sea ice then, with large quantities of <u>in situ</u> brine, one would expect the range of validity for a simple exponential dependence of creep on temperature to be substantially decreased.

Returning to the original hypothesis that sea ice is a thermorheologically simple material, how then do we decide upon a suitable shift function? Clearly the properties of sea ice are strongly dependent on temperature but also the way in which they depend is local to a small temperature range. The precipitation

of salts at temperatures of -8.2°C and -22.8°C, for example, will have considerable effect. With this in mind a suitable shift function might include an activation energy which is local to small temperature ranges within a total range from -1.8°C to -50.0°C, say. Clearly such a shift function poses serious problems in any mathematical analysis. For this reason we have chosen a considerably simplified shift function with parabolic form.

APPENDIX B

COMMUTATIVITY

COMMUTATIVITY

In the derivation of the plate equations in chapter 3 it was assumed that consecutive relaxation functions acting on the strain $\varepsilon(\underset{\sim}{x};t)$ under the operation $\circ$ were commutative. The operation defined by (3.12) is rewritten here for convenience

$$\mu \circ \varepsilon = \mu(0)\varepsilon(\underset{\sim}{x};t) - \int_{-\infty}^{t} \varepsilon(\underset{\sim}{x},\tau)\frac{\partial}{\partial\tau}\mu(\xi_t - \xi_\tau)\,d\tau, \tag{B.1}$$

where

$$\xi_t = \int_0^t \chi\left[\vartheta(\underset{\sim}{x};s)\right]ds, \tag{B.2}$$

and the subscript refers to the upper limit of integration. It is assumed that the relaxation operator $\mu(t)$ belongs to H^1 and the strain $\varepsilon(t)$ is bounded for all t. The shift function $\chi(\vartheta)$ is required to satisfy the following conditions:

$$\chi(\vartheta_0) = 1, \quad \frac{d\chi}{d\vartheta} > 0. \tag{B.3}$$

Then, following the change of variable outlined in Muki and Sternberg (1961) we invert (B.2), since ξ_t and ξ_τ are monotonically increasing functions of t, and write

$$t = t(\underset{\sim}{x}, \xi_t). \tag{B.4}$$

Whence, we define a new strain function $\hat{\varepsilon}(\underset{\sim}{x};\xi)$ such that

$$\varepsilon(\underset{\sim}{x};t) = \hat{\varepsilon}(\underset{\sim}{x};\xi_t) = \varepsilon\left[\underset{\sim}{x};\, t(\underset{\sim}{x};\xi_t)\right]. \tag{B.5}$$

The operation $\mu \circ \varepsilon$ may therefore be rewritten explicitly in terms of ξ_t:

$$\mu \circ \hat{\varepsilon} = \mu(0)\hat{\varepsilon}(\underset{\sim}{x};\xi_t) - \int_{-\infty}^{\xi_t} \hat{\varepsilon}(\underset{\sim}{x};\xi_\tau)\frac{\partial}{\partial\xi_\tau}\mu(\xi_t - \xi_\tau)\,d\xi_\tau, \tag{B.6}$$

where we have assumed that the temperature tends to the reference temperature for prior times sufficiently distant from the current time. (B.6) belongs to a general class of operators of the form

$$Af = a_1 f + \int_{-\infty}^{t} a_2(t-\tau)f(\tau)\,d\tau, \tag{B.7}$$

where a_1 is a constant and $a_2(\cdot)$ is continuous (or piecewise continuous). We require to prove that

$$BAf = ABf, \tag{B.8}$$

where B is another operator of the same form. Clearly, such a proof reduces to a change in the order of integration in the expression

$$\int_{-\infty}^{t} b_2(t-\tau)\left[\int_{-\infty}^{\tau} a_2(\tau-s)f(s)\,ds\right]d\tau. \tag{B.9}$$

Such a change is permissible for bounded relaxation functions and strain $\hat{\varepsilon}$ (Burkill, 1951, sect.5.4). Proceeding, we obtain

$$\int_{-\infty}^{t} f(s)\left[\int_{s}^{t} b_2(t-\tau)a_2(\tau-s)\,d\tau\right]ds, \tag{B.10}$$

so substituting $u=\tau-s$, we obtain

$$\int_{-\infty}^{t} f(s)\left[\int_{0}^{t-s} a_2(u)b_2(t-s-u)\,du\right]ds. \tag{B.11}$$

The inner integral is in the standard form of a convolution so that the roles of $a_2(\cdot)$ and $b_2(\cdot)$ may be interchanged. Hence the necessary commutativity between consecutive relaxation functions operating on $\varepsilon(\underline{x};t)$ has been proved.

APPENDIX C

INTERCHANGEABILITY

INTERCHANGEABILITY

In the derivation of the plate equations in chapter 3 it was necessary to assume that the operation of differentiation with respect to time could be interchanged with the operation $\mu\circ(.)$. That is

$$\frac{\partial}{\partial t}\mu\circ(\cdot) = \mu\circ\frac{\partial(\cdot)}{\partial t}. \tag{C.1}$$

We will show here that this interchangeability is valid for thermorheologically simple materials at constant temperature state. We rewrite equation (3.12) here for convenience:

$$\mu\circ\varepsilon = \mu(0)\varepsilon(\underset{\sim}{x};t) - \int_{-\infty}^{t}\varepsilon(\underset{\sim}{x};\tau)\frac{\partial}{\partial\tau}\mu(\xi_t - \xi_\tau)d\tau, \tag{C.2}$$

where

$$\xi_t = \int_0^t \chi\left[\vartheta(x;s)\right]ds, \tag{C.3}$$

and the subscript refers to the upper limit of integration. Clearly differentiation with respect to time may be interchanged with the operation $\circ$ in (C.2) as far as the first term is concerned and we need only consider the integral. Then, from Hildebrand (1965),

$$\begin{aligned}\frac{\partial}{\partial t}\int_{-\infty}^{t}\varepsilon(\underset{\sim}{x};\tau)\frac{\partial}{\partial\tau}\mu(\xi_t-\xi_\tau)\,d\tau \\ = \int_{-\infty}^{t}\varepsilon(\underset{\sim}{x};\tau)\frac{\partial}{\partial t}\left[\frac{\partial}{\partial\tau}\mu(\xi_t-\xi_\tau)\right]d\tau + \varepsilon(\underset{\sim}{x};\tau)\frac{\partial}{\partial\tau}\mu(\xi_t-\xi_\tau)\Big|_t\end{aligned} \tag{C.4}$$

The proof is therefore dependent on

$$\frac{\partial}{\partial t}\left[\frac{\partial}{\partial\tau}\mu(\xi_t-\xi_\tau)\right] = -\frac{\partial^2}{\partial\tau^2}\mu(\xi_t-\xi_\tau), \tag{C.5}$$

for if this is true, an integration by parts gives

$$\int_{-\infty}^{t}\frac{\partial}{\partial\tau}\varepsilon(x;\tau)\frac{\partial}{\partial\tau}\mu(\xi_t-\xi_\tau)d\tau, \tag{C.6}$$

the desired result. However, condition (C.5) is not true in general since a simple substitution gives

$$\frac{\partial}{\partial t}\left[\frac{\partial}{\partial \tau}\mu(\xi_t - \xi_\tau)\right] = -\frac{\partial}{\partial \tau}\left\{\frac{\chi[\vartheta(x;t)]}{\chi[\vartheta(x,\tau)]}\frac{\partial}{\partial \tau}\mu(\xi_t - \xi_\tau)\right\}, \qquad (C.7)$$

which reduces to (C.5) only for constant temperature states.

BIBLIOGRAPHY

BIBLIOGRAPHY

Abramowitz, M., and I.A. Stegun. 1965. Handbook of Mathematical Functions, Dover Publications, Inc., New York, 1046 pp.

Allan, A.J. 1975. The breaking of sea ice by ocean waves. Scott Polar Res.Inst.Field Report, 12 pp.

Allan, A.J. 1976. C-CORE goes to the Arctic. C-CORE News, 1(3), 1-3.

Allan, A.J., and W. Windsor. 1977. Industrial applications of ice strain measurements. Proceedings of 4th International Conference on Port and Ocean Engineering under Arctic Conditions, Memorial University of Newfoundland, Vol.2, 629-637.

Allan, A.J., and V.A. Squire. 1978. Naturally induced surface strain in fast ice. C-CORE publication. In press.

Anderson, D.L. 1960. The physical constants of sea ice. Research, 13(8), 310-318.

Anderson, D.L. 1963. Use of long-period surface waves for determination of elastic and petrological properties of ice masses. In Ice and Snow, ed. W.D. Kingery, M.I.T. Press, Cambridge, Mass., 63-68.

Assur, A. 1958. Composition of sea ice and its tensile strength. Arctic Sea Ice. Conference held at Easton, Maryland, Publn. 598 of Natn.Acad.Sciences - Natn.Res.Counc., Washington D.C. 106-138.

Assur, A. 1967. Flexural and other properties of sea ice sheets. Physics of Snow and Ice. Proceedings of the International Conference on Low Temperature Science, 1966, ed. H. Oura, Hokkaido Univ., Japan, Vol.1, 557-567.

Barnett, T.P., and J.C. Wilkerson. 1967. On the generation of ocean wind waves as inferred from airborne radar measurements of fetch-limited spectra. J.mar.Res., 25(3), 292-328.

Bendat, J.S., and A.G. Piersol. 1971. Random Data: Analysis and Measurement Procedures, Wiley-Interscience, New York, 407 pp.

Biot, M.A. 1954. Theory of stress-strain relations in anisotropic viscoelasticity and relaxation phenomena. J.appl.Phys., 25(11), 1385-1391.

Biot, M.A. 1955. Dynamics of viscoelastic anisotropic media. Proceedings of the Second Midwestern Conference on Solid Mechanics, Purdue Univ., 94-108.

Bowen, A.J., and D.L. Inman. 1971. Edge waves and crescentic bars. J.Geophys.Res., 76(36), 8662-8671.

Bretschneider, D.L. 1963. A one dimensional gravity wave spectrum. Ocean Wave Spectra. Natn.Acad.Sciences - Natn.Res.Counc. Conference held at Easton, Maryland, May 1-4, 1961. Prentice-Hall, Englewood Cliffs, 1963, 41-65.

Budden, K.G. 1961. Radio waves in the Ionosphere; The Mathematical Theory of the Reflection of Radio Waves from Stratified Ionised Layers. Camb.Univ.Press, Cambridge, England, 542 pp.

Burkill, J.C. 1951. The Lebesgue Integral, Camb.Univ.Press., (Camb. Tracts in Math. and Math.Phys., No.40), Cambridge, England, 87 pp.

Carslaw, H.S., and J.C. Jaeger. 1973. Conduction of Heat in Solids, Univ. Press, Oxford, 2nd ed., 510 pp.

Chirgwin, B.H., and C. Plumpton. 1969. A Course of Mathematics for Engineers and Scientists, Volume 5, Pergamon Press, Oxford, 202 pp.

Christensen, R.M. 1971. Theory of Viscoelasticity: An Introduction, Academic Press, Inc., New York, 245 pp.

Cox, G.F.N., and W.F. Weeks. 1975. Brine drainage and initial salt entrapment in sodium chloride ice. RR 345, U.S. Army Cold Regions Research & Engineering Laboratory, Hanover, New Hampshire, 85 pp.

Crary, A.P., Cotell, R.D., and J. Oliver. 1952. Geophysical studies in the Beaufort Sea, 1951. Trans.Am.geophys.Un., 33(2), 211-216.

Crary, A.P., and N. Goldstein. 1957. Geophysical studies in the Arctic Ocean. Deep Sea Res., 4, 185-201.

Dally, J.W., and W.F. Riley. 1965. Experimental Stress Analysis and Motion Measurement, McGraw-Hill Book Co., Inc., New York, 520 pp.

Dean, C.H. 1965. Ocean waves and pack ice in the Antarctic Evershed News (London), 8(1), 10-11.

Dettman, J.W. 1970. Applied Complex Variables, Macmillan , New York, 481 pp.

Doronin, Y.P., and D.E. Kheisin. 1977. Sea Ice, Published for the Office of Polar Programs and National Science Foundation, Washington D.C., by Amerind Publishing Co., Pvt. Ltd., New Delhi, 322.

Dove, R.C., and P.H. Adams. 1964. Experimental Stress Analysis and Motion Measurement (Theory, Instruments and Circuits, Techniques), Charles E. Merrill Pub.Co., Columbus, Ohio, 515 pp.

Dykins, J.E. 1970. Ice engineering - tensile properties of sea ice grown in a confined system. Naval Civil Engineering Laboratory, Technical Report R689, Port Hueneme, Calif., 56 pp.

Eide, L.I., and S. Martin. 1975. The formation of brine drainage features in young sea ice. J. Glaciol., 14(70), 137-154.

Evans, D.V., and T.V. Davies. 1968. Wave-ice interaction. Rep. 1313, DL 3207/084, Contract Nonr. 263(36), Office of Naval Research. Supported by the Arctic Research Project of the U.S. Naval Ordnance Laboratory, 102 pp.

Ewing, M., Crary, A.P., and A.M. Thorne. 1934. Propagation of elastic waves in ice, part I. Physics, 5, 165-168.

Ewing, M., and A.P. Crary. 1934. Propagation of elastic waves in ice, part II. Physics, 5, 181-184.

Flügge, W. 1975. Viscoelasticity, Springer-Verlag, Berlin, 2nd ed., 194 pp.

Frankenstein, G., and R. Garner. 1967. Equations for determining the brine volume of sea ice from -0.5° to -22.9°C. J. Glaciol., 6(48), 943-944.

Frederking, R., and N.K. Sinha. 1977. Ice action on wharf at Strathcona Sound. Proceedings of 4th International Conference on Port and Ocean Engineering under Arctic Conditions, Memorial University of Newfoundland, Vol.2, 707-717.

Glen, J.W. 1955. The creep of polycrystalline ice. Proc. R.Soc. Lond. A., 228(1175), 519-538.

Goodman, D.J. 1977. Creep and Fracture of Ice and Surface Strain Measurements on Glaciers and Sea Ice, Ph.D. dissertation, Univ. of Cambridge, England, 150 pp.

Goodman, D.J., Allan, A.J., and R.G. Bilham. 1975. Wire strainmeters on ice. Nature, Lond., 255(5503), 45-46.

Goodman, D.J., and C. Neal. 1977. A 1 m strainmeter for use on sea ice. Scott Polar Res.Inst. Report III. In press.

Gradshteyn, I.S., and I.M. Ryzhik. 1965. Tables of Integrals, Series and Products, Academic Press, New York, 4th ed., 1086 pp.

Graff, K.F. 1975. Wave Motion in Elastic Solids, Clarendon Press, Oxford, 649 pp.

Greenhill, A.G. 1887. Wave motion in hydrodynamics. Am.J.Math., 9, 62-112.

Gurtin, M.E., and E. Sternberg. 1962. On the linear theory of viscoelasticity. Archs ratin.Mech. Analysis, 11, 291-356.

Guza, R.T., and R.E. Davies. 1974. Excitation of edge waves by waves incident on a beach. J.Geophys.Res., 79(9), 1285-1291.

Heading, J. 1964. Electromagnetic Theory and Special Relativity, University Tutorial Press, London, 302 pp.

Hendrickson, J.A. 1966. Interaction theory for a floating elastic sheet of finite length with gravity waves in water of finite depth. Rep. NBy-62185 by Natn.Engng. Science Co., Pasadena, Calif. for U.S. Naval Civil Engng.Lab., Port Hueneme, Calif., 178 pp.

Hendrickson, J.A., and L.M. Webb. 1963. Theoretical investigation of semi-infinite ice floes in water of infinite depth. Rep. NBy-32225 by Natn.Engng. Science Co., Pasadena, Calif. for U.S. Naval Civil Engng.Lab., Port Hueneme, Calif., 43 pp.

Hendrickson, J.A., Webb, L.M., and R.T. Quigley. 1962. Study of natural forces acting on floating ice fields. Rep. NBy-32215 by Natn.Engng. Science Co., Pasadena, Calif. for U.S. Naval Civil Engng.Lab., Port Hueneme, Calif., 72 pp.

Henry, C.J. 1968. Wave-ice interaction model experiments. Rep.1314, CL 3207/084, Contract Nonr. 263(36), Office of Naval Research. Supported by the Arctic Ordnance Laboratory, 46 pp.

Hetényi, M.I. 1946. Beams on Elastic Foundations; Theory with Applications in the Fields of Civil and Mechanical Engineering, Ann Arbor, University of Michigan Press, (Univ. of Mich. Studies. Scientific Series, Vol.16), 255 pp.

Hildebrand, F.B. 1965. Methods of Applied Mathematics, Prentice-Hall, Inc., New Jersey, 2nd ed., 362 pp.

Hobbs, P.V. 1974. Ice Physics, Clarendon Press, Oxford, 837 pp.

Holdsworth, G. 1969. Flexure of a floating ice tongue. J. Glaciol., 8(54), 385-397.

Holdsworth, G. 1971. Calving from Ward-Hunt ice shelf, 1961-1962. Can.J. Earth Sci., 8(2), 299-305.

Holdsworth, G. 1974. Erebus glacier tongue, McMurdo Sound, Antarctica. J. Glaciol., 13(67), 27-35.

Holister, G.S. 1967. Experimental Stress Analysis, Principles and Methods, Camb.Eng. Series, ed. Sir John Baker, Camb.Univ. Press, Cambridge, England, 62-76.

Hunkins, K. 1962. Waves on the Arctic Ocean. J. Geophys.Res., 67(6), 2477-2489.

Hunter, S.C. 1961. Tentative equations for the propagation of stress, strain and temperature fields in viscoelastic solids. J. Mech.Phys. Solids, 9, 39-51.

Huntley, D.A. 1976. Long-period waves on a natural beach. J. Geophys.Res., 81(36), 6441-6449.

Hutter, K. 1973. On the fundamental equations of floating ice. Mitteilung Nr. 8 der Versuchsanstalt für Wasserbau, Hydrologie und Glaziologie an der ETH, Zürich, 150 pp.

Hutter, K.. 1975a. A general theory for floating ice plates. Archives of Mechanics. 27(4), 617-638.

Hutter, K. 1975b. A general nonlinear viscoelastic plate theory and its application to floating ice. Acta Mechanica, 21, 313-327.

Hutter, K. 1975c. Floating sea ice plates and the significance of the dependence of the Poisson ratio on brine content. Proc. R.Soc. Lond. A., 343(1632), 85-108.

Hutter, K. 1976. The significance of the shear rigidity and of Poisson ratio for sea ice plates. Proceedings of the 3rd International Conference on Port and Ocean Engineering under Arctic Conditions, Univ. of Alaska, Vol.1, 247-267.

Hutter, K. 1977. On the mechanics of floating ice sheets. Lecture notes, Memorial University of Newfoundland, St Johns, Nfld., Canada, 90 pp.

Hutter, K. 1978. On the mechanics of floating ice sheets. Mitteilung Nr. 28 der Versuchsanstalt für Wasserbau, Hydrologie und Glaziologie an der ETH, Zürich, 103 pp.

Jaeger, J.C. 1956. Elasticity, Fracture and Flow with Engineering and Geological Applications, Methuen and Co., Ltd., New York, 152 pp.

Jeffreys, H., and B. Jeffreys. 1972. Methods of Mathematical Physics, Camb.Univ.Press, 3rd ed., Cambridge, England, 718 pp.

Jellinek, H.H.G., and R. Brill. 1956. Viscoelastic properties of ice. J. appl.Phys., 27(10), 1198-1209.

Katona, M.G. 1974. Ice engineering; viscoelastic finite element formulation. Tech. Rep. R 803, Naval Civil Engng.Lab., Port Hueneme, Calif., 55 pp.

Keliher, T.E. 1976. An investigation of the effect of large-amplitude ocean waves on Antarctic pack ice. AIDJEX Bulletin No.34, 114-135.

Keller, J.B., and E. Goldstein. 1953. Water wave reflection due to surface tension and floating ice. Trans. Am. geophys.Un., 34(1), 43-48.

Keller, J.B., and M. Weitz. 1953. Reflection and transmission coefficients for waves entering or leaving an icefield. Communs pure appl.Math., 6(3), 415-417.

Kerr, A.D., and W.T. Palmer. 1970. The deformations and stresses in floating ice plates. New York University, School of Engineering and Science, Dept. of Aeronautics and Astronautics, Rep. No. S-70-3, NYU-AA-70-17, 22 pp.

Kheisin, D.Y. 1967. Dinamika ledyanogo pokrova [Dynamics of ice cover], Leningrad, Gidrometeorologicheskoye Izdatel'stvo, Section 19, 216 pp.

King, J.C.P., and R.G. Bilham. 1973. Strain measurements instrumentation and techniques. Phil. Trans. R.Soc. A, 274, 209-217.

Kinsman, B. 1965. Wind Waves, Prentice-Hall, Inc., Englewood Cliffs, New Jersey, 676 pp.

Kiviniemi, A. 1975. Measurements of wave motion in the ice surface. Rep. of Finnish Geodetic Inst., ISBN 951-711-017-0, Helsinki, 13 pp.

Lathi, B.P. 1965. Communication Systems, John Wiley & Sons, Inc., New York, 431 pp.

Lau, G., and J.R. Rossiter. 1978. Physical properties of fast ice near Twillingate, Newfoundland. C-CORE Tech. Rep. 78-1, 95 pp.

LeSchack, L.A. 1964. Long-period vertical oscillation of the ice recorded by continuous gravimeter measurements from drift station T-3. Arctic, 17(4), 272-279.

LeSchack, L.A. 1965. On the generation and directional recording of waves in the Arctic Ocean. U.S. Naval Oceanogr. Office, Washington D.C., Tech. Rep. TR-179, 44 pp.

LeSchack, L.A., and R.A. Haubrich. 1964. Observations of waves on an ice-covered ocean. J. Geophys.Res., 69(18), 3815-3821.

Lewis, E.L. 1971. Introduction to Arctic sea ice. Engng. J., 54(1/2), 10-14.

Lockett, F.J. 1972. Nonlinear Viscoelastic Solids, Academic Press, London, 195 pp.

Longuet-Higgins, M.S., Cartwright, D.E., and N.D. Smith. 1963. Observations of the directional spectrum of sea waves using the motions of a floating buoy. Ocean Wave Spectra, Natn. Acad. Sciences - Natn.Res.Counc. Conference held at Easton, Maryland, May 1-4, 1961. Prentice-Hall, Englewood Cliffs, 1963, 111-136.

Lorrain, P., and D. Corson. 1970. Electromagnetic Fields and Waves, W.H. Freeman & Co., San Francisco, 2nd ed., 706 pp.

Meier, J.H. 1950. Strain rosettes. In Handbook of Experimental Stress Analysis, ed. M. Hetényi, John Wiley and Sons, New York, 390-437.

Mills, D.A. 1969. Waves, pressure disturbances and floating ice fields. Res. paper 33, Horace Lamb Centre for Oceanogr.Res., Flinders Univ. of S. Aust., Bedford Park, 27 pp.

Mills, D.A. 1972. On waves in a sea ice cover. Res. paper 53, Horace Lamb Centre for Oceanogr.Res., Flinders Univ. of S. Aust., Bedford Park, 64 pp.

Mindlin, R.D. 1951. Influence of rotatory inertia and shear on flexural motions of isotropic, elastic plates. J. appl.Mech., 18, 31-38.

Morland, L.W., and E.H. Lee. 1960. Stress analysis for viscoelastic materials with temperature variation. Trans. Soc.Rheol., 4, 233-263.

Muki, R., and E. Sternberg. 1961. On transient thermal stresses in viscoelastic materials with temperature-dependent properties. J. appl.Mech., 28, Trans. ASME, 83, Series E, 193-207.

Murphy, G., Hausrath III, A.H., and P.W. Peterson. 1957. Response of resistance strain gauges to dynamic strains. IX Congres Int. de Mecan.Appl., Actes. [1956], Tom 8, 448-456.

Nakaya, U., and J. Muguruma. 1962. Physical properties of the ice of Fletcher's ice island (T-3) AFCRL-62-463, Scientific Report No.2, Geophysic Research Directorate, Air Force. Cambridge Research Laboratories, Bedford, Mass., 34 pp.

National Engineering Science Company Staff. 1965. Experimental investigation of ice floe under wave action. Rep. NBy-32256 by Natn.Engng. Science Co., Pasadena, Calif. for U.S. Naval Civil Engng.Lab., Port Hueneme, Calif., 34 pp.

Nevel, D.E. 1966. Time dependent deflection of a floating ice sheet. RR 196, U.S. Army Cold Regions Research & Engineering Laboratory, Hnover, New Hampshire, 9 pp.

Nevel, D.E. 1976. Creep theory for a floating ice sheet. SR 76-4, U.S. Army Cold Regions Research & Engineering Laboratory, Hanover, New Hampshire, 98 pp.

Newman, M., and M. Forray. 1962. Thermal stresses and deflections in thin plates with temperature-dependent elastic moduli. J. Aerospace Sci., 29, 372-373.

Ofuya, A.O., and A.J. Reynolds. 1967. Laboratory simulation of waves in an ice floe. J. Geophys.Res., 72(14), 3567-3583.

Oliver, J., Crary, A.P., and R. Cotell. 1954. Elastic waves in Arctic pack ice. Trans. Am.geophys.Un., 35(2), 282-2 2.

Peters, A.S. 1950. The effect of a floating mat on water waves. Communs pure appl.Math., 3, 319-354.

Pierson, W.J., and L. Moskowitz. 1964. A proposed spectral form for fully developed wind seas based on the similarity theory of S.A. Kitaigorodskii. J. Geophys.Res., 69(24), 5181-5190.

Pipkin, A.C. 1972. Lectures on Viscoelasticity Theory, George Allen & Unwin Ltd., London, 180 pp.

Pounder, E.R. 1965. The Physics of Ice, Pergamon Press, Oxford, 151 pp.

Press, F., Crary, A.P., Oliver, J., and S. Katz. 1951. Air-coupled flexural waves in floating ice. Trans. Am.geophys.Un., 32(2), 166-172.

Read, W.T. 1950. Stress analysis for compressible viscoelastic materials. J. appl.Phys., 21, 671-674.

Robin, G. de Q. 1963a. Wave propagation through fields of pack ice. Phil.Trans. R.Soc. A, 255(1057), 313-339.

Robin, G. de Q. 1963b. Ocean waves and pack ice. Polar Rec., 11(73), 389-393.

Robin, G. de Q. 1966. Pack ice and waves. SCAR/SCOR/IAPO/IUBS Symposium on Antarctic Oceanography, Santiago, Chile, Sept.13-16, 1966. Publ. by Scott Polar Res.Inst., Cambridge, for Sci. Comm. on Antarctic Res., 191-197.

Rossiter, J.R., Langhorne, P., Ridings, T., and A.J. Allan. 1977. Study of sea ice using impulse radar. Proceedings of 4th International Conference on Port and Ocean Engineering under Arctic Conditions, Memorial University of Newfoundland, Vol.1, 556-567.

Sala, I., and E. Olkkonen. 1973. Visco-elastic strain caused by a monotonously increasing stress. Geophysica, 13(1), 83-88.

Schwarz, J., and W.F. Weeks. 1977. Engineering properties of sea ice. J. Glaciol., 19(81), 499-531.

Schwarzl, F., and A.J. Staverman. 1952. Time-temperature dependence of linear viscoelastic behaviour. J. appl.Phys., 23(8), 838-843.

Shapiro, A., and L.S. Simpson. 1953. The effect of a broken icefield on water waves. Trans. Am.geophys.Un., 34(1), 36-42.

Spain, B., and M.G. Smith. 1970. Functions of Mathematical Physics, Van Nostrand Reinhold Co., London, 208 pp.

Squire, V.A. 1978. An investigation into the use of strain rosettes for the measurement of propagating cyclic strains. J. Glaciol., 29(83), 425-431.

Squire, V.A., and A.J. Allan. 1979. Propagation of flexural gravity waves in sea ice. A Symposium on Sea Ice Processes and Models, Seattle, U.S.A., Sept. 6-9, 1977. In press.

Stoker, J.J. 1957. Water Waves. The Mathematical Theory with Applications, Interscience, New York, 567 pp.

Sytinskiy, A.D., and V.P. Tripol'nikov. 1964. Some results of investigations of the natural vibrations of ice fields of the central Arctic. Izv. Akad. Nauk SSSR Geofiz., 4, 615-621.

Tabata, T. 1955. A measurement of visco-elastic constants of sea ice. J. oceanogr.Soc. Japan, 11(4), 1-5.

Tabata, T. 1958a. Studies on visco-elastic properties of sea ice. Arctic Sea Ice, Conference held at Easton, Maryland, Publn. 598 of Natn.Acad.Sciences - Natn.Res.Counc., Washington D.C., 139-147.

Tabata, T. 1958b. Studies on mechanical properties of sea ice. I. On the static visco-elasticity of sea ice. Low Temp.Sci., Ser.A, 17, 135-145.

Tabata, T. 1959. Studies on mechanical properties of sea ice. IV. Measurement of internal friction. Low Temp.Sci., Ser.A, 18, 131-147.

Timoshenko, S., and S. Woinowsky-Krieger. 1959. Theory of Plates and Shells, McGraw-Hill, New York, 2nd ed. 580 pp.

Ursell, F. 1947. The effect of a fixed vertical barrier on surface waves in deep water. Proc. Camb. phil.Soc. math.phys. Sci., 43, 374-382.

Vaudrey, K.D., and M.G. Katona. 1975. Viscoelastic finite element analysis of sea ice sheets. International Association of Hydraulic Research, 3rd International Symposium on Ice Problems. CRREL, Hanover, New Hampshire, 515-525.

Wadhams, P. 1973a. Attenuation of swell by sea ice. J. Geophys. Res., 78(18), 3552-3563.

Wadhams, P. 1973b. The Effect of a Sea Ice Cover on Ocean Surface Waves, Ph.D. dissertation, Univ. of Cambridge, England, 223 pp.

Wadhams, P. 1978. Wave decay in the marginal ice zone measured from a submarine. Deep Sea Res., 25, 23-40.

Weeks, W.F. 1966. Understanding the variations of the physical properties of sea ice. SCAR/SCOR/IAPO/IUBS Symposium on Antarctic Oceanography, Santiago, Chile, Sept. 13-16, 1966. Publ. by Scott Polar Res.Inst., Cambridge, for Sci.Comm. on Antarctic Res., 173-190.

Weeks, W.F., and A. Assur. 1967. The mechanical properties of sea ice. Report II-C3, U.S. Army Cold Regions Research & Engineering Laboratory, Hanover, New Hampshire, 80 pp.

Weeks, W.F., and O.S. Lee. 1958. Observations on the physical properties of sea ice at Hopedale, Labrador. Arctic, 11(3), 134-155.

Weeks, W.F., and O.S. Lee. 1962. The salinity distribution in young sea-ice. Arctic, 15(2), 93-108.

Weeks, W.F., and G. Lofgren. 1967. The effective solute distribution coefficient during the freezing of NaCl solutions. Physics of Snow and Ice. Proceedings of the International Conference on Low Temperature Science, 1966, ed. H. Ôura, Hokkaido, Japan, Vol.1, 579-597.

Weitz, M., and J.B. Keller, 1950. Reflection of water waves from floating ice in water of finite depth. Communs pure appl.Math., 3(3), 305-318.

Williams, F.M. 1976. Time dependent deflections of nonhomogeneous ice plates. Acta Mechanica, 25, 29-44.

PLATES

1

Wire strainmeters and telemetry system at Main Tickle

2

Rosette of three rod strainmeters at Starve Harbour

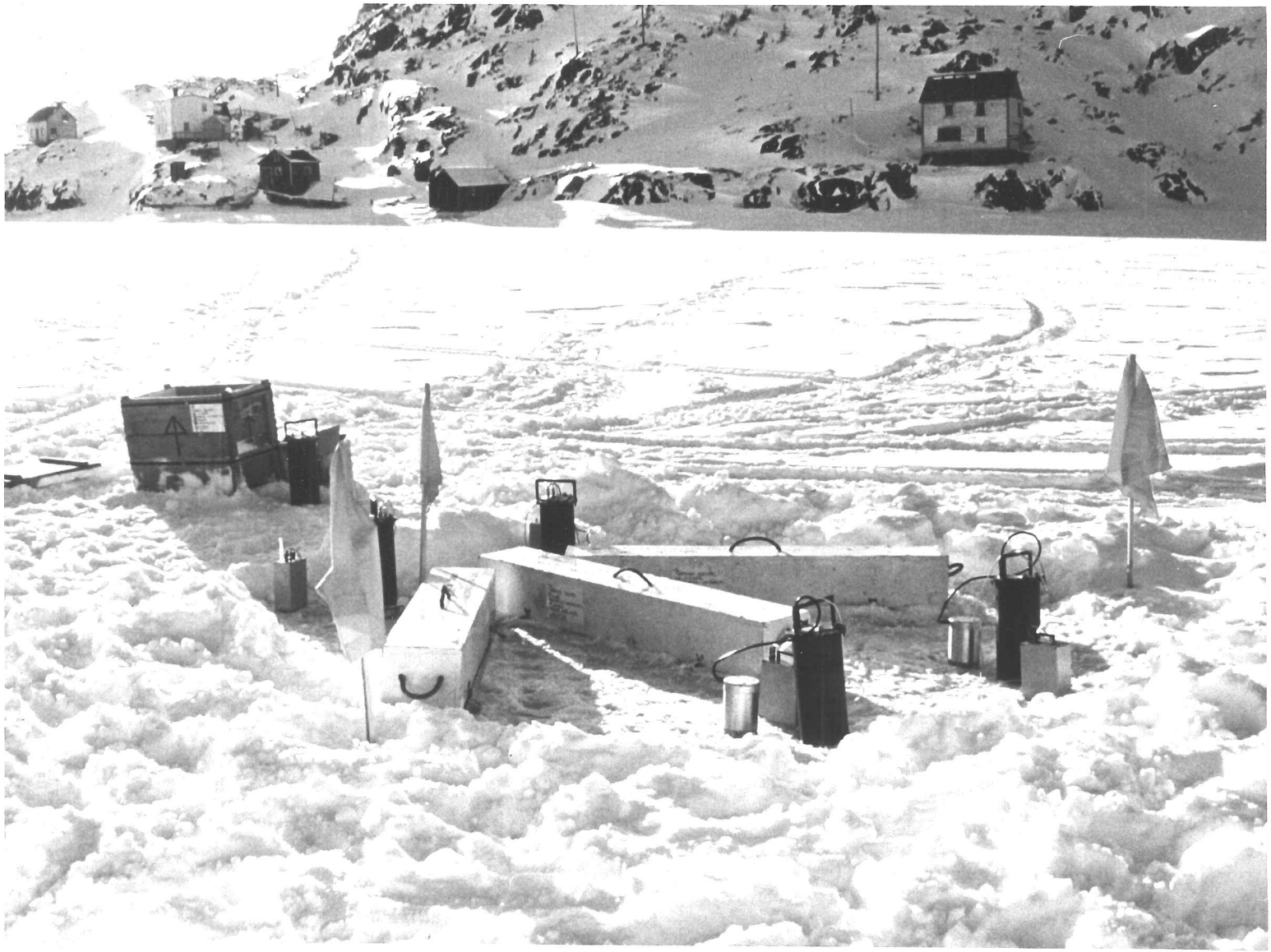

3

Wave break-up at St. Anthony Bight

4

Wave break-up at
St. Anthony Bight

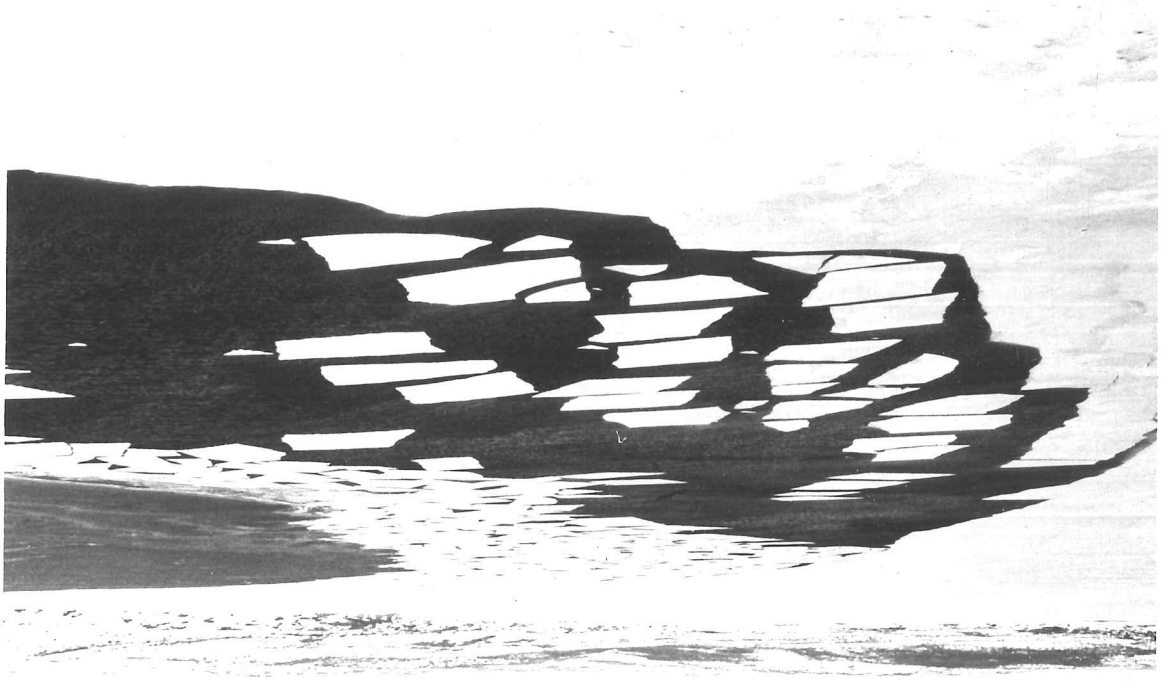

5

Crystal structure of sea ice core from L'Anse Amour

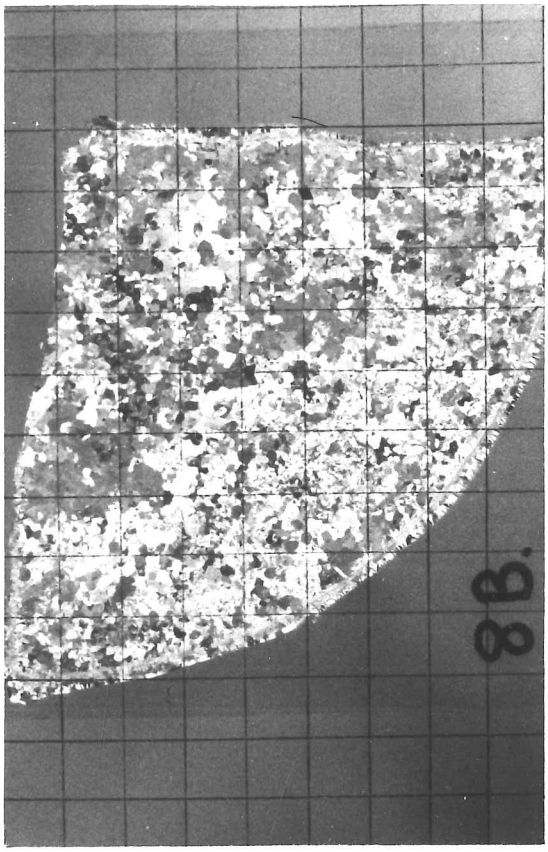
8B.

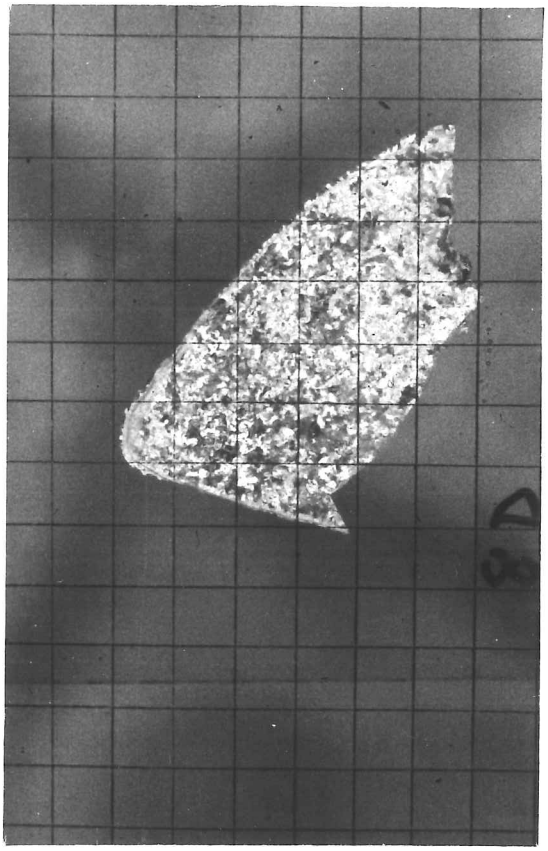
8D

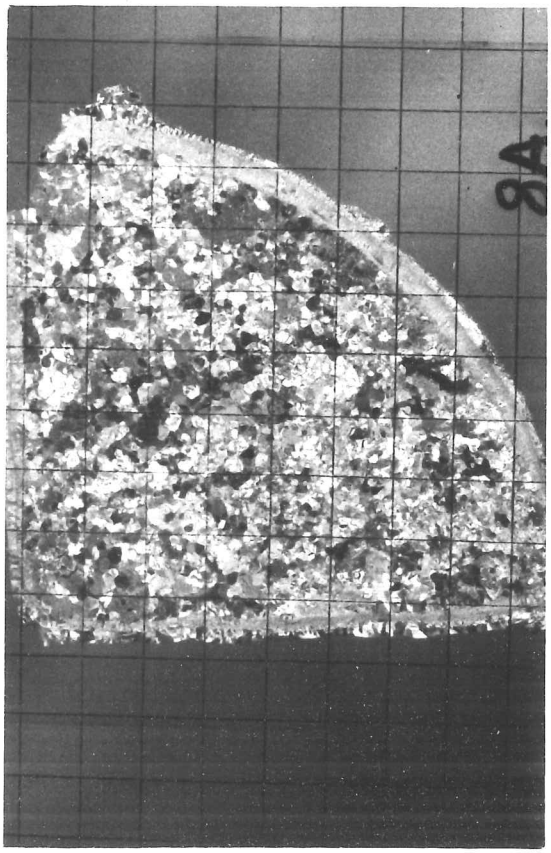
8A

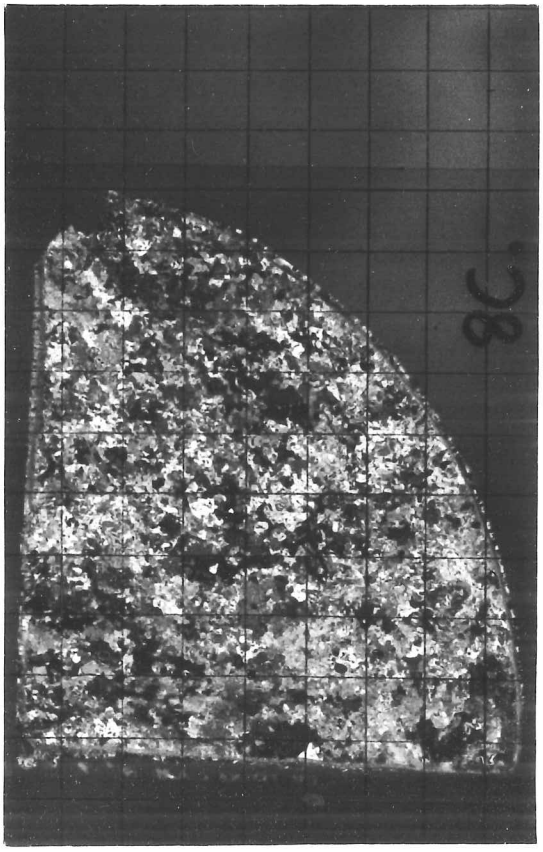
8C.

6

Crystal structure of sea ice core from Forteau Bay